TURBULENT INCOMPRESSIBLE FLOW IN ANNULAR DIFFUSERS

by

S.J. Stevens

A Thesis

submitted for the degree of

Doctor of Philosophy

Loughborough University of Technology

Department of Transport Technology - October 1970

SUMMARY

Low speed tests have been made to investigate the performance of three annular diffusers having centre bodies of uniform diameter and conically diverging outer walls. The diffusers had a common area ratio of 2.0 : 1, an inlet radius ratio of 0.833, and non-dimensional lengths of 5.0, 7.5 and 10.0 respectively. The tests were carried out with fully developed flow at inlet; the inlet conditions were obtained by natural development in a long annular entry length.

The overall static pressure rise coefficient was in good agreement with published data after applying a correction to take account of the increased boundary layer thickness at inlet. In addition to the overall performance characteristics, a detailed study has been made of the growth of the boundary layer along the inner and outer walls in each of the three diffusers. Measurements have been made of the mean velocity profiles and turbulence structure at a number of stations along the length of the diffusers. The data shows excellent symmetry of flow, and the momentum-balance plots are in good agreement.

The results indicate an asymmetric growth of the boundary layers along the inner and outer walls. The rate of increase in the shape parameters becoming significantly greater on the outer wall as the outer wall angle increases. This asymmetry is mainly attributed to the disturbance associated with the change in outer wall angle at inlet. The measured shear stress distributions exhibit considerable lag, and a large gradient of

shear stress near the wall in regions of severe adverse pressure gradient.

An integral approach has been used to predict the boundary layer growth, based on the assumption that no net mass transfer takes place between the inner and outer wall boundary layers. Within the limits of experimental error, this assumption has been verified. For the diffusers having non-dimensional lengths of 7.5 and 10.0, good agreement, sufficient for most engineering purposes, has been achieved between the theoretical and experimental values of overall and internal performance. However, this agreement was only obtained by commencing the calculations downstream of the disturbance associated with the inlet bend. In the case of the minimum length diffuser, the predicted values of shape parameter along the outer wall are too low. This is considered to be due to a failure of the accepted methods of velocity profile representation in severe adverse pressure gradients.

ACKNOWLEDGMENTS

The author wishes to express his gratitude to Professor K.L.C. Legg, Head of the Department of Transport Technology, for his continued support and encouragement, particularly in the early days of the Internal Aerodynamics Research Programme; also to the Science Research Council whose financial support made possible the completion of the work reported in this Thesis.

Gratitude is also due to Professor E. Markland, Head of the Department of Mechanical Engineering, University College, Cardiff, for his unfailing encouragement, and to Dr. H.E. Imbach, Brown-Boveri Co. Ltd., who made many helpful suggestions.

The author is indebted to Mr. G. Bowler who helped design and construct the experimental apparatus, and to Miss D. Gray and Mrs. R. Stevens who helped edit and proof read the manuscript. Thanks are also due to Mrs. Gretsch who carried out the typing, and to Mr. M. Proctor who prepared some of the Figures.

LIST OF CONTENTS

APPENDICES

VOLUME 2

VOLUME 3

LIST OF FIGURES

Appendices

LIST OF TABLES

LIST OF PRINCIPAL SYMBOLS

A	area of cross-section
A_B	blocked Area, A - Ae
A_E	effective Area $\int_0^A \frac{u}{U} dA$
AR	area Ratio
B	blocked area fraction, A_B/A
C_D	coefficient of Discharge or Dissipation Coefficient
Cf	local Skin Friction Coefficient , $\tau_\omega / \frac{1}{2}\rho U^2$
$\overline{Cp}$	pressure recovery coefficient based on $\frac{1}{2}\rho \overline{u}_1^2$
$\overline{Cp}'$	pressure recovery for ideal, one-dimensional flow , $1 - 1/AR^2$
$\overline{Cp}*$	the locus of maximum pressure recovery coefficient at prescribed non-dimensional length
$\mathcal{D}$	dissipation Integral
D	diameter of cross section
Dh	hydraulic mean diameter, Do - Di
E	effective area fraction, Ae/A
$\mathcal{E}$	overall effectiveness, $\overline{C}_P / \overline{C}_P'$
H	shape parameter δ^*/θ
$\overline{H}$	energy shape parameter δ^{**}/θ
ℓ	Prandtl mixing length $\left[-\overline{u'v'} / \left\lvert \frac{du}{dR} \right\rvert \frac{du}{dR} \right]^{1/2}$
L	mean wall length for annular diffusers
Le	length of approach pipe upstream of diffuser
n	exponent in power law velocity profile equation
N	diffuser axial length
N.S.C.	Reynolds Normal Shear Stress Coefficient

P	static pressure
PT	total or stagnation pressure
ΔP	actual static pressure rise
$\Delta P'$	static pressure rise for ideal, one-dimensional flow
Q	volume flow rate, $\int_0^A u\,dA = \bar{u}A$
$\bar{q}$	dynamic pressure based on mass-averaged velocity
R	radius
R_e	Reynolds number, $U D_h / \nu$
R_m	radius at which the axial velocity is equal to U
ΔR	annulus height, $R_o - R_i$
u	local axial velocity
$\bar{u}$	mass-averaged velocity
u_τ	friction velocity, $\sqrt{\tau_w / \rho}$
$\sqrt{\overline{u'}^2}$	r.m.s velocity fluctuation in x direction
$\overline{u'v'}$, $\overline{u'w'}$	Reynolds stresses
U	maximum velocity in cross section
$\sqrt{\overline{v'}^2}$	r.m.s. velocity fluctuation in R - direction
$\sqrt{\overline{w'}^2}$	r.m.s. velocity fluctuation in the circumferential direction
x	axial distance from diffuser inlet
y	distance normal to surface
W	local width of a two-dimensional diffuser
α	kinetic-energy-flux velocity profile parameter, $\frac{1}{A}\int_0^A \left(\frac{u}{\bar{u}}\right)^3 dA$
β	momentum-flux velocity profile parameter, $\frac{1}{A}\int_0^A \left(\frac{u}{\bar{u}}\right)^2 dA$
γ	pressure gradient parameter, $\frac{\nu}{\rho u_\tau^3}\frac{dP}{dx}$
δ	boundary layer thickness
δ_o^*	displacement thickness of boundary layer on outer wall, $\int_{R_m}^{R_o}\left(1 - \frac{u}{U}\right)\frac{R}{R_o}\,dR$

δ_i^* displacement thickness of boundary layer on inner wall,

$$\int_{R_i}^{R_m} \left(1 - \frac{u}{U}\right) \frac{R}{R_i}\, dR$$

δ_o^{**} energy thickness of boundary layer on outer wall,

$$\int_{R_m}^{R_o} \left(1 - \left(\frac{u}{U}\right)^2\right) \frac{u}{U} \frac{R}{R_o}\, dR$$

δ_i^{**} energy thickness of boundary layer on inner wall,

$$\int_{R_i}^{R_m} \left(1 - \left(\frac{u}{U}\right)^2\right) \frac{u}{U} \frac{R}{R_i}\, dR$$

ε eddy viscosity, $-\overline{u'v'} \Big/ \left(\frac{du}{dR}\right)$

θ_o momentum thickness of boundary layer on outer wall,

$$\int_{R_m}^{R_o} \left(1 - \frac{u}{U}\right) \frac{u}{U} \frac{R}{R_o}\, dR$$

θ_i momentum thickness of boundary layer on inner wall,

$$\int_{R_i}^{R_m} \left(1 - \frac{u}{U}\right) \frac{u}{U} \frac{R}{R_i}\, dR$$

λ loss coefficient

ν kinematic viscosity

ρ fluid density

τ shear stress

τ_w shear stress at the wall

ϕ diffuser wall angle

ψ correction factor applied to boundary layer thickness

Subscripts

i inner wall

o outer wall

m maximum

1 diffuser inlet

2 diffuser outlet

3 station in downstream settling length at which maximum pressure occurs

SECTION 1

INTRODUCTION

1 -1 The Diffuser

In many internal fluid flow systems it is often necessary to reduce the kinetic energy of the flow. This may be accomplished by allowing the fluid to pass through a duct of increasing area known as a diffuser. The reduction in kinetic energy is accompanied by a corresponding increase in the pressure energy of the fluid.

However, due to the adverse pressure gradient which occurs, the boundary layer thickens, and if the pressure gradient is too severe, separation will occur and the fluid will tend to flow back in the direction of the pressure gradient. Eddies formed by separation result in some kinetic energy being converted into random or disordered energy, thus reducing the amount of energy available for conversion into pressure energy. Consequently in all diffuser applications it is desirable to minimise the loss of available energy, and therefore attention can be focused on the velocity-decrease or pressure-increase objective in various installations.

In order to avoid excessive losses in engine components it is often necessary to reduce the velocity of the gases; a typical example is the design of a pure jet engine exhaust system. In most installations a diffuser is fitted downstream of the turbine to reduce the velocity in the jet pipe to an acceptable level. Diffusers are also used at exit of the compressor in a gas turbine engine. Again the objective is to reduce the velocity level to prevent excessive losses in a downstream component, namely the combustion chamber.

The use of a diffuser at exit of a power turbine is an example of an application where the pressure rise characteristic is important. The diffuser increases the expansion ratio across the turbine thus increasing the power output.

In addition to the overall performance characteristics, the velocity profile and stability of flow at exit may be equally important if the diffuser is linked to a downstream component whose performance is sensitive to inlet conditions. Such considerations apply to the intake diffuser of an aircraft gas turbine engine, since the surge line and efficiency of the compressor are known to depend on the flow conditions at inlet.

1-2 Diffuser Geometry

The simple, two-dimensional diffuser may be described by three geometric parameters : the area ratio (AR), the wall divergence angle (ϕ), and the ratio of wall length to entry width (L/W_1).

They are related by the expression

$$AR = 1 + 2\frac{L}{W_1}\sin\phi \qquad \text{1-2-1}$$

It is usual to plot the diffuser characteristics against (AR - 1) and L/W_1, the wall angle entering as a dependent parameter. Conical diffusers have three parameters related in a similar manner

$$AR = 1 + 2\frac{L}{R_1}\sin\phi + \left(\frac{L}{R_1}\sin\phi\right)^2 \qquad \text{1-2-2}$$

where R_1 is the radius at diffuser inlet.

The nomenclature used to define the geometric characteristics of annular diffusers are shown in Fig. 1-2-1. In the general case where both wall angles vary the relationship between the geometric parameters is more complex :

$$AR = 1 + 2\frac{L}{\Delta R_1}\left(\frac{\sin\phi_o + \frac{R_i}{R_o}\sin\phi_i}{\left(1+\frac{R_i}{R_o}\right)}\right) + \frac{L^2}{(\Delta R_1)^2}\left(1-\frac{R_i}{R_o}\right)\left(\frac{\sin^2\phi_o - \sin^2\phi_i}{\left(1+\frac{R_i}{R_o}\right)}\right) \qquad \text{——— 1-2-3}$$

where $\Delta R_1 = (R_o - R_i)_1$ is the annulus height at diffuser inlet, and L is the average wall length ($L \simeq L_o$ & L_i providing the difference between the wall angles is not very large). Thus, two additional parameters, the inlet radius-ratio, and a wall angle, are required to specify the geometry of simple straight walled annular diffusers.

The larger number of parameters increases the difficulties involved in attempting to generalise the performance characteristics.

Some simplification can be introduced by considering the case of a constant inner diameter diffuser (see Fig. 1-2-1) since,

$$AR = 1 + 2\frac{L}{\Delta R_1}\frac{\sin\phi_o}{\left(1+\frac{R_i}{R_o}\right)} + \frac{L^2}{(\Delta R_1)^2}\sin^2\phi_o\frac{\left(1-\frac{R_i}{R_o}\right)}{\left(1+\frac{R_i}{R_o}\right)} \qquad \text{——— 1-2-4}$$

As the inlet radius ratio $\left(\frac{R_i}{R_o}\right)_1$ approaches 1.0 the relationship tends towards that of a plane diffuser, a conical diffuser being the limiting case as $\left({}^{R_i}/_{R_o}\right)_1$ approaches zero.

All the preceding remarks apply to diffusers that are "clean", or free from any internal obstructions. However, in many engineering applications aerofoil-shaped struts are incorporated to transmit auxiliary drives, and air supplies, across the annulus. Such obstructions may modify the diffuser geometry considerably.

1-3 Performance Parameters

A large number of parameters have been suggested as suitable criteria for evaluating diffuser performance. Most are based on the static pressure recovery because of the particular ease with which the static pressure rise can be measured, since in the absence of swirl and streamline curvature the static pressure at any section can be based on the wall value.

The pressure recovery coefficient $\overline{C}p$ relates the actual pressure rise to the maximum attainable assuming uniform flow at inlet and an infinite area ratio.

$$\overline{C}_P = \frac{P_2 - P_1}{\frac{1}{2}\rho \bar{u}_1^2} \qquad \text{1-3-1}$$

The overall diffuser effectiveness relates the actual pressure rise to that achievable with inviscid one-dimensional flow, thus

$$(P_2 - P_1)' = \frac{1}{2}\rho\left(\bar{u}_1^2 - \bar{u}_2^2\right) = \frac{1}{2}\rho\bar{u}_1^2\left(1 - \frac{1}{\left(\frac{A_2}{A_1}\right)^2}\right)$$

$$\therefore \quad \overline{C}_P' = \frac{P_2 - P_1}{\frac{1}{2}\rho\bar{u}_1^2} = 1 - \frac{1}{AR^2} \qquad \text{1-3-2}$$

and the effectiveness $\mathcal{E}$.

$$\mathcal{E} = \frac{\overline{C}P}{\overline{C}_P'} = \frac{P_2 - P_1}{\frac{1}{2}\rho\bar{u}_1^2\left(1 - 1/AR^2\right)} \qquad \text{1-3-3}$$

With non-uniform inlet flow the kinetic energy flux entering a diffuser is greater than it would be for the same mass flow rate entering under uniform conditions, and it is therefore possible for the effectiveness to exceed unity. The relation defining effectiveness has often been referred to as the "efficiency", but efficiency is associated with a loss of available energy, and Eqn. 1-3-3 describes the effectiveness of a diffuser of fixed area ratio to recover pressure energy.

1-3-2 Loss Coefficient

If the flow is incompressible, and the static pressure constant across the section, the mass-mean total pressure can be expressed as

$$P_T = P + \alpha \frac{1}{2}\rho \bar{u}^2$$

where $\alpha \left(\frac{\int u^3 dA}{\bar{u}^3 A} \right)$ is the energy coefficient of the velocity profile, the value of α rising from unity as the non-uniformity or distortion increases. Writing the energy equation between inlet and exit we have

$$P_1 + \alpha_1 \frac{1}{2}\rho \bar{u}_1^2 = P_2 + \alpha_2 \frac{1}{2}\rho \bar{u}_2^2 + \Delta P_T \qquad 1\text{-}3\text{-}1$$

where ΔP_T is the mass averaged total pressure loss in the diffuser and is a measure of the loss of available energy. The loss coefficient λ_{1-2} is defined as;

$$\lambda_{1-2} = \frac{\Delta P_T}{\frac{1}{2}\rho \bar{u}_1^2} \qquad 1\text{-}3\text{-}2$$

Rearranging Equation 1-3-1 we obtain

$$\bar{C}_P = \frac{P_2 - P_1}{\frac{1}{2}\rho \bar{u}_1^2} = \left[\alpha_1 - \frac{\alpha_2}{AR^2} \right] - \lambda_{1-2} \qquad 1\text{-}3\text{-}3$$

$$\therefore \quad \bar{C}_P = \left[\alpha_1 - \frac{1}{AR^2} \right] - \left[\frac{\alpha_2 - 1}{AR^2} \right] - \lambda_{1-2} \qquad 1\text{-}3\text{-}4$$

Considering the terms in Eqn. 1-3-4, the first term $\alpha_1 - \frac{1}{AR^2}$ represents the pressure coefficient which would be attained if the flow were uniform at exit. The value of $(\alpha_2 - 1)$ in the second term is a measure of the distortion of the outlet velocity profile and therefore the term $\frac{\alpha_2 - 1}{AR^2}$ represents the reduction in pressure recovery due to excess kinetic energy at exit. The pressure recovery or effectiveness can therefore be lowered by insufficient diffusion as represented by the second term or inefficient diffusion as represented by the loss coefficient. Thus, apart from the static pressure rise, measurements of the inlet and outlet velocity profiles are required in order to determine the loss coefficient. However, due to possible asymmetry and the unsteadiness of flow at exit it is difficult to obtain reliable values of α_2, and therefore most of the published information on diffuser performance is in the form of pressure recovery characteristics. Experimentally it has been shown that:

Diffuser Effectiveness = f (Diffuser Geometry, inlet boundary layer characteristics, external influences, inlet Mach No., Reynolds No., entry swirl, surface finish.)

1-4 Factors Affecting Diffuser Performance

1-4-1 Diffuser Geometry

Extensive and systematic testing is required to determine the influence of diffuser geometry. Such an investigation has been carried out for two-dimensional diffusers by Renau, Johnston, & Kline.[1]

A contour plot of $\overline{C}p$ as a function of area ratio AR, and non-dimensional length N/W_1 is shown in Fig. 1-4-1. The values of AR and N/W_1 prescribe the overall pressure gradient, which is the principal factor governing the boundary layer development and consequently the values of exit energy coefficient α_2, loss coefficient λ_{1-2}, and overall performance.

Two optimum lines have been added to the performance chart. The line $\overline{Cp}^*$ is the locus of points which define the diffuser area ratio producing maximum pressure recovery at a given non-dimensional length. The other, line $\overline{Cp}$,** is the locus of points which define the non-dimensional length producing maximum pressure recovery at a given area ratio. The location of the $\overline{Cp}^{**}$ line is somewhat arbitrary, since at a fixed area ratio, $\overline{Cp}$ remains almost constant for values of N/W_1 greater than those defining the Cp* line.

Of equal importance in assessing the influence of diffuser geometry is the Flow-Regime charts, due to Kline, Abbott, & Fox,[2] and shown in Fig. 1-4-1. Four different flow regimes exist, three of which have reasonably "steady" flow. The region of no-appreciable-stall is steady and uniform whilst the region of transitory stall is unsteady and non-uniform. However, the line defining the onset of transitory stalling is approximate since it is based on observed flow patterns. This line has been plotted on Fig. 1-4-1 and it will be seen that optimum Cp* diffusers operate in or near the region of transitory stalling. It follows that in many engineering applications where a diffuser has to match with upstream and downstream components, the minimum length diffuser is chosen consistent with "steady" flow conditions at exit.

1-4-2 Inlet Boundary Layer Characteristics

It has been shown by Livesey, and Turner[3] in work on conical diffusers, and more recently by Wolf, and Johnston[4] for two-dimensional diffusers; that inlet conditions are not specified simply by the boundary layer thickness, but also by the "previous history" of the flow, or the way in which the inlet conditions have been generated. Consider the case of inlet conditions developed naturally in entry lengths.

(i) Naturally Developed Inlet Conditions

It has been shown in Section 1-2 that the effectiveness is determined by the energy coefficient of the outlet velocity profile α_2, and the loss coefficient λ_{1-2}. Both values depend on the development of the boundary layer, in particular the value of α_2 is determined by the shape of the velocity profile which under certain circumstances can be characterised by the shape parameter H. It has been shown theoretically by Schlichting and Gersten(5), and verified experimentally by Sprenger(6), that the outlet shape parameter is strongly dependent on the inlet boundary layer thickness (δ^* or θ). Therefore initial attempts(54) to correlate the influence of inlet conditions were based on inlet boundary momentum thickness. In view of the difficulty in obtaining reliable values of α_2, and doubts surrounding the significance of λ_{1-2}, Sovran and Klomp adopted an alternative approach.

Writing the total pressure at the point of maximum velocity we have

$$P_{T_m} = P + \frac{1}{2}\rho U^2 \qquad 1\text{-}4\text{-}1$$

If the static pressure is uniform across all sections of the diffuser, then the static pressure rise along the streamline of maximum velocity will be the same as that for the diffuser and can be expressed as;

$$P_2 - P_1 = \frac{1}{2}\rho\left(U_1^2 - U_2^2\right) - \Delta P_{T_m}$$

where ΔP_{T_m} is the total pressure loss along the streamline of maximum velocity. Therefore the effectiveness $\mathcal{E}$ can be written as;

$$\mathcal{E} = \left(\frac{U_1}{\bar{u}_1}\right)^2 \left[\frac{1 - \left(\frac{U_2}{U_1}\right)^2}{1 - \frac{1}{AR^2}}\right] - \frac{\lambda m_{1-2}}{\left[1 - \frac{1}{AR^2}\right]} \qquad 1\text{-}4\text{-}2$$

and λm_{1-2} is the loss coefficient $\Delta P_{T m_{1-2}} / \frac{1}{2}\rho \bar{u}_1^2$

The maximum velocities can be related by introducing the concept of effective and blocked area. The effective area is defined as;

$$A_e U = \int_0^A u \, dA = \bar{u} A \quad \text{and} \quad A_e = \int_0^A \frac{u}{U} \, dA \tag{1-4-3}$$

also $\int_0^A u \, dA = \bar{u} A$ and $\frac{\bar{u}}{U} = \frac{A_e}{A}$ 1-4-4

Thus the greater the degree of non uniformity ($\frac{\bar{u}}{U} < 1.0$) the smaller the effective area. The blocked area is defined as the difference between the geometric and effective areas i.e.

$$A_B = A - A_e = \int_0^A \left(1 - \frac{u}{U}\right) dA \tag{1-4-5}$$

expressing both areas as fractions of the geometric area A we have;

$$E = 1.0 - B \quad \text{where } E = \frac{A_e}{A} \quad \text{and} \quad B = \frac{A_B}{A}$$

From Eqn. 1-4-4 : $E = \frac{A_e}{A} = \frac{\bar{u}}{U}$ 1-4-6

Thus the velocity profile parameter E can be obtained without taking a detailed velocity traverse, if the flow rate and maximum velocity are known. (Some of the attraction of this approach is removed in annular diffusers due to asymmetry problems at outlet). From the continuity equation we have

$$\frac{U_2}{U_1} = \left(\frac{A_1}{A_2}\right)\left(\frac{E_1}{E_2}\right) \tag{1-4-7}$$

Introducing this into Eqn. 1-4-2 we have

$$\mathcal{E} = \frac{1}{E_1^2}\left[\frac{1 - \frac{(E_1/E_2)^2}{AR^2}}{1 - \frac{1}{AR^2}}\right] - \frac{\lambda m_{1-2}}{\left[1 - \frac{1}{AR^2}\right]} \tag{1-4-8}$$

The term λm_{1-2} will be zero if an inviscid core exists throughout the length of the diffuser. However, Sovran and Klomp reasoned that even when this was not the case, λm_{1-2} could be neglected in comparison with the first term in Eqn. 1-4-8, since the shear stress in the vicinity of the position of maximum velocity would be very small. They therefore went on to conclude that the first term in Eqn. 1-4-8 largely accounts for the variation in effectiveness, even in cases where separation occurs the reduction in effectiveness is considered to be due to a large increase in blockage rather than internal losses. Sovran and Klomp have shown that for optimum diffusers on the $\bar{C}p^*$ line, in which pressure forces dominate the growth of the boundary layer, the effective area fraction E_2 correlates with inlet blockage and area ratio. The correlation which was based on experimental results from tests with naturally developed inlet conditions on two-dimensional, conical, and annular diffusers is shown in Fig. 1-4-2.

(ii) Artificially Generated Inlet Conditions

The inlet conditions considered in the previous section comprised of boundary layer types of non-uniformity which are frequently combined with inviscid core flow. In many engineering applications however, this simple flow model is not applicable because of various upstream flow conditions such as, wakes from blockages, and energy gradients from compressors. The effect of certain types of non-uniformity on the performance of two-dimensional diffusers has been investigated by Waitman, Reneau, & Kline(8), Livesey & Turner(3), and Wolf & Johnston(4). Wolf & Johnston considered uniform and non-uniform shear flow as illustrated below;

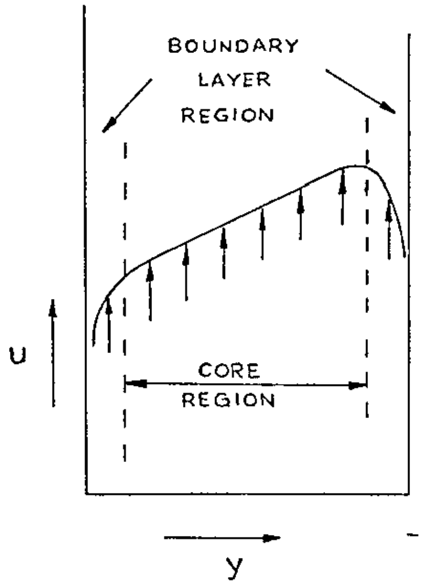

UNIFORM SHEAR

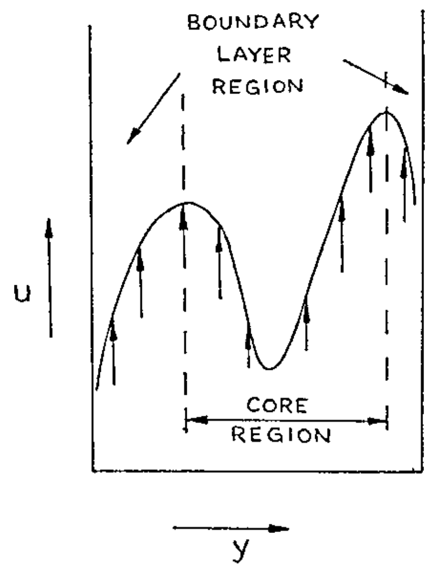

NON-UNIFORM SHEAR

The shear stress in the core region having a linear velocity profile is constant (assuming constant eddy viscosity). Hence no net shear force exists and the slope of the profile remains constant. In the terminology of Livesey & Turner this profile can be said to have a low decay rate. However, in the non-uniform profile, large velocity gradients in the core region generate large net shear forces that "mix" the profile towards uniform conditions, such a profile is said to have a large decay rate. These are just two examples of the many flow situations that could exist, in addition an increase in the turbulence intensity of boundary-layer-type profiles has been shown by Migay[9], and Waitman et al.[8] to influence diffuser performance.

Wolf & Johnston attempted to correlate the outlet velocity profile parameter E_2 using the method due to Sovran

& Klomp, the results are shown in Fig. 1-4-4. The following effects were observed with profiles exhibiting a low velocity near the wall:

a) The onset of transitory stalling occurred at a lower value of area ratio for fixed N/W_1 (see Fig. 1-4-1).

b) The values of peak pressure recovery at constant N/W_1 are decreased relative to the performance obtained with naturally developed inlet conditions.

With wake flow at inlet, in several diffuser geometries the performance increased above that obtained with naturally developed inlet conditions.

Whilst the maximum blockage fraction investigated by Wolf & Johnston was 0.23, Tyler & Williamson[10] have carried out tests on conical diffusers with blockage fractions as high as 0.65. Their results when compared with the correlation due Sovran & Klomp show that agreement is restricted to the "boundary layer" range of inlet blockage values, beyond which the values of E_2 depart significantly. Unfortunately it is not possible to categorise the type of profile presented to the diffuser as detailed inlet velocity traverses were not carried out.

As yet no acceptable parameter, or group of parameters, has been found to correlate the effect of inlet velocity profile distortion. The most successful attempts to date have been made by studying the influence of certain types of velocity profile. However complete elucidation of the dependence of diffuser performance on initial turbulence level and decay rate awaits further investigation.

1-4-3 Entry Swirl

Very little published data is available on the influence of inlet swirl. Schwartz[11] carried out tests on an annular diffuser of constant outer diameter and concluded that swirl angles up to 10° produced little effect on performance, but further increases in swirl angle produced a rapid deterioration.

1-4-4 Reynolds Number

Gibson[12] reported that Reynolds number did not have a significant effect on diffuser performance. More recently McDonald & Fox[13] have shown that for Reynolds numbers greater than 7×10^4 no variation in performance can be detected.

1-4-5 Inlet Mach Number

Tests carried out by Young & Green,[14] and Little & Wilbur,[15] indicate that the pressure recovery is essentially independent of Mach number until the flow becomes locally supersonic around the corner at inlet. Little & Wilbur found that the mean Mach number at which recovery is seriously affected was decreased from 0.82 to 0.72 by increases in inlet boundary layer thickness ($\frac{2\delta^*}{D_1}$ = 0.012 to 0.06).

1-4-6 Surface Finish

An increase in surface roughness has been shown by Little & Wilbur[15] to inhibit separation whilst leaving the pressure recovery unaltered. Migay[16] investigated the influence of transverse ribs, and found that for conical diffusers at very large wall angles ($\phi_o > 20^{\circ}$) the loss coefficient is reduced considerably. Very little attention has been paid to this effect despite its considerable practical importance.

1-4-7 External Influences

(i) Settling Length

If a constant area duct, or settling length, follows the diffuser, a recovery of pressure may occur. Writing the energy equation over the settling length from station 2 at diffuser exit to station 3 where recovery is complete, gives

$$P_2 + \alpha_2 \tfrac{1}{2}\rho\bar{u}_2^2 = P_3 + \alpha_3 \tfrac{1}{2}\rho\bar{u}_3^2 + \Delta P_{T_{2-3}}$$

and $$\frac{P_3 - P_2}{\frac{1}{2}\rho\bar{u}_2^2} = (\alpha_2 - \alpha_3) - \lambda_{2-3}$$

Hence a pressure rise occurs due to turbulent mixing reducing the degree of distortion in the velocity profile ($\alpha_3 < \alpha_2$). Renau, et al.(1) found that for two-dimensional types the performance of the diffuser is unaffected by the presence of the settling length. The fraction of $\bar{C}p$ occurring in the settling length is small (up to approx. 7%)for diffuser geometries below peak recovery, and increases as the amount of stalling (distortion) in the diffuser increases. For diffusers operating in the region of transitory stall as much as 30% of the recovery may take place in the settling length.

(ii) Downstream Obstructions

It is possible that the performance of a diffuser could be improved by placing a restriction in the centre of the stream at the downstream end, thereby forcing the flow to follow the diverging walls more closely. Such a suggestion has been investigated by Henderson(17) who placed circular discs or "target plates" at exit of a conical diffuser. The results indicated that the losses due to the restriction outweighed any improvements in the diffusion process. The influence of streamlining the plate was not considered since the increased length was undesirable for the particular application considered viz. rocket pump diffusers.

Such a situation can exist in the diffuser which is situated between the exit of the compressor and the entry to the combustion system of a gas turbine, depending on the design philosophy. Fig. 1-4-5 shows typical installations in current aircraft gas turbines, it will be seen that in Type A the head plate can influence the flow in the exit region of the diffuser. In Type B the obstruction, i.e. the "snout", extends into the diffuser, and diffusion takes place in the surrounding annulus.

1-5 Boundary Layer Thickness Definitions

The blocked area concept suggested by Sovran & Klomp[7] for equating inlet velocity profiles to diffusers of various cross-sectional shapes can be used to define the axisymmetric boundary layer parameter δ^*;

Since $$A_B = \int_0^A \left(1 - \frac{u}{U}\right) dA \qquad \text{1-4-5}$$

then $$A_B = 2\pi R_o \delta^* = 2\pi R_o \int \left(1 - \frac{u}{U}\right) \frac{R}{R_o}\, dR$$

and $$\delta^* = \int_0^{R_o} \left(1 - \frac{u}{U}\right) \frac{R}{R_o}\, dR \qquad \text{1-5-1}$$

for a circular cross section of radius R_o. Comparison of Eqn. 1-5-1 with the two-dimensional definition of displacement thickness

$$\delta^*_{II} = \int_0^{R_o} \left(1 - \frac{u}{U}\right) dR$$

shows that $\delta^*_{II} \neq \delta^*$, thus the concept of wall displacement valid for two-dimensional boundary layers is not applicable in axisymmetric flows.

Okiishi & Servoy[18] have adopted similar definitions for an annular cross section. For the outer wall boundary layer

$$\delta_o^* = \int_{Rb_o}^{R_o} \left(1 - \frac{u}{U}\right) \frac{R}{R_o} \, dR \qquad 1\text{-}5\text{-}2$$

where the integral extends to Rb_o, the radius at the limit of the outer wall boundary layer. For the inner wall

$$\delta_i^* = \int_{R_i}^{Rb_i} \left(1 - \frac{u}{U}\right) \frac{R}{R_i} \, dR \qquad 1\text{-}5\text{-}3$$

Rb_i being the radius at the limit of the inner wall layer. Equations 1-5-2 & 1-5-3 can be combined to give

$$\frac{\bar{u}}{U} = E = 1 - B = 1 - \frac{2}{R_o + R_i} \left[\frac{R_o \delta_o^*}{R_o - R_i} + \frac{R_i \delta_i^*}{R_o - R_i} \right] \qquad 1\text{-}5\text{-}4$$

In experiments on symmetrical annular diffusers in which $R_i \rightarrow 0$ the definitions of Eqns. 1-5-2 & 1-5-3 are not satisfactory, and Stevens & Markland[19] therefore adopted the following definitions:

$$\delta_o^{*'} = \int_{Rb_o}^{R_o} \left(1 - \frac{u}{U}\right) \frac{R}{(R_o - R_i)} \, dR \quad \& \quad \delta_i^{*'} = \int_{R_i}^{Rb_i} \left(1 - \frac{u}{U}\right) \frac{R}{(R_o - R_i)} \, dR \qquad 1\text{-}5\text{-}5$$

which combine to give

$$\frac{\bar{u}}{U} = 1 - B = 1 - \frac{2}{R_o + R_i} \left[\delta_o^{*'} + \delta_i^{*'} \right] \qquad 1\text{-}5\text{-}6$$

Whilst the displacement thickness δ^* and momentum thickness θ are calculated for two-dimensional and axisymmetric definitions (based on the local radius and the annulus height) in Appendices 4/6/8, throughout the remainder of this thesis the axisymmetric definitions based on local radii (Eqns 1-5-2 & 1-5-3) will be implied unless specifically stated otherwise.

To summarise;

Axisymmetric value of:	Outer Wall	Inner Wall
Displacement Thickness δ^*	$\int_{R_m}^{R_o}\left(1-\frac{u}{U}\right)\frac{R}{R_o}\,dR$	$\int_{R_i}^{R_m}\left(1-\frac{u}{U}\right)\frac{R}{R_i}\,dR$
Momentum Thickness θ	$\int_{R_m}^{R_o}\frac{u}{U}\left(1-\frac{u}{U}\right)\frac{R}{R_o}\,dR$	$\int_{R_i}^{R_m}\frac{u}{U}\left(1-\frac{u}{U}\right)\frac{R}{R_i}\,dR$
Energy Thickness δ^{**}	$\int_{R_m}^{R_o}\frac{u}{U}\left(1-\left(\frac{u}{U}\right)^2\right)\frac{R}{R_o}\,dR$	$\int_{R_i}^{R_m}\frac{u}{U}\left(1-\left(\frac{u}{U}\right)^2\right)\frac{R}{R_i}\,dR$
Shape Parameter H	$\frac{\delta_o^*}{\theta_o}$	$\frac{\delta_i^*}{\theta_i}$
Energy Shape Parameter $\bar{H}$	$\frac{\delta_o^{**}}{\theta_o}$	$\frac{\delta_i^{**}}{\theta_i}$

1-6 Review of Previous Work on Annular Diffusers

Many diffuser applications, particularly in turbomachinery where the fluid stream has to flow over and around a central shaft, involve diffusion in an annular passage. However, the annular diffuser has been the subject of considerably less investigation than have other diffuser geometries partly due to the difficulties involved in the study of the larger number of geometrical parameters and in the presentation of the data.

A considerable amount of information must have been obtained about the performance of particular configurations used in the many power plants built in the last decade but the amount of published data is still rather small, and limited exclusively to tests under laboratory conditions.

Some of the first experiments were carried out at the National Gas Turbine Establishment by Ainley[20] and Johnston[21] on symmetrical diffusers of fixed area ratio (3.19) but varying wall divergence angle. Using almost uniform inlet conditions Ainley established the diffuser geometries for maximum pressure recovery and the onset of transitory stalling. In addition, measurements were made of the pressure recovery in the downstream settling length; the results being in accordance with the findings of Renau, et al.[1], in that the recovery increased as the amount of stalling increased. For operation at a wall angle of 19^{o},35% of the recovery took place in the downstream settling length. Ainley also noted that the settling length was considerably shorter than the six diameters generally required with conical diffusers. The effect of non-uniform inlet conditions produced by gauzes was studied by Johnston but as these were in close proximity to the inlet, the effects of inlet boundary layer thickness and of decay rate cannot be separated. A similar conclusion has been reached by Wolf[4], in a recent analysis of Johnston's experiments.

The work done at N.A.S.A. which has been reported by Wood and Higginbotham[22] concerns improvements in performance obtained by incorporating vortex generators in annular diffusers with constant diameter at the outer wall. The results obtained are shown in Fig. 1-6-1. Vortex generators improved the performance, whilst the introduction of inlet swirl produced a slight deterioration. Nevertheless doubts must be expressed concerning the accuracy of these results in view of the asymmetry in the inlet velocity profile, as there was a 35% variation in outer wall momentum thickness between the four radial stations. Further attempts at improving performance using suction and injection have been reported by Wilbur, and Higginbotham.[23]

The influence of inlet swirl on the diffuser tested by Wood and Higginbotham was investigated by Schwartz[11] who concluded that swirl angles up to 10^{o} produced little effect on performance, although further increases in swirl angle produced a rapid deterioration. Quite recently Horlock[24] has reported an experiment by Hoadley on the influence of free vortex flow on the performance of an optimum $\overline{Cp}$* diffuser having a centre body of uniform diameter. Fig. 1-6-2 shows the total pressure distributions with and without swirl. Severe separation occurred on the outer wall when there was no swirl, but separation moved to the inner wall when large swirl angles were introduced at inlet.

Early attempts to correlate the performance of annular diffusers (Henry, et al.[25]) had been frustrated by a general lack of data, and some of that which was available was of doubtful accuracy on diffusers of poor performance. Sovran and Klomp[7] remedied this situation by measuring pressures recoveries of about one hundred different geometries, ninety-three of which had expanding centre bodies, and the value of inlet radius ratio was 0.55 or 0.70. The range of geometries tested is shown in Fig. 1-6-3. The test programme was conducted with an inlet Mach No. less than 0.3, a Reynolds No. of 4.8×10^5 to 8.5×10^5, and a single inlet velocity profile. The inlet boundary layers were fairly thin (inlet blockage fraction $\simeq 0.02$), and the diffusers had a free discharge. In order to obtain a correlation the geometrical parameters were divided into two groups, those expected to have the greatest influence on diffuser performance, and those expected to produce only second-order effects. Following the technique of Renau, et al.[1] the area ratio AR and non-dimensional length $L/\Delta R_1$ were chosen as the primary group, as they prescribe the overall pressure gradient. The choice of the inlet annulus height ΔR_1 as the normalising factor was based on Eqn. 1-2-4, since in this way it was possible to plot the performance characteristics of, two-dimensional, conical, and annular types on the same set of axes. Analysis of the results revealed that the area ratio for maximum pressure recovery ($\bar{C}p^*$) at a given non-dimensional length was relatively independent of the wall angle-inlet radius ratio combination adopted. A similar conclusion was reached for the geometry defining the optimum $\bar{C}p^{**}$ performance. The qualitative variation of recovery away from the region of the optimum lines was established by investigating the performance of a family of diffusers having a 15° outer wall angle and an inlet radius ratio of 0.70. The performance chart obtained is shown in Fig. 1-6-3. Analysis of these results indicate that all the optimum $\bar{C}p^*$ diffusers have an approximately constant effectiveness of 80%. Based on the results obtained for conical and two-dimensional diffusers Sovran & Klomp assumed that the optimum geometries would be independent of inlet boundary layer thickness. A comparison of the optimum lines for the various diffuser types is shown in Fig. 1-6-3. Although the boundary layers were not measured, the effect of variation of inlet velocity profile, and of the growth of boundary layers along the diffuser, were discussed in terms of the area-blockage concept outlined in Section 1-5.

The influence of inlet velocity profile distortion on the performance of two optimum $\overline{Cp}$*, constant inner diameter annular diffusers, having AR - $L/\Delta R_1$ combinations of; 2.25-6.5, and 3.25-12.0 respectively, has been investigated by Tyler and Williamson.(10) The Reynolds No., based on diffuser inlet diameter, was in the range 0.3×10^6 to 1.3×10^6. The inlet Mach No. did not exceed 0.35. By placing the entry flare in the working section of a wind tunnel, in a plane normal to the direction of flow, blockage fractions as high as 0.70 were produced (see Fig. 1-6-4). The results shown in Fig. 1-6-4 indicate that the correlation of effective outlet area fractions due to Sovran & Klomp is restricted to essentially "boundary-layer" types of inlet distortion, beyond which the performance deteriorates significantly. In addition the optimum area ratio at a given non-dimensional length was found to be reduced by as much as 50% for high blockage fractions. Unfortunately, no measurements were made of the inlet velocity profile, and in view of possible asymmetry, due to the way in which the inlet conditions were generated, the results obtained should be treated with caution.

Howard, et al.(26) have reported tests on symmetrical annular diffusers, and diffusers having constant inner diameter, using fully developed flow conditions at inlet. The inlet radius ratios were 0.515 and 0.775; the range of geometries covered is shown in Fig. 1-6-5. The symmetrical diffusers showed lines of first stall and optimum pressure recovery at constant non-dimensional length close to those of two-dimensional diffusers with which they share a common relationship between AR, $L/\Delta R_1$, and ϕ_o. Annular diffusers with constant inner diameter showed characteristics intermediate between two-dimensional and conical diffusers. Insufficient data was obtained to determine explicitly the effect of inlet radius ratio.

Whilst most of the published work has centred on the overall performance characteristics of annular diffusers Stevens and Markland[19] investigated the growth of the boundary layer along the walls of two symmetrical diffusers having an area ratio of 4.0:1. The divergence angle of the outer wall, and the convergence angle of the inner wall, was 2.5^o in one diffuser, and 5^o in the other, the geometry of the diffusers is shown in Fig. 1-6-6. The conditions at inlet were varied by adjusting the approach lengths, and for the 2.5^o wall-angle diffuser only, by annular gauzes placed some 20 hydraulic diameters upstream of the inlet. The overall performance was in excellent agreement with the results of Howard, et. al., and the variation of effectiveness with inlet blockage is shown in Fig. 1-6-6. Measurements of the pressure recovery in the downstream settling length confirmed the findings of Ainley in that the recovery increased as the amount of stalling increased. The growth of the boundary layers was investigated with fully developed flow at inlet, the results are summarised in Fig. 1-6-6. Although the flow in the 2.5^o wall angle diffuser did not separate, there was a noticeable asymmetry. The shape parameters on both inner and outer walls grew rapidly at the start. Subsequently, the shape parameters decreased as turbulent mixing predominated in a region of low pressure gradient. The flow in the 5° wall angle diffuser separated from the outer wall at $X/N \simeq 0.35$ and beyond this point very considerable asymmetry was apparent. No separation was detected on the inner body, Howard et al.[26] and Horlock[24] have also reported separation only on the outer wall. Further results are given in reference 27. According to reference 26 the 2.5° wall angle diffuser lies in the zone of large transitory stall which is clearly incorrect. Also reference 26 indicates that the 5° wall angle diffuser lies on the optimum $\bar{C}p^*$ line. Whilst the value of recovery is 5% lower than the value predicted by Sovran & Klomp, separation and asymmetry render this diffuser useless for practical applications. The work of Stevens & Markland therefore confirmed the published values of overall performance but cast some doubt on the flow regime charts of Howard, et al.

Although not specifically related to annular diffusers, Moses[28] and Goldberg[29] have measured the boundary layer growth on a cylinder in axially symmetric internal flow. The influence of various types of pressure gradient was investigated, two of which are of interest in relation to the behaviour of the boundary layer on the centre body of an annular diffuser. These experiments are particularly important since not only the mean velocity profile but the turbulence structure of the flow was measured.

Although a number of attempts, notably by Imbach[30] and Nicoll, & Ramaprian[31], have been made to predict the boundary layer growth in conical diffusers, very little attention has been focused on annular diffusers. Soo[32] extended the three-dimensional momentum integral equation to explore flow over bodies of revolution. Separation was predicted by extending the two-dimensional relations for shape parameter and an annular diffuser design based on imminent separation was illustrated.

In common with almost all methods, Soo's method relied on the existence of a potential core throughout the length of the diffuser. The author[33] extended the work reported in reference 27 and applied the axially symmetric form of the momentum integral equation to the calculation of the flow in annular diffusers, based on the assumption of power law velocity profiles. The method is restricted to the case of fully developed inlet flow with no potential core. Good agreement between the predicted and measured shape parameters has been achieved for a conical diffuser of 5° wall angle, and along the outer wall of a 5° wall angle symmetrical annular diffuser.[19]

From the above it can be seen that a considerable amount of data exist notably due to Sovran & Klomp, which enable the prediction of overall performance to be made to the limits of engineering accuracy. Such predictions are limited to "boundary-layer" types of inlet non-uniformity, and to "clean" or unobstructed diffusing passages. Considerable doubt however surrounds the precise location of the lines of first stall on the flow-regime charts for annular diffusers.

There is therefore, as concluded by Sovran & Klomp, "a need for detailed performance data which can serve as a basis for analytical studies". Such detailed data must include measurements of the boundary layer growth. This requirement has been brought into sharper focus by the recent AFOSR-IFP-Stanford 1968 Conference on Computation of Turbulent Boundary layers; where both the Evaluation Committee[34] and Coles[34] stress the urgent need for good detailed experimental data. It should be noted that in almost all of the data submitted to the conference three-dimensional effects were present, and in only one case (Stratford[35]) was the adverse pressure gradient as severe as those experienced in optimum ($\bar{C}p^*$) diffusers. The only investigation of boundary layer growth in annular diffusers (Stevens & Markland[19]) showed strong three-dimensional effects, and therefore at present no suitable data exist on which a theoretical prediction method can be assessed.

In view of the larger number of geometrical variables, and the need to investigate such effects as boundary layer suction, there is considerable stimulus for a theoretical approach to annular diffuser design. Many of the prediction methods available are capable of being applied, but in their present form are restricted by the need to assume the existence of a potential core. Moreover, the methods are all correlative and it is uncertain how well they will extrapolate beyond the range of the original data, i.e. to large adverse pressure gradients. More serious is the fact that all methods fail to predict accurately what is one of the main objects; namely the onset of stalling. The Evaluation Committee of the Stanford Conference drew no conclusions regarding the prediction of separation on the grounds that; (i) no theory presented applies there, and (ii) the data is nearly all suspect in this region. Thus at present no universally acceptable method is available to the designer.

1-7 Choice of Diffuser Geometry to be Investigated

In selecting the annular diffuser configuration to be investigated it was noted that most of the published data had been obtained on diffusers with inlet radius ratios in the range, 0.50 to 0.70, these figures being typical of most gas turbine exhaust annulus diffusers. However, an equally important application is that of the diffuser at compressor exit, and in such applications radius ratios as high as 0.94 have been used. In view of this it was decided to design for the highest possible inlet radius ratio, the value finally chosen being 0.83. This figure was decided by practical limitations outlined in Section 2. An area ratio of 2.0 was chosen as being the limiting value for most engineering applications. The selection of wall angles was influenced by the programme of research being carried out in the Department. The choice lay between a diffuser incorporating a large turning angle at inlet (see Fig. 1-4-5) and one in which the air had a relatively straight passage into the diffuser. An investigation was already in hand on the former alternative[36] and the straight entry was therefore selected. A diffuser with a constant inner diameter was chosen as a gas turbine configuration yielding data of practical utility. Since the flow turning occurred only on the outer wall, the influence of the disturbance associated with the change in outer wall angle at inlet could be investigated. In addition the flow on the inner wall would be of general interest since the flow would have a well defined history of development.

A fully annular configuration was to be used, the large radius ratio indicating a tendency towards two-dimensional conditions. It was hoped that, providing significant separation was avoided, no serious three-dimensional effects would be present.

The diffuser non-dimensional length was based on the optimum performance lines of Sovran & Klomp[7] for an area ratio of 2.0

(i) An optimum $\bar{C}p^*$ diffuser - $L/\Delta R_1 = 5.0$

(ii) An optimum $\bar{C}p^{**}$ diffuser - $L/\Delta R_1 = 7.5$

(iii) A calibration diffuser of $L/\Delta R_1 = 10.0$

1-8 Objectives and Scope of Present Investigation

The general objective of this work is to provide performance data on optimum annular diffusers having centre bodies of uniform diameter and conically diverging outer walls. Fully developed flow was chosen as the diffuser inlet condition, because it is more representative of the state of the flow in many applications than the thin boundary layer condition frequently used for diffuser research.

The specific objectives are:

(i) To measure the overall performance in terms of the pressure recovery and loss coefficient, paying particular regard to the stability of the outlet flow.

(ii) To achieve a diffusing flow free from any significant three-dimensional effects.

(iii) To measure in detail the growth of the boundary layer along the inner and outer walls; the measurements to include not only the mean velocity profiles, but the shear stress and turbulence intensity distributions.

(iv) To measure the pressure recovery, and velocity profiles in the downstream settling length.

(v) To compare the experimental data with the prediction method outlined by the author.[33]

(vi) To introduce the Coles two parameter velocity profile representation into the prediction method.

The experimental data is analysed in Section 4, and the theoretical analysis based on both the single and two-parameter velocity profiles is developed in Section 5. The results are compared with the theoretical predictions in Section 6. In view of the current interest in the turbulence structure of boundary layers the actual test observations are included in the Appendix.

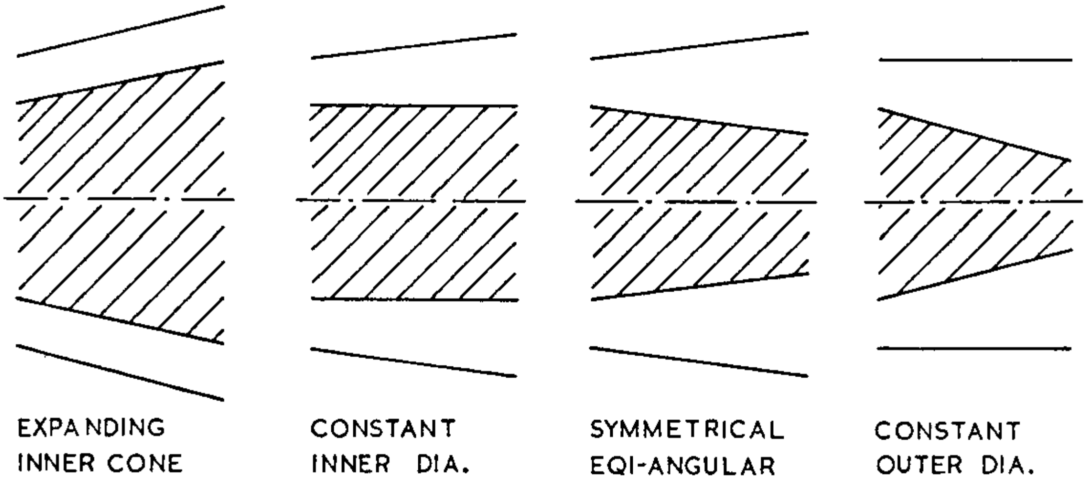

TYPES OF ANNULAR DIFFUSER

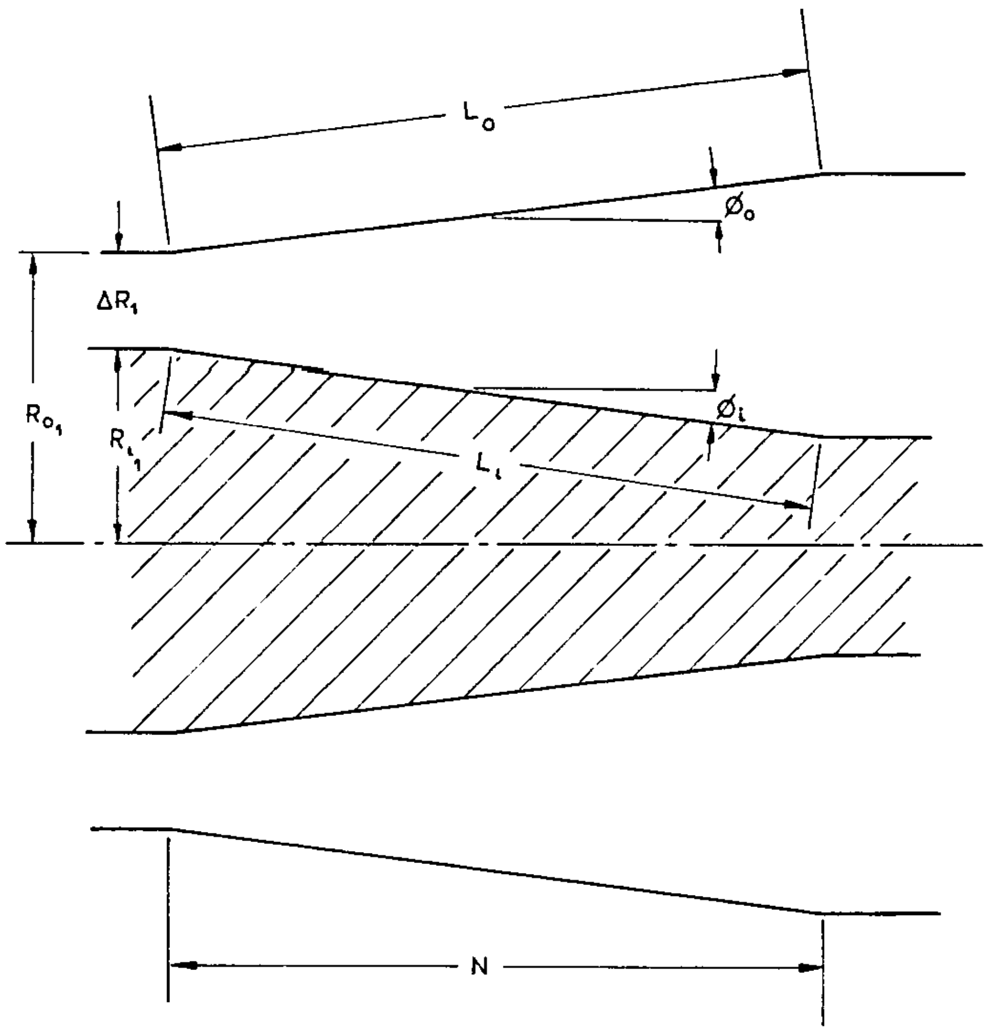

$$AR = \left[\varnothing_o, \varnothing_i, (R_i/R_o)_1, L/\Delta R_1\right]$$

FIG. 1-2-1 GEOMETRIC CHARACTERISTICS OF STRAIGHT WALLED ANNULAR DIFFUSERS

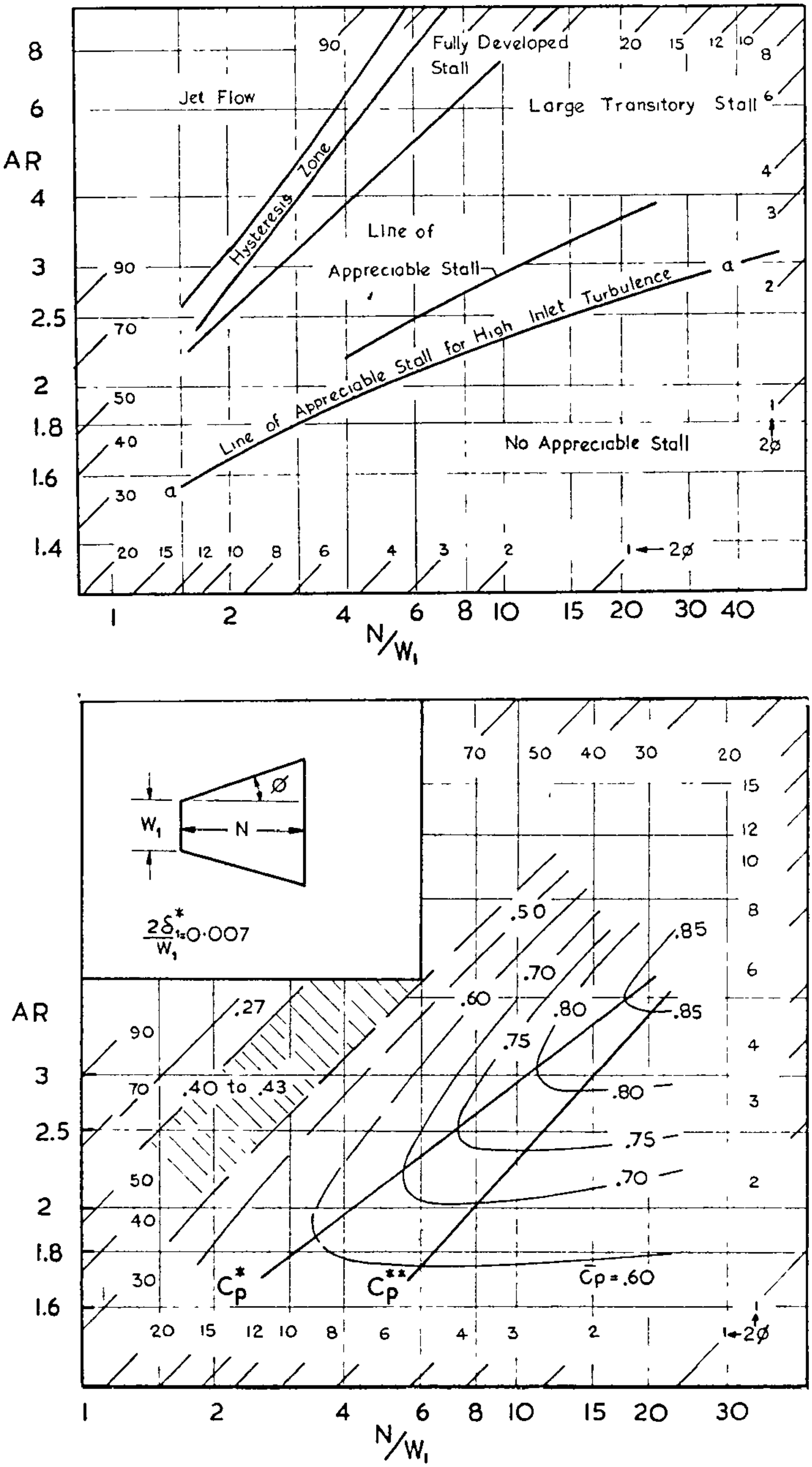

FIG. 1-4-1 PERFORMANCE AND FLOW REGIME CHARTS FOR TWO-DIMENSIONAL DIFFUSERS AFTER RENEAU ET AL. (1)

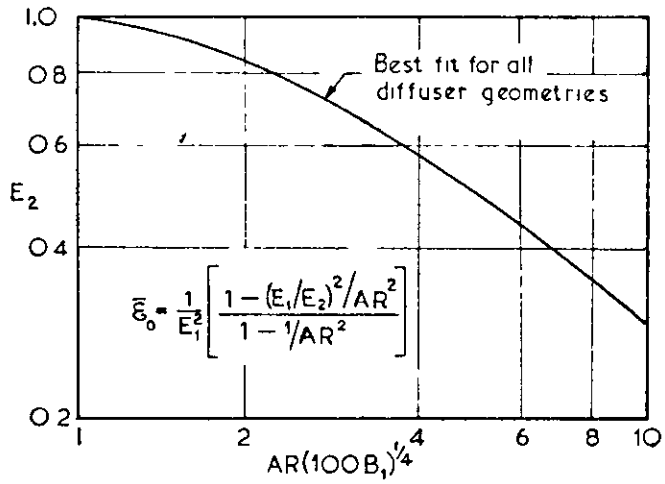

FIG.1-4-2 EFFECT OF INLET-BOUNDARY-LAYER-BLOCKAGE ON THE PERFORMANCE OF DIFFUSERS ON & NEAR C_p^* AFTER SOVRAN & KLOMP[7]

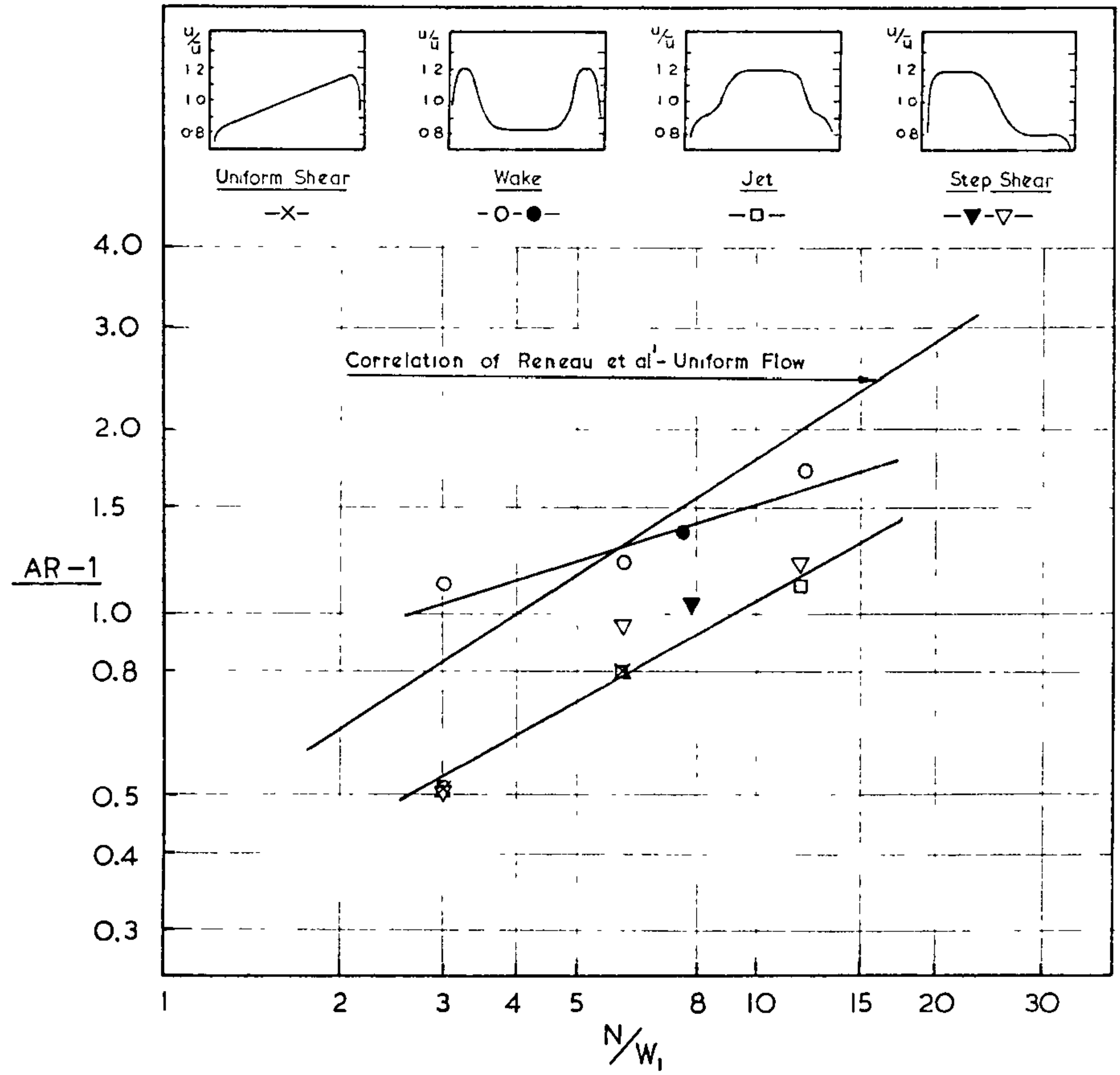

FIG. 1-4-3 INFLUENCE OF NON-UNIFORM INLET VELOCITY PROFILES ON THE OPTIMUM GEOMETRY (C_p^*) OF TWO-DIMENSIONAL DIFFUSERS AFTER WOLF & JOHNSTON (4)

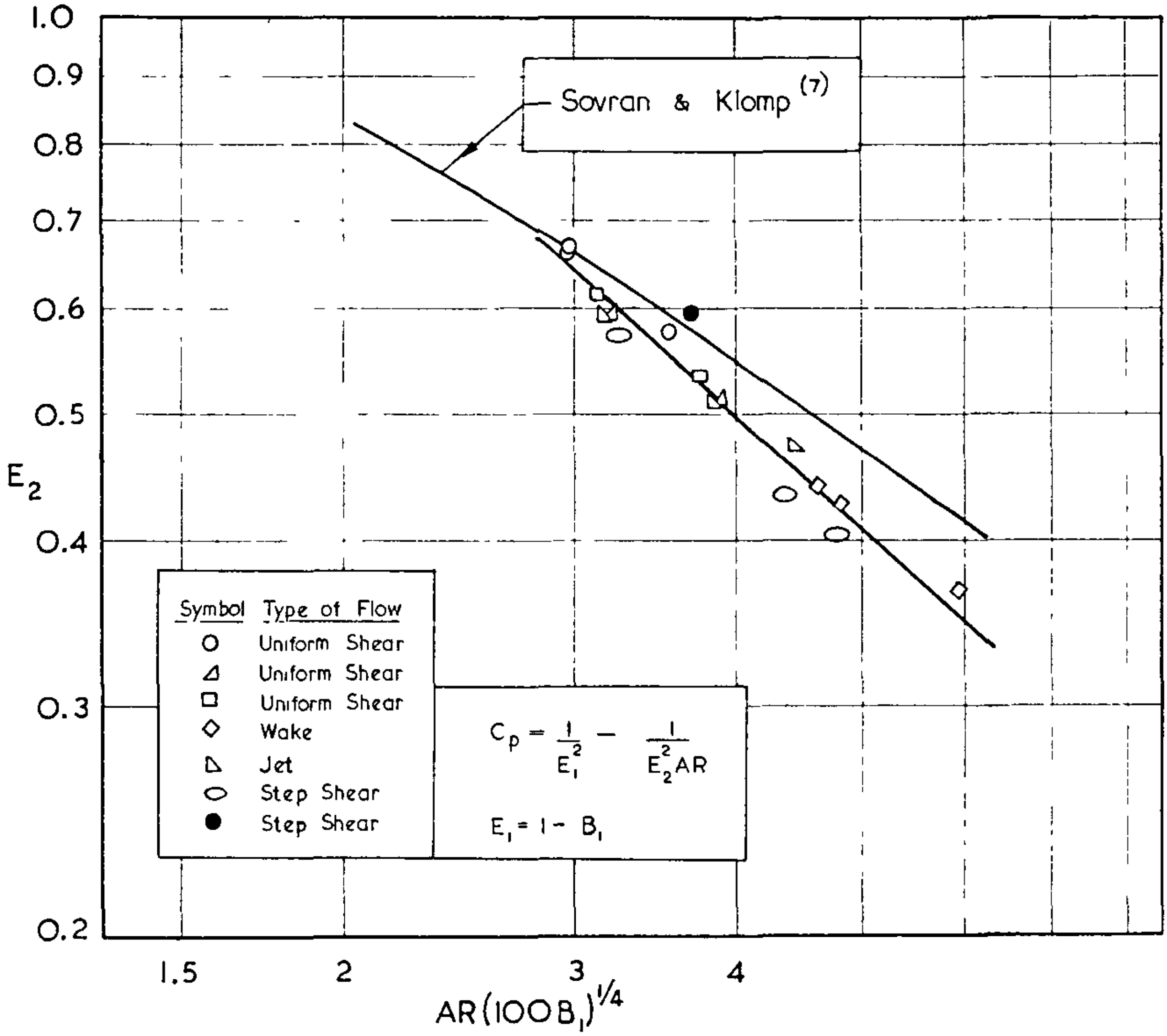

FIG. 1-4-4 EFFECT OF NON-UNIFORM INLET VELOCITY PROFILES ON THE PERFORMANCE OF TWO-DIMENSIONAL DIFFUSERS AFTER WOLF & JOHNSTON (4)

TYPE A

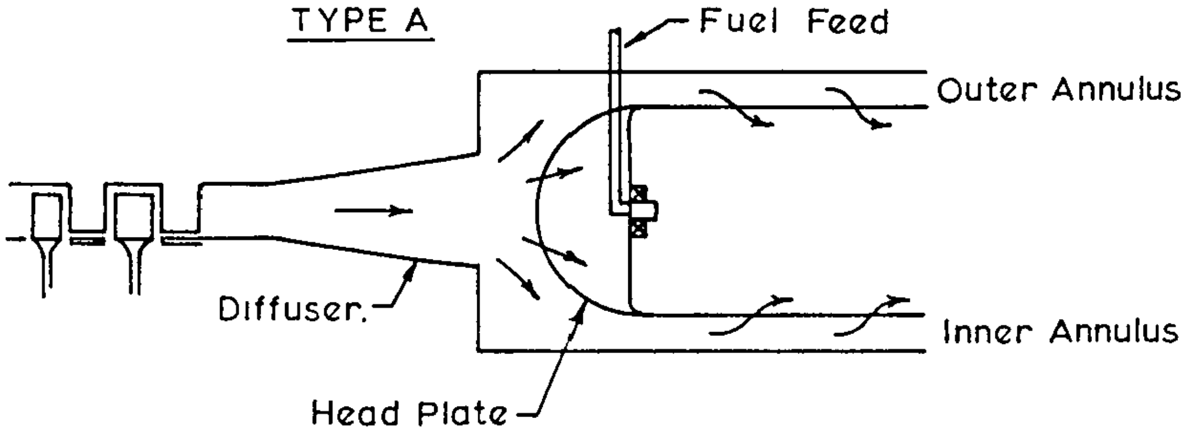

TYPE B

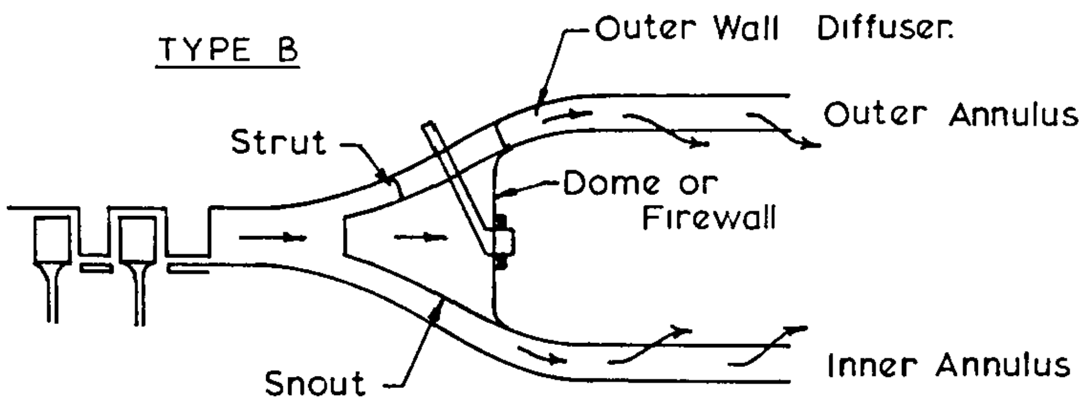

FIG 1-4-5 TYPICAL GAS TURBINE COMBUSTION CHAMBER DIFFUSERS

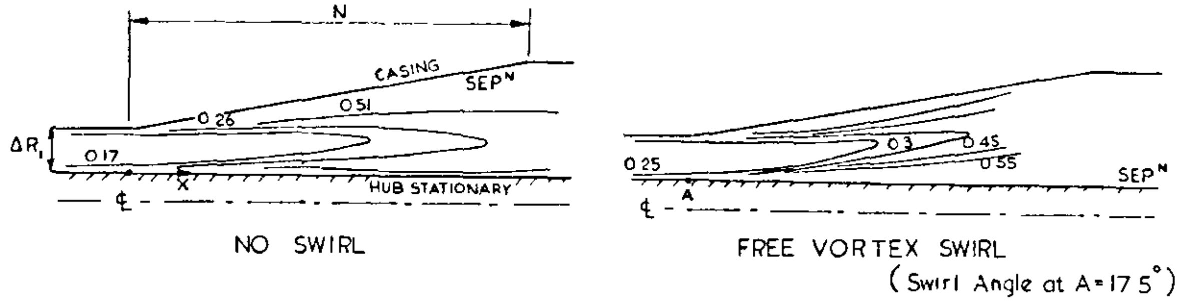

DIFFUSER GEOMETRY ~ $N/\Delta R_1 = 19\ 1$, AR = 4 57.
SEP^N Indicates SEPARATION

FIG 1-6-2 TOTAL PPESSURE CONTOURS $(P_{atm} - P_o)/(P_{ref} - P_{atm})$ IN ANNULAR DIFFUSERS DATA OF HOADLEY REPORTED BY HORLOCK (24)

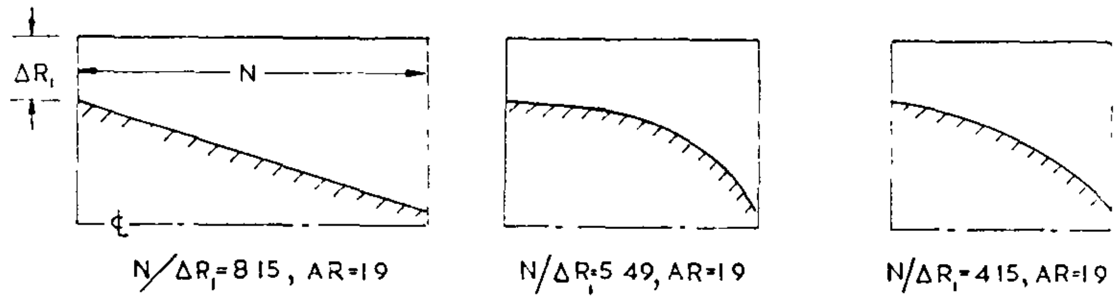

INLET CONDITIONS

$M_1 = 0.4$, $Re_D = 1\ 28 \times 10^6$, $H_o = 1\ 11$, $\delta_o^* = 0.122$ ins

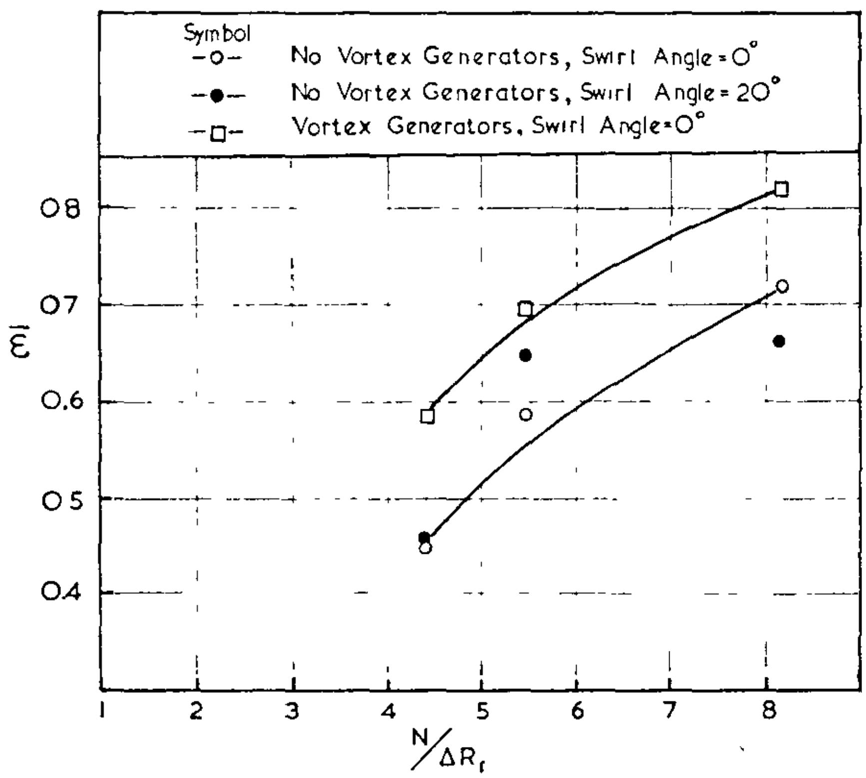

FIG. 1-6-1 ANNULAR DIFFUSER PERFORMANCE AFTER WOOD AND HIGGINBOTHAM (22)

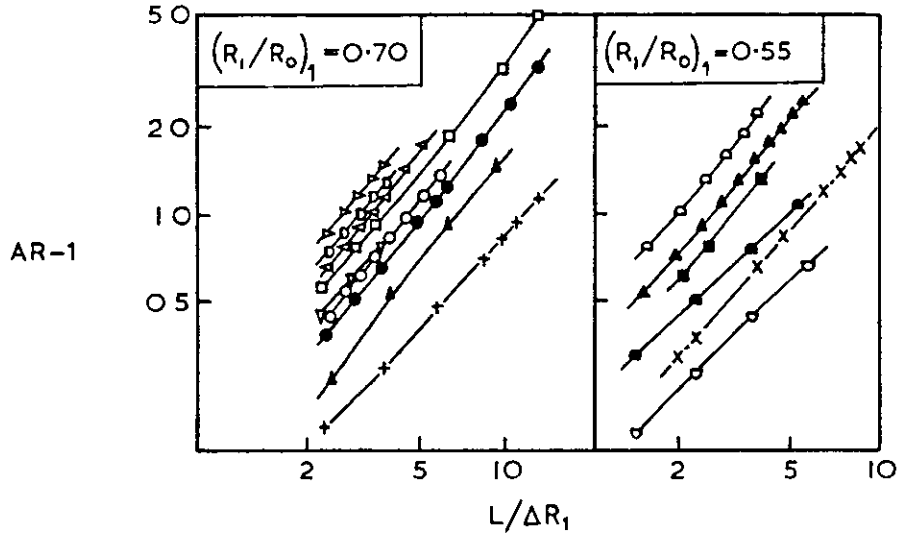

ANNULAR DIFFUSER GEOMETRIES TESTED

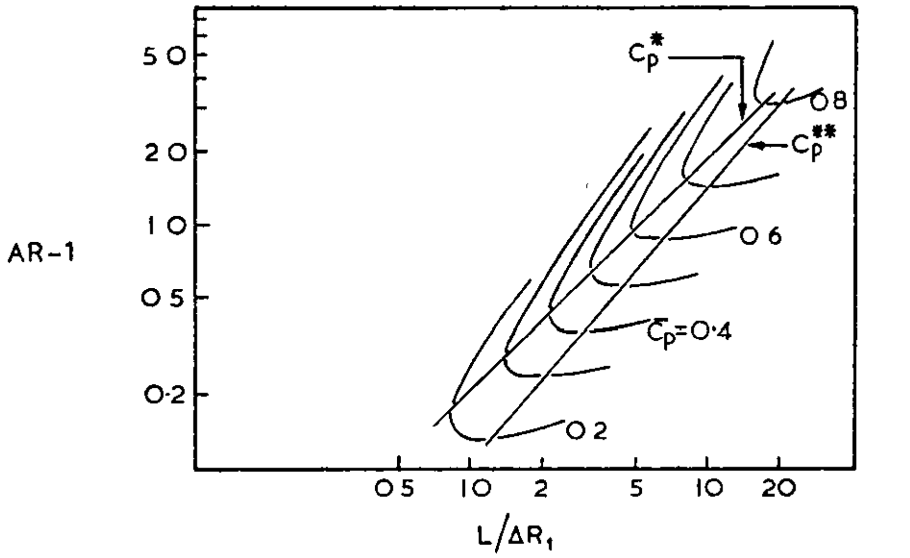

ANNULAR DIFFUSER PERFORMANCE CHART $B_1 \cong 0.02$

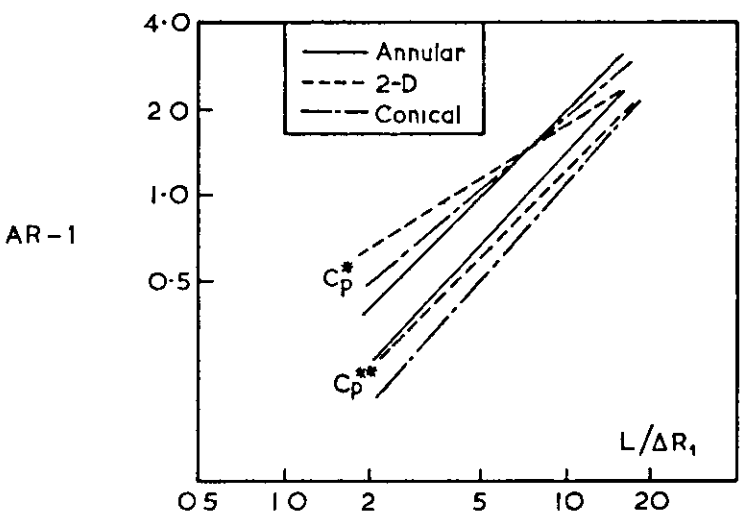

OPTIMUM LINES

FIG. 1-6-3 ANNULAR DIFFUSER PERFORMANCE AFTER SOVRAN & KLOMP (7)

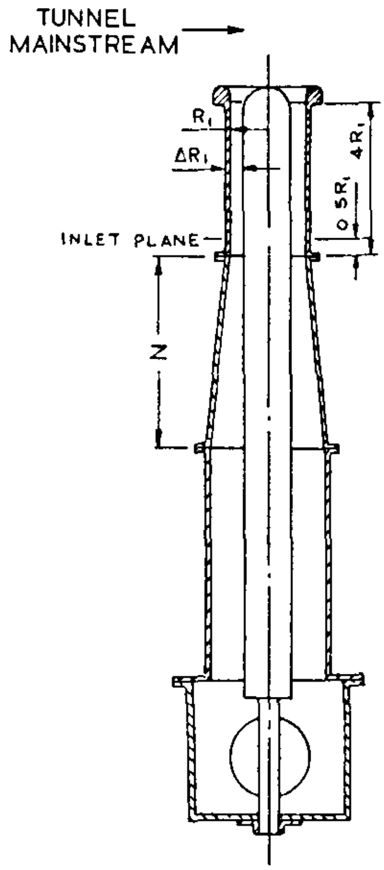

DIFFUSER ASSEMBLY

$N/\Delta R_1$	AR	R_i/R_o
6.5	2.25	0.47
12.0	3.25	0.47

DIFFUSER GEOMETRY

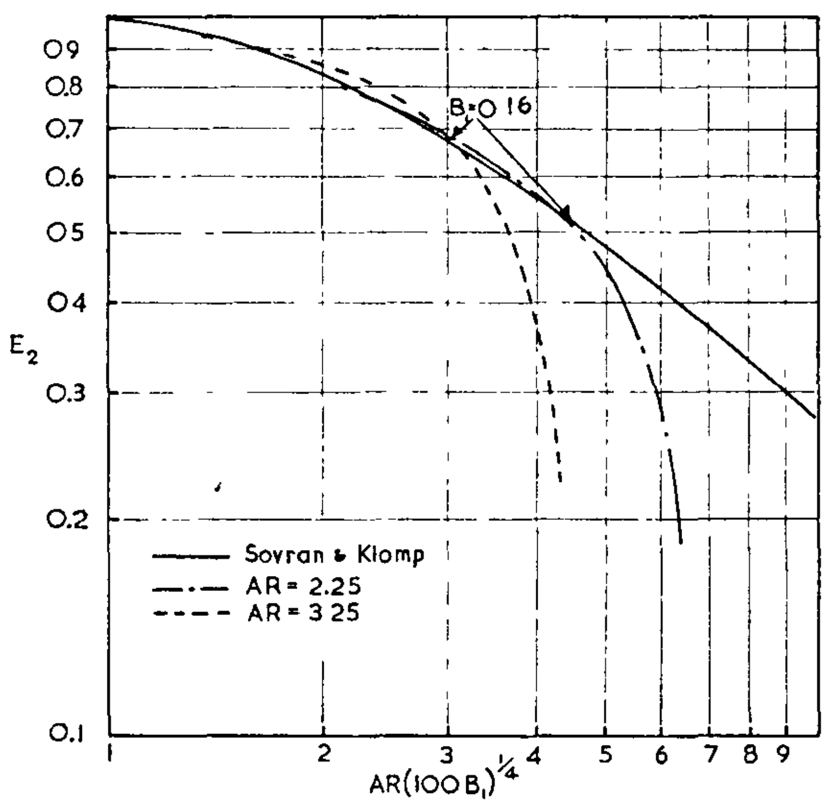

FIG. 1-6-4 DIFFUSER PERFORMANCE WITH DISTORTED INFLOW -TYLER AND WILLIAMSON (10)

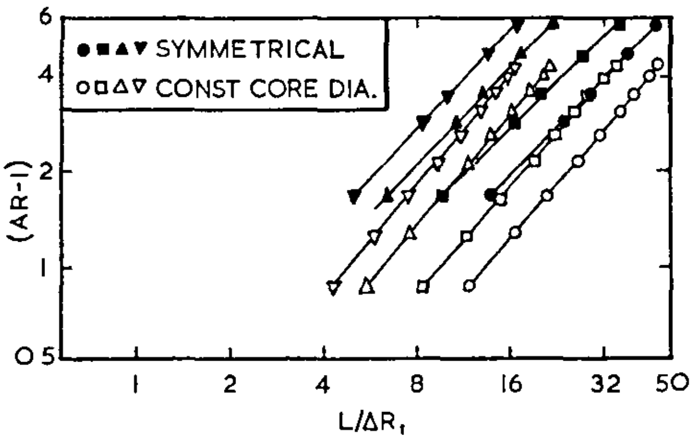

ANNULAR DIFFUSER GEOMETRIES TESTED

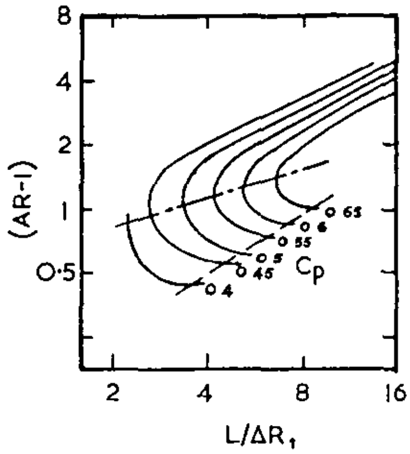

PRESSURE RECOVERY FOR SYMMETRICAL DIFFUSERS

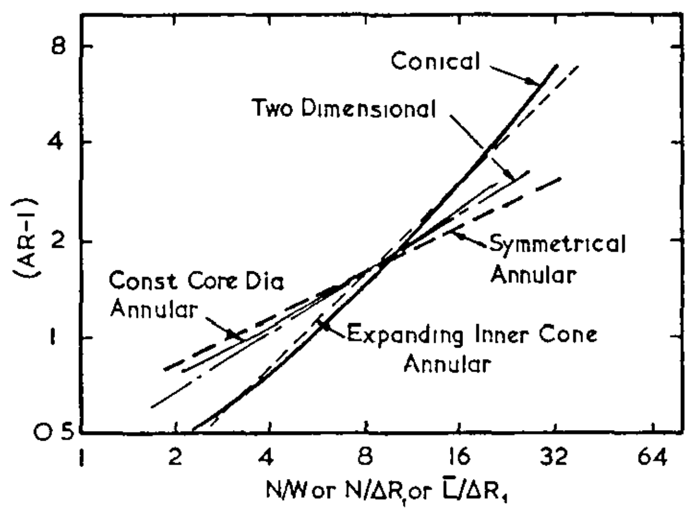

AREA RATIO FOR OPTIMUM PERFORMANCE AT CONSTANT NON DIMENSIONAL LENGTH

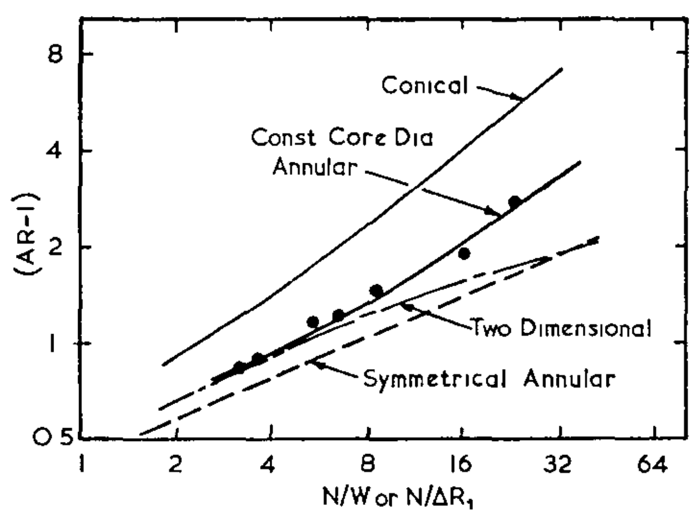

LINES OF FIRST STALL.

FIG. 1-6-5. ANNULAR DIFFUSER PERFORMANCE AFTER HOWARD HENSELER & THORNTON-TRUMP (26).

$\Phi_o = -\Phi_i$ (degrees)	2·5	5 0
AR	4 0	4 0
R_{i_1} (in)	2·25	2 25
R_{o_1} (in)	3 75	3 75
$D_{h_1} = 2\Delta R_1$ (in)	3·0	3 0
$L/\Delta R_1$	34 4	17 2
$N/\Delta R_1$	34 4	17 1

DIFFUSER GEOMETRIES

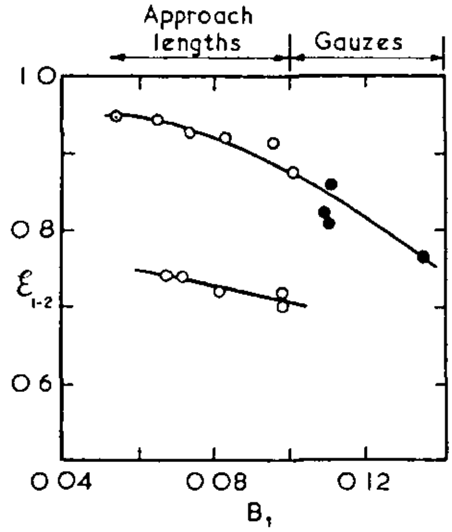

VARIATION OF EFFECTIVENESS WITH BLOCKAGE FRACTION.

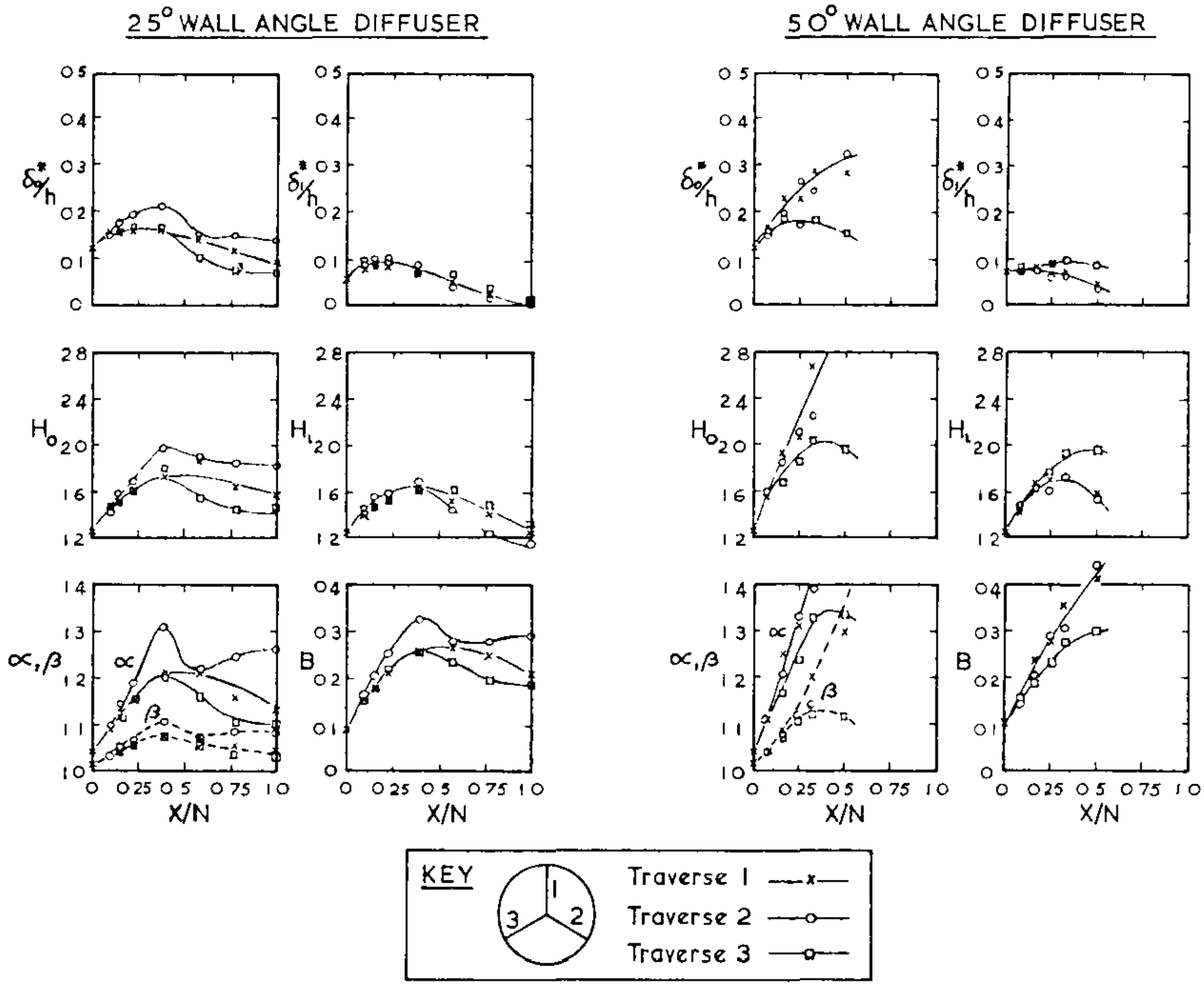

VARIATION OF BOUNDARY LAYER PARAMETERS ALONG DIFFUSERS WITH FULLY DEVELOPED FLOW AT INLET.

FIG 1-6-6 ANNULAR DIFFUSER PERFORMANCE AFTER STEVENS & MARKLAND (19).

SECTION 2

EXPERIMENTAL FACILITY

2 -1 Design of Apparatus

As stated in Section 1, diffusers which have centre bodies of uniform diameter are to be investigated, having fully developed flow at inlet. It was decided that the inlet conditions would be achieved by natural development in a long annular entry length. This method was chosen, rather than artificial thickening, due to uncertainties regarding the turbulence structure of such layers. A suction layout was chosen in order that the inlet boundary layer would have a well defined upstream history, although such a layout produced a rather inflexible rig. The dimensions of the rig were determined by the following considerations:-

i) Space available

ii) The need to achieve an inlet Reynolds No. $> 1 \times 10^5$.

iii) To test at an inlet velocity consistent with a measurable outlet dynamic pressure

iv) Adequate annulus height at inlet for boundary layer traverses.

v) Diffuser Geometry: Area Ratio 2.0 : 1, Max. $L/\Delta R_1 = 10.0$.

vi) To design for a high inlet radius ratio (R_i/R_o)

Bearing in mind the considerations listed above, it was decided to design for the largest practical inlet diameter. Tubing to a very high standard of accuracy (typically 10.0 $^{+0.005}_{-0.000}$ ins. O.D. over a length of 30 ins) was required, since experience with an earlier rig [27] had shown that minor eccentricity of the annulus core had a marked effect on the circumferential uniformity of the mean velocity profile. No commercial tubing to such close tolerances was available, and therefore the manufacture had to be carried out within the department. Machining capacity limited the maximum tube diameter to 13.75 ins. and the following dimensions were therefore chosen:

Outer wall diameter at inlet - 12.0 ins.

Inner wall diameter at inlet - 10.0 ins.

Outer wall diameter at outlet - 13.75 ins.

Inlet radius ratio - 0.833

Inlet annulus height - 1.0 ins.

The "design" operating conditions were:

Mean inlet velocity - 120 ft./sec.

Mean outlet dynamic pressure - 0.82 ins. water gauge

Inlet Reynolds No. $\left(\frac{\overline{u}\,(D_o - D_i)}{\nu}\right)$ — 1.28×10^5.

It was necessary to check the overall length of the rig, assuming a diffuser having $L/\Delta R_1 = 10.0$

<u>Estimated Length of Rig</u>

Entry Flare	1 ft. 6 ins.
Entry Length (assuming a length equal to $50\,(D_o - D_1)_1$ to achieve fully developed flow)	8 ft. 4 ins.
Diffuser	0 10 ins.
Settling length (based on a length equal to $8\,(D_o - D_i)_2$)	2 ft. 6 ins.
Total length	13 ft. 2 ins.

One of the main problems associated with the design of an earlier rig [27] was the large number of struts required to centralise the inner tube in the entry length. In view of the uncertainties regarding the influence of wakes from support struts on the subsequent growth of the boundary layer in the diffuser it was decided to mount the rig vertically (see Fig. 2-1-2). The advantage of this arrangement was that as all the inner tubes were spigotted together they could be positioned simply by three struts in the entry flare, the weight of the tubes being supported by two rods at the end of the settling length (see Fig. 2-1-1). In this way the influence of entry length supports was reduced to a minimum. The rig was mounted on a plenum chamber (6 ft. x 2 ft. x 3 ft.), and the clearance between the entry flare and the roof of the laboratory was 4 ft.

A suitable fan with a volume flow of 1800 ft.^{3}/min. at a pressure rise of approximately 4 ins. water gauge was selected; the drive was provided by an electric motor with a resistive speed control. In order to facilitate flow visualisation studies the tubing and diffusers were constructed in $\frac{3}{8}$ ins. clear perspex sheet. The tubes were manufactured by shrinking a heated perspex sheet, which had been joined with Tensol No. 3 cement, onto an accurately machined former. Using this technique a tube could be constructed to an accuracy of 0.003 ins. on a diameter of 12.0 ins. and this tolerance maintained over a length of 30 ins. The entry length comprised of three tube assemblies, each 30 ins. long, spigotted together to produce surfaces which mated accurately.

A flared intake and nose bullet followed by a 10 ins.

length of tubing, made up the inlet section. The design of the intake flare was based on a standard I.S.A. nozzle. Transition on the flare and nose bullet was stabilised by trip wires. Assuming that the Reynolds number based on wire diameter must exceed 600 to achieve transition[37] wires of 0.020 ins. diameter were attached to the surfaces of the tubes downstream of the throat. To avoid any problems associated with deposition of dirt on hot wire probes and small bore pitot tubes a fine mesh cloth filter was fitted around the intake flare.

The settling length comprised of perspex tubing 30 ins. long, at the end of which a Dufaylite honeycomb was fitted to ensure that no swirl was induced in the flow by prerotation at fan inlet. To prevent fan vibrations from reaching the test section a flexible hose was used to connect the inlet of the fan to the plenum chamber.

2 -2 Diffuser Geometry

The particulars of the diffusers tested are tabulated below

Do_1 (ins.)	12.0	12.0	12.0
Di_1 (ins.)	10.0	10.0	10.0
ϕ o (degrees)	5.0	6.62	10.0
ϕ i (degrees)	0	0	0
Area Ratio	2.0	2.0	2.0
$L/\Delta R_1$	10.01	7.514	5.018
$N/\Delta R_1$	10.0	7.5	5.0
$(Ri/Ro)_1$	0.833	0.833	0.833

In view of the small differences between $L/\Delta R_1$ and $N/\Delta R_1$, the values of $L/\Delta R_1$ will be quoted as 10.0, 7.5, and 5.0 respectively throughout this thesis.

2-3 Instrumentation

2-3-1 Pressure Measurements

The following wall static pressure measurements were taken:-

i) Throat of entry flare (3 off)

ii) Upstream of diffuser inlet on inner and outer walls (18 off)

iii) Along the length of the diffuser on inner and outer walls (6 off at each station)

iv) Diffuser exit (6 off)

v) Downstream settling length on inner and outer walls of stations 3.75 ins apart (6 off at each station)

All static pressure holes were 0.031 ins. diameter, and at each station three tappings were made, equally spaced round the circumference of the inner and outer walls. The axial location of the stations is shown in Fig. 2-3-1

Total pressure traverses were made along three equally spaced radii at a station 3 ins. upstream of diffuser inlet, and at various stations along the length of the diffuser and downstream settling length (see Fig. 2-3-2). The end section of the total head tube was flattened to a rectangular shape 0.040 x 0.015 ins. Separate probes were used for inner and outer wall traverses, each being bent slightly, to ensure that only the tip of the probe was in contact with the surface of the tube. The traverses were carried out normal to the walls of the tubes using micrometers (see Fig. 2-3-3) which, after removing any backlash, could be set to an accuracy of 0.0005 ins. When the traverse holes were not in use they were plugged with screwed inserts. All pressures were recorded on Betz projection manometers.

2-3-2 Hot-Wire Measurements

Turbulence measurements were carried out using a D.I.S.A. 55A01 constant temperature anemometer. The D.C. component of the output was monitored on a Weir D.V.M. Type 500. D.I.S.A. probe elements Type 55A53 and 55A54 were used, the wires were of platinum-plated tungsten 5 microns diameter, 0.45 m.m. long (see Fig. 2-3-4). No suitable commercial X-probe was available for making shear stress measurements, and therefore a single 45° slant wire was used. The technique used was to present the wire at an angle of 45° to the mean direction of flow, and then to turn the wire through an angle of 180° as indicated below

This technique is the same as that employed by Goldberg[29] and Lee[63]. In order to facilitate the re-orientation of the wire the probe element was mounted in a square sectioned carrier, and fitted into the traverse gear. With the square sectioned carrier the wires could be placed in four positions relative to the flow viz. the u'-v', and u'w' planes. The carrier and probe element are shown in Fig. 2-3-4, and a cross-sectional view is given overleaf:

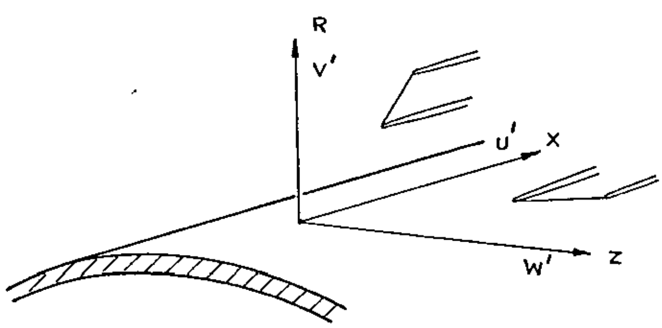

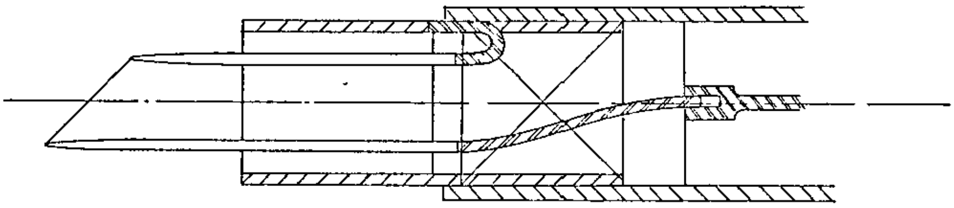

CROSS SECTIONAL VIEW OF PROBE AND CARRIER

A single straight wire probe (Type 55A53)was used to determine the longitudinal component of the turbulent fluctuations.

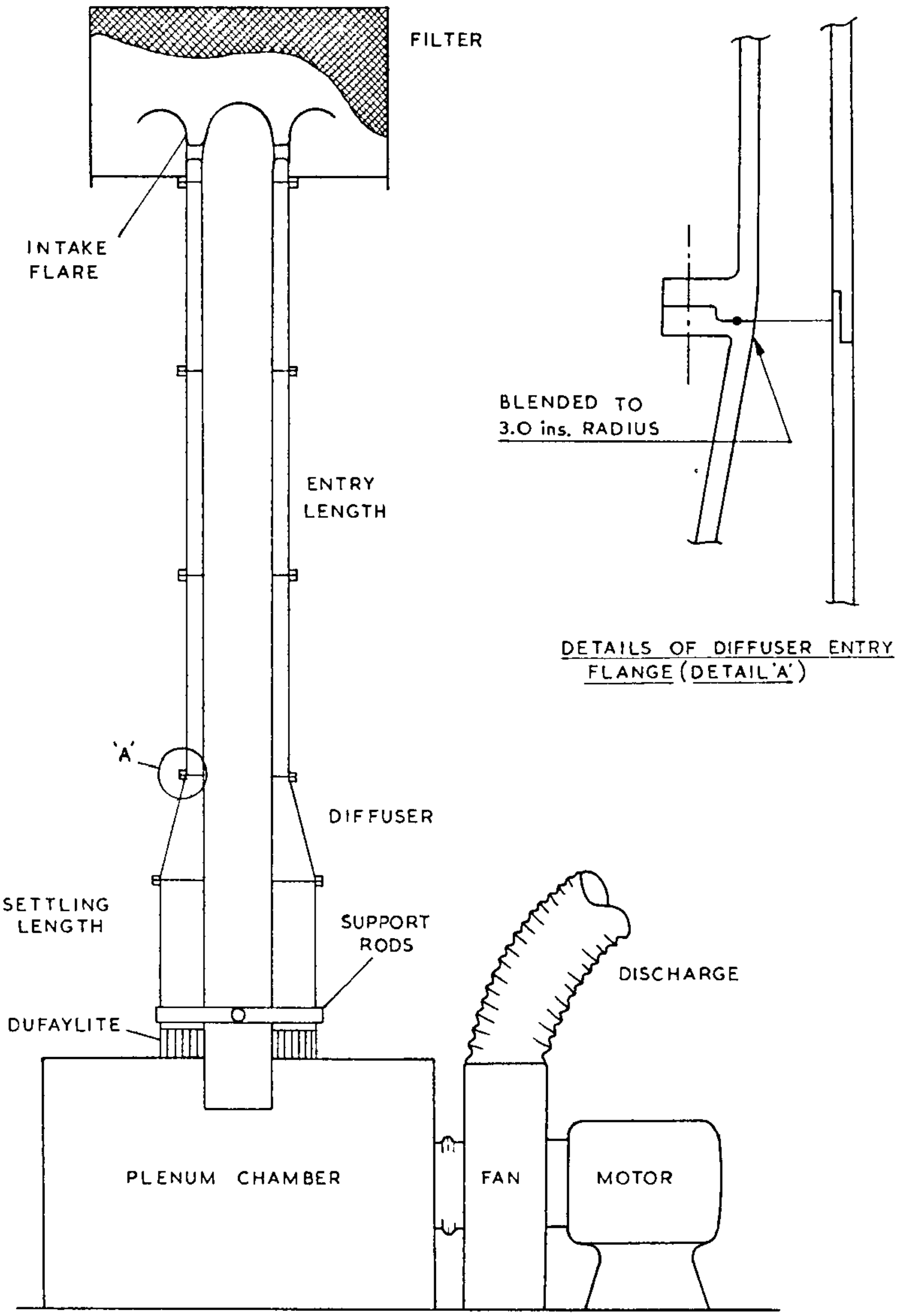

FIG. 2-1-1 LAYOUT OF APPARATUS

FIGURE 2 - 1 - 2 ANNULAR DIFFUSER TEST RIG

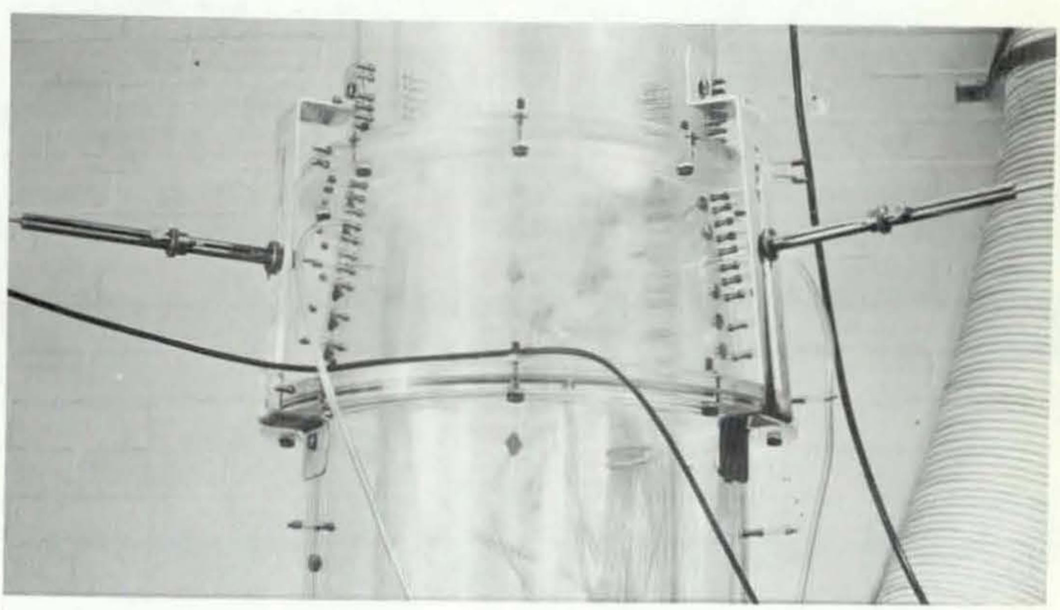

FIGURE 2 - 3 - 2 TEST DIFFUSER

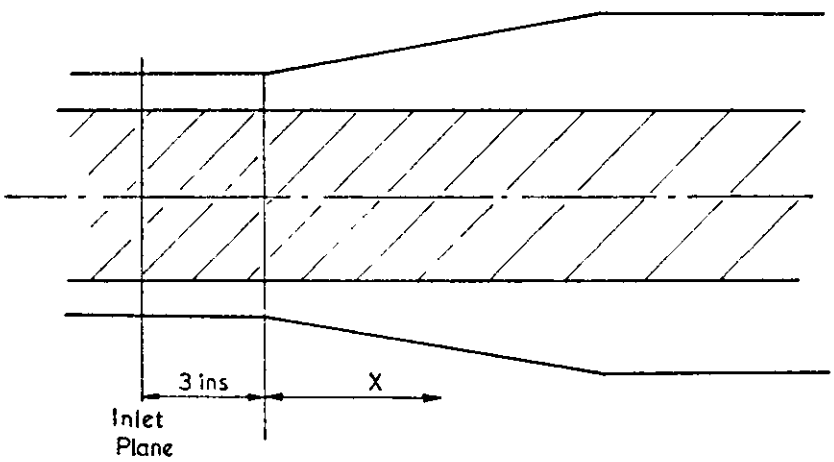

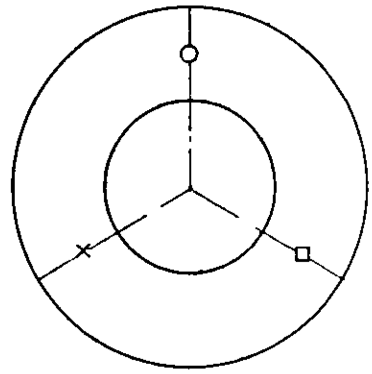

RADIAL LOCATION OF TRAVERSES

DIFFUSER											
$L/\Delta R_1 = 5.0$				$L/\Delta R_1 = 7.5$				$L/\Delta R_1 = 10.0$			
X ins	X/L	Velocity Traverses	Turbulence Traverses	X ins	X/L	Velocity Traverses	Turbulence Traverses	X ins	X/L	Velocity Traverses	Turbulence Traverses
-30		✓	✓	-3.0		✓	✓	-3.0		✓	✓
0.30	.06	✓	✓	0.30	.04	✓		0.30	.03	✓	
0.75	.15	✓	✓	0.75	.10	✓		0.75	.075	✓	
1.35	.27	✓	✓	1.25	.167	✓	✓	1.00	.10	✓	✓
1 95	.39	✓	✓	1.70	.226	✓		1.45	.145	✓	
2.55	.51	✓	✓	2.20	.293	✓	✓	2.15	.215	✓	
3.15	.63	✓	✓	2.65	.354	✓		2.25	.225	✓	✓
3.75	.75	✓	✓	3.15	.42	✓	✓	2.70	.27	✓	
4.28	.856	✓		3.60	.48	✓		3.25	.325	✓	✓
4.85	.97	✓	✓	4.10	.546	✓	✓	3.70	.37	✓	
				5.05	.674	✓	✓	4.25	.425	✓	✓
				6.00	.80	✓	✓	4.70	.47	✓	
				7.35	.98	✓	✓	5.45	.545	✓	✓
								5.90	.59	✓	
								7.25	.725	✓	✓
								7.70	.77	✓	
								9.85	.985	✓	✓
8.75	1.75	✓	✓	11.25	1.50	✓	✓	13.75	1.37	✓	✓
17.5	2.5	✓	✓	15.0	2.0	✓	✓	17.5	1.75	✓	✓
16.25	3.25	✓	✓	18.75	2.50	✓	✓	21.25	2.13	✓	✓

LOCATION OF INSTRUMENTATION

FIG. 2-3-1

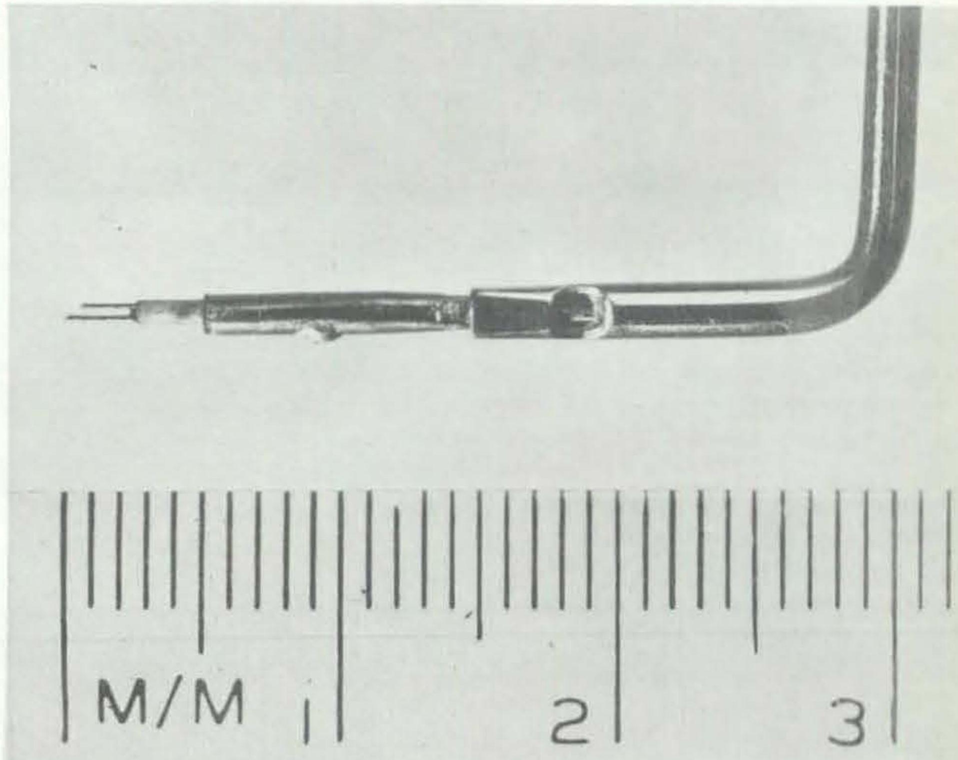

FIGURE 2 - 3 - 4 HOT- WIRE PROBE

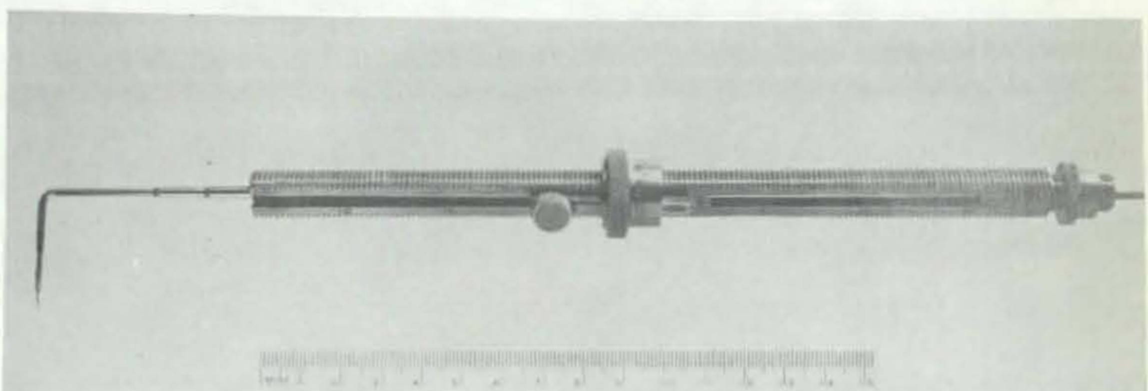

FIGURE 2 - 3 - 3 TRAVERSE GEAR

SECTION 3

EXPERIMENTAL WORK

3-1 Scope of Experimental Work

Low speed tests were carried out on three annular diffusers having centre bodies of uniform diameter and conically diverging outer walls. The diffusers had a common area ratio of 2.0:1 and non-dimensional lengths ($^L/\Delta R_1$) of 5.0, 7.5, and 10.0 respectively. The tests, using air as the working fluid, were carried out with a fully developed inlet velocity profile having a maximum velocity of approximately 140 ft./sec. The inlet Reynolds No. was 1.30 x 10^5.

To enable the overall performance and boundary layer growth to be determined, the static pressures and mean velocity profiles were measured at, on average, 16 stations along the length of each diffuser and the downstream settling length. At a number of stations measurements were taken of the distribution of Reynolds shear stresses ($\overline{u'v'}$ & $\overline{u'w'}$) and the longitudinal, radial, and transverse components of the turbulent velocity fluctuations.

3-2 Experimental Technique

For most of the tests the speed of the fan was adjusted to give approximately the same differential head across the entry flare, in this way inlet conditions were maintained as near constant as possible. The fan was then run for 20 mins. to allow conditions to settle. The test programme was split into two phases, one concerned with the overall performance, the other with the internal performance.

3-2-1 Overall Performance

In these tests all the static pressures were recorded relative to a reference static pressure measured on the outer wall 3.0 ins. upstream of the diffuser inlet. No instability of pressure was noted.

3-2-2 Internal Performance

Mean Velocity Profiles

Total head traverses were carried out along three equally spaced radii at the stations shown in Fig. 2-3-1. The velocity was calculated from the measured difference between the total and wall static pressures on the assumption that the static pressure along each radial traverse, was the same as that measured at the wall. At each station all three total head probes were traversed at the same time; the technique adopted was to traverse in from the outer wall for some distance past the point of maximum velocity, and then with the rig still running to change probes and static pressure connections; and traverse from the inner wall. When the probes were in contact with the wall, the micrometer was set at a distance corresponding to the effective displacement of the centre of the probe. Using the correction due to Young and Maas[38] the centre of the probe was assumed to be 0.015 ins. from the wall.

Turbulence Measurements

Most of the measurements were carried out at one radial location, although at inlet, exit, and one or two stations in the diffuser, measurements were taken along all three radii.

Inner and outer wall traverses were again carried out separately. Five traverses were made from each wall as detailed below:

i) straight wire probe — u'-v' plane.

ii) slant wire probe – u'-v' plane.

iii) slant wire probe turned through 180° – u'-v' plane.

iv) slant wire probe – u'-w' plane

v) slant wire probe turned through 180° — u'-w' plane

(For further details see Appendix 11)

Considerable care was taken to ensure that the probes were correctly aligned to the flow, and accurately positioned from the wall. Also the hot-wires were examined at frequent intervals under a microscope, to check for contamination with dirt, and cleaned when necessary with Kistler contact cleaner (Freon 1001). For further information on the precautions taken to avoid "drift" due to dirt see Appendix 13.

3-3 Computational Methods and Reduction of Results

3-3-1 Mean Velocity Profiles

A detailed analysis of a typical set of experimental data is given in Appendix 1. The values of non-dimensional velocity ($^u/U$) were calculated by hand, and plotted graphically at each station. A mean line was drawn through the data, and values taken from the mean line were tabulated at appropriate intervals. The tabulated data was punched on I.C.T. cards, and an I.C.T. 1905 Digital Computer was used to reduce the data further. The computer programme used to process the inner and outer wall velocity profiles is detailed in Appendix 2.

Using this programme values of displacement thickness, momentum thickness, energy thickness, shape parameter, and energy shape parameter, were calculated for two-dimensional definitions, and axi-symmetric definitions based on local radius and annulus height. Values of the ratio of mean to maximum velocity, momentum coefficient, energy coefficient, volume flow, and the percentage flow entrained in the outer wall layer, were also calculated.

3-3-2 Turbulence Structure

The reduction of a typical set of turbulence measurements is illustrated in Appendix 11. Values of the R.M.S. voltage were plotted against distance from the wall, and the square of the bridge D.C. volts was plotted against the square root of the local velocity ratio ($^u/U$). Mean lines were drawn through the data, and tabulated values fed to a computer programme (see Appendix 12). This programme was used to compute values of,

$$\frac{\sqrt{\overline{u'^2}}}{U}, \frac{\sqrt{\overline{v'^2}}}{U}, \frac{\sqrt{\overline{w'^2}}}{U}, \frac{1}{2U^2}\left(\overline{u'^2}+\overline{v'^2}+\overline{w'^2}\right), \; \frac{2\,\overline{u'v'}}{U^2}, \; \& \; \frac{2\,\overline{u'w'}}{U^2}.$$

After the turbulence measurements had been processed, a further programme (Appendix 18) was used to calculate the Reynolds normal stress, dissipation coefficient, mixing length, and eddy viscosity at a specified number of points across the layer. The analysis of a typical set of data is detailed in Appendix 17.

3-4 Estimated Experimental Accuracy

Pressure measurements were taken throughout using Betz manometers which could be read to an accuracy of 0.01 ins. water-gauge. Therefore the error in non-dimensional velocity ($^u/U$) near the wall at inlet should be approximately $\pm$ 1%

rising to $\pm$ 2% at exit. However, whilst a correction was made for the effective displacement of the probe, positioning errors could increase the values quoted to $\pm$ 2% near the wall at inlet. No corrections were made for the effects of turbulence, or streamline curvature. In general the degree of scatter is within the limits of experimental error, and the accuracies quoted are confirmed by the fact that the volume flows obtained by integrating the mean velocity profiles, agree to within $^{+2.0}_{-1.5}$ % of the inlet value. (see Appendices 4/6/8). This is considerably better than the accuracy achieved in earlier diffuser investigations, where the volume flow at exit is, typically, 5 - 10% higher than the measured inlet value.(15)

The values of static pressure rise coefficient are considered to be within $\pm$ 3%. The loss coefficient was not measured directly but calculated as the difference between the ideal and measured values of pressure rise coefficient, and therefore suffered in accuracy due to the fact that a small difference was calculated from two relatively large quantities. The error could be as high as $\pm$ 20%, nevertheless the loss coefficient is small, typically, 0.06.

The accuracy of the turbulence measurements is considerably more difficult to quantify, due to such problems as drift, orientation of the hot-wires, high turbulence levels, and large vertical components of velocity as the flow approaches separation. The significance of these effects is discussed in Appendix 13, and the following accuracies are suggested:

Early stages of diffusion	5% in	$\sqrt{\overline{u'^2}}/U$
	10-15% in	$2\,\overline{u'v'}/U^2$

Latter stages of diffusion 20% in $\sqrt{\overline{u'^2}}/U$

20-40% in $2\,\overline{u'v'}/U^2$

However, in the outer regions of the layers further errors in $\overline{u'v'}$ may be incurred due to misalignment of the slant wire probes.

The accuracy of the boundary layer parameters, is approximately $\pm$ 3% near diffuser inlet and $\pm$ 4% at exit.

3-5 Calibration Tests

Initial calibration tests were carried out on the $^L/\Delta R_1$ = 10 diffuser, since the flow in this diffuser was expected to be free from transitory stalling.

3-5-1 Symmetry of Flow

Initially flow visualisation checks were carried out using wool tufts. At no point in the test diffuser or the downstream settling length could any swirl be detected. Next, the circumferential static pressure variation at each station was investigated, and, within experimental error, no variation could be detected. Finally, the velocity profiles at diffuser inlet and exit were measured; excellent symmetry of flow was observed, and the integrated volume flows at the two stations were within 1½%. Therefore no evidence of any three-dimensional flow could be detected.

3-5-2 Calibration of Intake Flare

It was originally proposed to fit an I.S.A. nozzle in the fan discharge, but in view of the excellent symmetry of flow it was decided that the mass flows calculated at diffuser inlet could be taken as the "correct" values. Tests carried out over a range of fan speeds indicated a mean discharge coefficient of

0.97 for the intake flare, a value of 0.975 has been obtained for a flare of similar design.[27]

3-5-3 <u>Influence of Intake Filter</u>

Measurements were carried out a station 3 ins. upstream of diffuser inlet with and without the filter around the intake flare. Within the limits of experimental error no difference could be detected in either the velocity profile or the shear stress distribution.

3-5-4 <u>Influence of Diffuser Inlet Bend</u>

The diffuser inlet static pressure is usually measured some distance upstream of the entry plane, because curvature of the flow produces a local reduction of pressure on the surface near the entry. At a later stage in the test programme, a survey of the static pressure distribution was made along the walls just upstream of the entry to the $^{L}/\Delta R_1 = 5$ diffuser. The results are shown in Fig. 3-5-1 ; also included are the results for the other two diffusers. The quoted diffuser inlet conditions are based on traverses carried out at a plane 3 ins. upstream of the entry, which is shown to be unaffected by the local curvature of the flow.

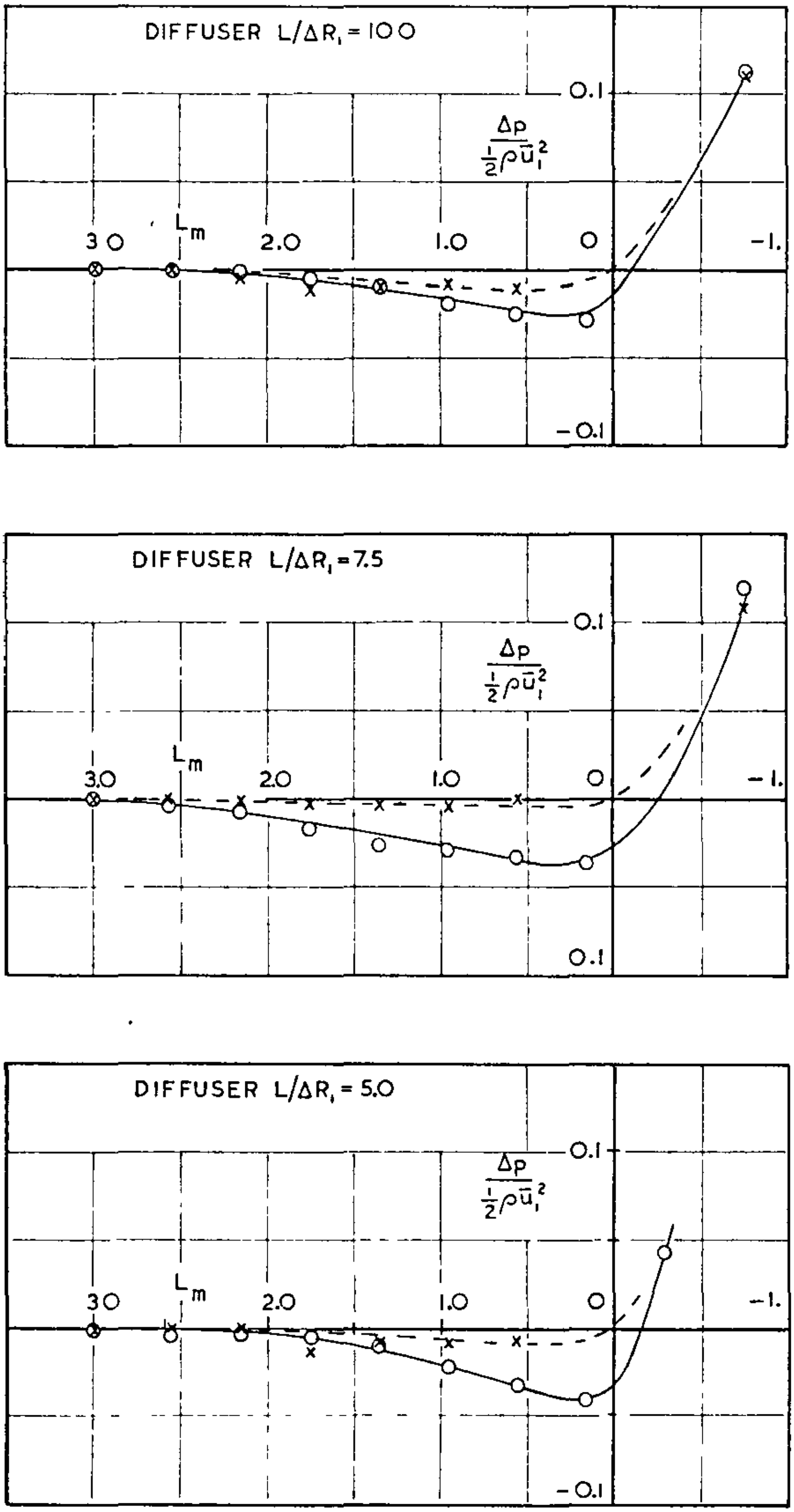

Δp DENOTES THE REDUCTION IN STATIC PRESSURE RELATIVE TO PRESSURE IN ENTRY LENGTH AT DISTANCE 3 ins UPSTREAM OF DIFFUSER INLET (X=O)

L_m DISTANCE OF STATIC PPESSURE TAPPING UPSTREAM OF DIFFUSER INLET - ins

FIG. 3-5-1 REDUCTION OF STATIC PRESSURE ON WALLS JUST UPSTREAM OF DIFFUSER INLET

SECTION 4

RESULTS AND DISCUSSION OF EXPERIMENTAL WORK

4-1 Diffuser Inlet Conditions

The mean velocity profile measured along three equally spaced radii at a station 3 ins. upstream of diffuser inlet (henceforward referred to DIFFUSER INLET) is shown in Fig. 4-1-1. The results are compared with those due to Brighton and Jones[39], for approximately the same Reynolds number, and a radius ratio, $^{Ri}/_{Ro} = 0.562$. The results are in good agreement; Howard et al[26] have produced a similar finding. Also the position of the point of maximum velocity in turbulent flow is much the same as that for laminar flow.

In order to verify that the data follows the well established "Law of the Wall", the results are shown in Fig. 4-1-2 in the form of a semilogarithmic plot. The law is;

$$\frac{u}{u_\tau} = \frac{1}{K} \log_e \left[\frac{(R_o - R)\, u_\tau}{\nu} \right] + C \qquad 4\text{-}1\text{-}1$$

Values of the constants, K & C, in annular flow have been quoted by Knudsen and Katz[40] as 0.38 and 3.0 respectively. In view of the large radius ratio it was considered more appropriate to use the values suggested by Coles[41] for two-dimensional flow i.e., 0.4 & 5.1. Similar assumptions have been made by Goldberg[29] in an experiment with annular flow at an equivalent radius ratio. Equation 4-1-1 can be expressed for the outer wall boundary layer in the form;

$$\frac{u}{U} = \sqrt{\frac{C_{f_o}}{2}} \left\{ 2.5 \log_e \left[\frac{(R_o - R)U}{\nu} \sqrt{\frac{C_{f_o}}{2}} \right] + 5.1 \right\} \quad - 4\text{-}2\text{-}2$$

and for the inner wall layer as;

$$\frac{u}{U} = \sqrt{\frac{C_{f_i}}{2}} \left\{ 2.5 \log_e \left[\frac{(R - R_i)U}{\nu} \sqrt{\frac{C_{f_i}}{2}} \right] + 5.1 \right\} - 4\text{-}2\text{-}3$$

Equations 4-2-2 and 4-2-3, have been plotted as a universal family for various values of Cf, the measured velocity profiles are also plotted, and the value of Cf determined by selecting the appropriate member of the family which best fits the experimental data. Whilst the velocity profiles on inner and outer walls follow a logarithmic variation, the experimental data lie on a line of greater slope than that predicted by Coles. This variation in slope makes it difficult to estimate values of Cf to better than $\pm 5\%$. The table below compares the estimated values with those predicted by Ludwieg and Tillmann[42] and Felsch[43] for the same values of Re_θ and H.

COMPARISON OF SKIN FRICTION COEFFICIENTS

	OUTER WALL	INNER WALL
Cf - Experiment	0.0033	0.0034
Cf - Ludwieg & Tillmann	0.00356	0.00378
Cf - Felsch	0.00357	0.0038

The lower experimental values are attributed to the lack of a suitable form of the universal law, Knudsen and Katz [40] in reviewing flow in annular passages state that "extensive investigation has failed to produce a satisfactory relationship".

The boundary layer momentum thickness ($\theta/(Ro - Ri)$) on inner and outer walls is 0.039 and 0.042 respectively, compared with values of 0.036 and 0.041 reported by the author[27] for a radius ratio of 0.60.

The Reynolds shear stress distribution (see Fig. 4-1-3) was found to be linear, indicating that the flow was also fully developed in terms of the turbulence structure. The shear stress distributions were extrapolated to the wall to give further estimates of the skin friction coefficients viz. $Cfo \simeq Cfi = 0.0031$

The distribution of longitudinal turbulence intensity is shown in Fig. 4-1-4 ; it will be seen that there is good agreement with the outer wall values due to Brighton and Jones, but the results are approximately 15% lower over a large proportion of the inner layer.

Thus on the basis of the mean velocity profiles and turbulent shear stress distributions it can be stated that fully developed flow has been established at diffuser inlet. It should be noted that these conditions have been achieved in an entry length of 50 hydraulic diameters with the aid of transition wires on the intake, compared with a length of 59 diameters used by the author(27) in an earlier investigation. Wood(22) using a similar arrangement required 45 diameters, whilst Brighton and Jones using gauzes and roughness elements required 35 diameters.

4-2 Outlet Conditions and Flow Stability

Fig. 4-2-1 shows the outlet velocity profiles for the three diffusers; the following points are noted:

(i) As the non-dimensional length of the diffuser is reduced, the distortion of the outlet velocity profile increases. The increased distortion is reflected in the progressive increase in the profile energy coefficient α_2.

(ii) The increased distortion is associated mainly with an increase in the shape parameter of the outer wall boundary layer.

(iii) Although considerable distortion of the flow has taken place, only in the case of the $^{L}/\Delta R_1 = 5$ diffuser is any asymmetry of flow observed. The symmetry of flow in the other diffusers is very good.

The imminence of separation at outlet of the $L/\Delta R_1 = 5$ diffuser is indicated by the asymmetry of flow, and the high outer wall shape parameter. However failure to measure a separated profile cannot be taken unreservedly as proof of the absence of separation, but merely indicates that separation has not occurred at the positions at which the measurements were made. Examination of the flow at outlet using wool tufts indicated that intermittent transitory stalling was occurring at varying positions on the outer wall between the outlet plane and a station approximately one inch upstream.

In the other two diffusers tested there was a general unsteadiness in the outlet flow but no stalling could be detected.

4-3 Static Pressure Distribution

The increase of pressure along the inner and outer walls of the diffusers is indicated in Figs. 4-3-1/2/3, in terms of the local pressure coefficient defined as

$$\bar{C}_P = \frac{P - P_1}{\frac{1}{2}\rho \bar{u}_1^2} \qquad 4\text{-}3\text{-}1$$

The experimental observations are given in Appendix 9. The inlet pressure P_1 is taken as the static pressure measured 3 ins. upstream of diffuser entry (see Section 3-5). A similar technique has been adopted by Howard et al.[26], and Stevens and Markland[19]. There is a significant difference in static pressure across the annulus in the vicinity of the diffuser entry due to the local curvature of flow. This pressure difference, which increases with outer wall angle, has the effect of increasing the local pressure gradient $(\frac{dP}{dx})$ on the outer wall in the initial stages of diffusion. Over the remaining length of the diffusers, with the exception of the $L/\Delta R_1$=5 diffuser, the pressures on the inner and outer walls at each station are indistinguishable. In the case of the $L/\Delta R_1$=5 diffuser, the small but detectable difference in pressures is not considered to be significant.

The measured values of pressure rise coefficient are lower than the ideal values calculated from Eqn. 1-3-2 due to the combined effects of increasing non-uniformity of flow and energy losses along the length of the diffuser. Neglecting energy losses, the pressure rise coefficient is obtained from Eqn. 1-3-3 as;

$$\overline{C}_P = \left[\alpha_1 - \frac{\alpha_2}{AR^2}\right] \qquad 4\text{-}3\text{-}2$$

The predicted values of $\overline{Cp}$ obtained by substituting the experimental values of velocity profile energy coefficient in Eqn. 4-3-2 are also shown in Figs. 4-3-1/2/3. It will be seen that the lower experimental values of $\overline{Cp}$ are due mainly to insufficient diffusion associated with the increased kinetic energy flux due to flow distortion, rather than inefficient diffusion due to energy losses.

4-4 Overall Performance

The overall performance of the diffusers is summarised below:

DIFFUSER $^L/\Delta R_1$	5.0	7.5	10.0
$\overline{Cp}$ 1-2	0.54	0.63	0.64
$\overline{Cp}'$ 1-2	0.75	0.75	0.75
ε_{1-2}= Cp/Cp′	0.72	0.84	0.85
α_1	1.045	1.045	1.045
α_2	*1.740	1.41	1.31
λ_{1-2}	0.08	0.065	0.077

*Arithmetic mean value

The calculation of the loss coefficients (λ 1-2) is detailed in Appendix 10, and the values of outlet velocity profile energy coefficient (α 2) are given in Appendices 4/6/8.

The results show that an increase in the non-dimensional length of the diffuser results in an improvement in the static pressure rise coefficient. However within the limits of experimental error the values of $\overline{Cp}_{1-2}$ for the $L/\Delta R_1$=7.5 and 10.0 diffusers are the same; this is due to the reduced distortion in the $L/\Delta R_1$=10.0 diffuser being offset by the slightly larger energy losses associated with the increased length of diffusion.

4-5 Comparison of Overall Performance with Published Data

Howard et al.[26] have carried out overall performance tests with fully developed flow at inlet, on a range of annular diffusers which had centre bodies of uniform diameter and inlet radius ratios of 0.775 and 0.515. Although the influence of inlet radius ratio was found to be significant, the higher value of 0.775 is reasonably close to the value used in the present tests and the results are compared in the table below.

DIFFUSER $L/\Delta R_1$	5.0	7.5	10.0
$\overline{Cp}_{1-2}$ (Expt)	0.54	0.63	0.64
$\overline{Cp}_{1-2}$ (Howard et al.)	0.53	0.59*	0.60

* Interpolated

It can be seen that within the limits of experimental error there is good agreement between the data.

Sovran and Klomp[7] have proposed a universal correlation to predict the influence of inlet boundary layer thickness on diffuser performance (Fig. 1-4-3). The correlation is restricted to diffusers having geometries on or near the optimum $\overline{Cp}$ * line i.e. the $L/\Delta R_1=5$ diffuser. Substitution of the appropriate values of area ratio and inlet blockage fraction yields a predicted value of $(\bar{U}/U)_2 = 0.60$ compared with the experimental value $\cong 0.62$. Using this result, and neglecting the total pressure loss along the streamline of maximum velocity, a static pressure rise coefficient of 0.555 is predicted, which is in excellent agreement with the measured value.

Very little published data is available on annular diffuser loss coefficients, however Henry et al.[25] have suggested a correlation based on the included wall angle. The experimental data is compared with this correlation in Fig. 4-5-1. It can be seen that there is reasonable agreement with the data due to Nelson and Popp.[82]

4-6 Influence of Downstream Settling Length

Measurements were made of the variation of static pressure, velocity profile, and turbulence structure along the length of the constant area duct downstream of the diffuser. Traverses were carried out at stations, 3.75, 7.50 and 11.25 ins. downstream of the diffuser exit plane. The velocity profiles are shown in Appendices 3/5/7, and the pressure distributions and turbulence data are given in Appendices 9/14/15/16.

There is an increase in pressure in the downstream settling length due to radial momentum transfer reducing the distortion or momentum coefficient of the velocity profile. This effect is shown in Fig. 4-6-1 where the reduction in distortion is indicated by the lower values of shape parameter. The momentum equation for flow in the settling length is;

$$\rho\frac{\pi}{4}\left(D_o^2-D_i^2\right)\left[\beta_3\bar{U}_3^2-\beta_2\bar{U}_2^2\right] = \frac{\pi}{4}\left(D_o^2-D_i^2\right)\left[P_2-P_3\right]-\tau_\omega\pi\left(D_o+D_i\right)dx \quad -4\text{-}6\text{-}1$$

Where τ_w is the mean wall shear stress, and β is the momentum coefficient defined as

$$\beta = \int u^2 dA \,/\, \bar{u}^2 A \qquad 4\text{-}6\text{-}2$$

If the flow is assumed to be near to separation at outlet, the term $\left[\tau_w \pi (Do + Di)\, dx\right]$ has a very small influence in the equation, and can be safely neglected. Equation 4-6-1 therefore reduces to

$$\frac{P_3 - P_2}{\frac{1}{2}\rho \bar{u}_1^2} = 2(\beta_2 - \beta_3)\left(\frac{A_1}{A_2}\right)^2 \qquad 4\text{-}6\text{-}3$$

In the table below the measured values of pressure rise coefficient are compared with the value obtained by substituting the experimental values of $\beta 2$ and $\beta 3$ in Eqn. 4-6-3.

DIFFUSER $L/\Delta R_1$	5.0	7.5	10.0
$\beta 2$	1.239*	1.142	1.106
$\beta 3$	1.024	1.017	1.017
$(P3-P2)/\frac{1}{2}\rho\bar{u}_1^2$ Eqn. (4-6-3)	0.107	0.062	0.044
$(P3-P2)/\frac{1}{2}\rho\bar{u}_1^2$ (expt)	0.125	0.043	0.050
$\overline{Cp}$-1-3	0.665	0.668	0.690
$\overline{Cp}$ 1-2	0.540	0.625	0.640
% increase in $\overline{Cp}$	23.0	7.0	8.0

* Arithmetic mean value

Within the limits of experimental error, there is good agreement. The discrepancy in the case of the $L/\Delta R_1=5$ diffuser is considered to be due, in part, to the difficulty in establishing an accurate value of β_2 for the asymmetric diffuser outlet velocity profile. It can be seen that the downstream settling length produces an appreciable increase in the static pressure rise coefficient, particularly in the case of the $L/\Delta R_1=5$ diffuser.

The overall loss coefficient, λ_{1-3}, for the diffuser - settling length combination has been obtained from:

$$\lambda_{1-3} = \left[\alpha_1 - \frac{\alpha_3}{(A_3/A_1)^2} \right] - \overline{C}_{P_{1-3}} \qquad 4\text{-}6\text{-}4$$

The values of λ_{1-3} are tabulated below:

DIFFUSER $L/\Delta R_1$	5.0	7.5	10.0
α_1	1.045	1.045	1.045
α_3	1.067	1.048	1.050
$\alpha_1 - \alpha_3/(A3/A1)^2$	0.778	0.783	0.783
$\overline{Cp}_{1-3}$ (exp$^{t.}$)	0.665	0.668	0.690
λ_{1-3}	0.113	0.115	0.093
λ_{1-2}	0.080	0.065	0.077
$\lambda_{2-3} = \frac{\Delta P_T}{\frac{1}{2}\rho \bar{u}_1^2}$	0.033	0.050	0.016
$\lambda_{2-3} = \Delta P_T / \frac{1}{2}\rho \bar{u}_2^2$	0.132	0.200	0.064
$Cp_{2-3} = \Delta P / \frac{1}{2}\rho \bar{u}_2^2$	0.500	0.172	0.200

Based on the results for the $L/\Delta R_1$=5 & 10 diffusers, the increased turbulent mixing has resulted in an increase of approximately 30% in the overall loss coefficient. These values are approximate, since they have been calculated from the difference between the ideal and actual static pressure rise coefficients, and as discussed in Section 3-4 this approach can lead to large errors, e.g. the results for the $L/\Delta R_1$=7.5 diffuser.

To summarise, the addition of a downstream settling length produced in all cases an improvement in the pressure rise coefficient, particularly in the case of the $L/\Delta R_1$ = 5 diffuser which exhibited the greatest flow distortion. In all cases the stability of flow in the settling length increased considerably. However, these improvements are obtained at the expense of an increase in the mean total pressure loss.

4-7 Mean Velocity Profiles and Boundary Layer Growth

4-7-1 Mean Velocity Profiles

The development of the mean velocity profile, at one circumferential position, along the inner and outer walls of the three diffusers is shown in Figs. 4-7-1 to 4-7-6. The profiles plotted against the non-dimensional distance from the inner wall are presented in Figs. 4-7-7 to 4-7-9, whilst the results of the traverses taken along the three equally spaced radii are given in Appendices 3/5/7. The boundary layer parameters quoted on the graphs are based on axi-symmetric definitions e.g.

$$\delta_i^* = \int_{R_1}^{R_m} \left(1 - \frac{u}{U}\right) \frac{R}{R_1}\, dR \quad , \quad \theta_i = \int_{R_1}^{R_m} \frac{u}{U}\left(1 - \frac{u}{U}\right) \frac{R}{R_1}\, dR \quad , \quad H_1 = \delta_1^*/\theta_1$$

The velocity profiles in Appendices 3/5/7, exhibit excellent symmetry of flow at all stations; only on the outer wall at exit of $L/\Delta R_1=5$ diffuser is any asymmetry noted.

4-7-2 Boundary Layer Growth

The boundary layer parameters at each station are listed in Appendices 4/6/8, and their rate of growth along the inner and outer walls is presented in Figs. 4-7-10 and 4-7-11.

There is a significant difference in the growth of the shape parameter H along the inner and outer walls. The rate of increase in the shape parameter $(\frac{dH}{dx})$ is greater on the outer wall, and this effect increases with outer wall angle, until in the case of the $^L/\Delta R_1=5$ diffuser a value of $H \simeq 3.5$ is obtained at exit. The exit shape parameter on the inner wall remains approximately constant at 1.70 in all three diffusers.

In order to explain these effects, the physical interpretation of profile distortion is briefly reviewed. The two-dimensional boundary layer equation for the mean flow may be written as

$$u\frac{\partial u}{\partial x} + v\frac{\partial u}{\partial y} = -\frac{1}{\rho}\frac{dP}{dx} - \frac{\partial \overline{u}^2}{\partial x} + \frac{1}{\rho}\frac{\partial \tau}{\partial y} \qquad 4\text{-}7\text{-}1$$

If the influence of Reynolds stresses is ignored and the term $v\frac{\partial u}{\partial y}$ is assumed to be small in the inner region of the layer, then the equation indicates that in the presence of a pressure gradient the change in velocity $\frac{\partial u}{\partial x}$ is inversely proportional to the local velocity. In a diffuser where $\frac{dP}{dx}$ is positive, there will therefore be a reduction in velocity. The reduction in velocity is greatest where the local velocity is smallest and the distortion of the flow is accentuated. This simplified approach is modified by the inclusion of the other terms in the equation, of which the most important is the Reynolds shear stress, which represents the mean transfer in the y direction of x - component momentum. Measurements of the shear stress distribution, in a boundary layer subjected to a strong adverse pressure gradient, indicate that the flow in the vicinity of the wall receives momentum from the outer regions of the layer which assists it to advance to a region of higher pressure. Therefore, in an adverse pressure gradient the Reynolds shear stress reduces the degree of distortion, and the changes in profile shape will therefore depend on the relative magnitude of the pressure gradient and Reynolds stress terms.

Since the static pressure is nearly constant across any station in the diffuser, the boundary layers on inner and outer walls must experience the same pressure gradient, and therefore the asymmetric growth of the boundary layer shape parameters is due to

(i) Initial distortion produced by the flow curvature at entry, and/or

(ii) Significantly different turbulence structures in the inner and outer wall layers.

Although a generous blending radius (see Fig. 2-1-1) was used to ensure a smooth change in flow direction on the outer wall at inlet, the measured static pressure distributions in the vicinity of the inlet flange indicate a significant pressure difference across the annulus as illustrated below.

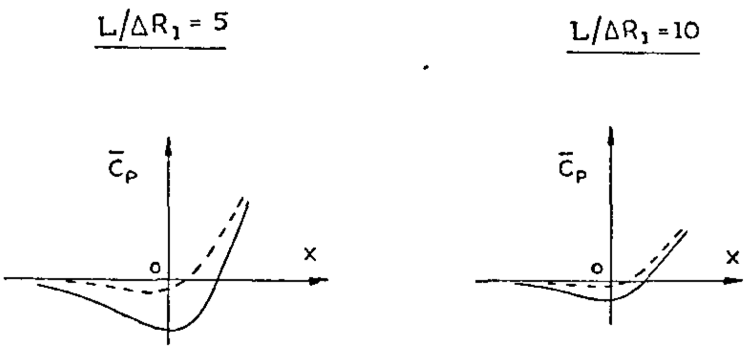

--- Inner Wall ——— Outer Wall

After the minimum pressure point the boundary layer on the outer wall experiences a more severe adverse pressure gradient which is reflected in a higher shape parameter on the outer wall at a station 0.3 ins. downstream of the inlet flange.

	UPSTREAM	DOWNSTREAM		
DIFFUSER $L/\Delta R_1$		5.0	7.5	10.0
Station (X ins)	-3.0	0.3	0.3	0.3
Outer Wall H_o	1.30	1.39	1.36	1.30
Inner Wall H_i	1.28	1.31	1.28	1.32

In the case of $L/\Delta R_1 = 5$ diffuser the initial pressure gradient is very large and, Coles[44] has suggested that under such conditions "the mean motion is determined by pressure forces alone." Therefore in the $L/\Delta R_1 = 5$ diffuser the asymmetric growth of the shape parameters is attributed to the initial distortion produced by flow curvature at inlet, which is then accentuated by a very severe adverse pressure gradient in which the turbulent Reynolds stresses play only a minor role.

A similar phenomenon has been reported by Stevens and Eccleston[36] in an experiment in which a diffuser was preceded by a 40° annular bend. Due to the distortion produced by the bend the shape parameters on the inner and outer walls at diffuser inlet were 1.22 and 1.43 respectively. The severe adverse pressure gradient in the diffuser ($L/\Delta R_1 = 6.2$, $A_2/A_1 = 2.0$) accentuated this distortion to produce shape parameters on inner and outer walls at diffuser exit of 1.28 and 3.0.

The asymmetric growth of the shape parameters is reduced as the outer wall angle is decreased, since not only the degree of initial distortion, but the pressure gradient also is reduced, and the turbulent Reynolds stresses exert a greater influence on the development of the mean motion.

As discussed in Section 4-2 intermittent transitory stalling was detected over approximately the last 20% of the outer wall of the $L/\Delta R_1 = 5$ diffuser. The experimental boundary layer parameters are compared in Fig. 4-7-12 with the correlations suggested by Sandborn and Liu[45] for predicting intermittent and fully developed separation. It can be seen that the conditions at diffuser exit correspond to fully developed separation. Whilst the shear stress at this point is very small, only a transitory stall could be detected. Furthermore, the correlation predicts the onset of stalling at a station approximately 3 ins. from diffuser inlet, whereas wool tuft observations indicated that transitory stalling did not occur until approximately 4 ins. from inlet. Therefore whilst Sandborn and Liu correlation is partially successful, like many other separation predictions it merely indicates the imminence of stalling.

4-8 Longitudinal Turbulence Intensity Distribution

The measured longitudinal turbulence intensities are presented in Figs. 4-8-1 to 4-8-6. The method of reducing the data is given in Appendix 11 and the results are tabulated in Appendices 14/15/16. It is emphasised that apart from plotting the test data to remove spurious points, the results are based on the raw test data with no corrections applied. Although the order of accuracy probably varies from 5-10% in the early stages of diffusion, to approximately 20% in the latter stages, the results do indicate general trends when results for the different diffuser geometries are compared.

The data shows that in an adverse pressure gradient the value of $\sqrt{\overline{u'^2}}/U$ near the wall develops to a maximum which increases and moves away from the wall as the flow proceeds downstream. Whilst the flow remains within the adverse pressure gradient the maximum level of $\sqrt{\overline{u'^2}}/U$ is maintained, but when the pressure gradient is relaxed in the downstream settling length the maximum falls rapidly.

Spangenberg et al[46] have suggested that areas of intermittent stalling occur when the root-mean-square intensity in the inner 10% of the layer exceeds about 33% of the local mean velocity. Using this criterion the data indicates the onset of intermittent stalling on the outer wall of the $L/\Delta R_1 = 5$ diffuser at a station approximately 2.50 ins. from inlet, and on the outer wall of the $L/\Delta R_1 = 7.5$ diffuser approximately 6.0 ins. from inlet. Careful investigation using wool tufts did not confirm these predictions. Intermittent stalling was confined to a region on the outer wall of the $L/\Delta R_1 = 5$ diffuser approximately 4 ins. from inlet, where r.m.s. fluctuations as high as 70% of the local velocity were recorded.

In the latter stages of diffusion, along the outer wall of the $L/\Delta R_1 = 5$ diffuser, there is a sharp fall in the value of $\sqrt{\overline{u'^2}}/U$, which suggests that in regions near to intermittent stalling the force opposing the pressure gradient is probably derived not only from the shear stress gradient, but also from the gradient of Reynolds normal stress.

The measured longitudinal turbulence intensities in the downstream settling length distal to the three diffusers are presented in Figs. A14-1/2, A15-1/2, and A16-1/2. The distributions are given along one radius at three stations located 3.75, 7.50, and 11.25 ins. from diffuser outlet. There are insufficient number of traverses to draw conclusions regarding the axial gradient of turbulence intensity but an indication is obtained of the level of values at the measuring stations. Figs. A15-2 and A16-2 indicate that the maximum value decreases as the flow approaches equilibrium. However, although the boundary layer shape parameters on inner and outer walls at the station 11.25 ins from outlet are in the range 1.37 to 1.28 the values of turbulence intensity are relatively high. Therefore the velocity profile is returning to equilibrium faster than the turbulence intensity distribution.

4-9 Turbulent Shear Stress Distribution

The distribution of turbulent shear stress $\left(\frac{2\overline{u'v'}}{U^2}\right)$ at one circumferential position for a number of stations in the three diffusers is presented in Figs. 4-9-1 to 4-9-3. The method of reducing the data is detailed in Appendix 11 and the results obtained using a computer programme (see Appendix 12) are tabulated in Appendices 14/15/16. To complete the shear stress distributions, the shear stress at the wall, estimated from the equation due to Ludwieg and Tillmann[42] has been added. The turbulent shear stress measured in the u'-w' plane was found to be extremely small, and is therefore not presented in a graphical form.

At a selected number of stations measurements were made of the shear stress distribution along three equally spaced radii; the results are tabulated in Appendices 14/15/16 and presented graphically in Figs. A14-5/6, A15-5, and A16-6. Within the limits of experimental error, the distributions are symmetrical, and only in the case of the measurements taken at exit of the $L/\Delta R_1 = 5$ diffuser is any marked asymmetry observed.

The shear stress distributions are very similar to the longitudinal turbulence intensity distributions, in that, near the wall a maximum develops which moves away as the flow proceeds downstream. It should be noted that despite the difficulties entailed in making accurate shear stress measurements the general trend of the results is very consistent. It is possible to see qualitatively on physical grounds how the shearing stress must be distributed across the layer. The shearing stress is always in such a direction that fluid layers further out pull on layers further in. When the pressure is either constant, or falling, all pull is ultimately exerted on the surface. Therefore the shearing stress must be at least as high at the surface as it is elsewhere and it would be expected to be a maximum there, as it must fall to zero outside the layer. When the pressure is rising, part of the pull must be exerted on that part of the fluid near the wall, which has insufficient energy of its own to progress to regions of higher pressure. In other words, the fluid in such layers must be pulled upon harder than it pulls upon the adjacent layer nearer the surface. This means that the shear stress must have a maximum away from the wall in regions of adverse pressure gradient.

An alternative approach is to write the mean flow equation (Eqn. 4-7-1)near the wall as

$$\frac{d\tau}{dy} = \frac{dP}{dx} \qquad 4\text{-}7\text{-}2$$

assuming that the remaining terms in the equation are negligible in the vicinity of the wall. Therefore in the initial stages of diffusion where the pressure gradient is at its maximum value, steep gradients of shear stress are observed near the wall. Then as the flow proceeds downstream, and the pressure gradient is relaxed so the gradient of shear stress normal to the wall is reduced. The region between the wall and the point of maximum shear stress is receiving energy per unit volume at each point at a rate given by $u\frac{\partial\tau}{\partial y}$, and therefore the positive slope $\frac{\partial\tau}{\partial y}$, is evidence that the shear stress is acting to prevent separation. The fall to near zero in shear stress on the outer wall at exit of the $L/\Delta R_1 = 5$ diffuser is attributed to the extremely low velocity in this region, and that a condition has developed in which no energy can be received.

A number of workers notably Bradshaw[34] and Spangenberg et al[46], have investigated the validity of Eqn. 4-7-2. Bradshaw found that $\frac{d\tau}{dy} \simeq \frac{1}{2}\frac{dP}{dx}$, and Spangenberg et al., in an investigation of a near separating layer, found that at no point near the wall did $\frac{d\tau}{dy}$ equal $\frac{dP}{dx}$; in fact close to separation $\frac{d\tau}{dy} \simeq 0.2\frac{dP}{dx}$. As separation was approached a condition of near zero wall shear stress was reached, and in this region the force required to overcome the pressure gradient was found to be derived mainly from the Reynolds normal stress term, a value of $\frac{d\overline{u'^2}}{dx} \simeq 0.6\frac{dP}{dx}$ being obtained near to separation. Examination of the experimental data along the outer wall of the $L/\Delta R_1 = 5$ diffuser revealed that $\frac{d\tau}{dy} \simeq 0.8\frac{dP}{dx}$ in the initial stages of diffusion, falling to $\frac{d\tau}{dy} \simeq 0.25\frac{dP}{dx}$ at a station 3.75 ins. from entry. The gradient of Reynolds normal stresses at a point 0.5 ins. from the wall, for the station 3.75 ins. from entry, was found to be equal to approximately $0.3\frac{dP}{dx}$. It appears therefore that at this point the other terms in the mean flow equation must be taken into account. For a detailed analysis of the flow, additional measurements are required near the wall.

It is of interest that despite the significant differences in mean flow development in the three diffusers, the maximum values of shear stress along inner and outer walls are very similar. This seems to suggest that the turbulence components have originated from sources other than the local mean velocity gradient.

The shear stress distribution at the three traverse stations in the downstream settling length are presented in Figs. A14 - 3/4, A15 - 3/4 and A16 - 3/4. It can be noted that in the $^{L}/\Delta R_1 = 5$ & 7.5 diffusers the maximum value of shear stress in the outer wall boundary layer continues to increase up to the station 7.5 ins. from diffuser outlet, reflecting the large amount of turbulent mixing which is occurring. Although in the inner wall boundary layer the maximum value of shear stress is decreasing continuously, there is evidence, particularly in the outer wall boundary layer, of the turbulence structure lagging behind the development of the mean velocity profile.

4-10 Distribution of Mixing Length and Eddy Viscosity

4-10-1 Mixing Length

The mixing length defined by Prandtl as

$$\ell = \left[\frac{-\overline{u'v'}}{\left|\frac{du}{dR}\right| \frac{du}{dR}} \right]^{1/2} \qquad 4\text{-}10\text{-}1$$

is often used to relate the turbulent shear stress to the mean velocity profile. It is frequently assumed that the mixing length stays constant in the outer 80% of the boundary layer and equal to 0.09δ, whilst for the inner region of the layer the Prandtl relationship, $\ell = 0.4\,y$, is used. A review of expressions for mixing length is given by Patanker & Spalding.(78)

The method used to obtain the values of mixing length is detailed in Appendices 17/18, and the results are tabulated in

Appendices 20/21/22. The values of mixing length have been non-dimensionalised with respect to displacement thickness, and are presented in Figs. 4-10-1/2, A21-1/2, and A22-1/2.

Brighton and Jones[39] have shown that in fully developed flow the mixing length, ℓ, goes to infinity as $R \rightarrow Rm$; the same effect is noted at the edge of a number of the test boundary layers, due to small differences between the radii of the point of maximum velocity ($\frac{du}{dR} = o$), and zero shear stress. The mixing length, ℓ, physically represents the distance over which a fluid particle migrates before exchanging momentum with fluid particles of different layers. Thus, it would be impossible to have values of ℓ of the order of δ or greater. This anomaly is confined however to a small portion of the flow.

Apart from conditions near to diffuser entry where mixing length increases with distance from the wall, the distributions agree reasonably well with the assumption of constant mixing length over most of the boundary layer, although the magnitude of this constant level varies considerably. As the flow proceeds along the diffuser the value of ℓ/δ^* is reduced, due to the turbulent shear stress distribution lagging behind the development of the mean velocity profile. In the downstream settling length the values of ℓ/δ^* increase rapidly. Similar results have been obtained by Goldberg[29] and Rotta[47].

It has been suggested by many research workers e.g. Bradshaw[48] and Reynolds[34] that mixing length theory is unsound when applied to conditions far removed from "local equilibrium". As a matter of interest, the mean values of ℓ/δ, ℓ/δ^*, and $\ell/$ Ro - Ri) in the outer portions of the layers were compared to see if the magnitude of the variations could be reduced by an alternative method of non-dimensionalising. The results are given in Table 4-1. The variation in the mean values of ℓ/δ and ℓ/δ^* is compared with the results due to Goldberg in the table below.

	Goldberg		Present Investigation		
	ℓ/δ^*	ℓ/δ	ℓ/δ^*	ℓ/δ	$\ell/(Ro-Ri)$
maximum value	0.55	0.10	0.40	0.098	0.043
minimum value	0.10	0.04	0.11	0.054	0.028

Whilst the variations in the present experiments are less than those obtained by Goldberg, the variations can be reduced still further by considering inner and outer wall boundary layers separately.

	ℓ/δ^*	ℓ/δ	$\ell/(Ro-Ri)$
inner wall	$0.35 \; {}^{+15}_{-30}\,\%$	$0.088 \; {}^{+11}_{-9}\,\%$	$0.038 \; {}^{+14}_{-12}\,\%$
outer wall	$0.20 \pm 45\,\%$	$0.062 \; {}^{+19}_{-15}\,\%$	$0.033 \; {}^{+30}_{-18}\,\%$

The values of ℓ/δ give the lowest percentage variation, the inner wall values being in good agreement with the correlation suggested by Spalding[(49)].

An unsuccessful attempt was also made to correlate the values of mixing length with the non-dimensional pressure gradient parameter ($\frac{\delta^*}{\tau_\omega}\frac{dP}{dx}$).

4-10-2 Eddy Viscosity

The eddy viscosity ε , defined in Eqn. 4-10-2, has also been used to relate the turbulent shear stress to the mean velocity profile.

$$\varepsilon = -\frac{\overline{u'v'}}{\frac{du}{dR}} \qquad 4\text{-}10\text{-}2$$

The simplest assumption of a constant value of ε in the outer region of the boundary layer was applied to equilibrium layers by Clauser[51] who suggested

$$\frac{\varepsilon}{U\delta^*} = 0.018 \qquad 4\text{-}10\text{-}3$$

The solution obtained in this way was joined with the universal law of the wall to give the velocity profile for the whole of the boundary layer. Bradshaw and Ferris[50], and more recently Goldberg[29], have shown that the assumption of constant eddy viscosity away from the wall does not hold in non-equilibrium flows. Also the variation of $\frac{\varepsilon}{U\delta^*}$ at fixed $\frac{y}{\delta}$, exhibits the same trend as the mixing length data, in that, $\frac{\varepsilon}{U\delta^*}$ decreases in an adverse pressure gradient, then increases rapidly in the downstream settling length. Goldberg attempted to determine a more appropriate normalisation of eddy viscosity, but found that even the best grouping, $\frac{\varepsilon}{u_\tau \theta}$, had maximum and minimum values of 1.4 and 0.51 respectively compared with values of 0.028 and 0.0048 for $\frac{\varepsilon}{U\delta^*}$.

The method used to obtain the values of eddy viscosity is detailed in Appendices 17/18, and the results are tabulated in Appendices 20/21/22. The values of eddy viscosity have been non-dimensionalised with respect to displacement thickness and annulus height. Although in the outer region of a number of layers, the value of $\frac{\varepsilon}{U\delta^*}$ is approximately constant, as in Goldberg's experiments, there is a considerable variation in the value of $\frac{\varepsilon}{U\delta^*}$ at fixed $\frac{y}{\delta}$, typical maximum and minimum values being 0.035 and 0.007 respectively. The variation of $\varepsilon/U\delta^*$ along the outer wall of the $L/\Delta R_1 = 5.0$ diffuser is presented in Figure A20-1.

4-11 Skin Friction Coefficients

No direct measurements were made of wall shear stress, and the local skin friction coefficient was estimated from the measured velocity profiles using the method due to Clauser[51]. The conventional form of the law of the wall (Equation 4-1-1) is replotted as a universal family for a range of values of C_f. The measured profile is then plotted and the value of C_f determined by selecting the appropriate member of the family which best fits the experimental data. It may be noted that during the initial stages of diffusion there is an absence of any clear logarithmic portion in the measured profiles and under these conditions the estimated values of C_f can only be considered as approximate. The Clauser plots are shown in Figs. 4-11-1 to 4-11-6 inclusive. The results are plotted in Figs. 4-11-7/8 and compared with the values predicted by Ludwieg and Tillmann[42], and Coles[41] for the same value of Re_θ and H. The results indicate a rapid decrease in skin friction coefficient during the initial stages of diffusion, and that on the outer wall at exit of the $^L/\Delta R_1 = 5$ diffuser a condition of near zero wall shear exists. Both Coles Law and the relation due to Ludwieg and Tillmann, overestimate the value of skin friction coefficient by as much as 35% in some cases. Discrepancies of a similar order have been noted by the author[27] and Goldberg[29] in experiments performed under conditions of severe adverse pressure gradient.

4-12 Balance of Momentum and Energy Equations

4-12-1 Balance of Momentum Equation

As a guide to the accuracy of the experimental data, and the relative significance of the terms in the momentum equations, momentum balances were carried out at a number of stations along the length of each diffuser. Writing the momentum integral equations (Appendix 25 and Reference 33) for the flow along the inner and outer walls as:

$$\frac{d\theta_o}{dx} = \frac{C_{f_o}}{2} - \frac{\theta_o}{R_o}\frac{dR_o}{dx} - \frac{\theta_o}{U}\frac{dU}{dx}(H_o+2) + \frac{R_o^2 - R_m^2}{R_o}\frac{1}{2\rho U^2}\left(\frac{dP_T}{dx}\right)_m + \frac{1}{U^2}\frac{d}{dx}\int_{R_m}^{R_o}(\overline{u'^2}+\overline{v_m'^2}-\overline{v'^2})\frac{R}{R_o}\,dR \qquad \text{4-12-1}$$

$$\frac{d\theta_i}{dx} = \frac{C_{f_i}}{2} - \frac{\theta_i}{R_i}\frac{dR_i}{dx} - \frac{\theta_i}{U}\frac{dU}{dx}(H_i+2) + \frac{R_m^2 - R_i^2}{R_i}\frac{1}{2\rho U^2}\left(\frac{dP_T}{dx}\right)_m + \frac{1}{U^2}\frac{d}{dx}\int_{R_i}^{R_m}(\overline{u'^2}+\overline{v_m'^2}-\overline{v'^2})\frac{R}{R_i}\,dR \qquad \text{4-12-2}$$

The momentum balance consists of using the experimental values of θ, H, U, R_m, etc., at a given station, to calculate the terms on the right hand side of the equation, and then to compare the calculated value of $\frac{d\theta}{dx}$ with the value estimated from the gradient of the measured values of momentum thickness. A similar technique has been adopted by McDonald and Stoddart(52) in analysing the data of Schubauer and Klebanoff(53), and by Coles and Hurst(34) in preparing the data for the recent AFOSR-IFP-Stanford Conference. The results obtained by McDonald and Stoddart are presented in Fig. 4-12-1; the descrepancy in $(\frac{d\theta}{dx})$ is generally attributed to three-dimensional effects and Coles(44) has found that a balance is rare in flows developed in a strong adverse pressure gradient.

Equation 4-12-1/2 differs from the usual form of the axi-symmetric momentum integral equation in the following respects:

(i) $\frac{R_o^2 - R_m^2}{R_o}\frac{1}{2\rho U^2}\left(\frac{dP_T}{dx}\right)_m$ & $\frac{R_m^2 - R_i^2}{R_i}\frac{1}{2\rho U^2}\left(\frac{dP_T}{dx}\right)_m$

are the terms which take account of the total pressure loss along the streamline of maximum velocity. In cases where an inviscid core flow is present

(ii) The Reynolds normal stresses $\frac{1}{U^2}\frac{d}{dx}\int\left(\overline{u'^2}+\overline{v_m'^2}-\overline{v'^2}\right)\frac{R}{R_1}\,dR$

The term containing $\overline{u'^2}$ comes directly from the x-momentum equation. The $\overline{v'^2}$ terms enter the equation through the R-momentum equation for the static pressure variation across the boundary layer. If inviscid core flow is present $\frac{d}{dx}\left(\overline{v_m'^2}\right) = 0$

The methods used to calculate the experimental values of pressure gradient and the other terms in momentum equations are detailed in Appendix 23. It should be stated that the calculations are sensitive to the methods used to smooth the data and obtain the differentials, nevertheless considerable care has been taken to provide data free from bias. The results are listed in Tables A23-1 to A23-6, and presented graphically in Figs. 4-12-2/3 and A23-1 to A23-4. The values of momentum thickness are compared with the values obtained from a graphical integration of the experimentally predicted values of $\left(\frac{d\theta}{dx}\right)$ in Figs. 4-12-4 and A23-5/6. It can be seen that in all cases the comparison between the left and right-hand sides of the momentum equations is very good, bearing in mind the large adverse pressure gradient. In view of this, it can be stated with confidence, that apart from the exit of the $L/\Delta R_1 = 5$ diffuser, the data is free from any significant three-dimensional effects. This conclusion is confirmed by wool tuft investigations, the symmetry of the mean velocity profiles, and the good agreement in integrated volume flows at all stations along the diffuser. The avoidance of three-dimensional effects is considered to be due to the fully annular configuration i.e. no sidewalls, and the high standard of accuracy maintained throughout the construction of the rig. This view is confirmed by Coles[34] in the paper "On the need for better experiments", in which he stated "I can see advantages in the use of an axially-symmetric configuration like that developed at M.I.T."

The main conclusions to be drawn from the momentum-balance results are:

i) Apart from the initial stages of diffusion the skin friction term is extremely small

ii) The Reynolds normal stress term is only of importance when the boundary layer is near to separation

iii) The term incorporating the total pressure loss along the streamline of maximum velocity is significant

iv) In all the cases considered the term incorporating the pressure gradient, $(H + 2)\frac{\theta}{U}\frac{dU}{dx}$, dominates the equation.

In fact, for engineering purposes, it would be sufficient to write the momentum equation as $\frac{d\theta}{dx} = \frac{\theta}{U}\frac{dU}{dx}(H+2)$

4-12-2 <u>Balance of Energy Equation</u>

The balance of the energy equation was investigated using the same technique as that outlined in the previous section, experimental values of U, δ^{**}, τ, etc. being used to calculate the right-hand-side of the energy integral equation. Neglecting the Reynolds normal stress term we may write:

$$\frac{d\delta_0^{**}}{dx} = (\delta - \delta_0^*)\frac{2}{\rho U^2}\left(\frac{dP_T}{dx}\right)_m + \frac{2\mathcal{D}_0}{\rho U^3} - 3\frac{\delta_0^{**}}{U}\frac{dU}{dx} \qquad 4\text{-}12\text{-}3$$

$$\frac{d\delta_1^{**}}{dx} = (\delta - \delta_1^*)\frac{2}{\rho U^2}\left(\frac{dP_T}{dx}\right)_m + \frac{2\mathcal{D}_1}{\rho U^3} - 3\frac{\delta_1^{**}}{U}\frac{dU}{dx} \qquad 4\text{-}12\text{-}4$$

Bearing in mind possible errors in the measurement of turbulent shear stress, and the large radius ratio, the two-dimensional form of the dissipation integral has been used without incurring any significant error. The remaining boundary layer parameters are based on axisymmetric definitions. Again a term is included to take account of the total pressure loss along the streamline of maximum velocity. The method of analysing the experimental data is outlined in Appendix 24, and the values listed in Tables A24-1 to A24-3. It can be seen that the right-hand-side of the energy equation is dominated by the term incorporating the pressure gradient $3\frac{\delta^{**}}{U}\frac{dU}{dx}$, the dissipation coefficient making a relatively small contribution. Values of the energy thickness δ^{**} calculated from equations 4-12-1/2 are compared with the values obtained from the mean velocity profile data in Figs. A24-1 to A24-3, again the general level of agreement is very good.

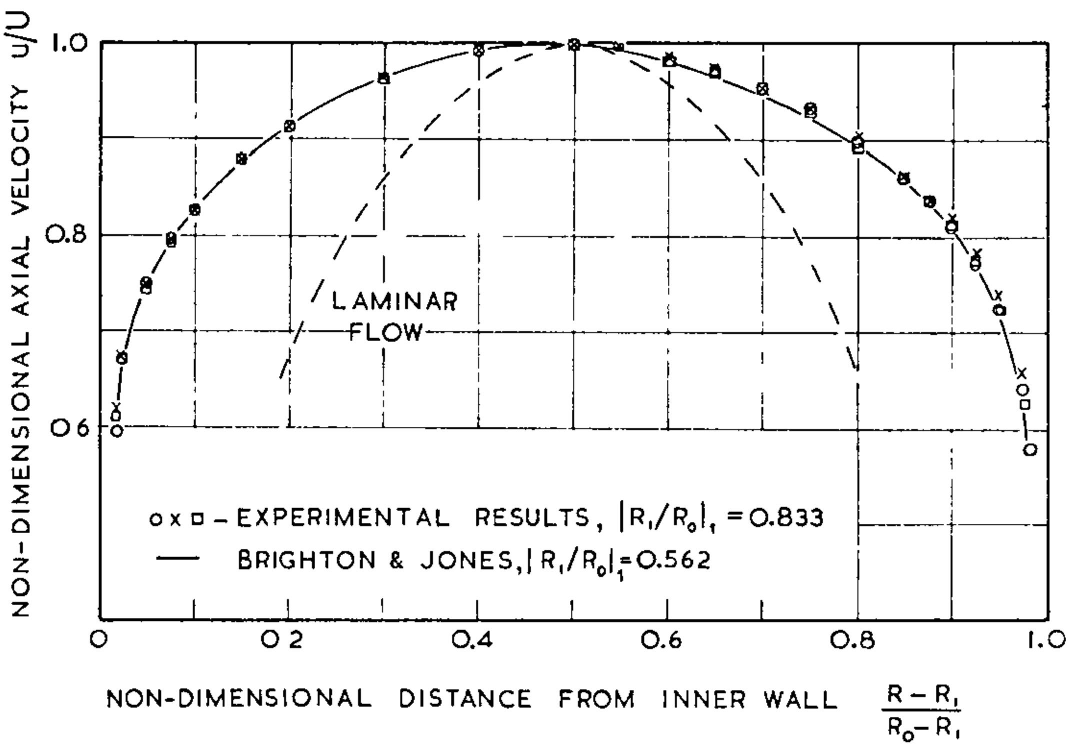

FIG. 4-1-1 COMPARISON OF FULLY DEVELOPED INLET VELOCITY PROFILE WITH RESULT OF BRIGHTON & JONES (39)

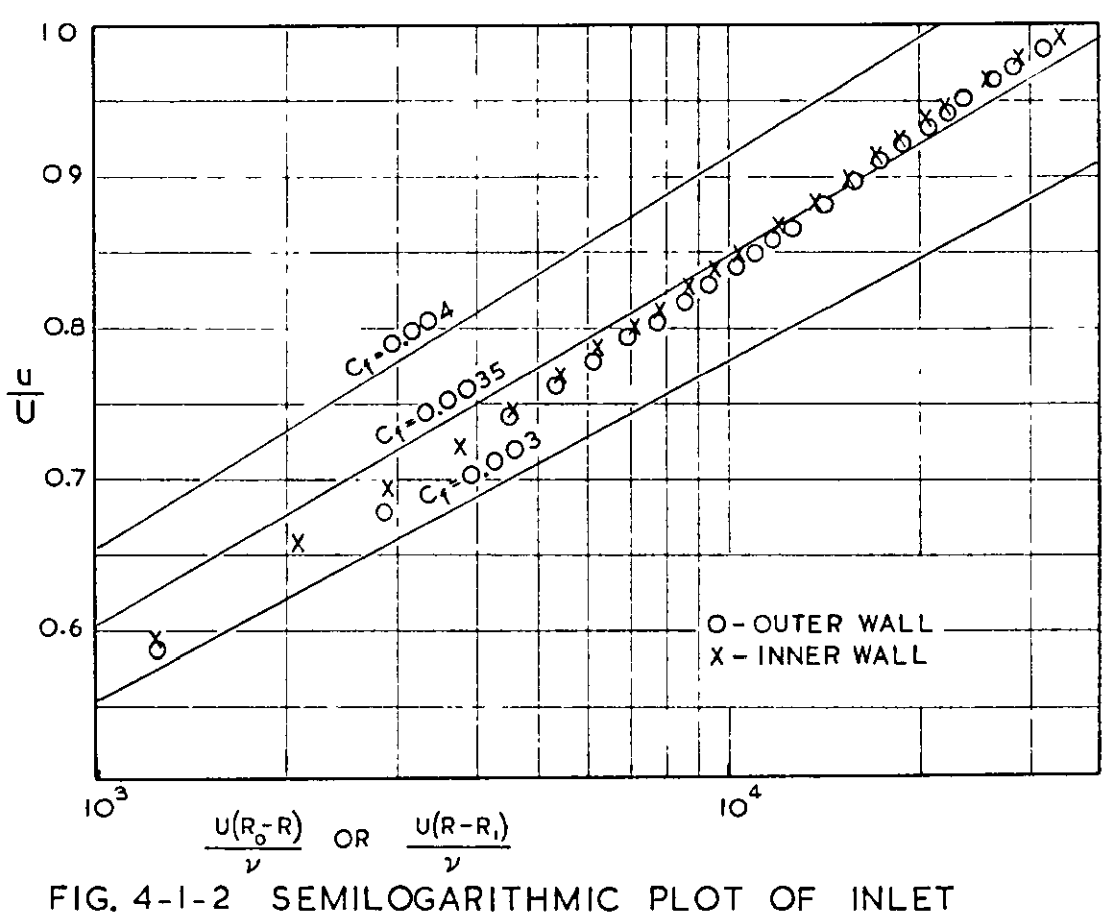

FIG. 4-1-2 SEMILOGARITHMIC PLOT OF INLET VELOCITY PROFILE

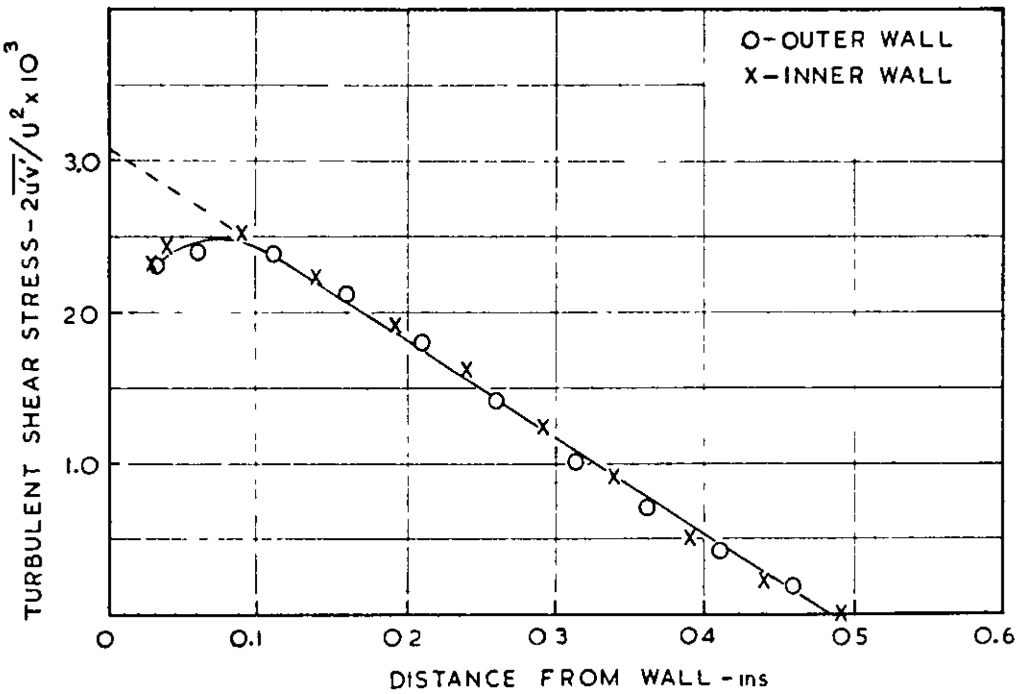

FIG. 4-1-3 TURBULENT SHEAR STRESS DISTRIBUTION AT INLET

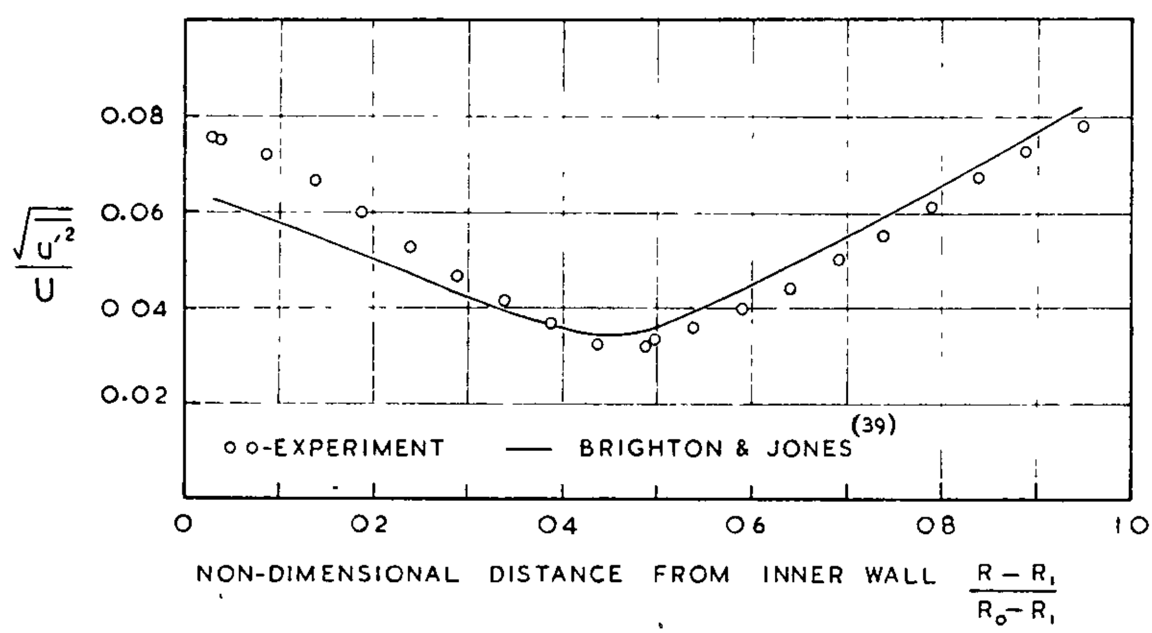

FIG. 4-1-4 AXIAL TURBULENCE INTENSITY DISTRIBUTION AT INLET

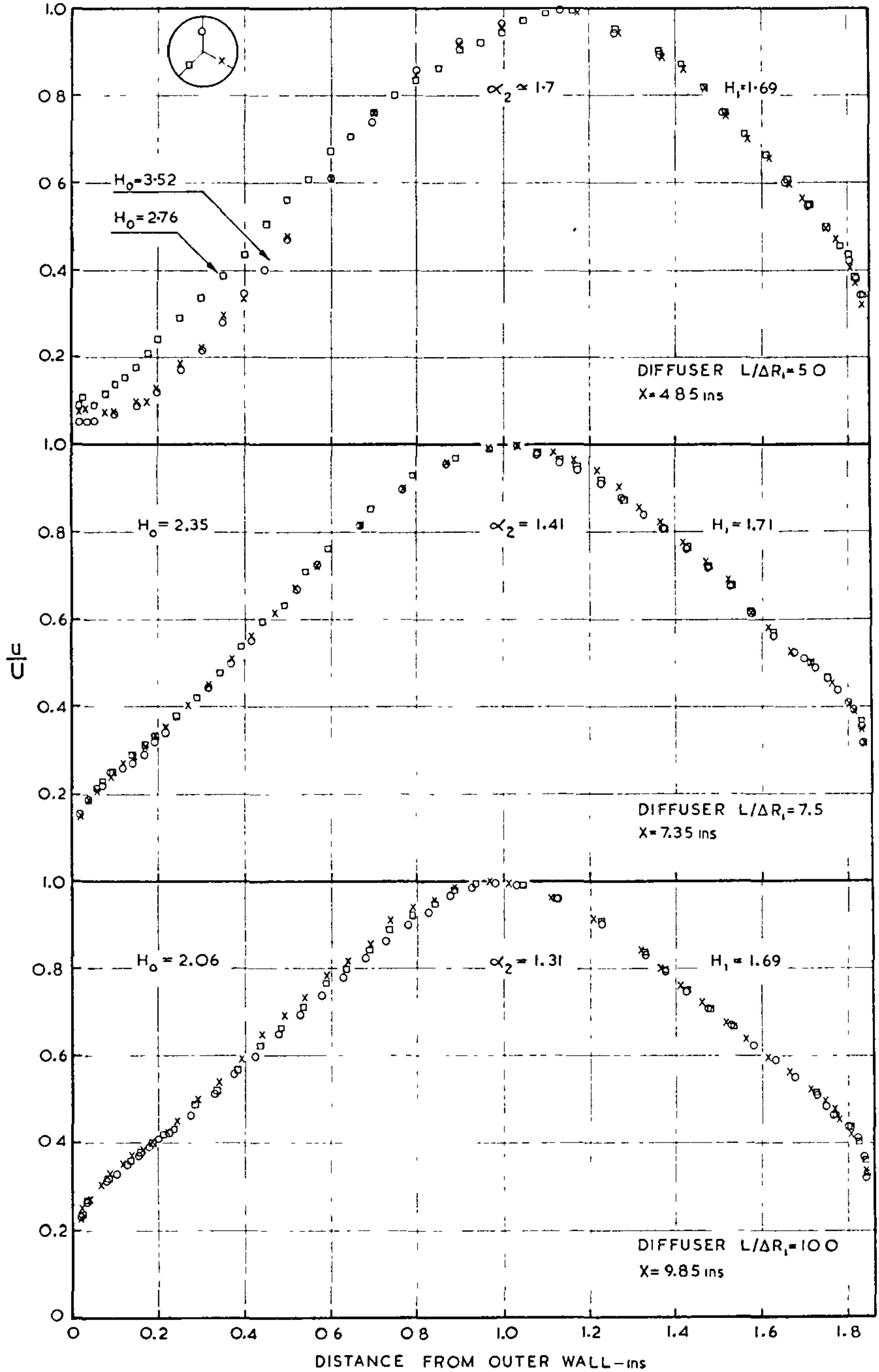

FIG. 4-2-1 DIFFUSER OUTLET VELOCITY PROFILES

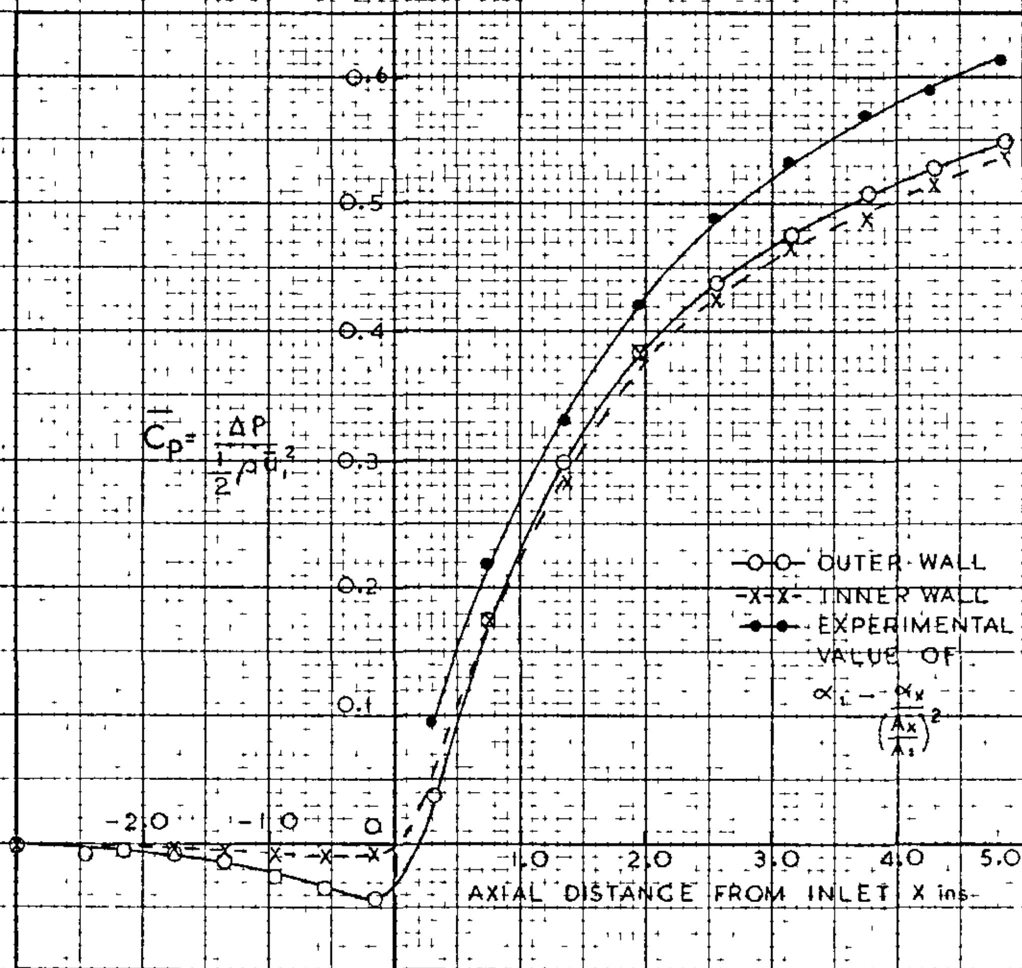

FIG. 4-3-1 STATIC PRESSURE RECOVERY IN THE $L/\Delta R_1 = 5.0$ DIFFUSER

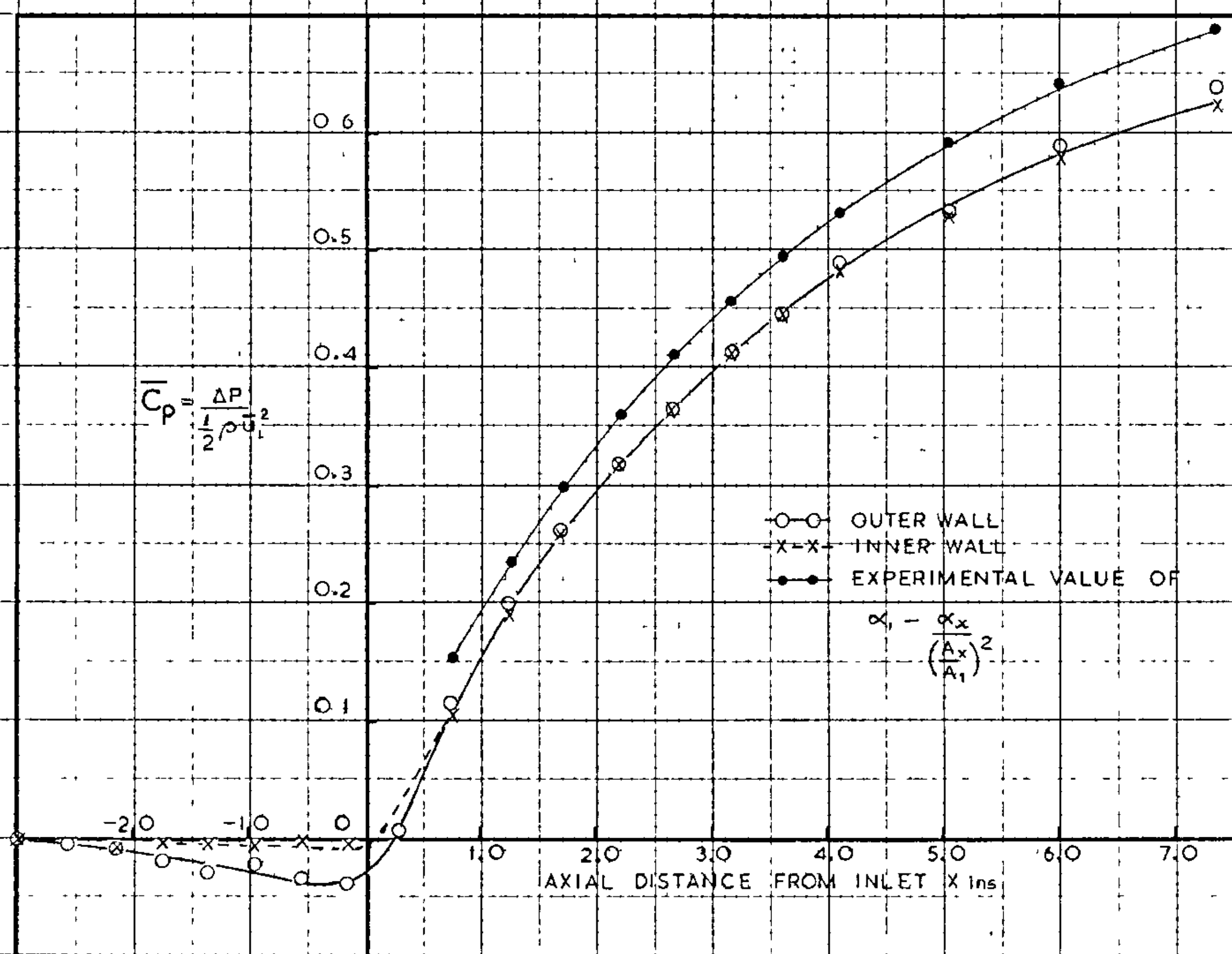

FIG. 4-3-2 STATIC PPESSURE RECOVERY IN THE $L/\Delta R_1 = 7.5$ DIFFUSER

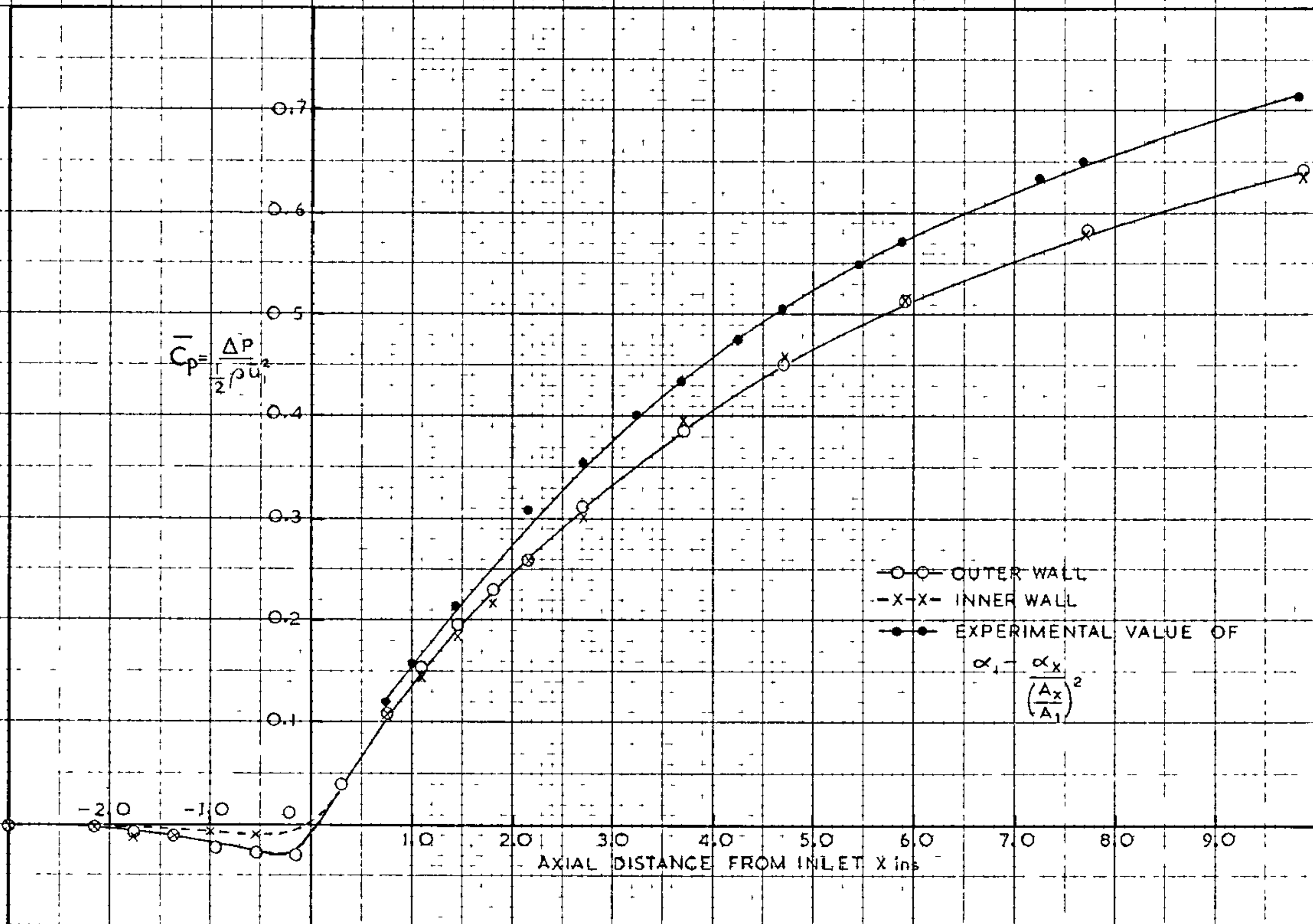

FIG. 4-3-3 STATIC PRESSURE RECOVERY IN THE $L/\Delta R_1 = 10.0$ DIFFUSER

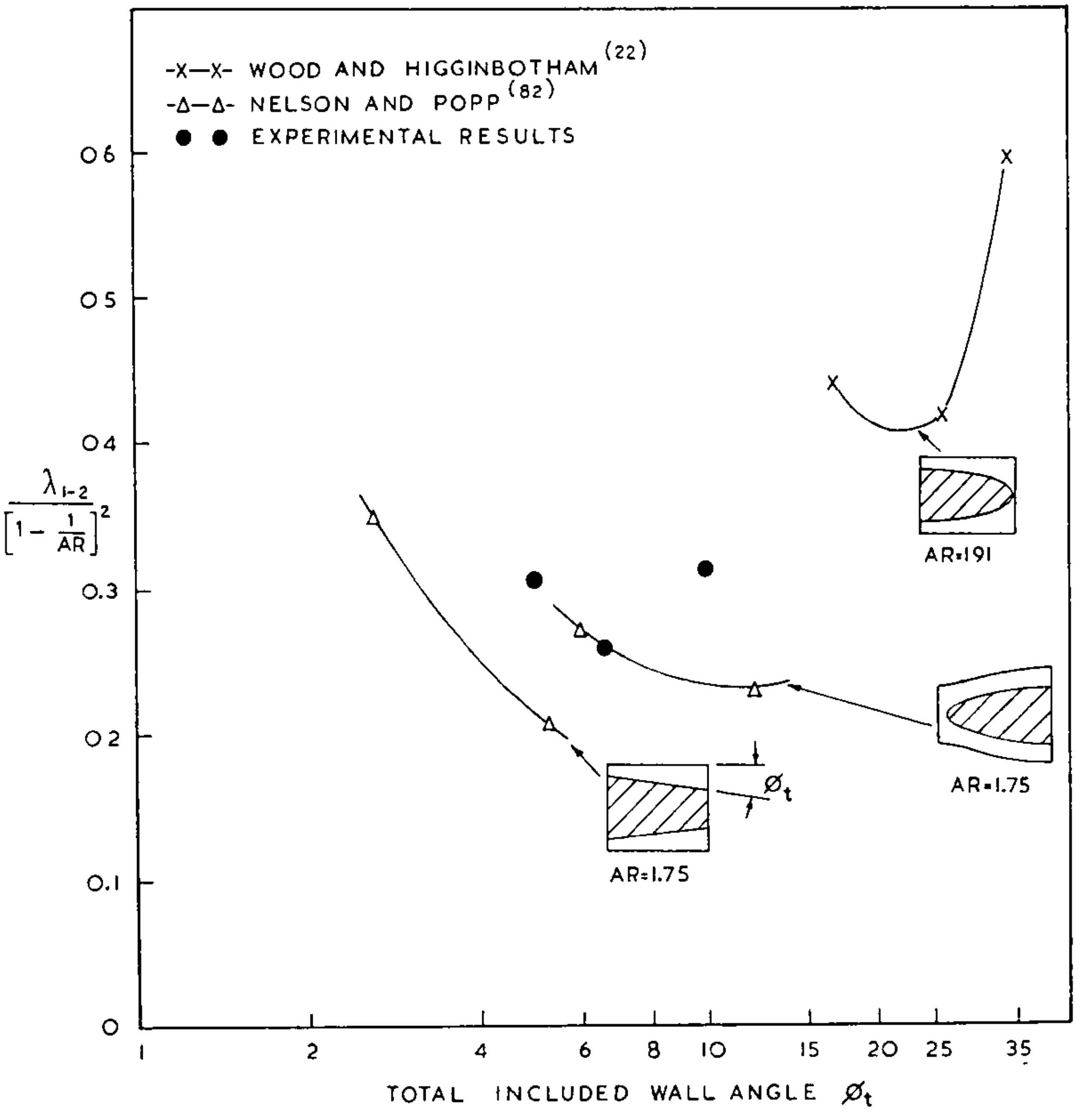

FIG. 4-5-1 COMPARISON OF ANNULAR DIFFUSER LOSS COEFFICIENTS

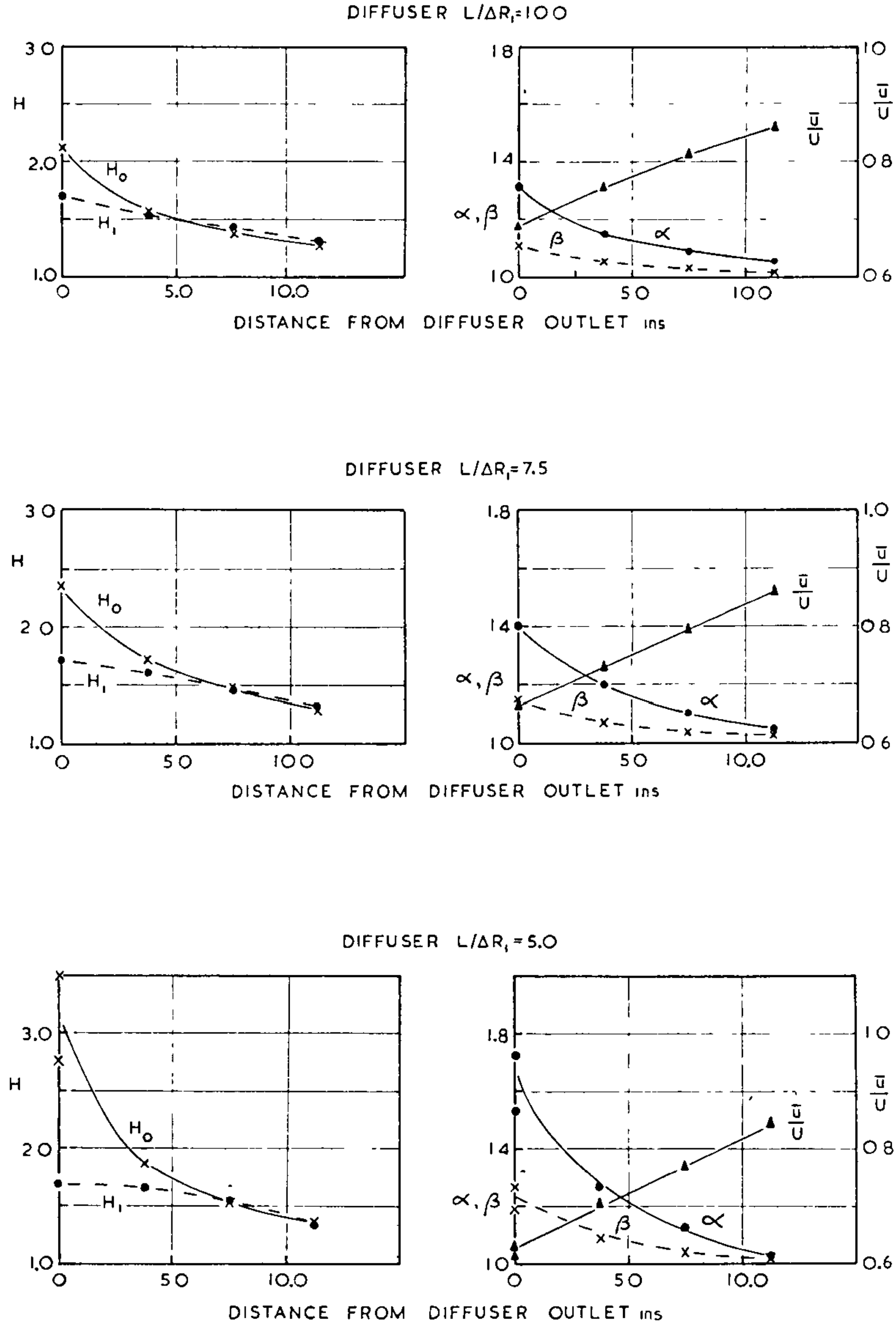

FIG. 4-6-1 VARIATION OF BOUNDARY LAYER PARAMETERS ALONG DOWNSTREAM SETTLING LENGTH

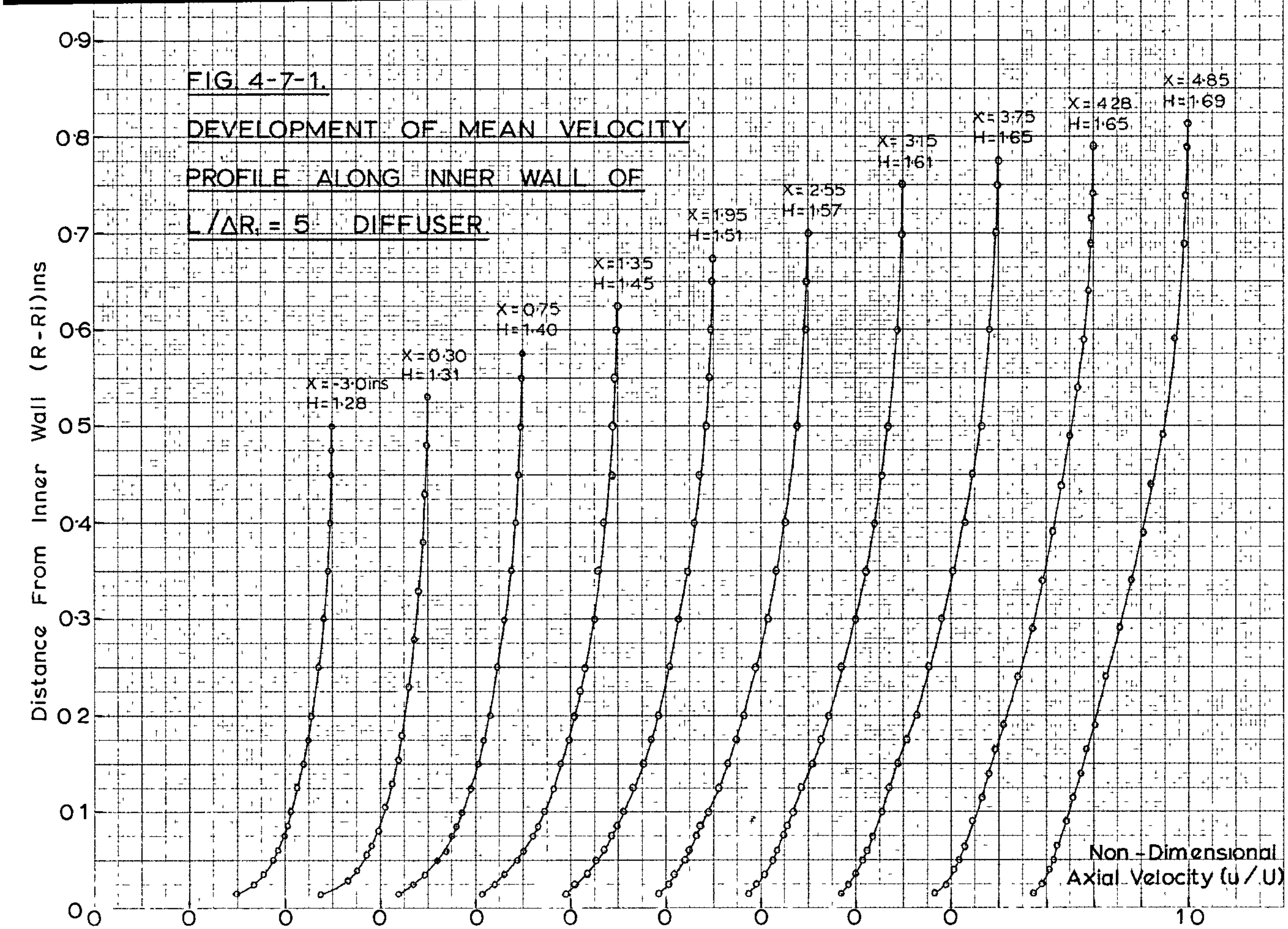

FIG. 4-7-1.
DEVELOPMENT OF MEAN VELOCITY
PROFILE ALONG INNER WALL OF
L/ΔR₁ = 5 DIFFUSER.
X = -3·0ins H = 1·28
X = 0·30 H = 1·31
X = 0·75 H = 1·40
X = 1·35 H = 1·45
X = 1·95 H = 1·51
X = 2·55 H = 1·57
X = 3·15 H = 1·61
X = 3·75 H = 1·65
X = 4·28 H = 1·65
X = 4·85 H = 1·69
Distance From Inner Wall (R-Ri) ins
0·9
0·8
0·7
0·6
0·5
0·4
0·3
0·2
0·1
0
Non-Dimensional Axial Velocity (u/U)
1·0

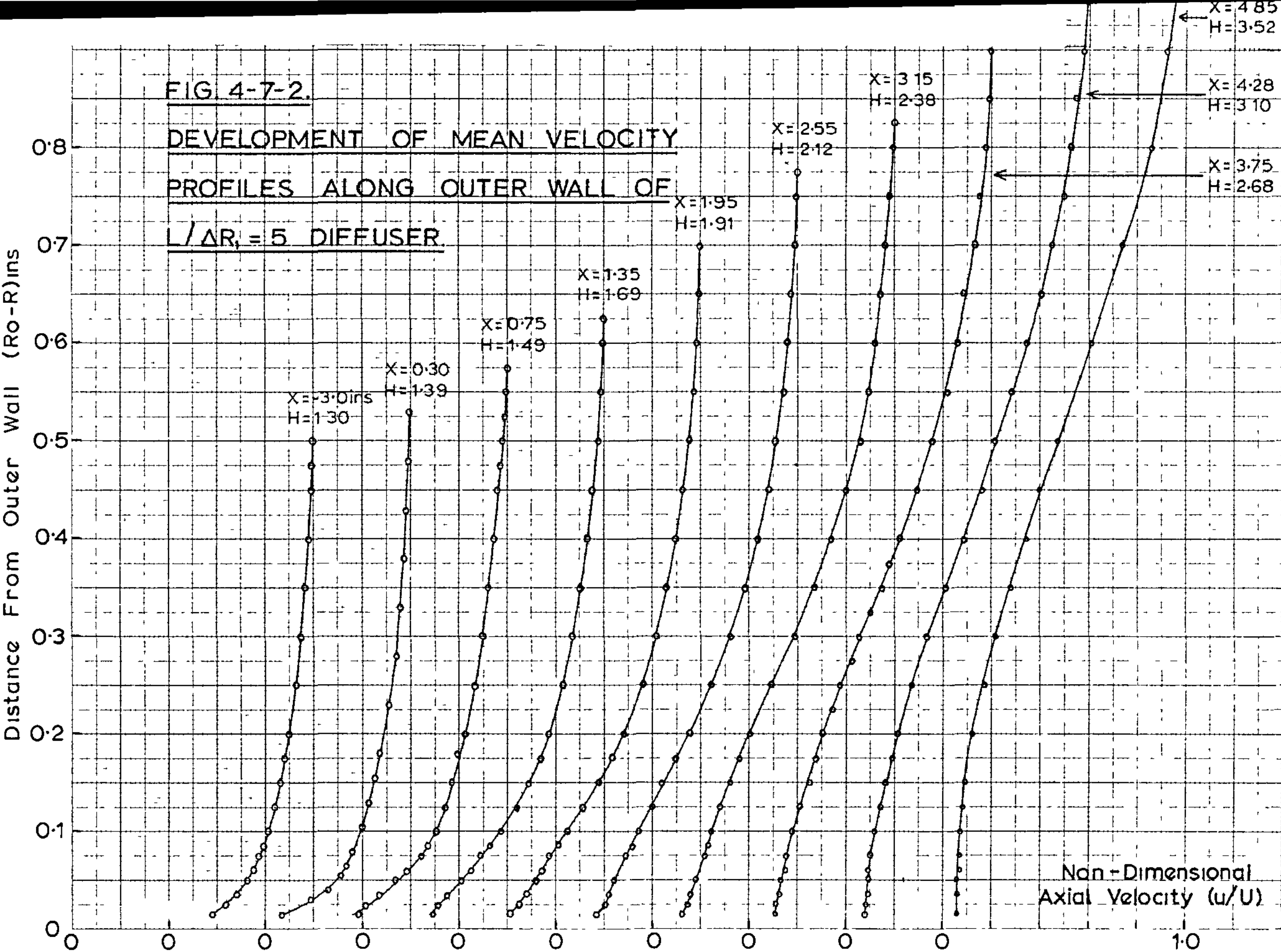

FIG. 4-7-2.
DEVELOPMENT OF MEAN VELOCITY PROFILES ALONG OUTER WALL OF $L/\Delta R_1 = 5$ DIFFUSER.

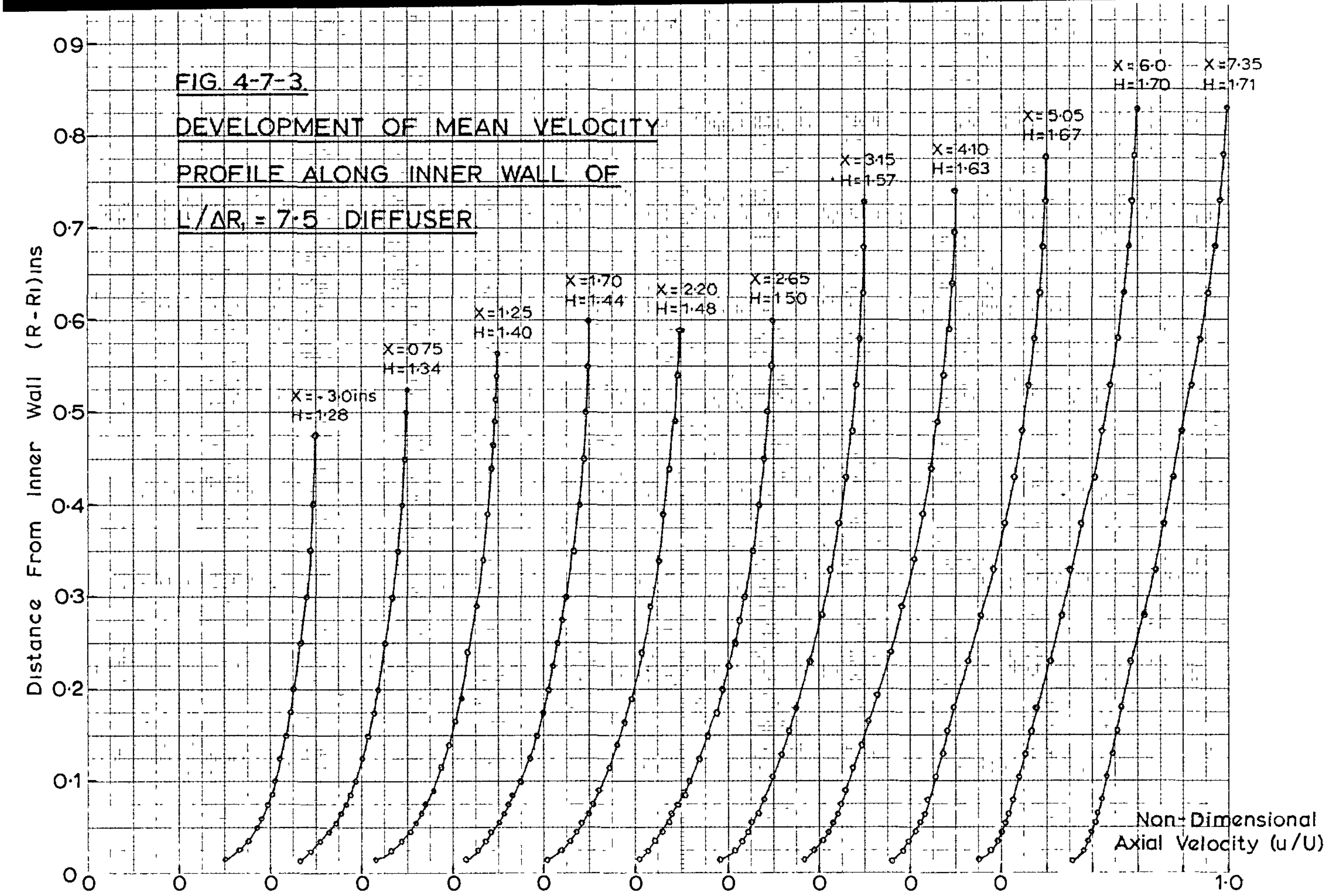

FIG. 4-7-3.
DEVELOPMENT OF MEAN VELOCITY PROFILE ALONG INNER WALL OF $L/\Delta R_1 = 7\cdot5$ DIFFUSER

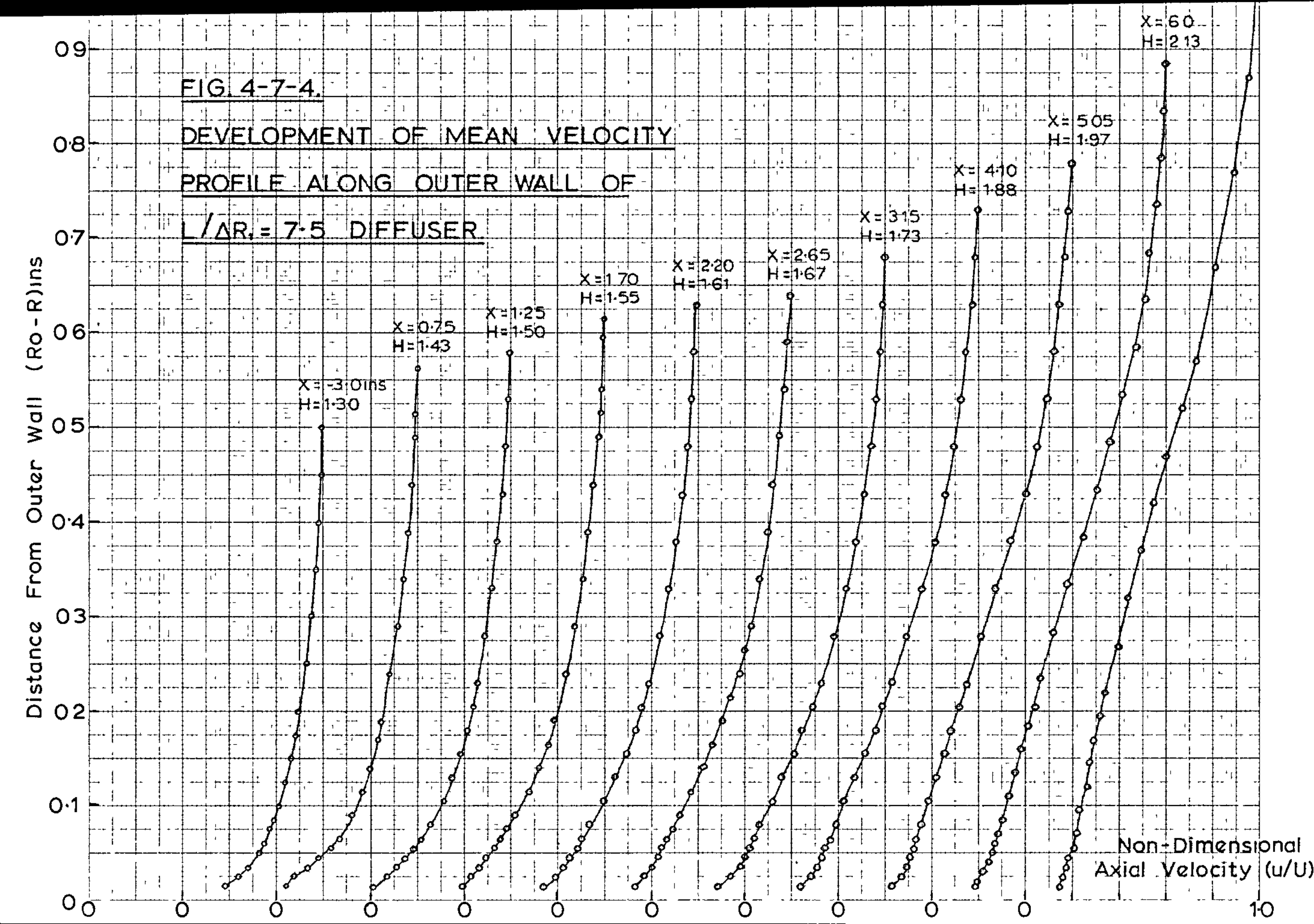

FIG. 4-7-4.
DEVELOPMENT OF MEAN VELOCITY PROFILE ALONG OUTER WALL OF L/ΔR₁ = 7·5 DIFFUSER
Distance From Outer Wall (Ro-R)ins
Non-Dimensional Axial Velocity (u/U)
X=-3·0ins H=1·30
X=0·75 H=1·43
X=1·25 H=1·50
X=1·70 H=1·55
X=2·20 H=1·61
X=2·65 H=1·67
X=3·15 H=1·73
X=4·10 H=1·88
X=5·05 H=1·97
X=6·0 H=2·13
0·9
0·8
0·7
0·6
0·5
0·4
0·3
0·2
0·1
0
1·0

96

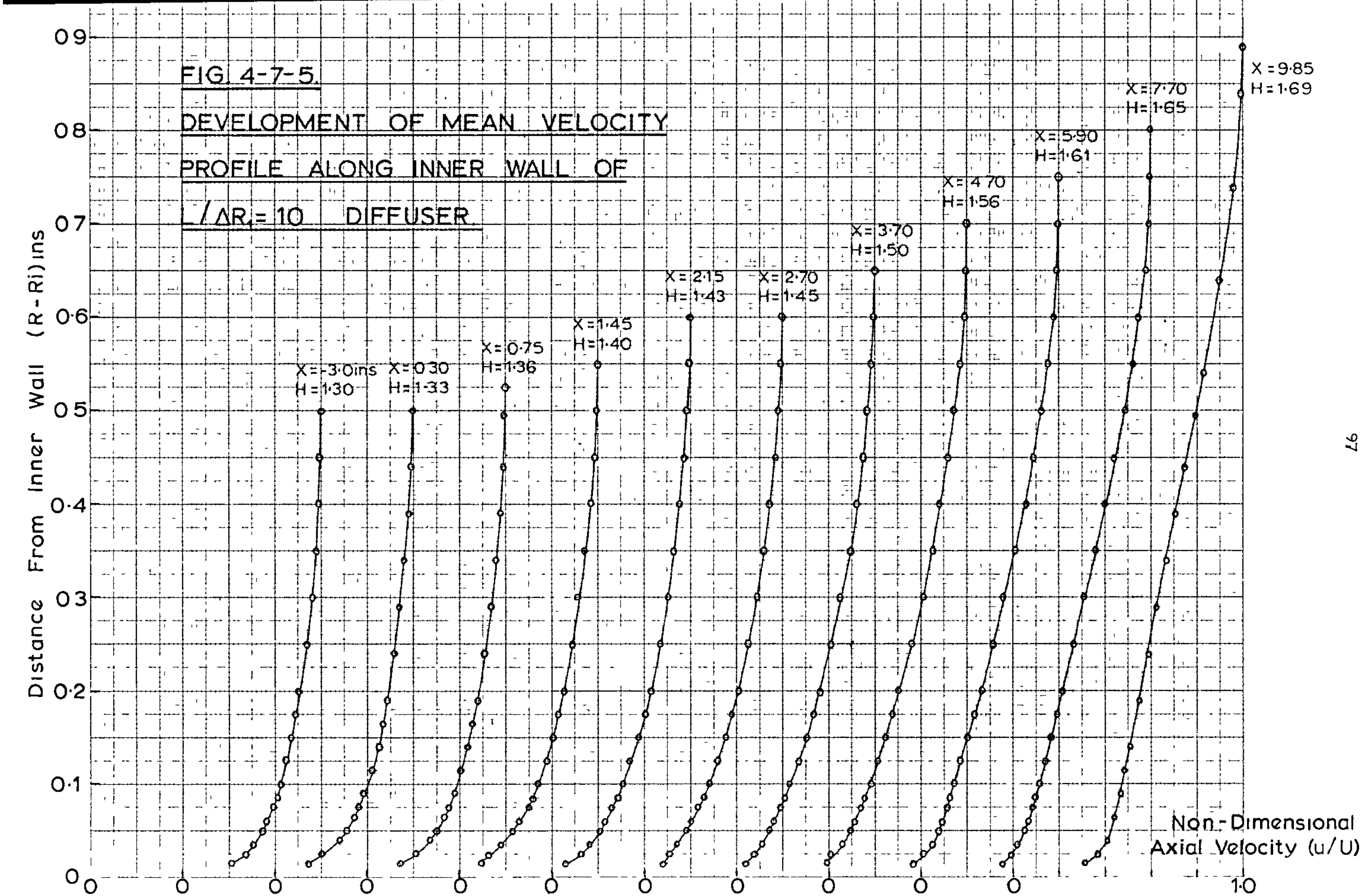

FIG. 4-7-5.
DEVELOPMENT OF MEAN VELOCITY PROFILE ALONG INNER WALL OF $L/\Delta R_1 = 10$ DIFFUSER

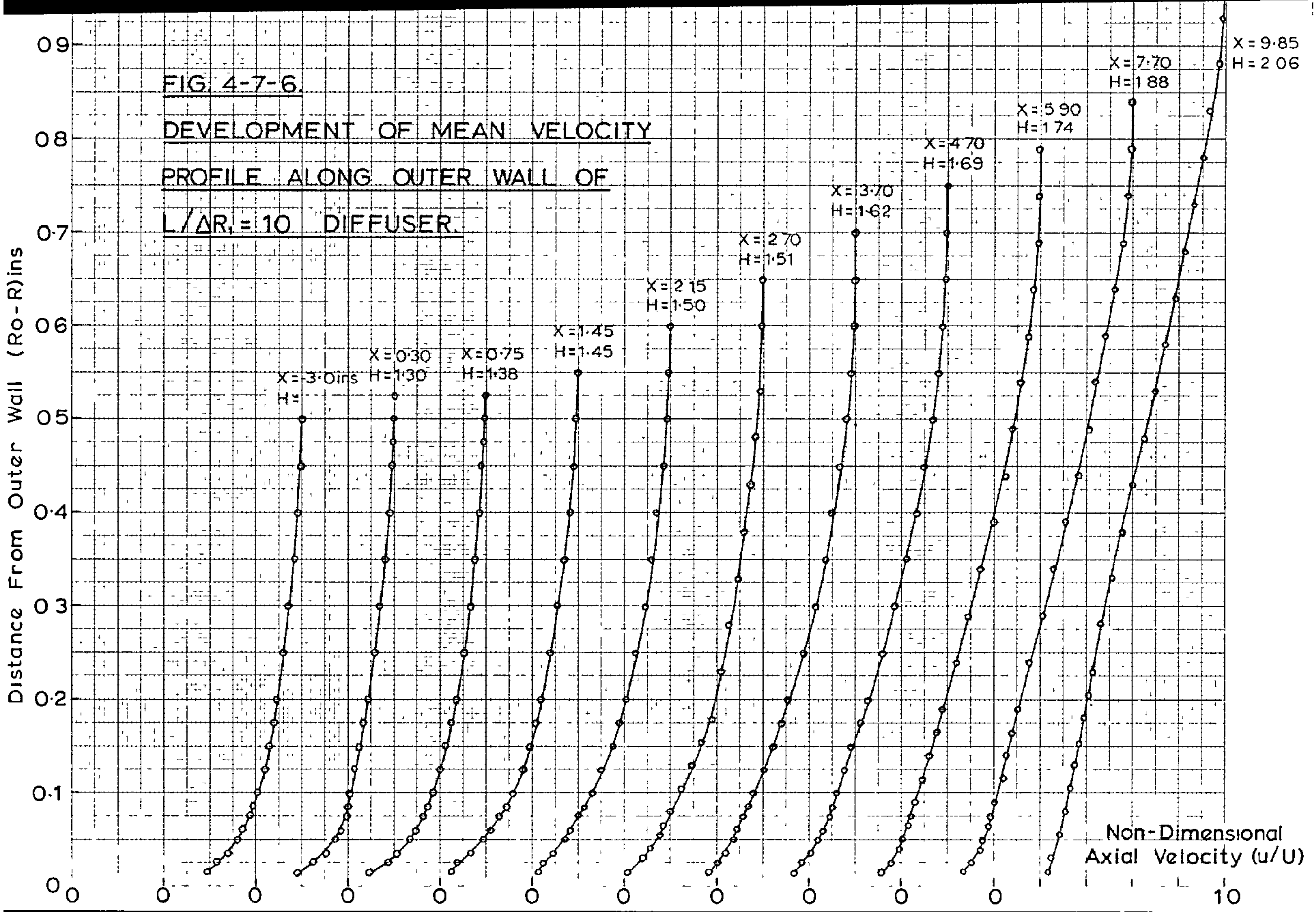

FIG. 4-7-6.
DEVELOPMENT OF MEAN VELOCITY PROFILE ALONG OUTER WALL OF L/ΔR, = 10 DIFFUSER.

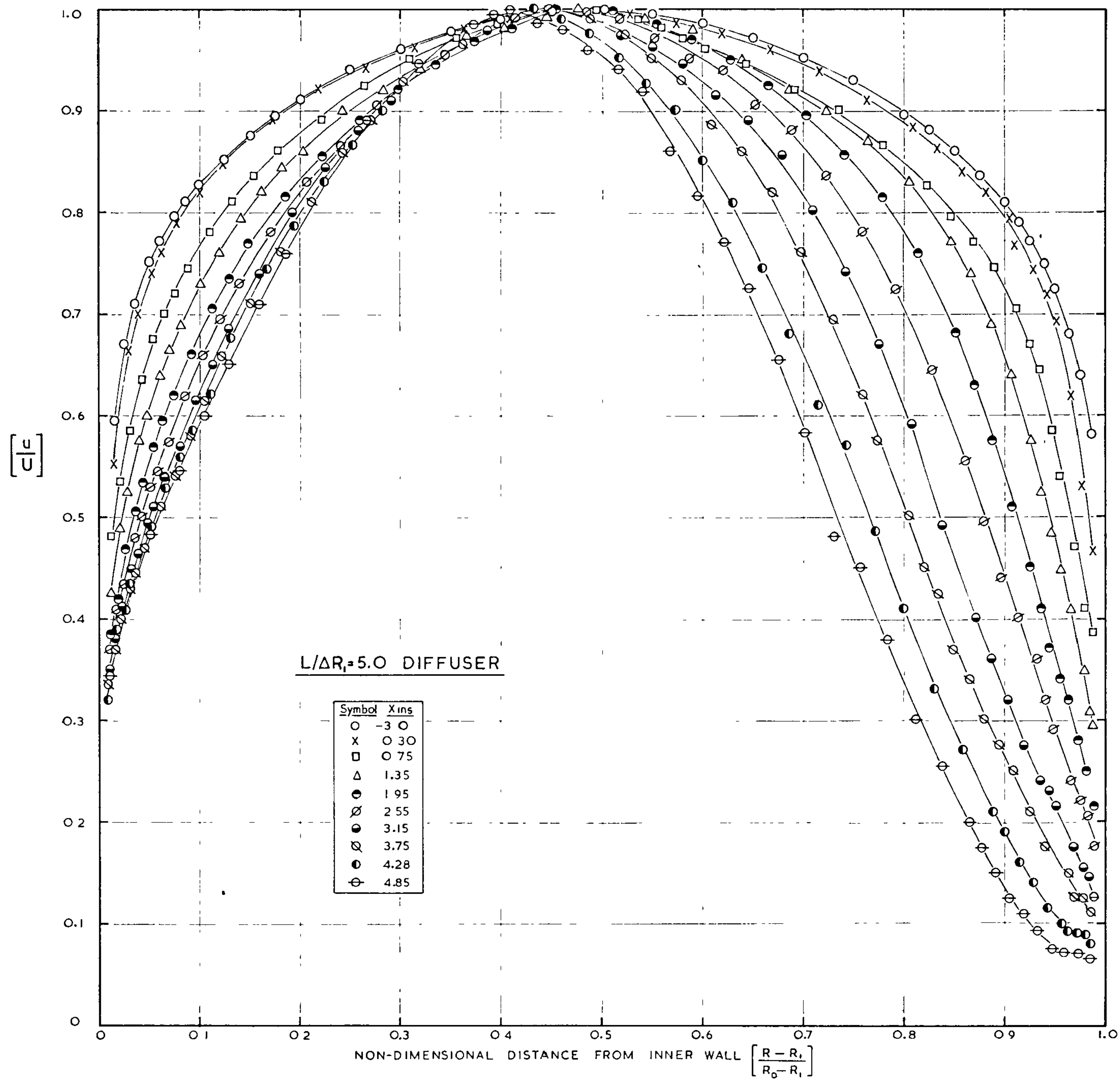

FIG. 4-7-7 NON-DIMENSIONAL VELOCITY PROFILES ALONG THE L/ΔR₁ = 5.0 DIFFUSER

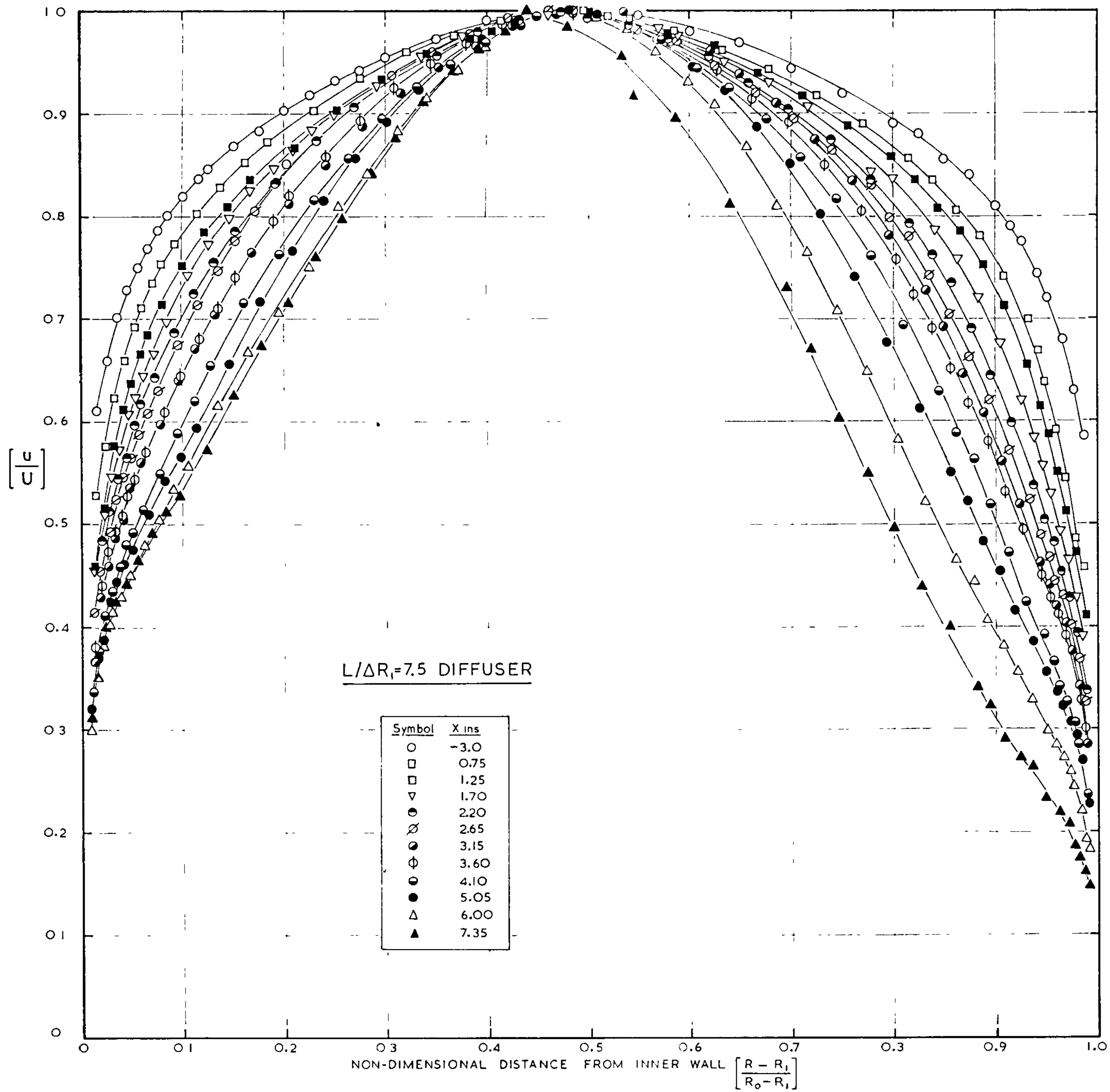

FIG. 4-7-8 NON-DIMENSIONAL VELOCITY PROFILES ALONG THE $L/\Delta R_1 = 7.5$ DIFFUSER

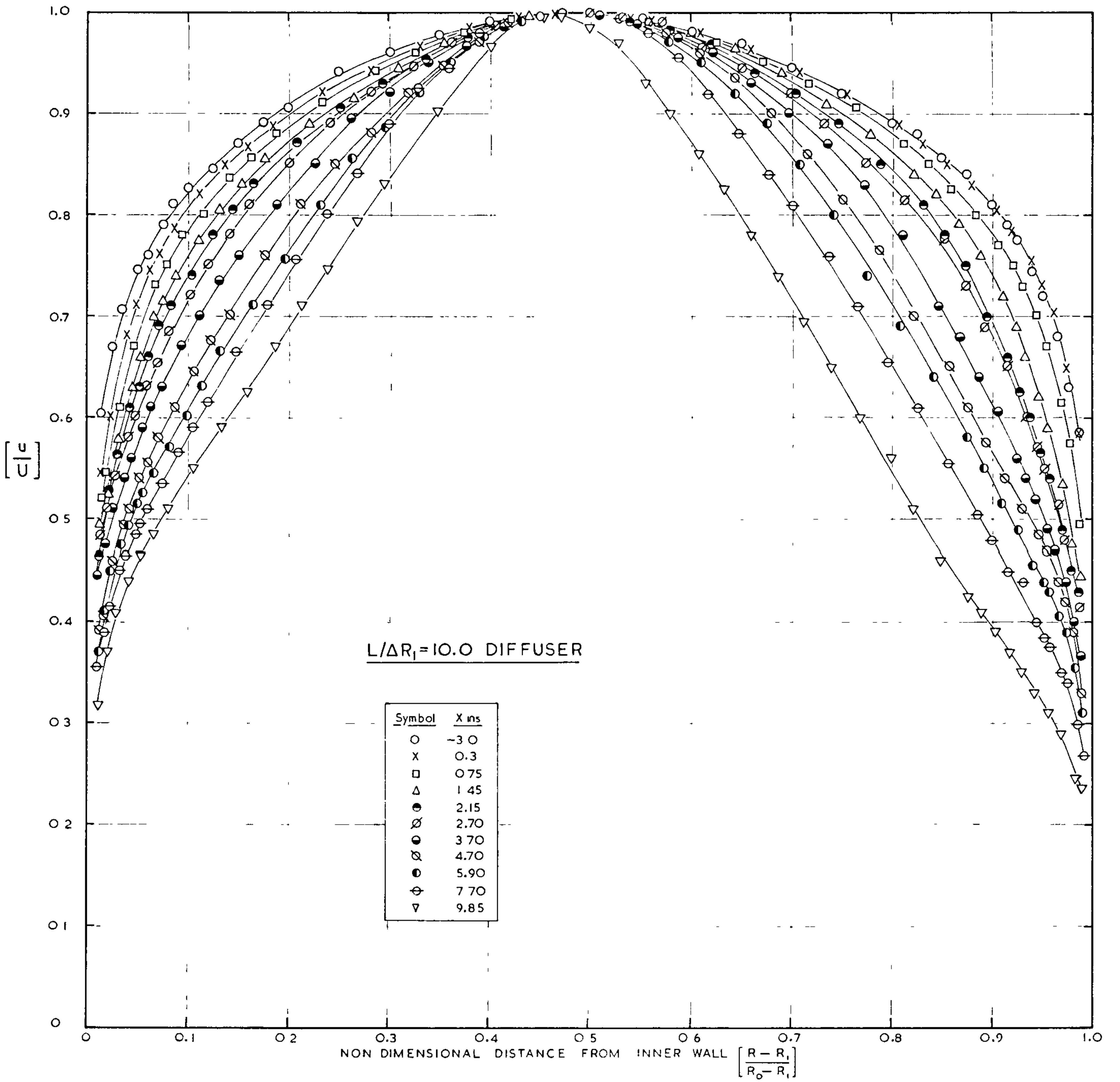

FIG. 4-7-9 NON DIMENSIONAL VELOCITY PROFILES ALONG THE $L/\Delta R_1 = 10.0$ DIFFUSER

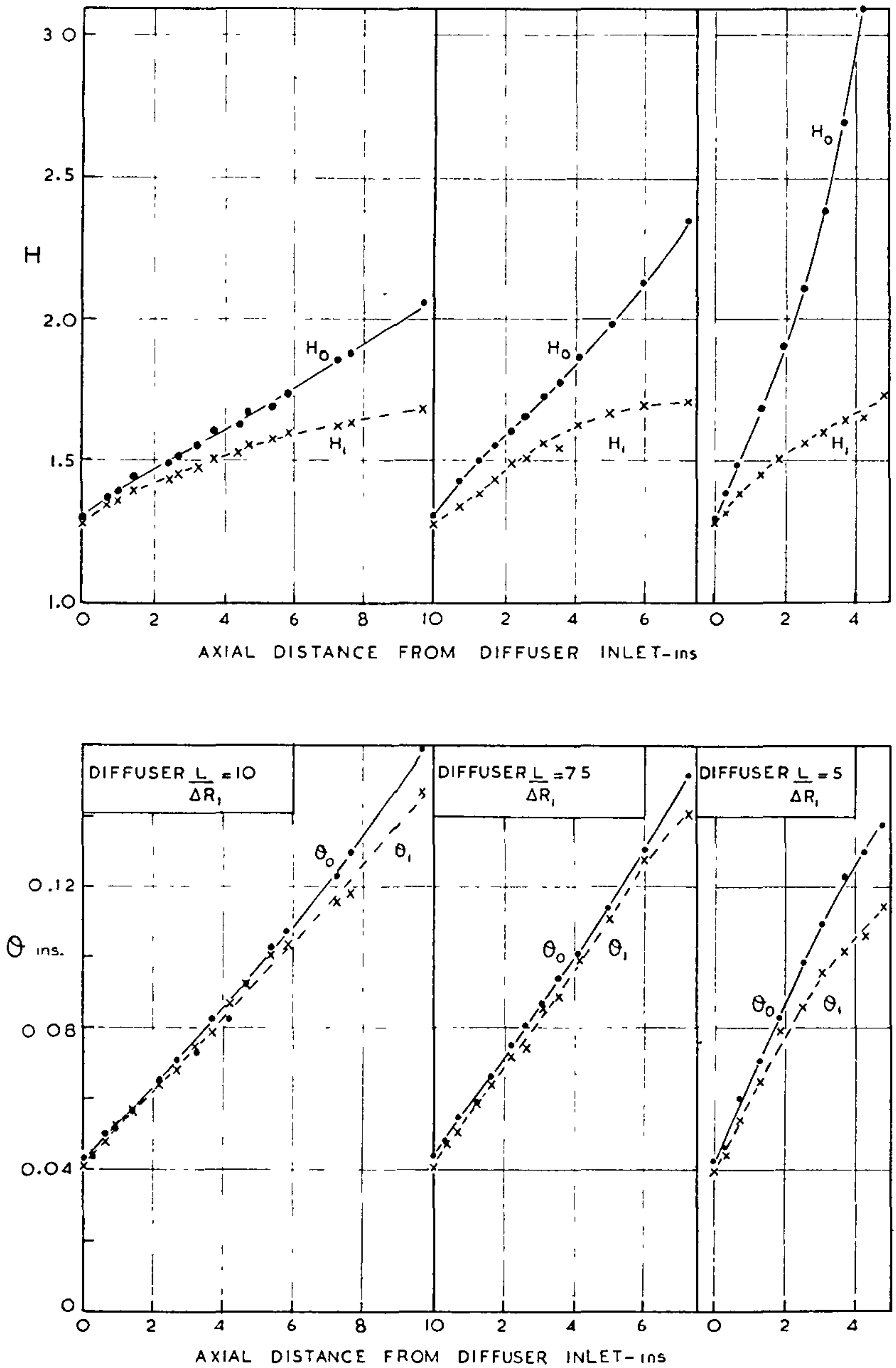

FIG. 4-7-10 VARIATION OF BOUNDARY LAYER PARAMETERS ALONG DIFFUSERS

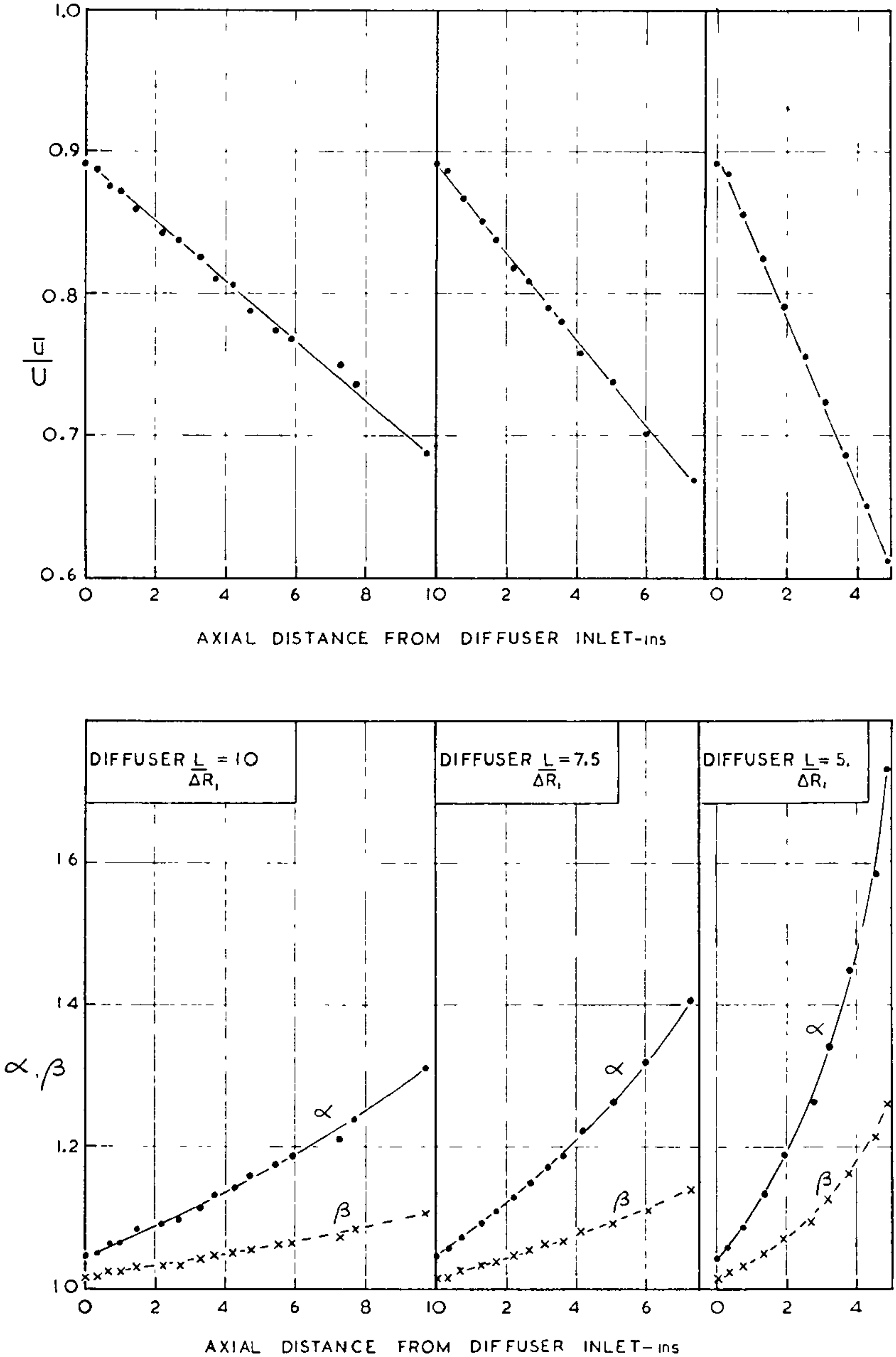

FIG. 4-7-11 VARIATION OF BOUNDARY LAYER PARAMETERS ALONG DIFFUSERS

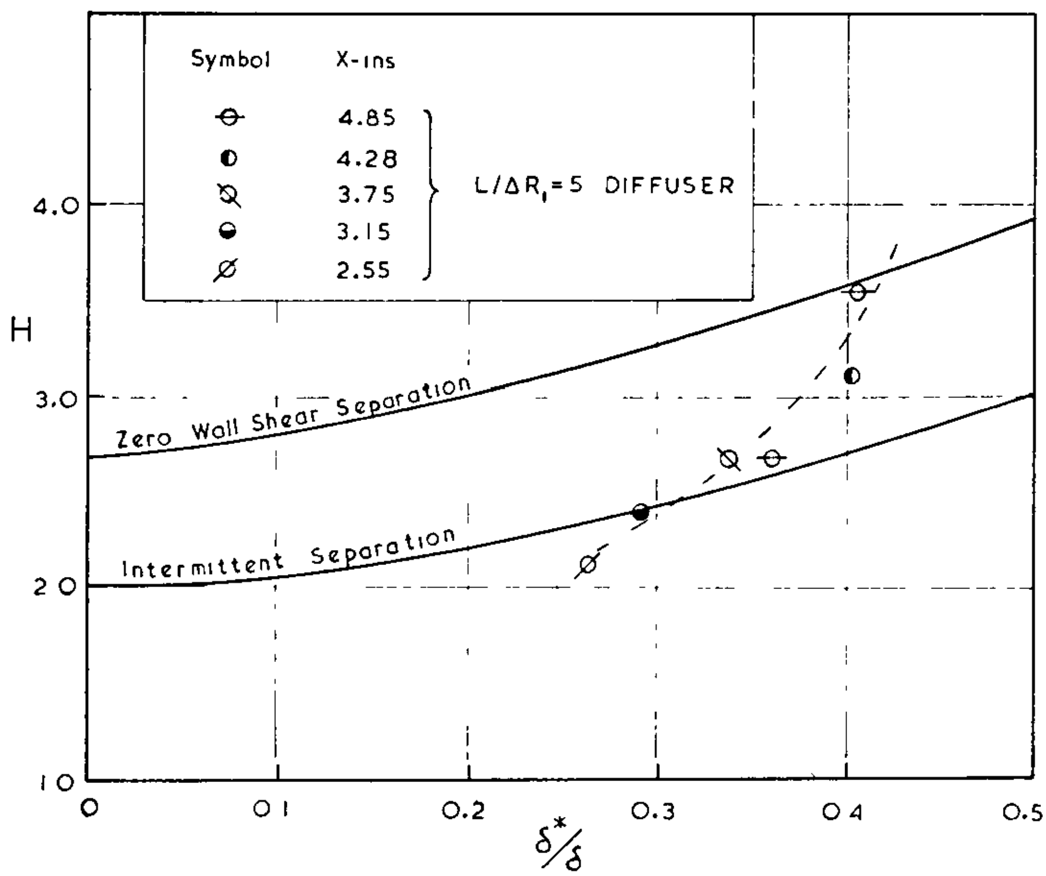

FIG. 4-7-12 COMPARISON OF EXPERIMENTAL DATA WITH SEPARATION CRITERIA DUE TO SANDBORN AND LIU (45)

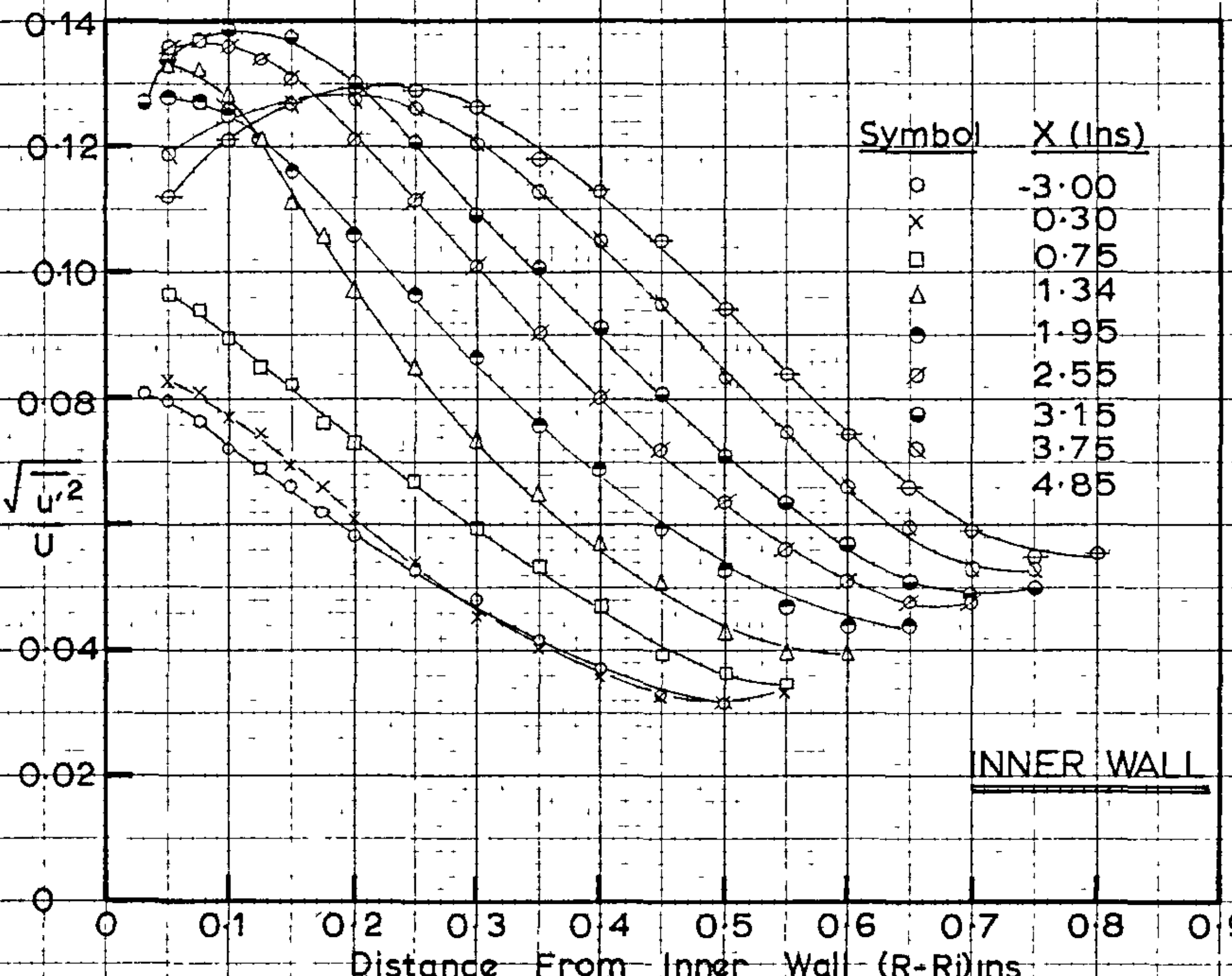

FIG. 4-8-1. EXPERIMENTAL LONGITUDINAL TURBULENCE INTENSITY DISTRIBUTIONS $L/\Delta R = 5$ DIFFUSER.

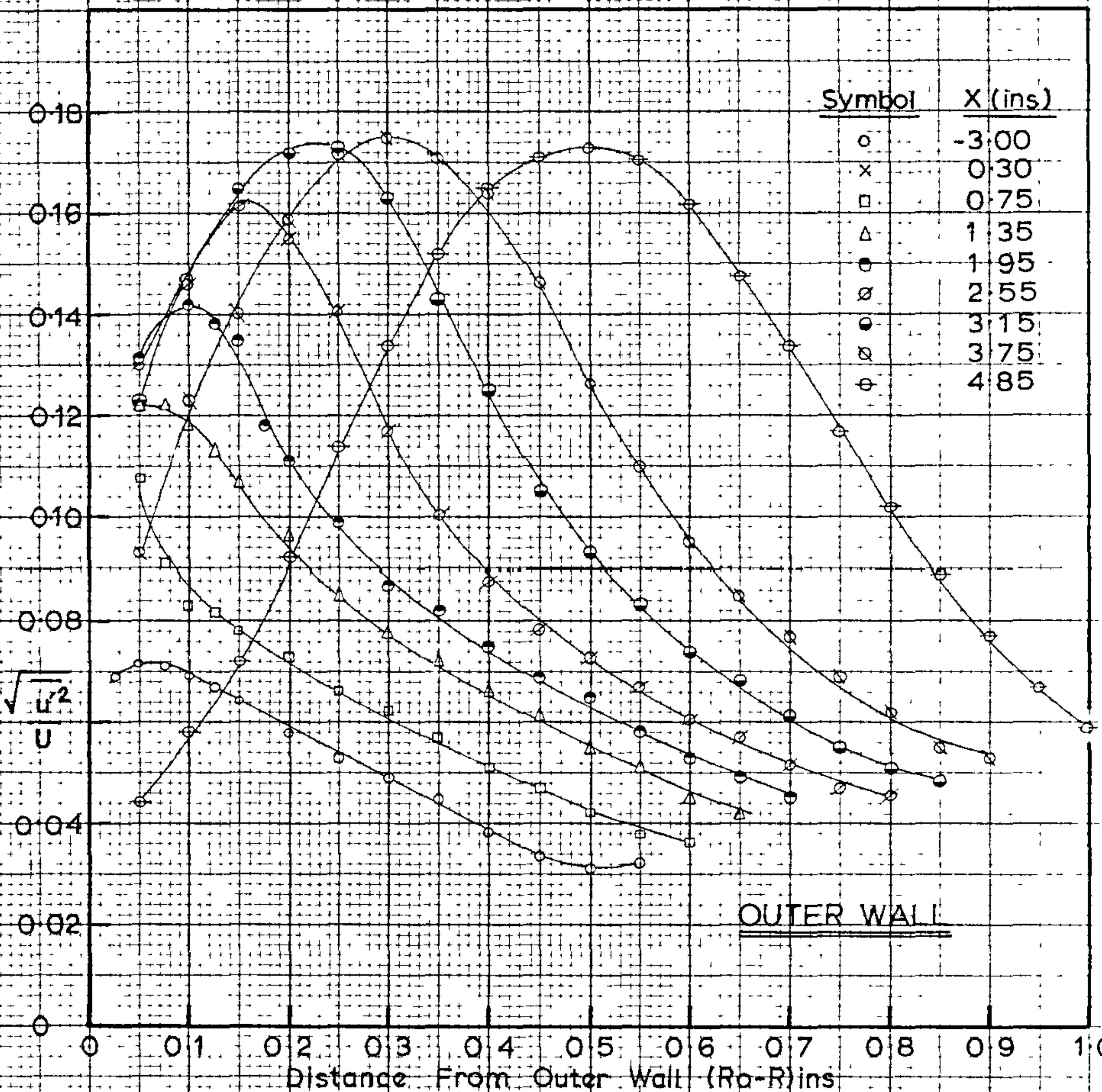

FIG. 4-8-2. EXPERIMENTAL LONGITUDINAL TURBULENCE INTENSITY DISTRIBUTIONS $L/\Delta R = 5$ DIFFUSER.

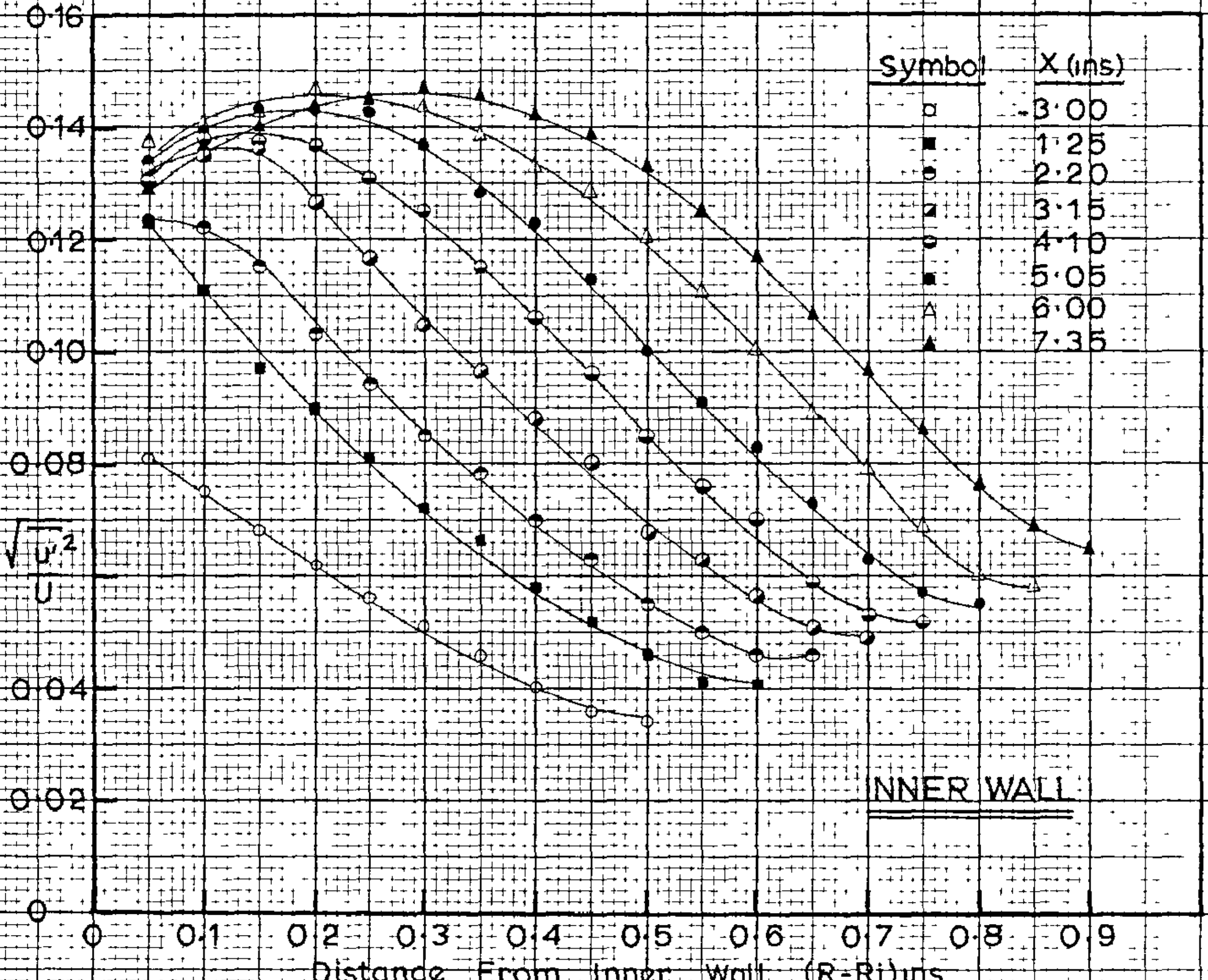

FIG. 4-8-3. EXPERIMENTAL LONGITUDINAL TURBULENCE INTENSITY DISTRIBUTIONS $L/\Delta R_i = 7{\cdot}5$ DIFFUSER

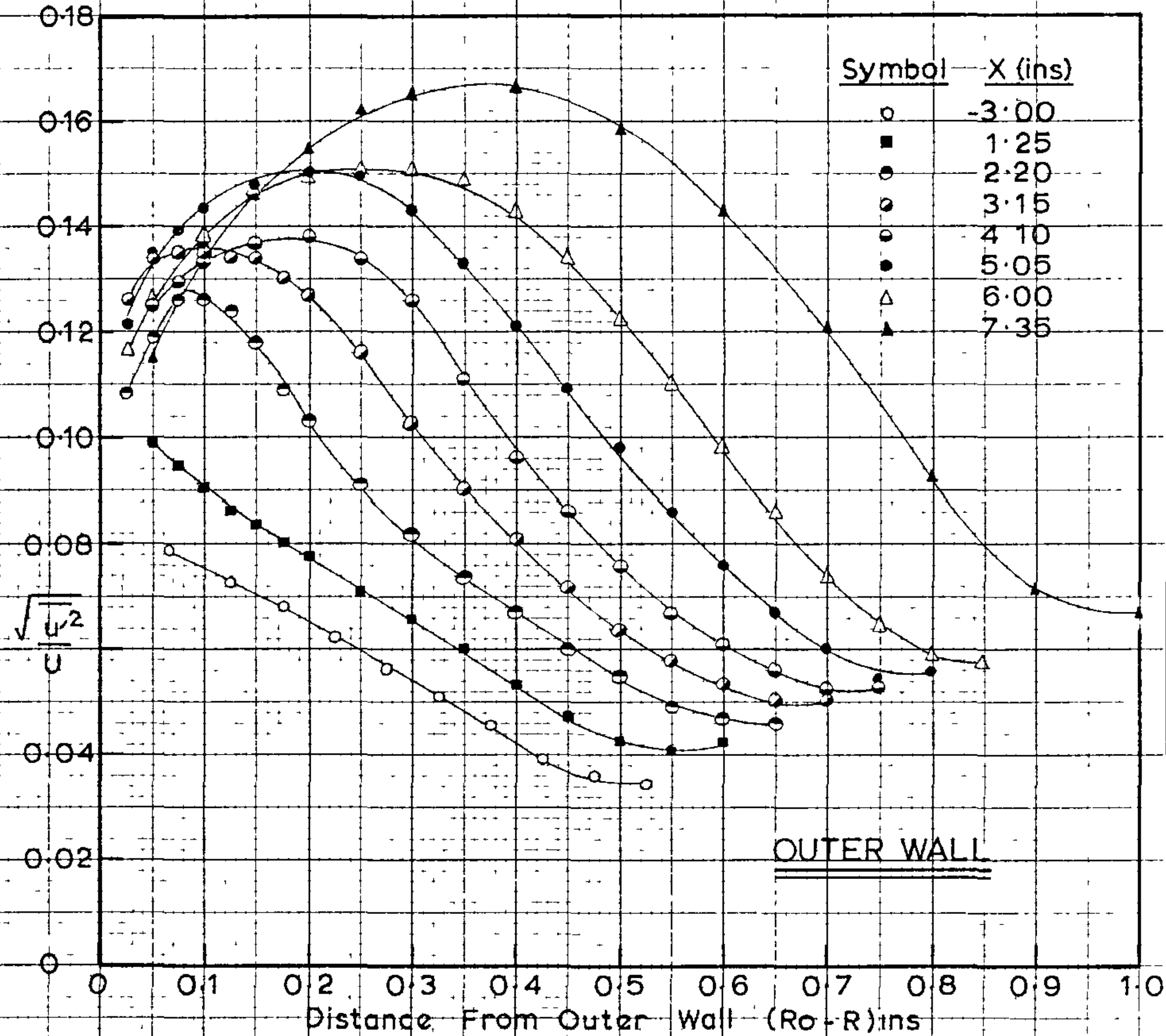

FIG. 4-8-4. EXPERIMENTAL LONGITUDINAL TURBULENCE INTENSITY DISTRIBUTIONS $L/\Delta R_1 = 7{\cdot}5$ DIFFUSER.

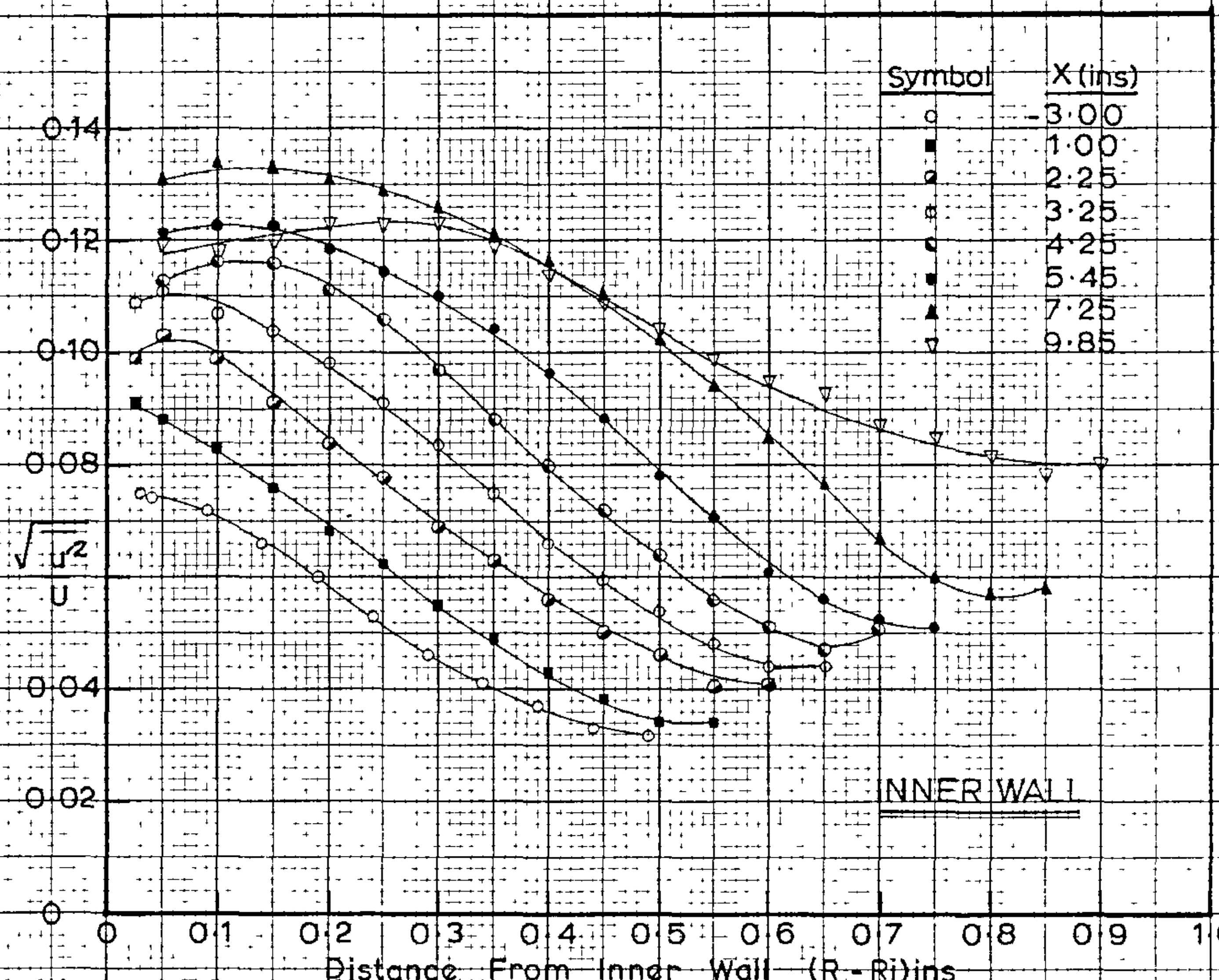

FIG. 4-8-5. EXPERIMENTAL LONGITUDINAL TURBULENCE INTENSITY DISTRIBUTIONS $L/\Delta R_1 = 10$ DIFFUSER.

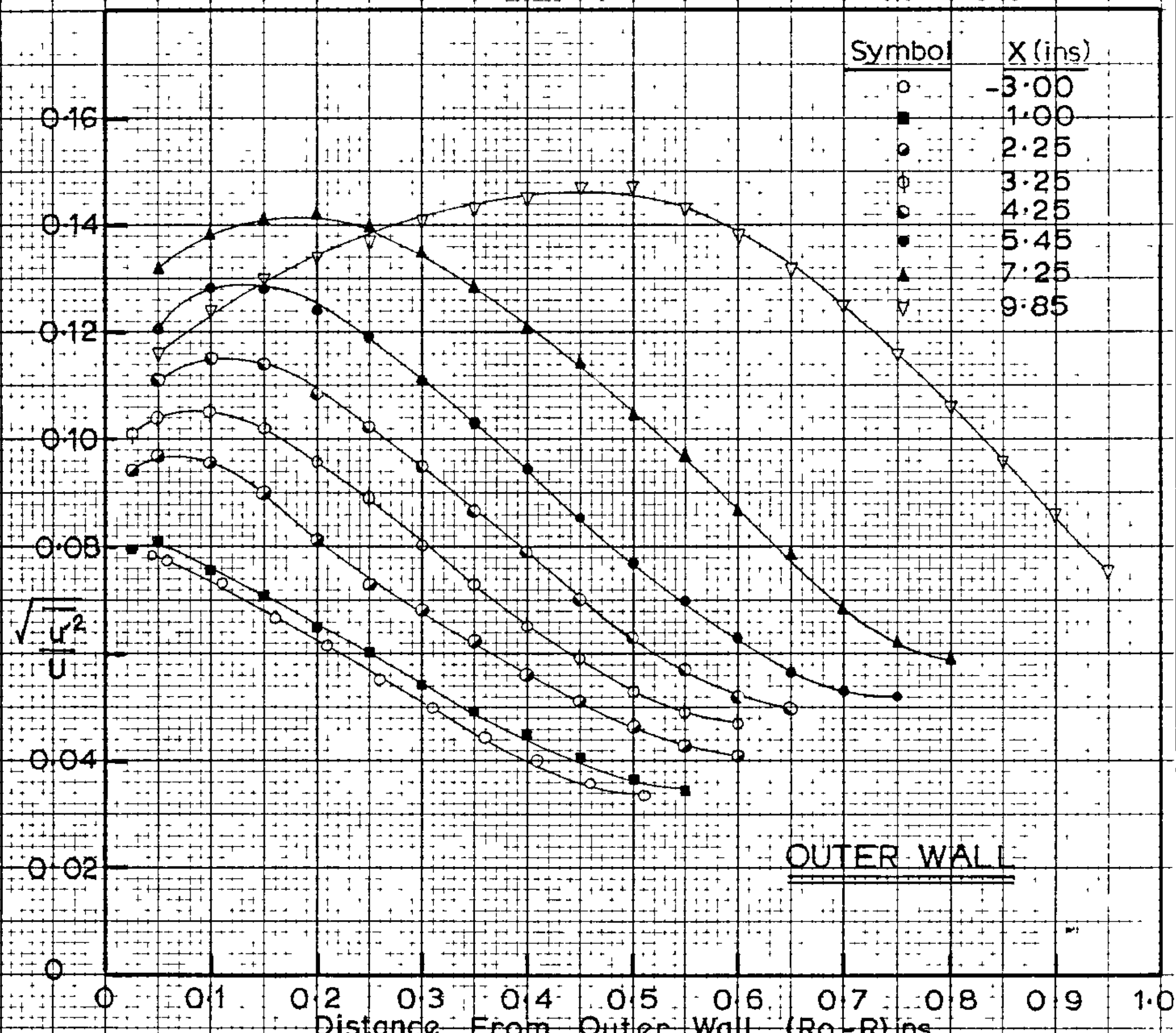

FIG. 4-8-6. EXPERIMENTAL LONGITUDINAL TURBULENCE INTENSITY DISTRIBUTIONS. L/ΔR₁ = 10 DIFFUSER.

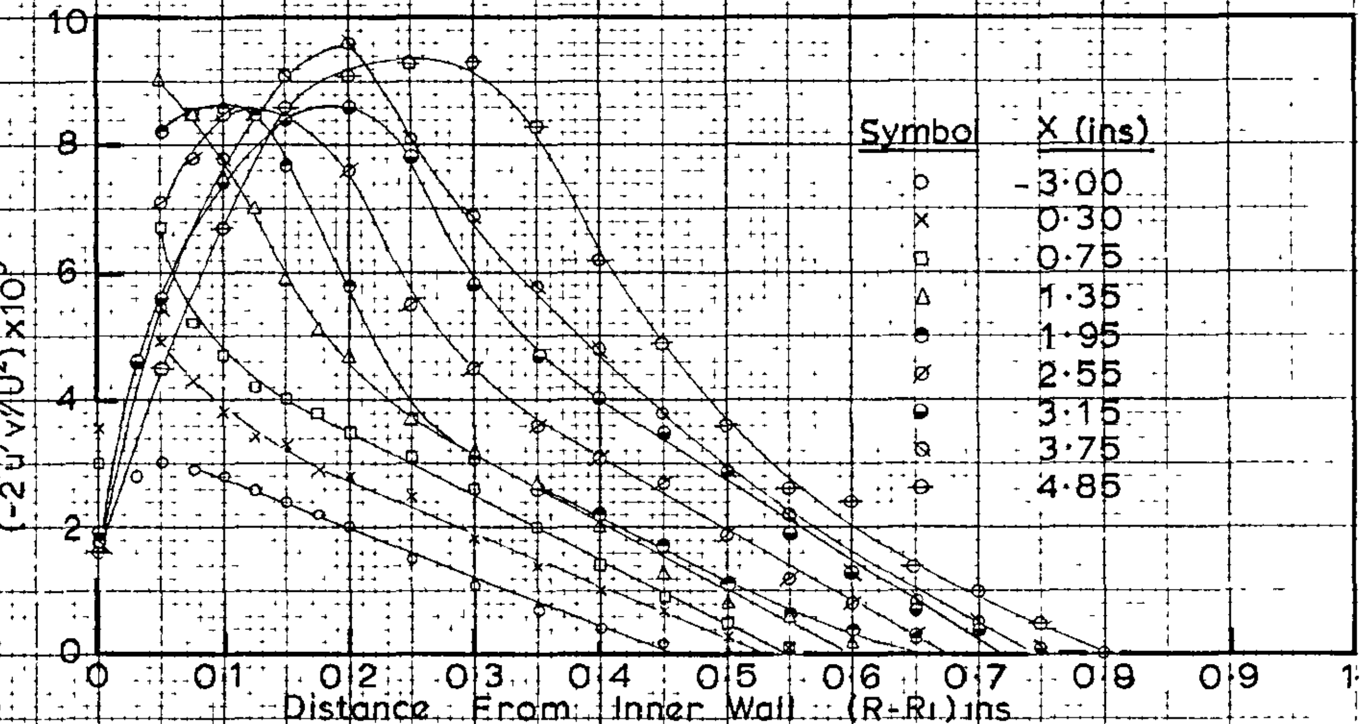

FIG. 4-9-1. EXPERIMENTAL SHEAR STRESS DISTRIBUTIONS

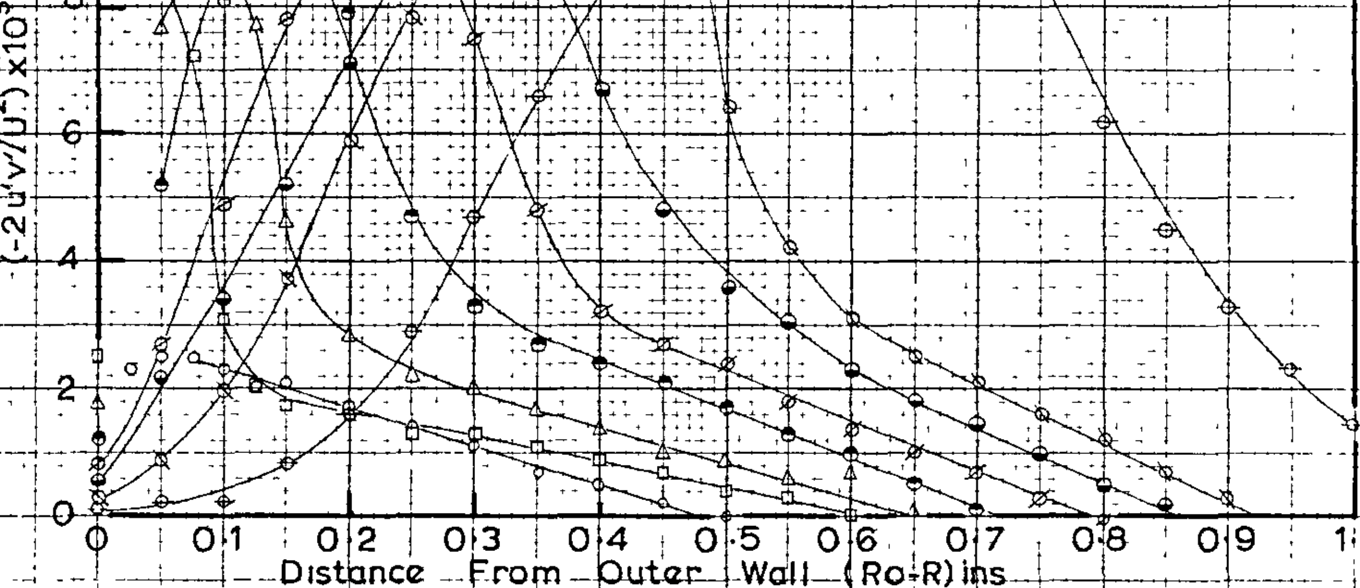

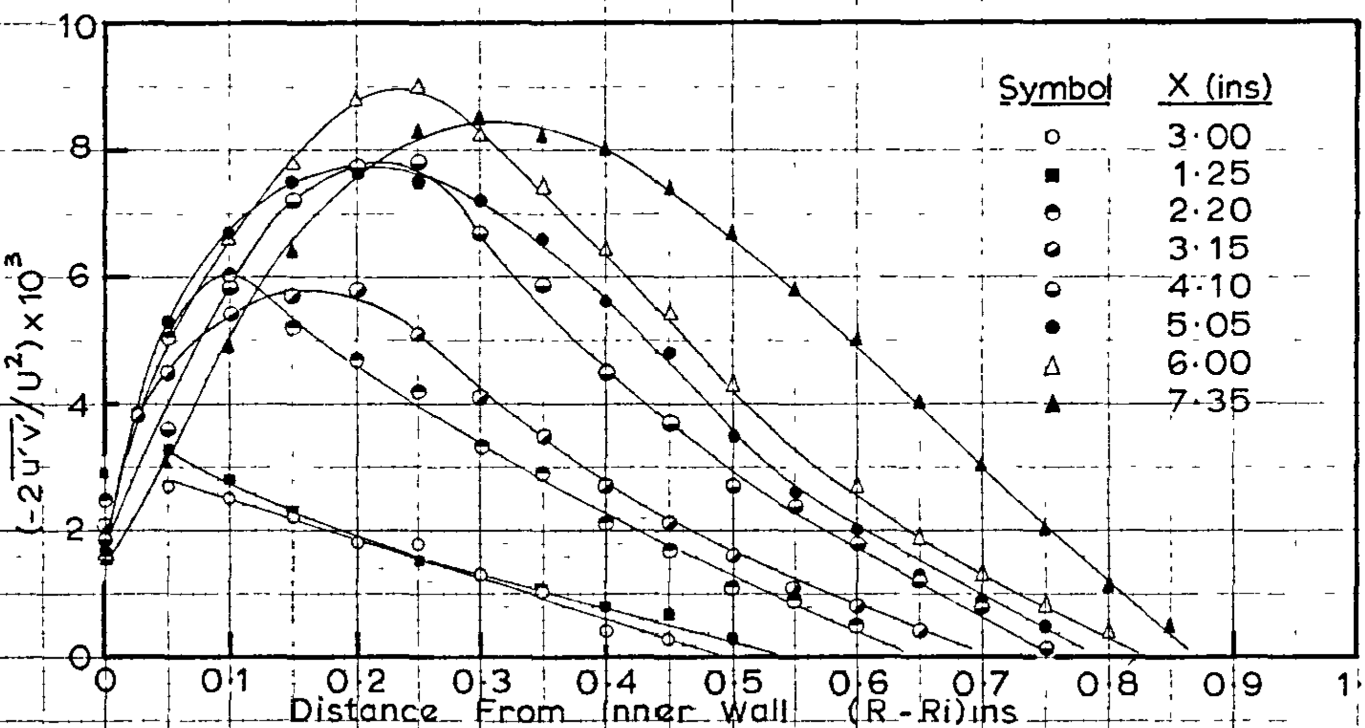

FIG. 4-9-2. EXPERIMENTAL SHEAR STRESS DISTRIBUTIONS.

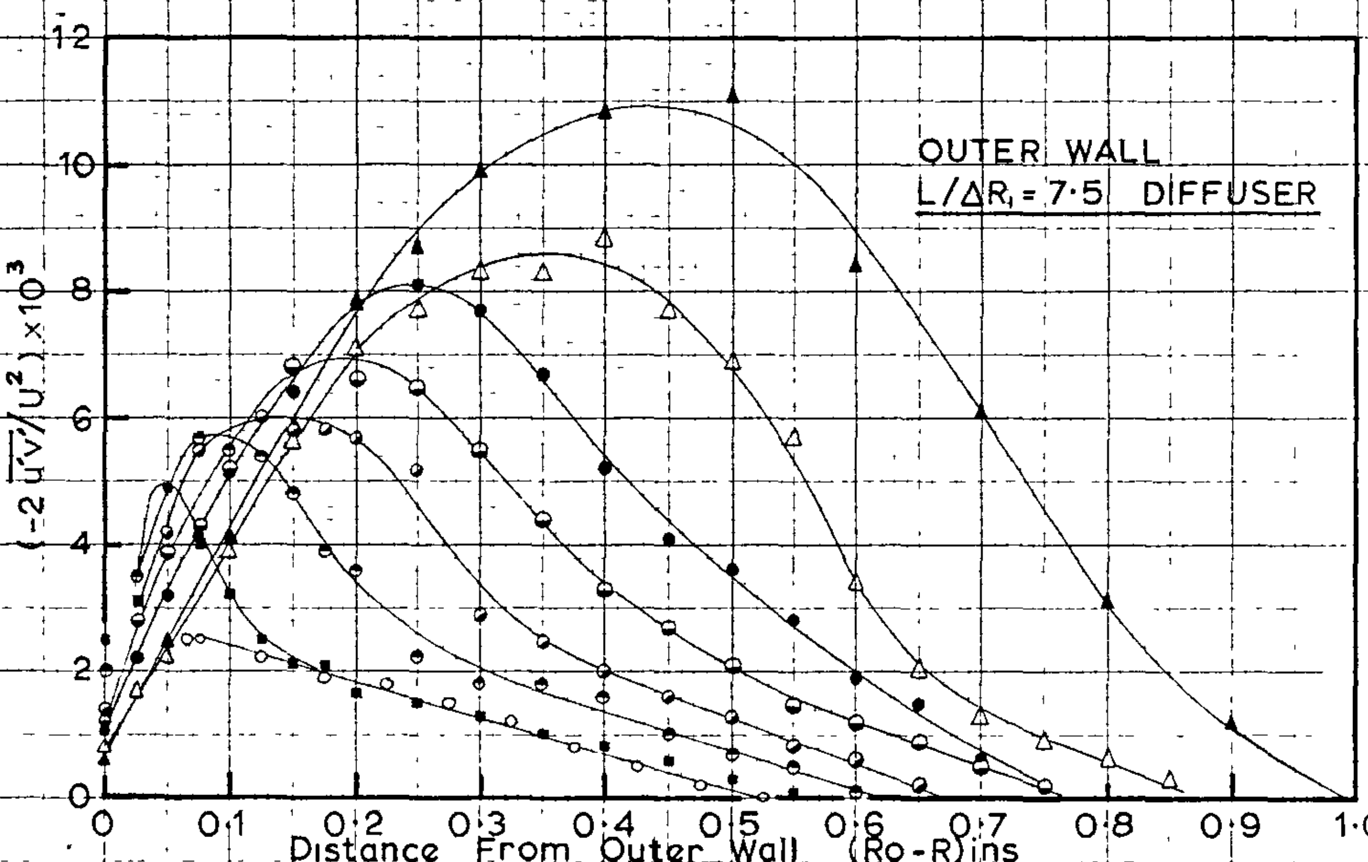

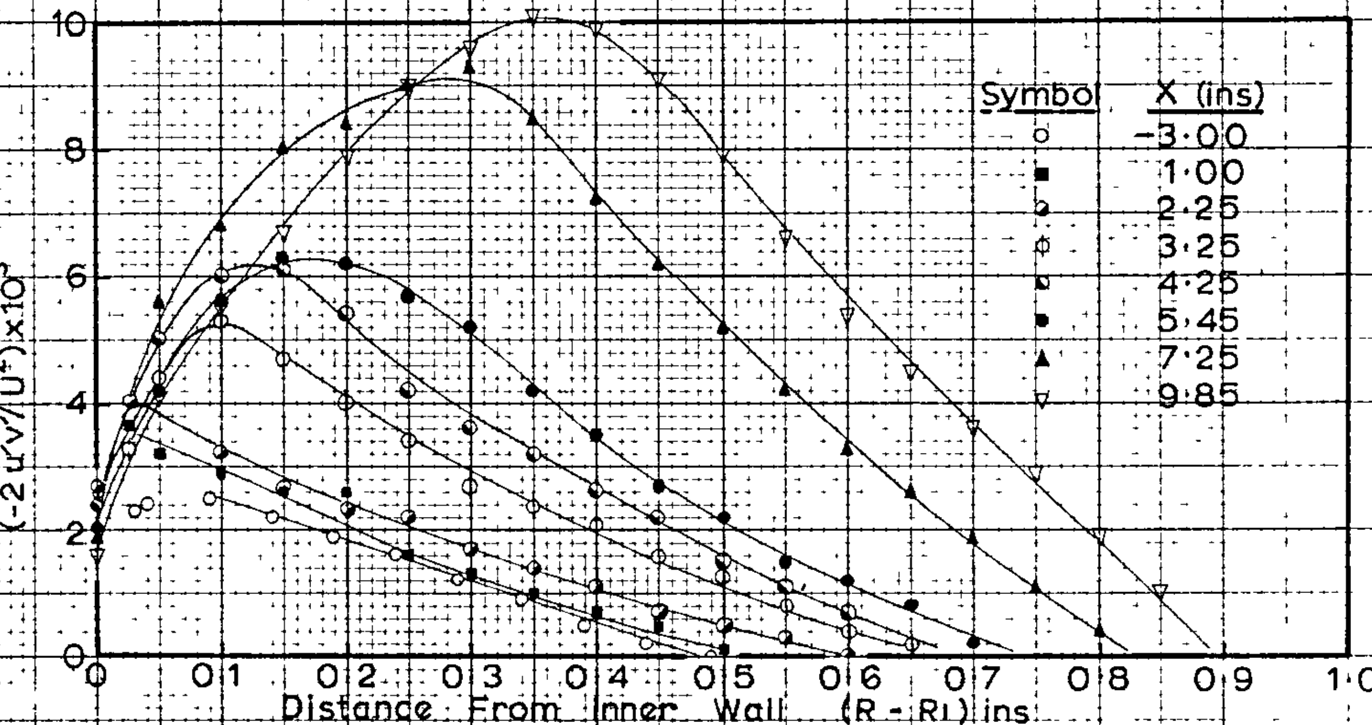

FIG. 4-9-3. EXPERIMENTAL SHEAR STRESS DISTRIBUTIONS

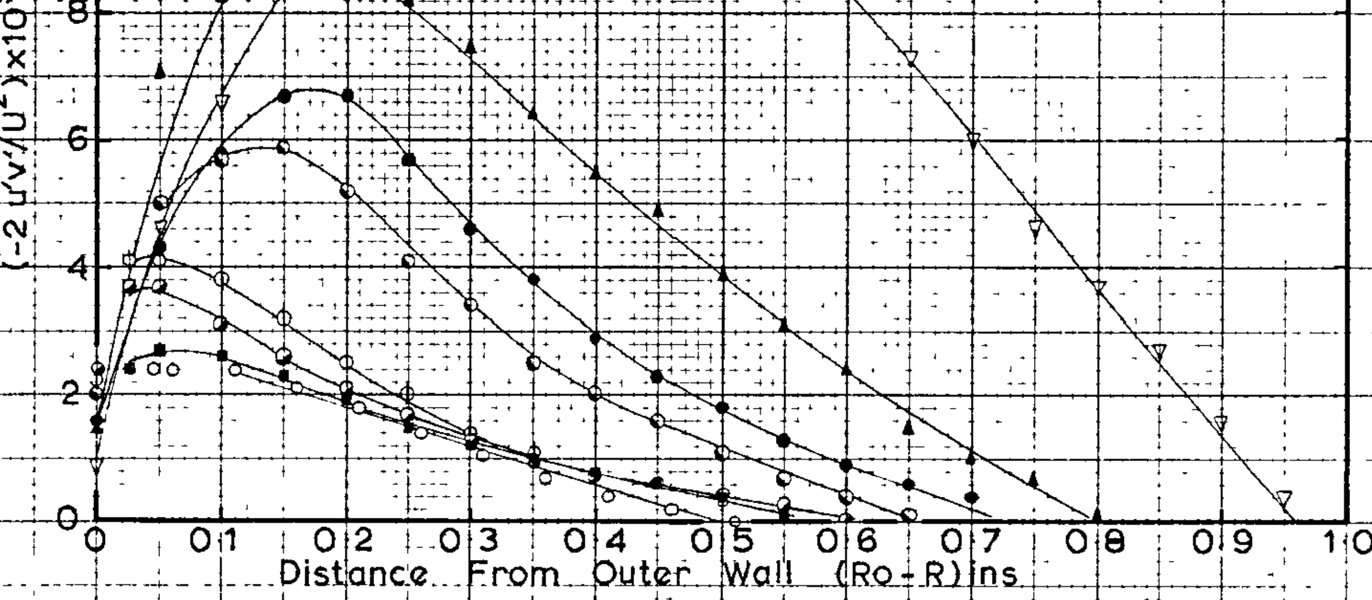

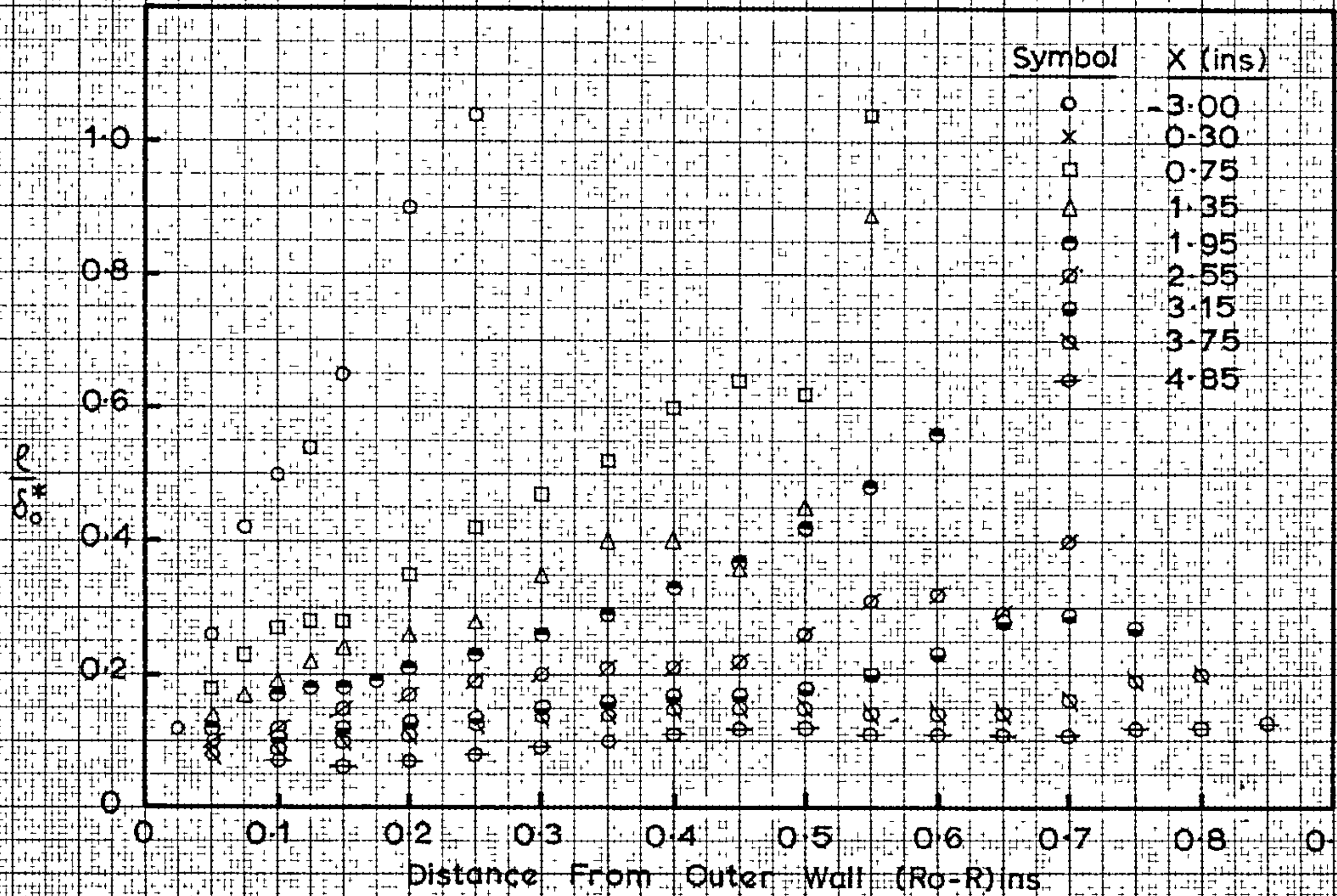

FIG 4-10-1 EXPERIMENTAL MIXING LENGTH DISTRIBUTIONS. $L/\Delta R_1 = 5$ DIFFUSER.

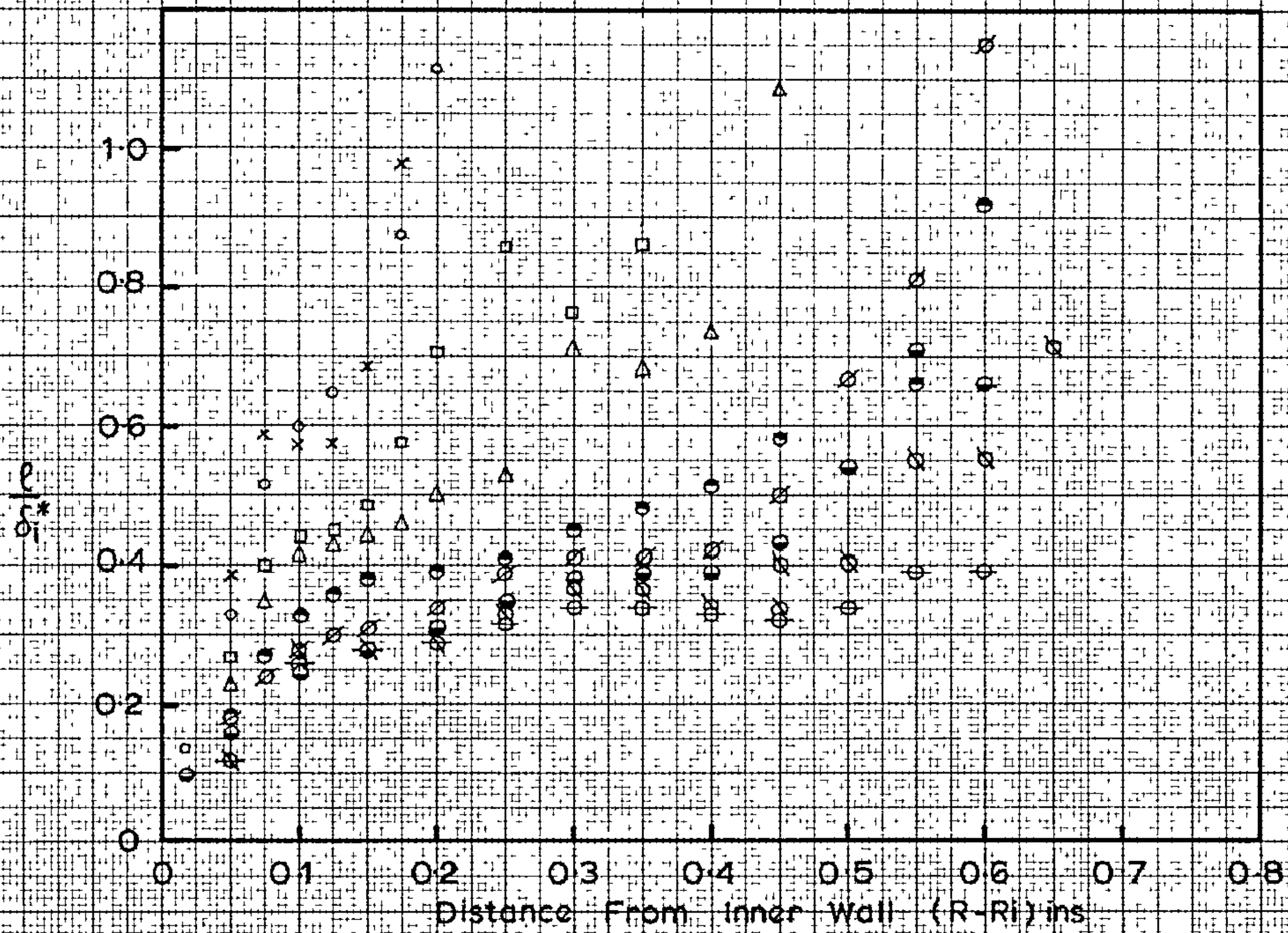

FIG. 4-10-2 EXPERIMENTAL MIXING LENGTH DISTRIBUTIONS L/ΔR$_1$=5 DIFFUSER

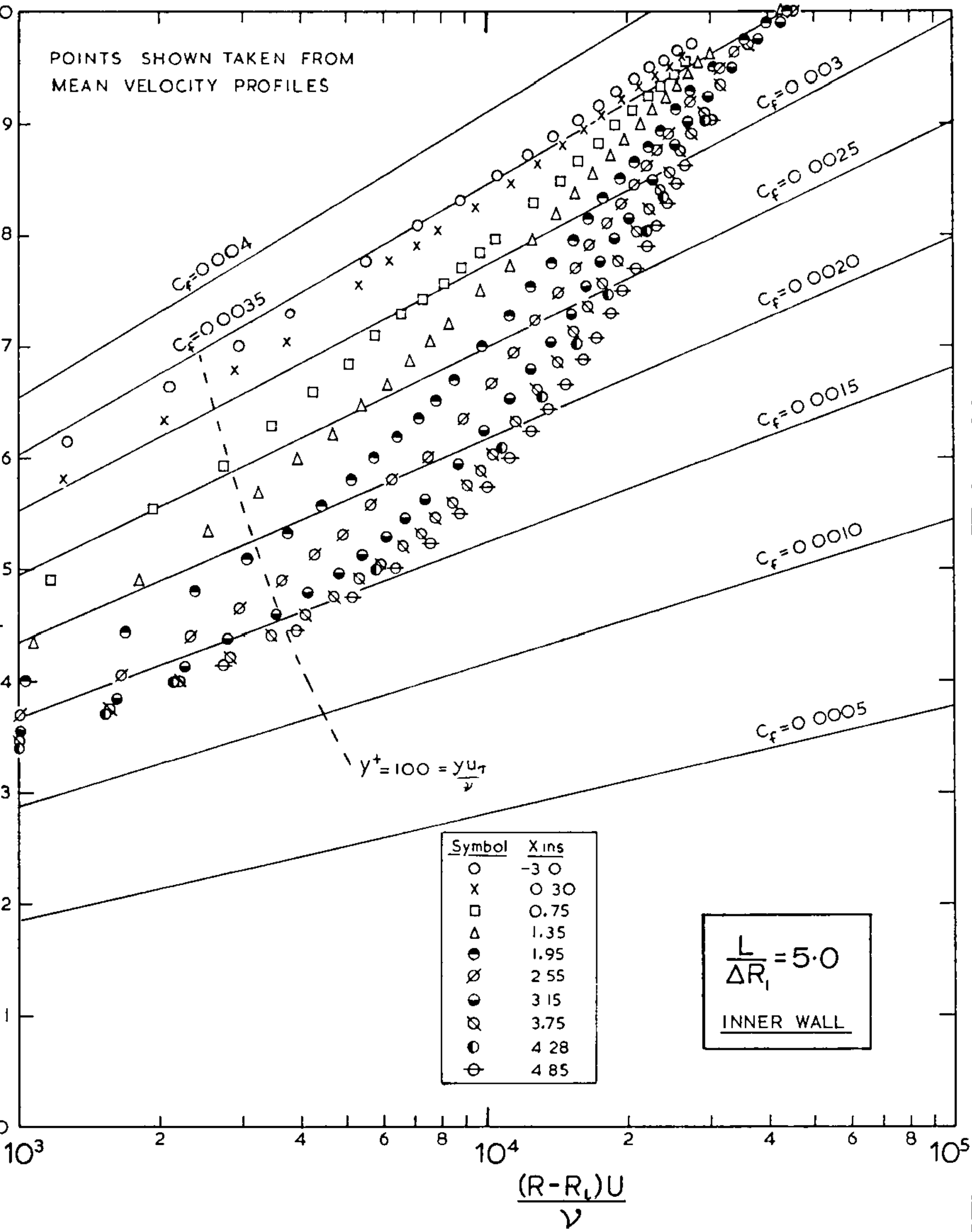

FIG. 4-11-1 SEMILOGARITHMIC PLOT OF INNER WALL VELOCITY PROFILES($L/\Delta R_1 = 5.0$ DIFFUSER)

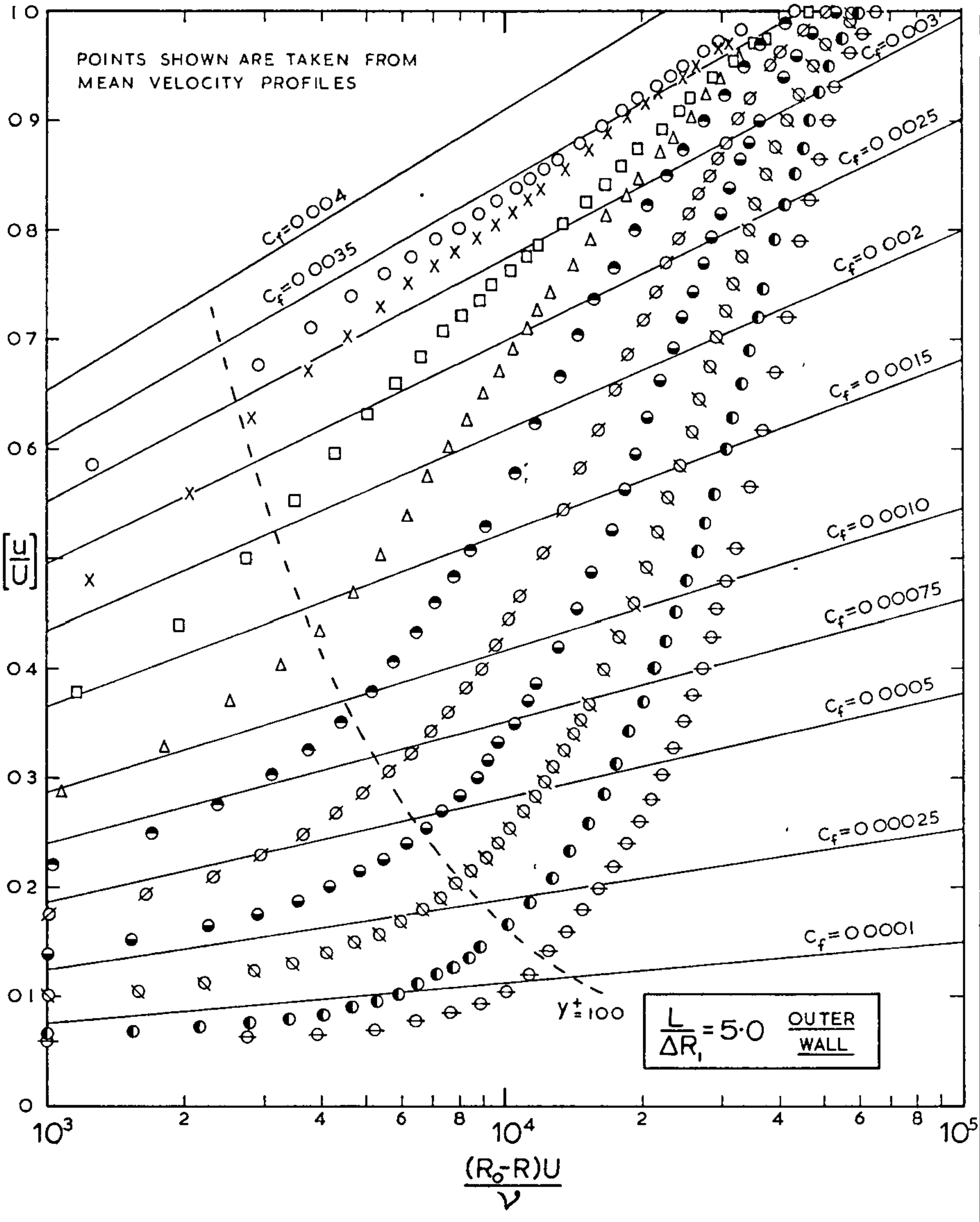

FIG. 4-II-2 SEMILOGARITHMIC PLOT OF OUTER WALL VELOCITY PROFILES ($L/\Delta R_1 = 5.0$ DIFFUSER)

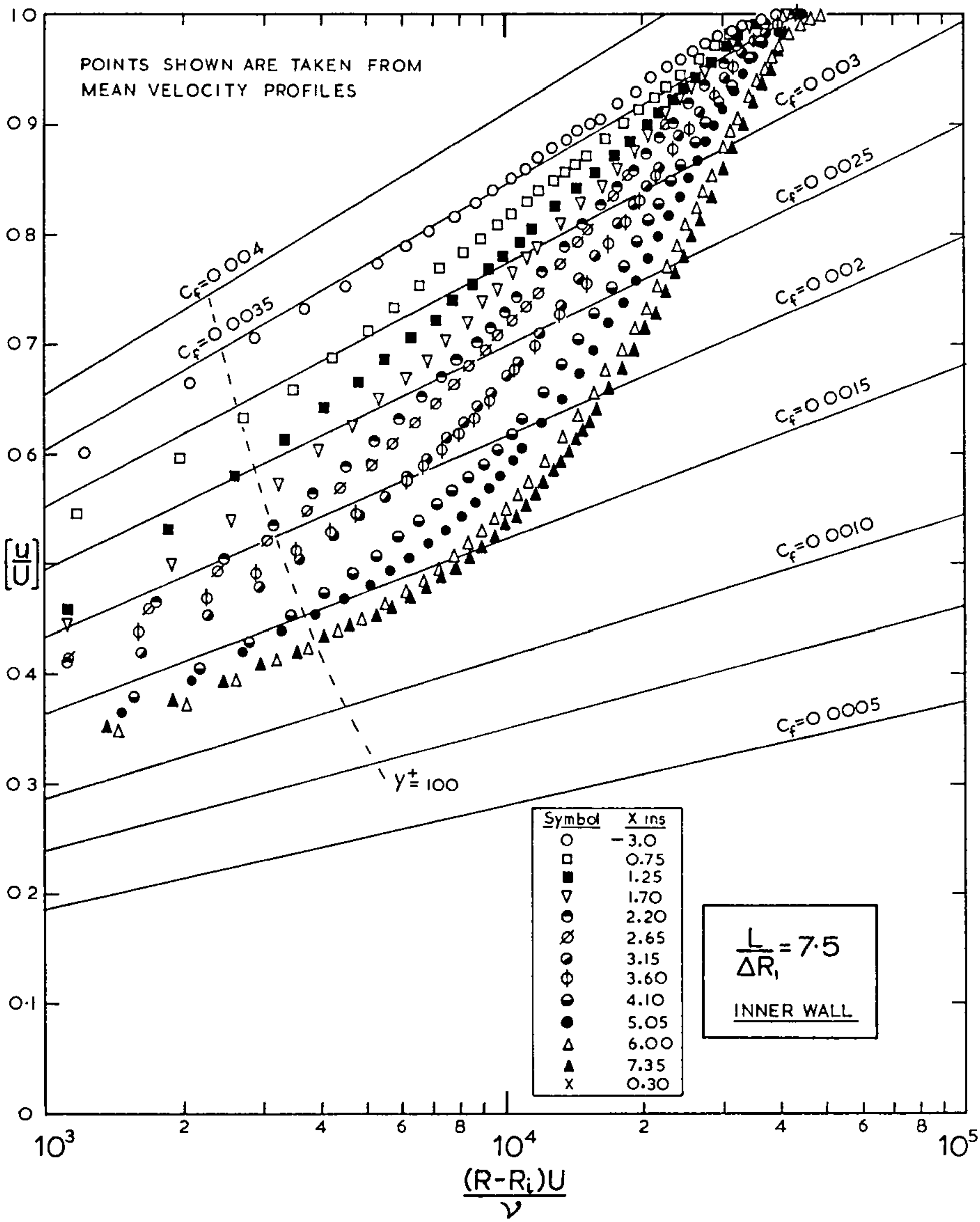

FIG. 4-11-3 SEMI-LOGARITHMIC PLOT OF INNER WALL VELOCITY PROFILES($L/\Delta R_1$ = 7.5 DIFFUSER)

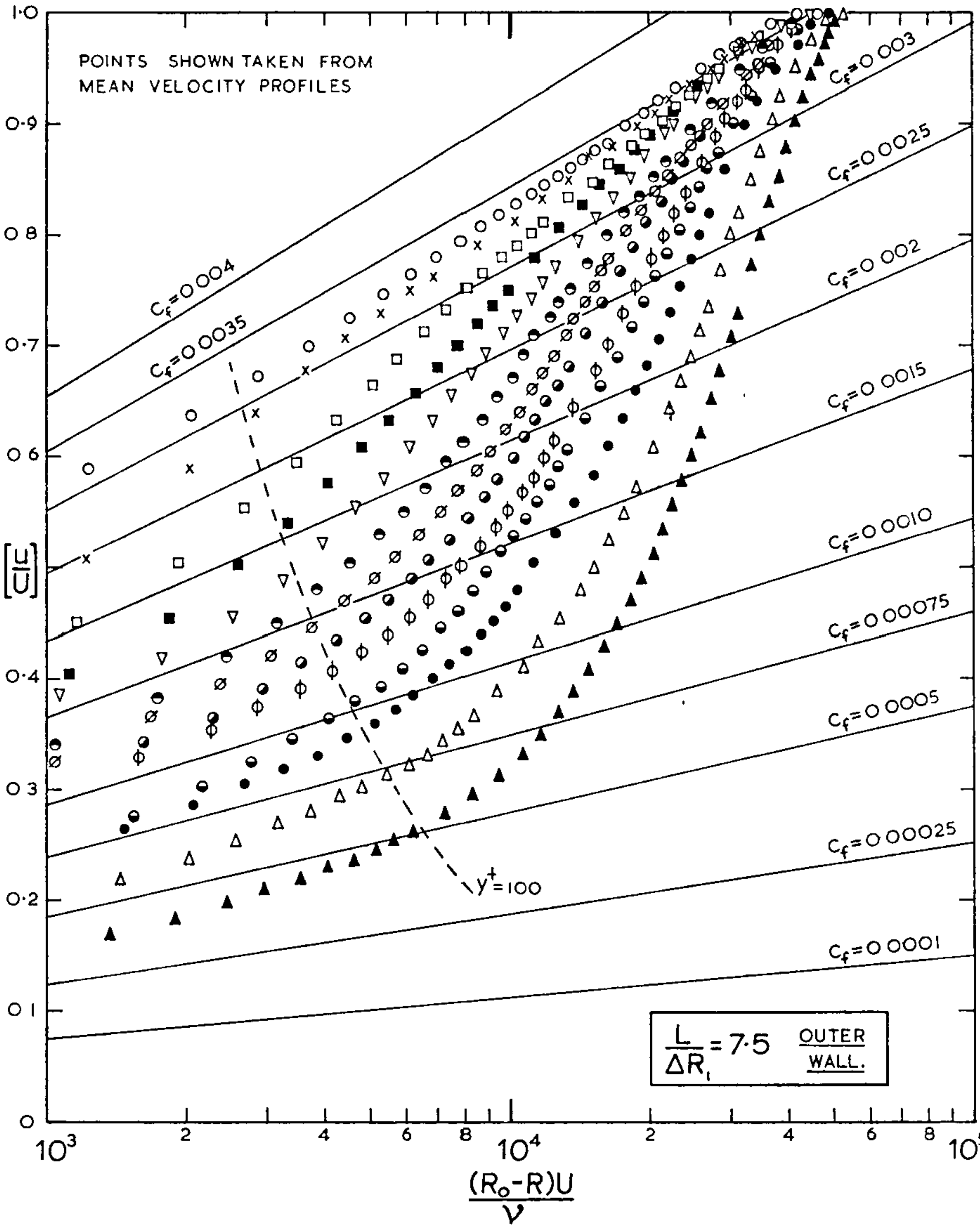

FIG. 4-11-4 SEMILOGARITHMIC PLOT OF OUTER WALL VELOCITY PROFILES($L/\Delta R_1$=7.5 DIFFUSER)

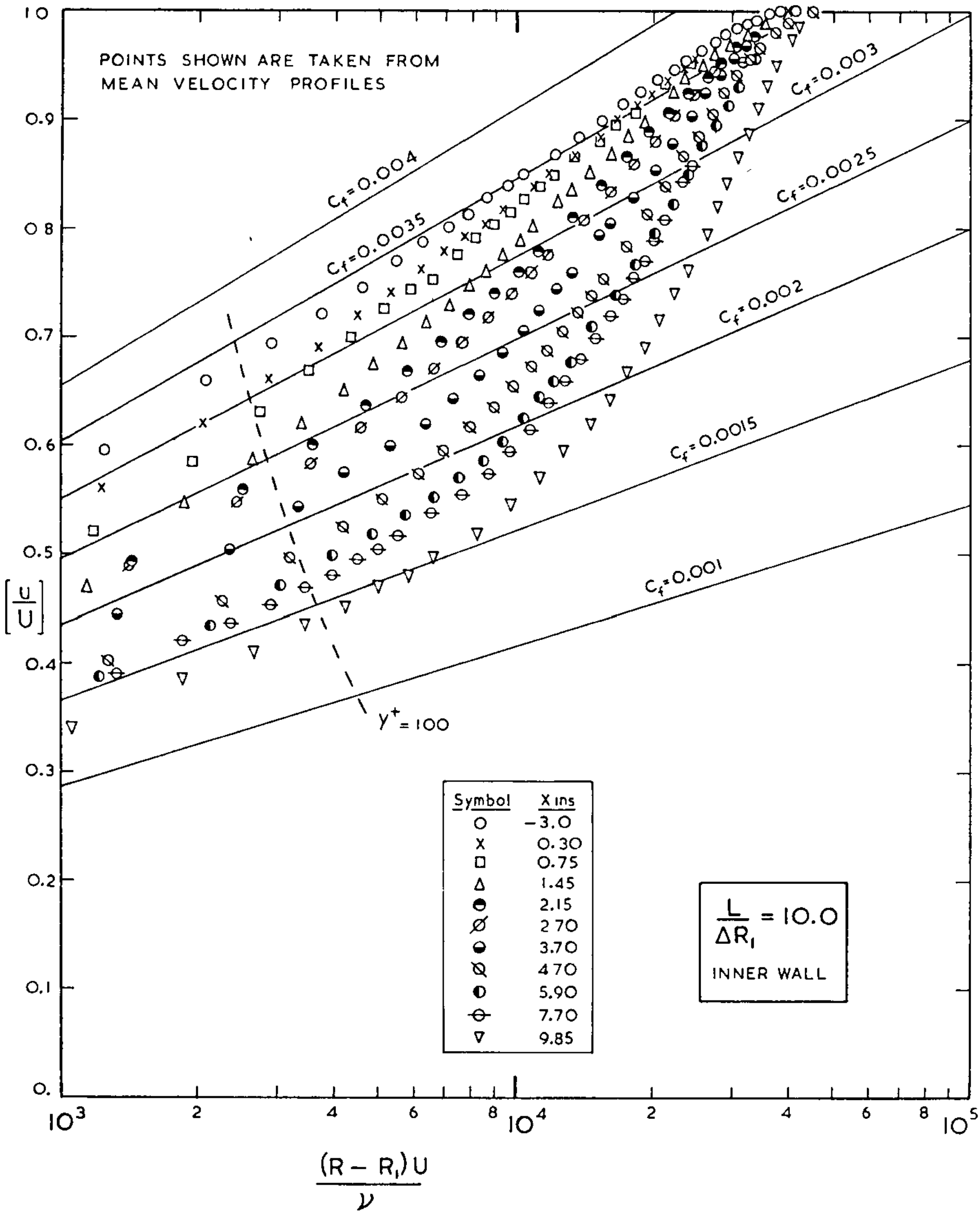

FIG. 4-11-5 SEMILOGARITHMIC PLOT OF INNER WALL VELOCITY PROFILES ($L/\Delta R_1 = 10.0$ DIFFUSER)

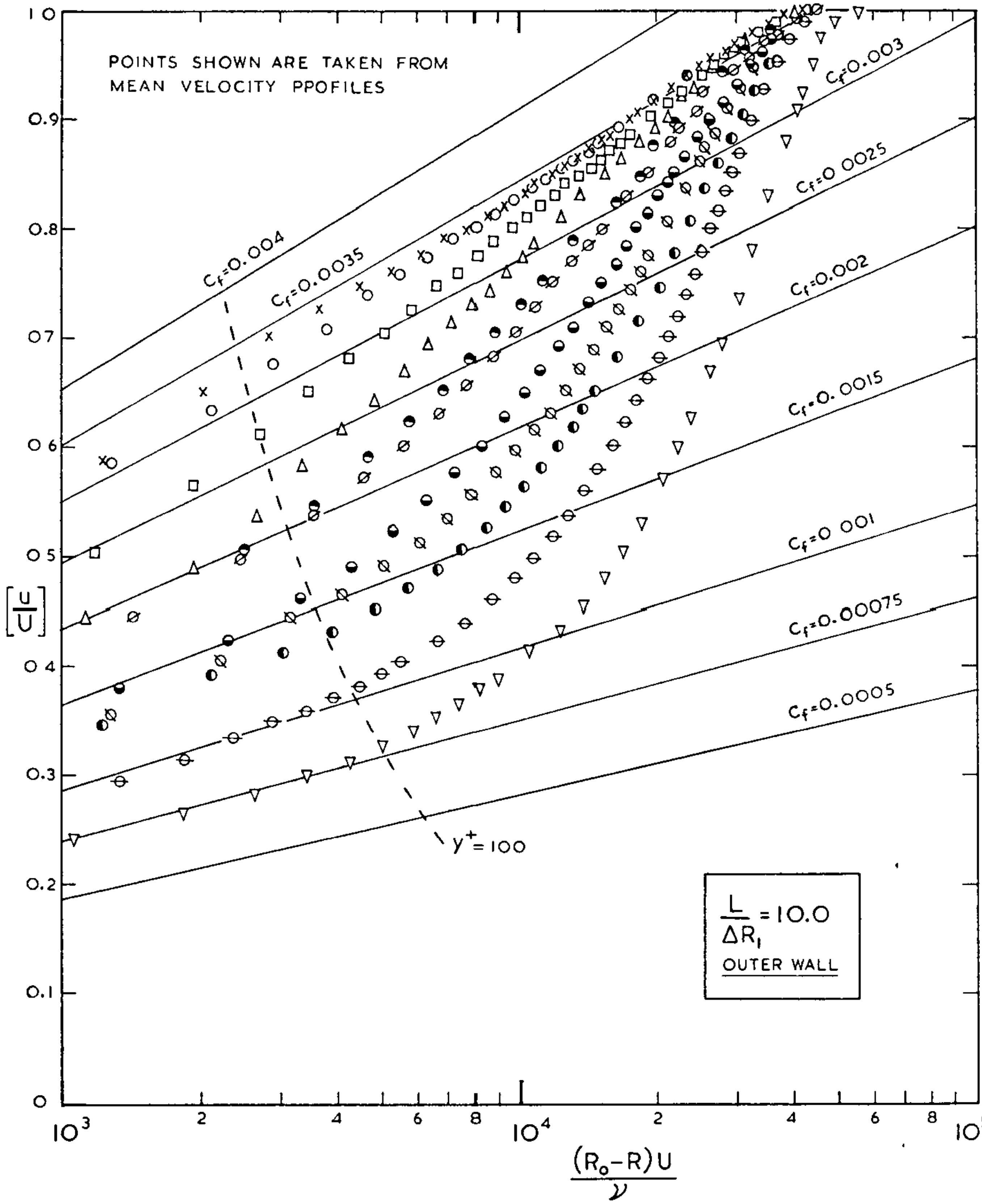

FIG. 4-II-6 SEMILOGARITHMIC PLOT OF OUTER WALL VELOCITY PROFILES ($L/\Delta R_1$ = 10.0 DIFFUSER)

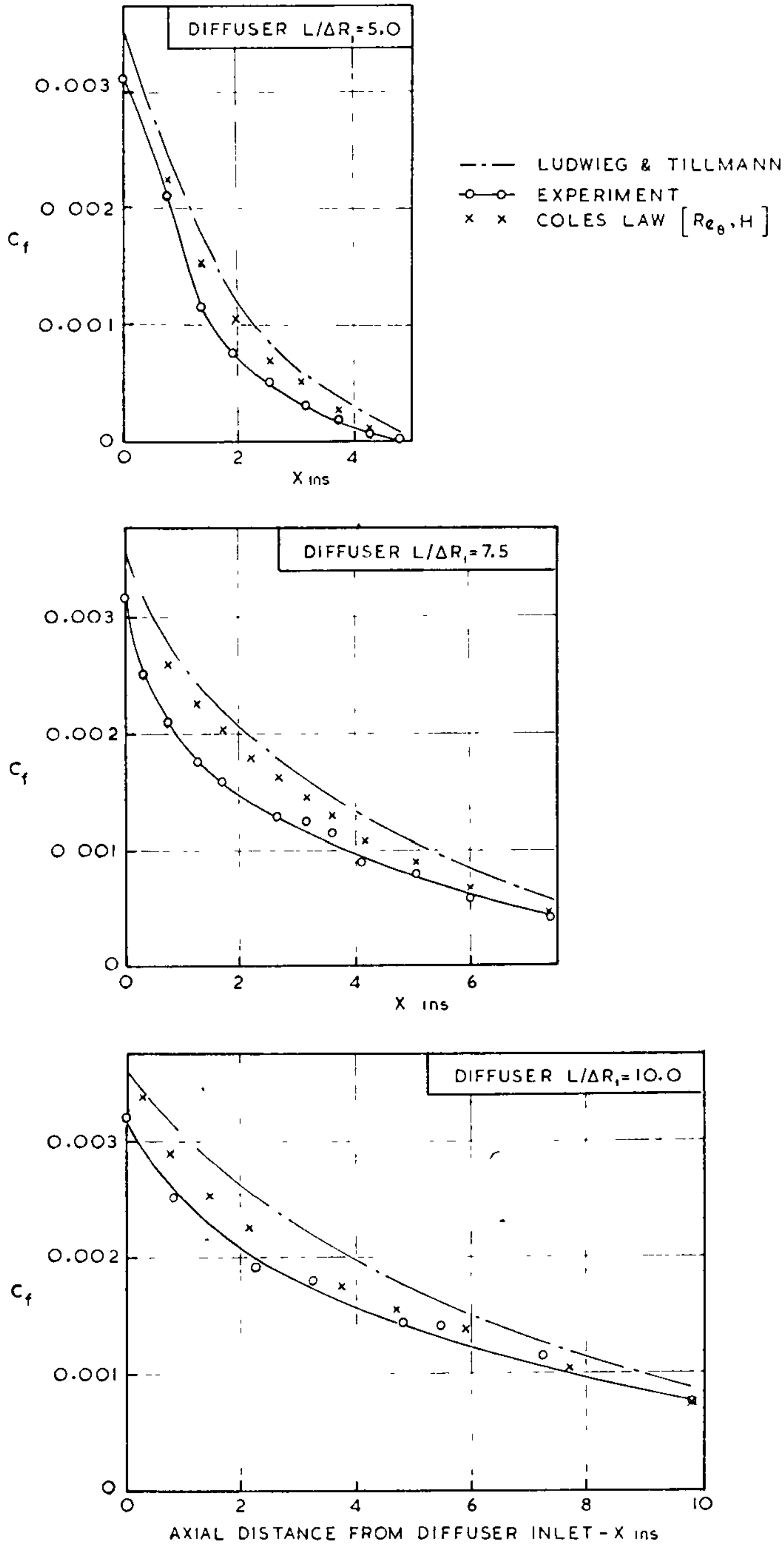

FIG. 4-11-7 COMPARISON OF SKIN FRICTION COEFFICIENTS - OUTER WALL

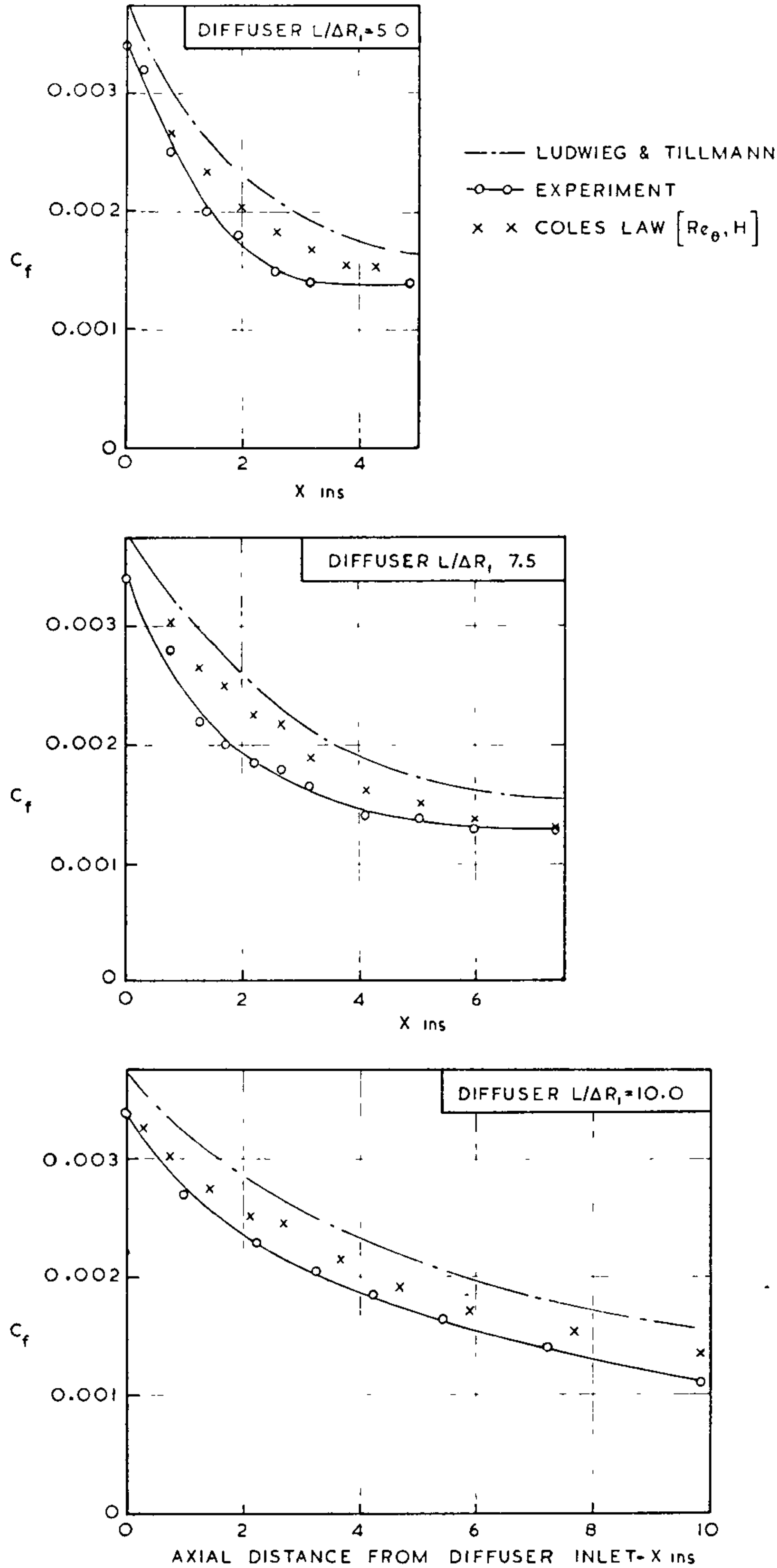

FIG. 4-11-8 COMPARISON OF SKIN FRICTION COEFFICIENTS -INNER WALL

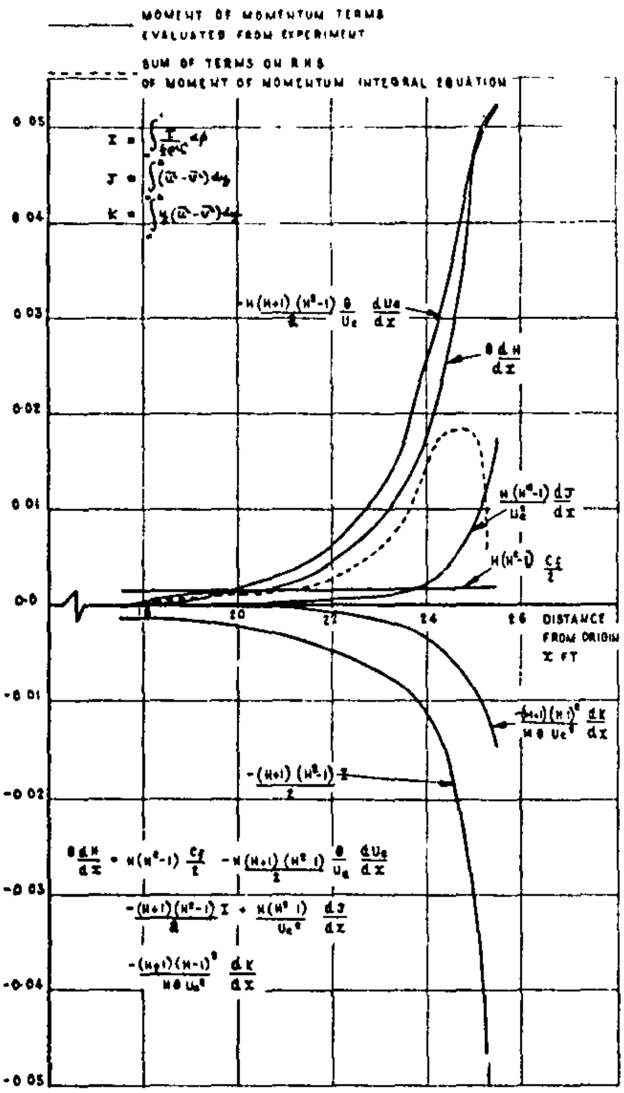

Two-dimensional moment of momentum balance for the N B S boundary layer

Schubauer and Klebanoff[28]

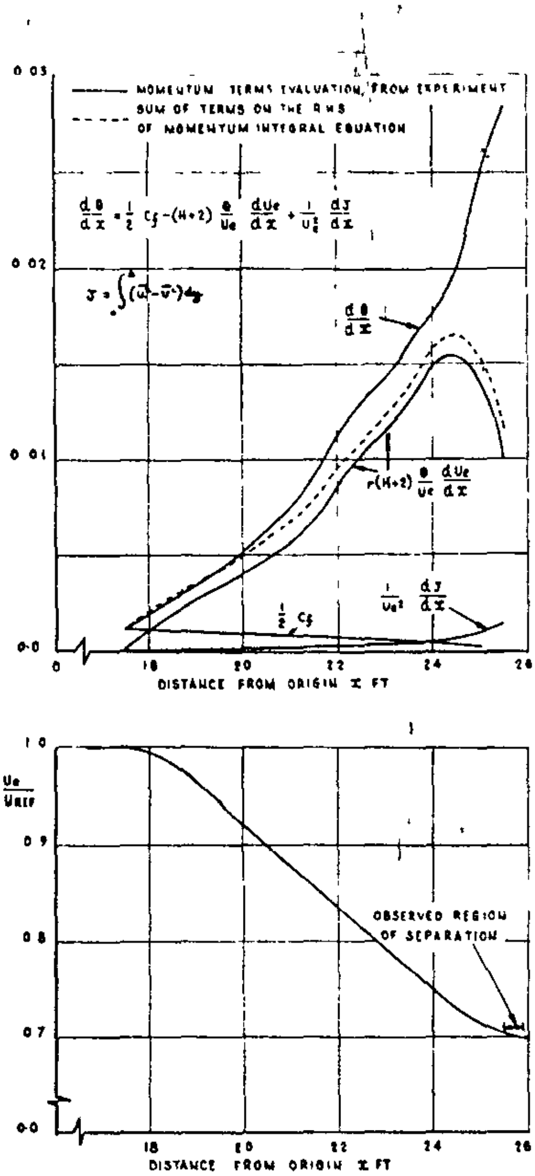

Two-dimensional momentum balance for the N B S boundary layer

Schubauer and Klebanoff[28]

FIG. 4-12-1 MOMENTUM BALANCE DUE TO McDONALD AND STODDART[52]

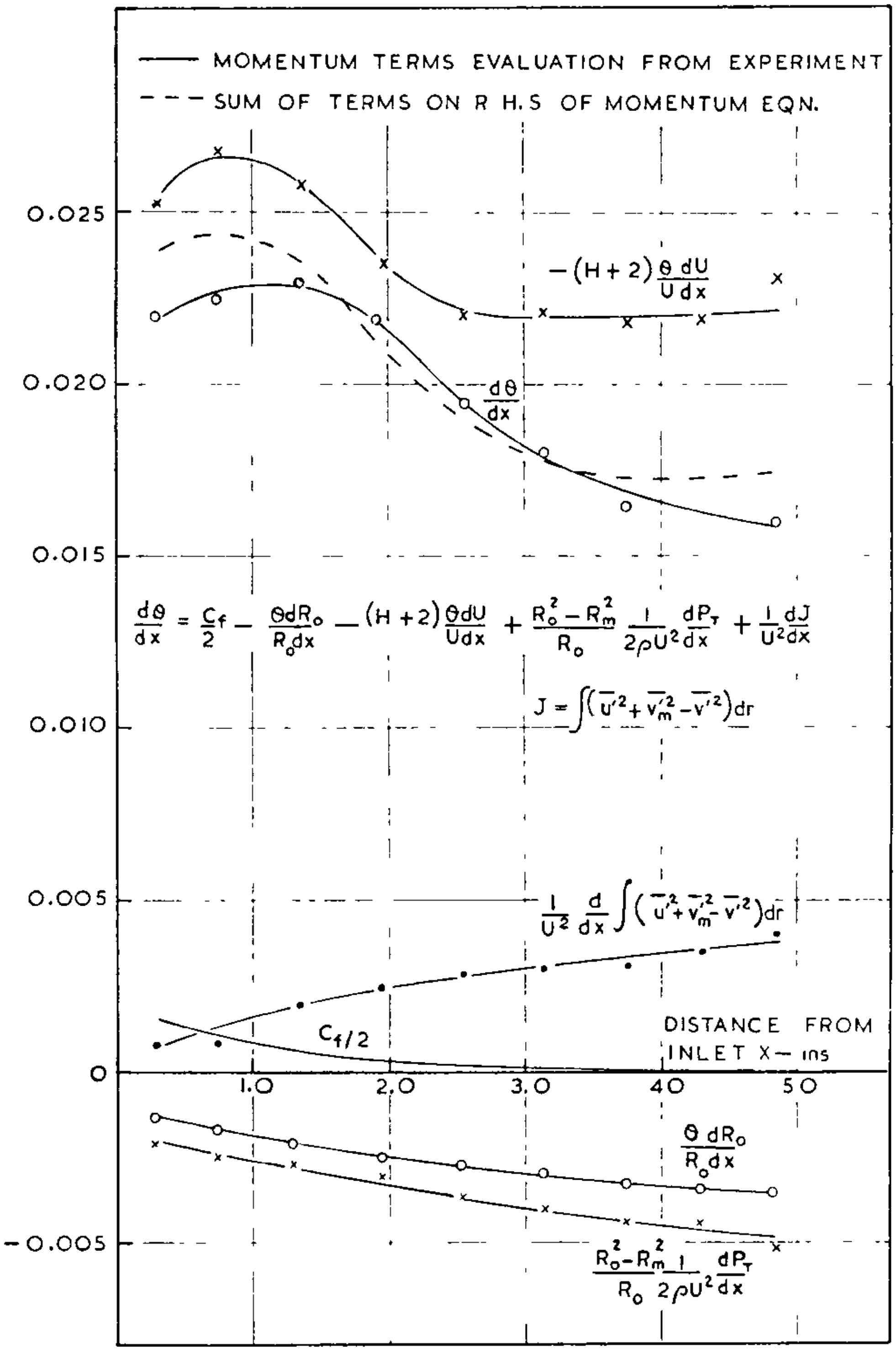

FIG. 4-12-2 MOMENTUM BALANCE FOR THE OUTER WALL BOUNDARY LAYER - $L/\Delta R_1 = 5.0$ DIFFUSER

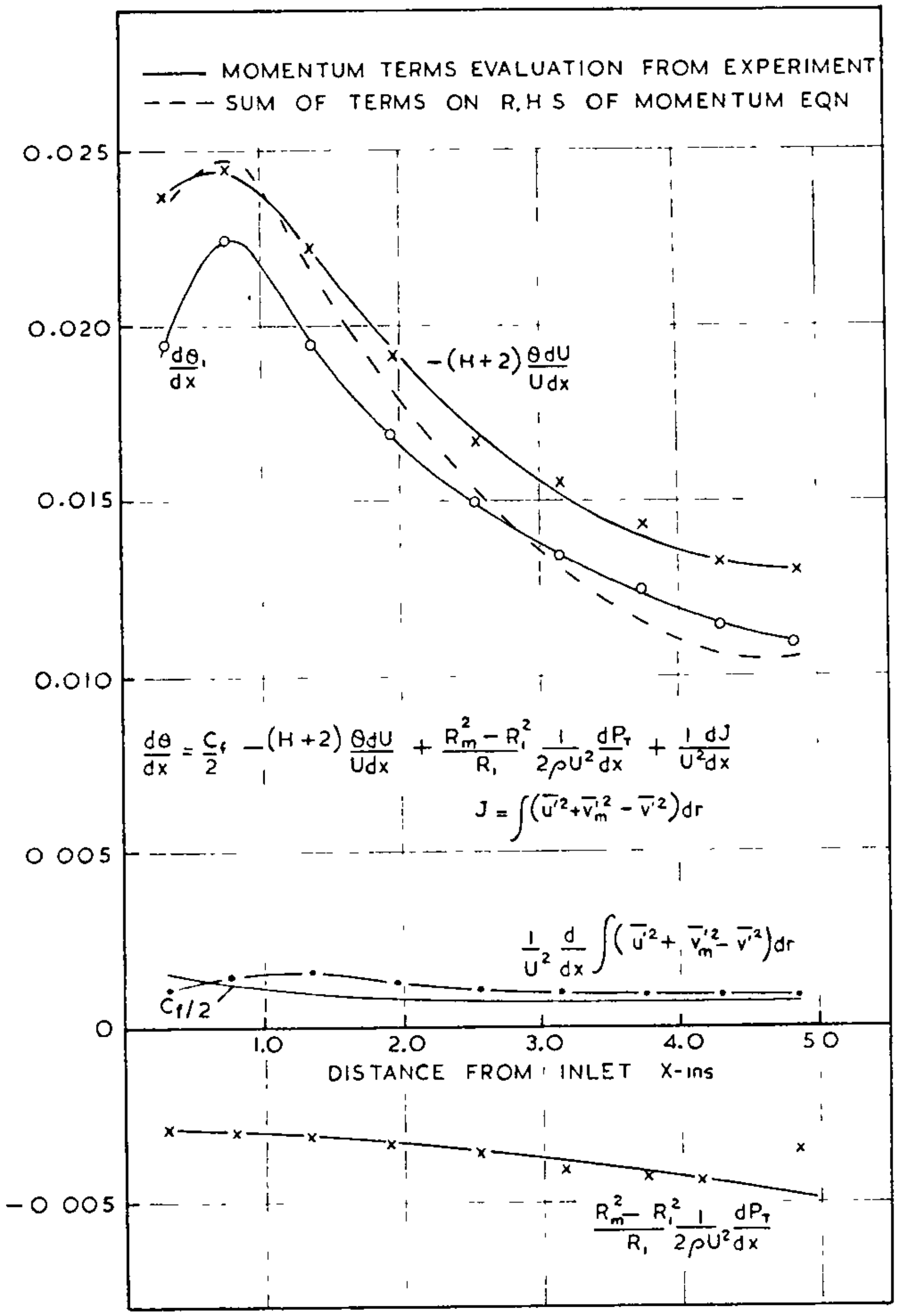

FIG. 4-12-3 MOMENTUM BALANCE FOR THE INNER WALL BOUNDARY LAYER – $L/\Delta R_1 = 5.0$ DIFFUSER

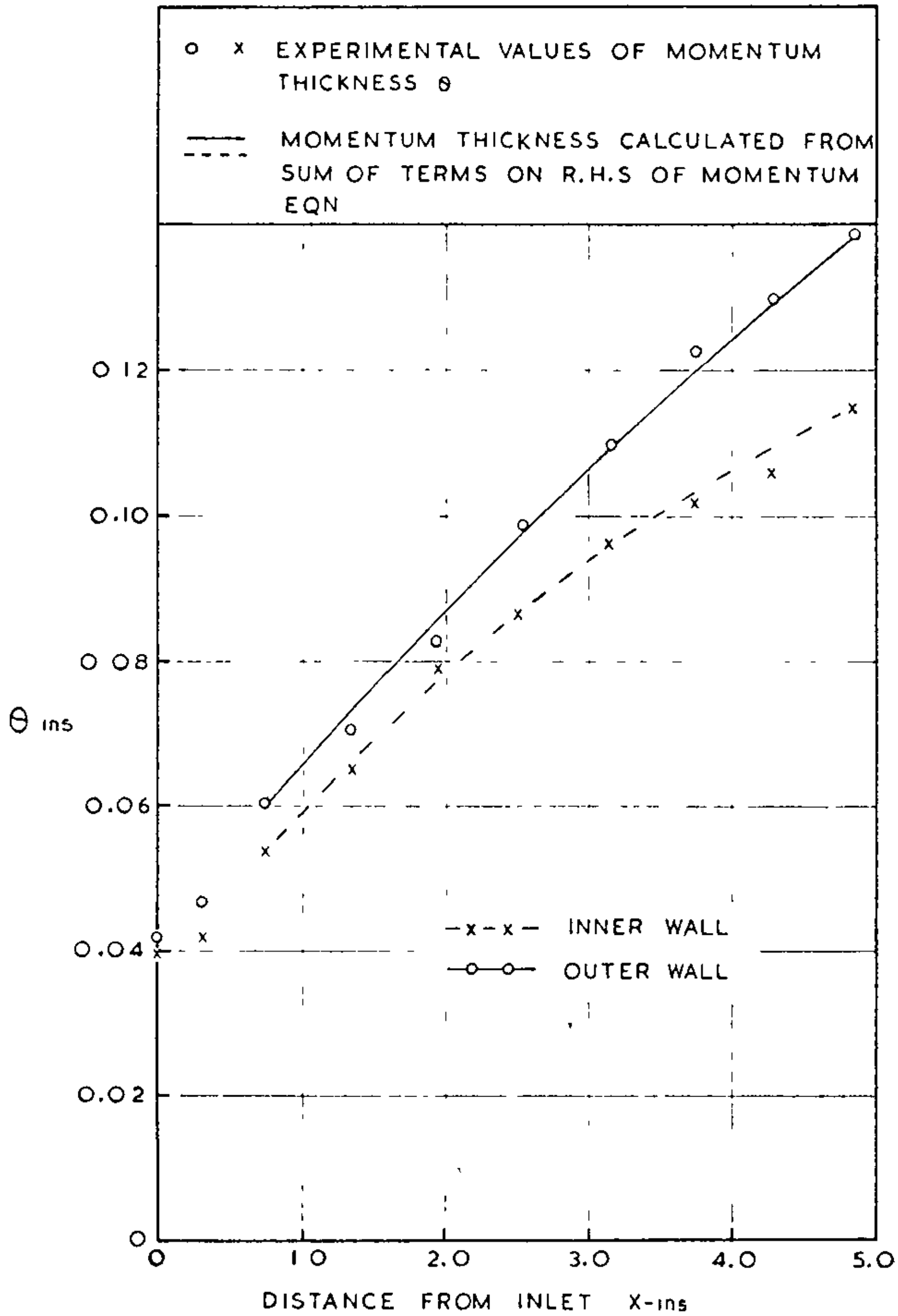

FIG. 4-12-4 COMPARISON OF MOMENTUM THICKNESS CALCULATIONS WITH DATA $L/\Delta R_1 = 5.0$ DIFFUSER

TABLE 4-1

VALUES OF MIXING LENGTH IN OUTER REGION OF

BOUNDARY LAYERS

OUTER PORTIONS ONLY

DIFFUSER $L/\Delta R_1 = 5$ OUTER WALL						Typical Mean Value
X ins	for values less than $x = 2.55$ ins. no significant const. region	2.55	3.15	3.75	4.85	
ℓ/δ_o^*		0.20	0.16	0.14	0.11	0.13
ℓ/δ_o		0.060	0.054	0.054	0.058	0.057
$\ell/(R_o-R_i)$		0.030	0.028	0.028	0.031	0.029
DIFFUSER $L/\Delta R_1 = 5$ INNER WALL						
X ins	”	2.55	3.15	3.75	4.85	
ℓ/δ_i^*		0.40	0.38	0.38	0.33	0.38
ℓ/δ_i		0.090	0.091	0.094	0.092	0.092
$\ell/(R_o-R_i)$		0.039	0.039	0.035	0.034	0.037

DIFFUSER $L/\Delta R_1 = 7.5$ OUTER WALL						Typical Mean Value
X ins	For $X < 4.10$ ins. $\ell/\delta^* \neq$ Const.	4.10	5.05	6.00	7.35	
ℓ/δ_o^*		0.23	0.20	0.19	0.18	0.20
ℓ/δ_o		0.064	0.060	0.062	0.065	0.063
$\ell/(R_o-R_i)$		0.031	0.031	0.032	0.037	0.033
X ins.	INNER WALL	4.10	5.05	6.00	7.35	
ℓ/δ_i^*	”	0.36	0.33	0.28	0.27	0.31
ℓ/δ_i		0.091	0.087	0.080	0.081	0.085
$\ell/(R_o-R_i)$		0.040	0.037	0.036	0.037	0.038

DIFFUSER $L/\Delta R_1 = 10$ OUTER WALL						Typical Mean Value
X ins	For $X < 4.25$ ins $\ell/\delta^* \neq$ Const.	4.25	5.45	7.25	9.85	
ℓ/δ_o^*		0.29	0.27	0.27	0.20	0.26
ℓ/δ_o		0.068	0.066	0.074	0.070	0.068
$\ell/(R_o-R_i)$		0.031	0.032	0.037	0.043	0.036
X ins	INNER WALL	4.25	5.45	7.25	9.85	
ℓ/δ_i^*	”	0.37	0.33	0.37	0.32	0.35
ℓ/δ_i		0.08	0.081	0.098	0.097	0.089
$\ell/(R_o-R_i)$		0.043	0.035	0.042	0.042	0.040

SECTION 5

THEORETICAL ANALYSIS

5-1 Introduction

Theoretical analysis of the flow in diffusers is effectively a problem in the calculation of the rate of growth of a turbulent boundary layer in an adverse pressure gradient. The objectives of the analysis are the prediction of:

i) The pressure recovery

ii) Imminence of separation or transitory stalling

iii) Energy losses

In contrast to the case of a body surrounded by a free stream, the pressure is no longer determined by the frictionless external flow, but by the development of the boundary layer itself. Therefore one of the main difficulties in calculating diffuser flows is that the pressure distribution is unknown to begin with, and is only obtained in the course of the calculations. Nearly all calculation methods assume that over the length of the diffuser there exists a core of fluid having constant total energy, in which case the pressure is only influenced by the boundary layer through the continuity relations. From measurements made by Sprenger(6) Cockrell(54) and the author(27) it is known that flow situations can occur in which the boundary layers merge together, and in these circumstances considerable discrepancies between theory and experiment can occur. Furthermore, many of the existing laws for calculating the turbulent boundary layer e.g. mean velocity profile, and skin friction, are based on data from experiments with relatively mild adverse pressure gradients, and because of this only the case of a diffuser with a modest overall pressure gradient operating with a thin inlet boundary layer can be predicted with confidence. (Cockanower et al[55]),

Finally, boundary layer theory will only give a criterion for the imminence of separation. Several authors, but notably Sandborn[45], have proposed the shape parameter H as a guide and predicted transitory stalling for values of H between 2.0 and 3.2, and separation between 2.6 and 4.0.

The present investigation in a minimum length diffuser operating with fully developed flow conditions at inlet represents an extremely severe test of boundary layer theory.

5-2 Summary of Prediction Methods

5-2-1 Differential Equations of Motion

The boundary layer equations are obtained from the Navier-Stokes equations, after suitable time-averaging of the fluctuating components and applying the normal boundary layer approximations (see Appendix 25).

The continuity equation for axially symmetric flow is

$$\frac{\partial}{\partial x}(Ru) + \frac{\partial}{\partial R}(RV) = 0. \qquad 5\text{-}2\text{-}1$$

The streamwise mean momentum equation is

$$u\frac{\partial u}{\partial x} + v\frac{\partial u}{\partial R} = -\frac{1}{\rho}\frac{dP}{dx} + \frac{1}{\rho R}\frac{\partial}{\partial R}(R\tau) - \frac{\partial}{\partial x}(\overline{u'^2}) \qquad 5\text{-}2\text{-}2$$

and the mean momentum equation normal to the wall reduces to

$$\frac{P}{\rho} + \overline{v'^2} = \text{Const.} \qquad 5\text{-}2\text{-}3$$

The constant of integration in equation 5-2-3 is obtained by writing the equation at the point of maximum velocity (R = Rm) to give

$$\frac{P}{\rho} = \frac{P_m}{\rho} + (\overline{v'^2_m} - \overline{v'^2}) \qquad 5\text{-}2\text{-}4$$

and

$$\frac{1}{\rho}\frac{dP}{dx} = \frac{1}{\rho}\frac{dP_m}{dx} + \frac{d}{dx}(\overline{v'^2_m} - \overline{v'^2}) \qquad 5\text{-}2\text{-}5$$

P_m is the static pressure at Rm, and is obtained by writing Bernoulli's equation at the point of maximum velocity

$$P_{T_m} = P_m + \frac{1}{2}\rho U^2 \qquad 5\text{-}2\text{-}6$$

Differentiating eqn. 5-2-6, and combining with eqn. 5-2-5, enables the streamwise momentum equation to be written as:

$$u\frac{\partial u}{\partial x} + v\frac{\partial u}{\partial R} = U\frac{dU}{dx} - \frac{1}{\rho}\left(\frac{dP_T}{dx}\right)_m + \frac{1}{\rho R}\frac{\partial(R\tau)}{\partial R} - \frac{d}{dx}\left(\overline{u'^2} + \overline{v'^2_m} - \overline{v'^2}\right) \qquad 5\text{-}2\text{-}7$$

A simplification normally made is that the last term in eqn. 5-2-7 is only of importance near separation. Imbach[30] has suggested that the total pressure gradient along the streamline of maximum velocity can be related to the shear stress gradient. Writing eqn. 5-2-2 at R_m, and neglecting the term $\frac{\partial \overline{u'}^2}{\partial x}$ yields

$$U\frac{dU}{dx} = \frac{1}{\rho}\left(\frac{dP}{dx}\right)_m + \frac{1}{\rho R_m}\left[\frac{\partial}{\partial R}(R\tau)\right]_{R_m}$$

$$\therefore \qquad \left(\frac{dP_T}{dx}\right)_m = \frac{1}{R_m}\left[\frac{\partial}{\partial R}(R\tau)\right]_{R_m} \qquad 5\text{-}2\text{-}8$$

The equations may be modified to take account of a transverse pressure gradient, although except near separation or in regions of large surface curvature, this modification may be safely neglected.

Neglecting Reynolds normal stresses, equations 5-2-1, 5-2-7 and 5-2-8 can be solved for a given distribution of U, providing the relations governing Reynolds' shear stress $\tau = -\rho\overline{u'v'}$ are known. It is the way in which this information is incorporated which accounts for the large number of prediction methods available. These methods fall into two broad categories, namely, integral, and differential.

5-2-2 Integral Approach

The need to assume something explicitly about the local Reynolds' stresses can be avoided by integrating Eqn. 5-2-7 across the boundary layer. The technique is detailed in Appendix 25, and the momentum integral equations for the inner and outer wall boundary layers are obtained.

$$\frac{d\theta_I}{dx} + \frac{\theta_I}{R_I}\frac{dR_I}{dx} + \frac{\theta_I}{U}\frac{dU}{dx}(H_I+2) = \frac{C_{f_I}}{2} + \frac{R_m^2-R_I^2}{R_I}\frac{1}{2\rho U^2}\left(\frac{dP_T}{dx}\right)_m + \frac{1}{U^2}\frac{d}{dx}\int_{R_I}^{R_m}(\overline{u'^2}+\overline{v'^2_m}-\overline{v'^2})\frac{R}{R_I}\,dR \qquad \text{- 5-2-9}$$

$$\frac{d\theta_o}{dx} + \frac{\theta_o}{R_o}\frac{dR_o}{dx} + \frac{\theta_o}{U}\frac{dU}{dx}(H_o+2) = \frac{C_{f_o}}{2} + \frac{R_o^2-R_m^2}{R_o}\frac{1}{2\rho U^2}\left(\frac{dP_T}{dx}\right)_m + \frac{1}{U^2}\frac{d}{dx}\int_{R_m}^{R_o}(\overline{u'^2}+v'^2_m-\overline{v'^2})\frac{R}{R_o}\,dR \qquad \text{- 5-2-10}$$

The velocity U is coupled with the displacement thickness δ^* in the continuity equation

$$\frac{\bar{u}}{U} = 1.0 - \frac{2R_o\delta_o^*}{R_o^2-R_I^2} - \frac{2R_I\delta_I^*}{R_o^2-R_I^2} \qquad \text{5-2-11}$$

To obtain a solution the unknowns in the equations must be inter-related with each other, and with known flow parameters. Some of the required relationships can be established if the velocity profiles are defined; the simplest possibility is to assume the velocity profile as a one-parameter family which may be approximated by a power law. In addition, an auxiliary equation will be required for the variation of the shape parameter. Thompson(56) has shown that the first order differential equations for the variation of the shape parameter assume that the shear stress profile depends only on the mean velocity profile, the Reynolds number, and the pressure gradient.

Therefore whilst the turbulent shear stress is not contained explicitly in Eqns. 5-2-9/10, as stated by Reynolds(34) "such assumptions amount to global assumptions about the implicit effects of the turbulence".

As an alternative to the semi-empirical auxiliary equation additional relationships can be derived to relate the mean flow properties e.g. the entrainment equation of Head(57), the energy integral equation(58), the moment of momentum equation(28), and the semi-integrated momentum equation(34). Frequently these additional relationships require assumptions to be made regarding the Reynolds stress distribution e.g. the dissipation integral ($\int \tau \, (du/dy) \, dy$) is contained in the energy integral equation.

5-2-3 Differential Approach

Differential methods fall into two groups, depending on the method of treatment of the Reynolds stress term

i) Mean-Field Methods

These methods relate the shear stress to the local mean velocity gradient. This can be done by introducing an eddy viscosity ε and writing

$$-\overline{u'v'} = \varepsilon \frac{du}{dR} \qquad 5\text{-}2\text{-}12$$

Clauser[51] has shown that for equilibrium boundary layers

$$\varepsilon = 0.18\, U \delta^{*} \qquad 5\text{-}2\text{-}13$$

Alternatively a mixing length model may be adopted

$$-\overline{u'v'} = \ell^{2} \left| du/dR \right| du/dR \qquad 5\text{-}2\text{-}14$$

Escudier & Spalding[59] have suggested that the mixing length is constant in the outer 80% of the layer and equal to $0.09\,\delta$. A summary of mixing length relations is given by Spalding[49].

ii) Turbulent Field Methods

In these methods the shear stress is assumed to be closely related to the turbulent kinetic energy $\frac{1}{2}\rho\left(\overline{u'^2}+\overline{v'^2}+\overline{w'^2}\right)$ the latter being governed by the turbulent energy equation.[61]

$$\frac{1}{2}\rho\left(u\frac{\partial \overline{q}^2}{\partial x} + \frac{\partial \overline{q}^2}{\partial y}\right) - \tau\frac{\partial u}{\partial y} + \frac{\partial}{\partial y}\left(\overline{pv} + \frac{1}{2}\rho\overline{q^2 v}\right) + \rho\varepsilon = 0.$$

advection production diffusion dissipation

where $\overline{q}^2 = \left(\overline{u'^2}+\overline{v'^2}+\overline{w'^2}\right)$, $\varepsilon = \nu\left(\partial u/\partial x\right)^2$

The longitudinal transfer of energy by normal stresses being neglected. Bradshaw and Ferris[60] in solving eqn. 5-2-15 define

$$a_1 \equiv \tau/\rho\overline{q}^2$$
$$L \equiv (\tau/\rho)^{3/2}/\varepsilon \qquad \text{5-2-16}$$
$$G \equiv \left(\frac{\overline{pv}}{\rho} + \frac{1}{2}\overline{q^2 v}\right)\Big/\left(\frac{\tau_{max}}{\rho}\right)^{1/2}\frac{\tau}{\rho}$$

Substitution of these relationships in equation 5-2-15 yields

$$u\frac{\partial}{\partial x}\left(\frac{\tau}{2a_1\rho}\right) + v\frac{\partial}{\partial y}\left(\frac{\tau}{2a_1\rho}\right) - \frac{\tau}{\rho}\frac{\partial u}{\partial y} + \left(\frac{\tau_{max}}{\rho}\right)^{\frac{1}{2}}\frac{\partial}{\partial y}\left(G\,\frac{\tau}{\rho}\right) + \frac{(\tau/\rho)^{3/2}}{L} = 0. \qquad \text{5-2-17}$$

Equation 5-2-17 together with the continuity and momentum equations give three equations in the three unknowns u, v, and τ. The equations form a hyperbolic set, and, providing adequate assumptions can be made for a_1, L, and G, the method of characteristics can be used to obtain a solution.

Other differential methods are reviewed by Reynolds[34]

5-3 History Effects in Turbulent Boundary Layers

It has been known for many years that the upstream development of the flow (history), as well as the mean velocity profile, plays an important part in establishing the turbulent shear stress distribution.

The early attempts to represent turbulent shear stress draw analogies between the behaviour of turbulent flow and the behaviour of the molecules of a gas according to the kinetic theory. The shear stress in the outer regions of a layer is now attributed, however, to the production of large eddies which originate near the wall and move out towards the high velocity free stream. Kline[62] has suggested that the production of eddies occurs via a local instability of the mean or instantaneous velocity profile. Bradshaw[48], and Rotta[34] consider that the lifetime of an eddy may correspond to a downstream travel of ten to five times the boundary layer thickness. It follows that the shear stress at a point has its origin in a disturbance propogated near the wall some distance upstream. It is this "memory" or upstream history effect which most integral, and some differential, prediction methods fail to take into account. Experimental evidence of history effects have been observed by, Lee[63] in an entry length, Sandborn and Slogar[64] in adverse pressure gradients, and Goldberg[29] in relaxing pressure gradients; in all cases a relaxation time is required for the values of shear stress to revert to those associated with local equilibrium.

In the light of such evidence the question arises, "Is it justifiable to base the calculation of shear stress on local conditions, e.g. mean velocity profile ?". Many workers have attempted to answer this question, and Reynolds[34] and Bradshaw[48] concluded that only when the boundary layer is changing very slowly (near to local equilibrium) can mean-field methods work successfully. However turbulent field methods are capable of taking such effects into account. History effects have been incorporated in integral methods by McDonald and Stoddart[52] and Goldberg[29]. In these methods auxiliary equations are used which incorporate the shear stress integral, which is calculated by relating its departure from the equilibrium value to the local non-dimensional pressure gradient.

5-4 Theoretical Approach Adopted

A mean-field approach was not adopted because of the argument expressed above concerning the inability of mean-field methods to take account of history effects, which were expected to be significant in practical diffuser flows. Turbulent-Field methods appeared attractive, but in attempting to apply the method due to Bradshaw et al.[60] a number of difficulties arose:

(i) The method required considerably more sophisticated assumptions, and at the time no experimental data was available to calculate the constants a, L, and G, in an extremely severe adverse pressure gradient.

(ii) In an experiment with fully developed inlet flow, or merged inner and outer wall layers, a position of zero shear stress must occur at a point where the turbulent kinetic energy has a finite value. Therefore the assumption that the shear stress is proportional to the turbulent kinetic energy needs to be revised.

Owing to the initial lack of suitable experimental data on which to base a modified version of the turbulent field method due to Bradshaw et al.[60], it was decided to postpone its application until integral methods had been fully investigated.

In a review of existing integral methods Thompson[56] has shown that of all the auxiliary equations available, the Entrainment equation due to Head[57] proved to be the most satisfactory. Recently the proceedings of the AFOSR-IFP-Stanford Conference on Computation of Turbulent Boundary Layers, have become available, and whilst considerable controversy arose regarding the inadequacy of mean-field methods (pp 399[34]), one indisputable fact emerged namely, that in strong adverse pressure gradients (Moses[44] case 3) the "better" integral method predicts the flow as well as the "better" differential method. The two methods being; integral - Head,[57] differential - Reyhner[34]. In view of the results of the Stanford Conference, and the comparative success achieved by the author in applying an integral method to calculate the flow in symmetrical and expanding inner cone annular diffusers (27) (80) it was decided to adopt an integral approach.

Whilst integral methods will probably be overshadowed eventually by subsequent differential methods, many workers are striving for a method which will be satisfactory for all classes of boundary layers, e.g. relaxing flows, severe adverse pressure gradients, etc. In practical diffuser systems only one class of flows is generally encountered, namely strong adverse pressure gradients, and by removing the catholicity of the requirements it was hoped that an integral approach would be reasonably successful.

5-5 Method of Solution for a Conical Diffuser

It is required to solve the momentum integral equations along inner and outer walls for the case of merged boundary layers. In order to illustrate the solution procedure the case of rotationally symmetric flow in a conical diffuser is considered first.

The procedure is outlined by the author in reference 33, ignoring Reynolds normal stresses we may write the momentum integral equation as

$$\frac{d\theta}{dx} + \frac{\theta}{R_o}\frac{dR_o}{dx} + \frac{\theta}{U}\frac{dU}{dx}(H+2) = \frac{\tau_w}{\rho U^2} + \frac{R_o}{2\rho U^2}\left(\frac{dP_T}{dx}\right)_m \qquad 5\text{-}5\text{-}1$$

where $H = \delta^*/\theta$ and R_o = wall radius

To solve the equation the following additional relations are required:

i) Continuity Equation

Using the axisymmetric definition of displacement thickness δ^* the continuity equation can be expressed as

$$Q = 2\pi R_o U\left(\frac{R_o}{2} - \delta^*\right) \qquad 5\text{-}5\text{-}2$$

ii) Mean Velocity Profile

The simplest possibility is to assume the velocity profiles as a one-parameter family which may be approximated by a power law.

$$\frac{u}{U} = \left(\frac{y}{\delta}\right)^{1/n} = \left(\frac{R_o - R}{\delta}\right)^{1/n} \qquad 5\text{-}5\text{-}3$$

Pretsch[65] has shown that for plane turbulent boundary layers in an adverse pressure gradient, admitting a varying exponent

$$\frac{1}{n} = \frac{1}{2}\left(H - 1\right)$$

using axisymmetric definitions of δ^* and θ we obtain

$$\delta^* = \int_0^{R_o} \left(1 - \frac{u}{U}\right)\frac{R}{R_o}\,dR = f_1\left[\frac{\delta}{R_o}, n\right] \qquad 5\text{-}5\text{-}4$$

$$\theta = \int_0^{R_o} \frac{u}{U}\left(1 - \frac{u}{U}\right)\frac{R}{R_o}\,dR = f_2\left[\frac{\delta}{R_o}, n\right] \qquad 5\text{-}5\text{-}5$$

iii) Diffuser Geometry

It is assumed that the initial value of Ro, and the wall angle $\left({}^{dR_o}/dx\right)$ will be specified

iv) Local Skin Friction Coefficient

Due to the dominating influence of the pressure gradient an equation for plane boundary layers due to Ludwieg and Tillmann[42] is sufficiently accurate. Using axisymmetric boundary layer parameters.

$$\frac{\tau_w}{\rho U^2} = 0.123 \Big/ \left(10^{0.678H} R_{e_\theta}^{\ 0.268}\right) \qquad 5\text{-}5\text{-}6$$

v) Total Pressure Gradient along the Streamline of Maximum Velocity

The total pressure gradient $\left(\frac{dP_T}{dx}\right)_m$ can be obtained empirically by correlation with a suitable mean flow parameter, say H, or as proposed by Imbach[30] from the shear stress gradient

$$\left(\frac{dP_T}{dx}\right)_m = -\frac{1}{R}\frac{d}{dR}\left[R\tau\right] \qquad 5\text{-}5\text{-}7$$

Imbach suggested that if the shear stress distribution in the immediate vicinity of $R = 0$ is approximated by a straight line then

$$\left(\frac{dP_T}{dx}\right)_m = -2\frac{d\tau}{dR} \qquad 5\text{-}5\text{-}8$$

Assuming an eddy viscosity(e.g. $\frac{\varepsilon}{U\delta^*}$ = 0.018) and a parabolic velocity distribution near the point of maximum velocity $\left(\frac{dP_T}{dx}\right)_m$ can be estimated from equation 5-5-8.

vi) Auxiliary Equation

In order to form a closed set of equations additional assumptions are required, which for a developing internal flow could be provided by a modified form of Head's[57] entrainment equation. The modification is required to take account of the reduction in entrainment area due to the growth of the boundary layer. However for fully developed flow at inlet, i.e. merged boundary layers over the length of the diffuser, there is no net entrainment, and provided the flow is symmetrical, the boundary layer thickness $\delta = R_o$. Closure is therefore effected by a simple, physically acceptable assumption, without the need to incorporate additional empiricism in the form of an auxiliary equation.

Substitution in equations 5-5-4, and 5-5-5 yields

$$\frac{\delta^*}{R_o} = \frac{1}{2} + \frac{n^2}{(n+1)(2n+1)} \qquad 5\text{-}5\text{-}9$$

$$\frac{\theta}{R_o} = n^2\left[\frac{1}{(n+1)(2n+1)} - \frac{1}{(2+n)(2+2n)}\right] \qquad 5\text{-}5\text{-}10$$

The momentum integral equation can now be solved, step-by-step, iterating for values of the exponent 'n'. The success of the method hinges on the correctness of the assumed velocity profile. A flow diagram is shown in Fig. 5-5-1, and a comparison between theory and experiment is also presented. It will be seen that there is good agreement.

5-6 Method of Solution for an Annular Diffuser

The momentum integral equations (see Reference 33 and Appendix 25) for the inner and outer wall boundary layers are

$$\frac{d\theta_o}{dx} + \frac{\theta_o dR_o}{R_o dx} + (H_o+2)\frac{\theta_o dU}{U\,dx} = \frac{\tau_{wo}}{\rho U^2} + \frac{R_o^2-R_m^2}{R_o}\frac{1}{2\rho U^2}\left(\frac{dP_T}{dx}\right)_m + \frac{1}{U^2}\frac{dJ_o}{dx} \qquad 5\text{-}6\text{-}1$$

$$\text{where} \quad J_o = \int_{R_m}^{R_o}(\overline{u'^2}+\overline{v_m'^2}-\overline{v'^2})\frac{R}{R_o}dR \quad \& \quad H_o = \delta_o^*/\theta_o$$

$$\frac{d\theta_i}{dx} + \frac{\theta_i dR_i}{R_i dx} + (H_i+2)\frac{\theta_i dU}{U\,dx} = \frac{\tau_{wi}}{\rho U^2} + \frac{R_m^2-R_i^2}{R_i}\frac{1}{2\rho U^2}\left(\frac{dP_T}{dx}\right)_m + \frac{1}{U^2}\frac{dJ_i}{dx} \qquad 5\text{-}6\text{-}2$$

$$\text{where} \quad J_i = \int_{R_i}^{R_m}(\overline{u'^2}+\overline{v_m'^2}-\overline{v'^2})\frac{R}{R_i}dR \quad \& \quad H_i = \delta_i^*/\theta_i$$

Following a similar technique to that outlined in Section 5-5 the following equations are required

(i) Continuity Equation

Using the axisymmetric definitions of displacement thickness

$$\delta_o^* = \int_{R_m}^{R_o}\left(1-\frac{u}{U}\right)\frac{R}{R_o}dR \qquad 5\text{-}6\text{-}3$$

$$\delta_i^* = \int_{R_i}^{R_m}\left(1-\frac{u}{U}\right)\frac{R}{R_i}dR \qquad 5\text{-}6\text{-}4$$

the continuity equation may be written as

$$Q = 2\pi R_o U\left[\frac{R_o^2-R_m^2}{2R_o} - \delta_o^*\right] + 2\pi R_i U\left[\frac{R_m^2-R_i^2}{R_i} - \delta_i^*\right] \qquad 5\text{-}6\text{-}5$$

(ii) Mean Velocity Profiles

In order to introduce the method of solution power law velocity profiles are assumed. The two-parameter presentation due to Coles[41] is considered in Section 5-6-1. Therefore in the outer wall boundary layer

$$\frac{u}{U} = \left(\frac{R_o-R}{\delta_o}\right)^{1/n_o} \qquad 5\text{-}6\text{-}6$$

and since there is no potential core $\delta_o = R_o - R_m$ and

$$\frac{u}{U} = \left(\frac{R_o-R}{R_o-R_m}\right)^{1/n_o} \qquad 5\text{-}6\text{-}7$$

the boundary layer parameters are obtained by integrating across the layer.[27]

$$\frac{\delta_o^*}{R_m - R_o} = \frac{R_o + R_m}{2R_o} - \frac{1}{R_o}\left[\frac{R_m n_o}{(1+n_o)} + \frac{(R_o - R_m)\, n_o^2}{(1+n_o)(1+2n_o)}\right] \qquad 5\text{-}6\text{-}8$$

and

$$\frac{\theta_o}{R_o - R_m} = \frac{R_m}{R_o}\left[\frac{n_o}{(1+n_o)} - \frac{n_o}{(2+n_o)}\right] + \frac{R_o - R_m}{R_o}\left[\frac{n_o^2}{(1+n_o)(1+2n_o)} - \frac{n_o^2}{(2+2n_o)(2+n_o)}\right] \qquad 5\text{-}6\text{-}9$$

Similarly, for the inner wall layer

$$\frac{u}{U} = \left(\frac{R - R_i}{\delta_i}\right)^{1/n_i} = \left(\frac{R - R_i}{R_m - R_i}\right)^{1/n_i} \qquad 5\text{-}6\text{-}10$$

$$\frac{\delta_i^*}{R_m - R_i} = \frac{R_m + R_i}{2R_i} - \frac{1}{R_i}\left[\frac{R_m n_i}{(1+n_i)} - \frac{(R_m - R_i)\, n_i^2}{(1+n_i)(1+2n_i)}\right] \qquad 5\text{-}6\text{-}11$$

$$\frac{\theta_i}{R_m - R_i} = \frac{R_m}{R_i}\left[\frac{n_i}{(1+n_i)} - \frac{n_i}{(2+n_i)}\right] - \frac{R_m - R_i}{R_i}\left[\frac{n_i^2}{(1+n_i)(1+2n_i)} - \frac{n_i^2}{(2+2n_i)(2+n_i)}\right] \qquad 5\text{-}6\text{-}12$$

(iii) Diffuser Geometry

The initial values of R_o and R_i together with $dR_o/_{dx}$ and dR_i/dx will be specified

iv) Local Skin Friction Coefficient

Again the equation due to Ludwieg and Tillmann[42] is assumed, namely $\dfrac{\tau_\omega}{\rho U^2} = 0.123\Big/\left(10^{0.678H}\, Re_\theta^{\;0.268}\right)$ 5-6-13

The inner and outer wall boundary layer parameters being used as appropriate.

v) Reynold's Normal Stress Coefficient

Since this term is only considered to be significant when the flow is near to separation it is assumed that no significant error will be incurred by writing, (see Appendix 25),

$$\frac{1}{U^2}\frac{d}{dx}\int_{R_m}^{R_o}\left(\overline{u'^2} + \overline{v'^2_m} - \overline{v'^2}\right)\frac{R}{R_o}\,dR = \frac{1}{U^2}\frac{d}{dx}\int_{R_m}^{R_o}\left(\overline{u'^2} - \overline{v'^2}\right)dR$$

in which case the correlation due to Goldberg[29] is assumed

$$\frac{1}{U^2}\frac{d}{dx}\int_0^{\delta}\left(\overline{u'^2} - \overline{v'^2}\right)dR = 0.0365\,(H - 1.0)\,\frac{d\delta^*}{dx} \qquad 5\text{-}6\text{-}14$$

Inner and outer wall boundary layer parameters being used as appropriate.

(vi) Total Pressure Gradient along the Streamline of Maximum Velocity

Whilst this term could be calculated from equation 5-5-7 by estimating the shear stress gradient at the position of maximum velocity, difficulties arose due to the power law velocity profile failing to satisfy the condition; $\frac{\partial u}{\partial R} \rightarrow 0$ as $R \rightarrow R_m$. In addition to this an assumed value of mixing length or eddy viscosity was required, and, it was decided therefore to obtain $(dP_T/dx)_m$ empirically. The experimental values of $\frac{D_o^2 - D_m^2}{D_o} \frac{2}{\rho U^2} \left(\frac{dP_T}{dx}\right)_m$ were plotted against the outer wall shape parameter Ho, and within the limits of experimental error a reasonable correlation was achieved (see Appendix 10).

The method of calculating $(dP_T/dx)_m$ for the two-parameter velocity profile equation due to Coles[41] is considered in Section 5-6-1

vii) Auxiliary Equations

Additional equations are required before a solution can be obtained; these could take the form of moment of momentum equations, or, possibly kinetic energy integral equations, but both approaches incorporate the integral of the shear stress across the layers. It was decided to abandon these approaches because of the lack of success of existing methods of estimating the shear stress, particularly in a severe adverse pressure gradient, and assume that no net mass transfer takes place between the inner and outer wall layers. Therefore;

$$Q_o = 2\pi R_o U \left[\frac{R_o^2 - R_m^2}{R_o} - \delta_o^* \right] = \text{constant} \qquad 5\text{-}6\text{-}15$$

$$Q_i = 2\pi R_i U \left[\frac{R_m^2 - R_i^2}{R_i} - \delta_i^* \right] = \text{constant} \qquad 5\text{-}6\text{-}16$$

Admittedly such an assumption is open to question, but a similar approach has met with reasonable success when applied to a conical and a symmetrical annular diffuser[33]. However, it must be emphasised that this approach can only be applied to the case of smooth walled diffusers with naturally developed boundary layers at inlet. It is not expected to hold in cases where the inlet boundary layers have a high rate of decay.

The momentum equations are solved separately iterating for values of the exponents $\frac{1}{n_o}$ and $\frac{1}{n_i}$, and the boundary condition that the maximum velocity in both layers should be the same is satisfied by iterating values of the radius of the position of maximum velocity Rm. The solution procedure is outlined in Fig. 5-5-2 and detailed in Appendix 28.

Because of the importance attached to the velocity profile equation, an additional computer programme was compiled using the two-parameter representation due to Coles[41]. The basic equations remain unaltered, and only those terms affected by the modified velocity profile equation will be discussed.

5-6-1 Calculation Procedure using Velocity Profile Equation Due to Coles

i) Coles Law

Coles[41] has shown that the velocity profile in a turbulent boundary layer can be expressed as the sum of two functions, one representing the "Law of the Wall" and the other in Coles' terminology the "Law of the Wake". This representation is based on the idea that, "a typical boundary layer can be viewed as a wake-like structure which is constrained by a wall," a schematic representation of a typical profile is shown overleaf

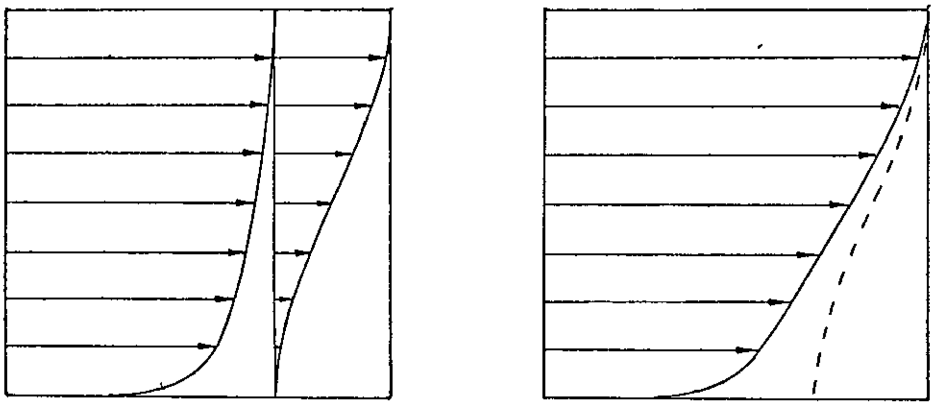

The equation takes the form

$$\frac{u}{u_\tau} = f\left(\frac{y u_\tau}{\nu}\right) + \frac{\Pi}{K} w\left(\frac{y}{\delta}\right) \qquad 5\text{-}6\text{-}17$$

where $u_\tau^2 = \tau_w/\rho$. The function f (the Law of the Wall) has the form

$$f\left(\frac{y u_\tau}{\nu}\right) = \frac{1}{K} \log_e \left(\frac{y u_\tau}{\nu}\right) + C \qquad 5\text{-}6\text{-}18$$

outside the sublayer. The constants K and C are taken as 0.40 and 5.1 respectively, independent of pressure gradient. The function $w\left(\frac{y}{\delta}\right)$ is the "Law of the Wake", which for analytical purposes is taken as

$$w\left(\frac{y}{\delta}\right) = 1 + \sin\left[\pi\left(\frac{y}{\delta} - 0.5\right)\right] \qquad 5\text{-}6\text{-}19$$

and satisfies the two normalising conditions

$$\left.\begin{aligned} w(1.0) &= 2.0 \\ \int_0^1 w \, d\left(\frac{y}{\delta}\right) &= 1.0 \end{aligned}\right\} \qquad 5\text{-}6\text{-}20$$

Π is a parameter which depends on the pressure gradient, and can be obtained by writing equation 5-6-17 at $y = \delta$

$$\frac{U}{u_\tau} = \sqrt{\frac{2}{C_f}} = \frac{1}{K} \log_e\left(\frac{\delta u_\tau}{\nu}\right) + C + \frac{2\Pi}{K}$$

given K, C, ν, and U, this equation determines any one of the three parameters u_τ, δ, Π, if the other two are known.

However considerable care is necessary in applying Coles' formulation, particularly when δ and u_τ are the known parameters. Coles Law is shown below in a semi-logarithmic plot

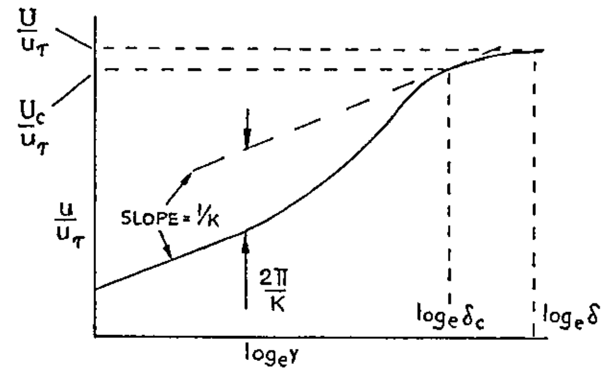

In Coles' formulation δ_c is the value of y at which the slope of the velocity profile $\partial(u/u_\tau) / \partial(\log_e y u_\tau/\nu)$ near the edge of the layer is equal to the slope which the logarithmic profile has near the wall viz. $\frac{1}{K}$. In his original paper Coles assumed that the velocity (U_c) at δ_c was experimentally indistinguishable from U the free stream velocity, and although this is an acceptable assumption, he went on to assume that δ_c was equal to δ, the value of y at U. It is this assumption, recognised by Bull(66) which can have serious effects on profile representation. In a more recent paper Coles(44) has limited his method of analysis to values of $\frac{y}{\delta} \leq 0.9$. This solution to the problem of the "corner effect" may be acceptable in analysing experimental data but it does not assist in the theoretical prediction of velocity profiles.

Titcomb and Fox(67) using Coles Law in its original form have shown (see Fig. 5-6-1) that for a given Reynolds number, $\frac{\theta}{\delta} \simeq f(H)$. Therefore, since the integral method adopted predicts θ, for assumed values of H and δ ($\delta = R_o - R_m$), the predicted value of θ will be affected directly by errors in δ. This approach should be compared with normal methods where H and

θ are obtained from the auxiliary and momentum equations respectively. The experimental velocity profile is then compared with Coles representation for given values of θ and H. Consequently errors in δ of the order of 10% are frequently accepted, provided good agreement is achieved in the inner regions of the layer. It is, therefore, critical to the success of the integral method adopted, that the correct value of δ_c is used in Coles Law. It has been suggested by Bull(66) that the ratio (δ_c/δ) should be correlated with the parameter Π , which depends on the pressure gradient. The correlation is shown in Fig. 5-6-2, the data shows that as the pressure gradient increases, the assumption $(\delta_c \cong \delta)$ becomes more accurate. When attempts were made to use the correlation due to Bull difficulty was experienced in obtaining the correct initial values of momentum thickness. It was found that a different correlation was required depending on whether the calculations were initiated upstream or downstream of the inlet bend. This was considered to be due to the fact that whereas the velocity profiles were in equilibrium upstream of the inlet bend, downstream in the diffusing section, grossly non-equilibrium profiles were present. Two correlations were therefore used as indicated in Fig. 5-6-2. The lack of agreement with the data due to Bull is thought to be due to history effects, and the higher turbulence intensities at the edge of the test boundary layers. The predicted values of θ and δ^* were obtained by numerical integration as detailed in Appendix 28.

(ii) Local Skin Friction Coefficient

The skin friction coefficient was obtained from Coles Law (see Appendix 28).

(iii) Total Pressure Gradient along the Streamline of Maximum Velocity

Apart from the empirical correlation discussed in Section 5-5, the total pressure loss was calculated from the shear stress gradient near the edge of the outer wall boundary layer assuming a value of mixing length equal to 0.20 δ_o^* . In view of the large radius ratio (Ri/Ro) it was assumed that $\frac{1}{R}\frac{\partial}{\partial R}(R\tau) \simeq \frac{\partial \tau}{\partial R}$ (see Appendix 24).

An attempt was also made to obtain $(dP_T/dx)_m$ from the energy integral equation.

$$\frac{d\delta^{**}}{dx} = (\delta - \delta^*)_o \frac{2}{\rho U^2}\left(\frac{dP_T}{dx}\right)_m + 2\mathcal{D} - 3\frac{\delta_o^{**}}{U}\frac{dU}{dx}$$

The dissipation integral being obtained using the expressions due to Goldberg[29] and Rotta[61].

The calculation procedure was very similar to that outlined in Fig. 5-5-2, differing only in the following respects;

i) Skin friction coefficient obtained from Coles Law

ii) That the solution of the momentum integral equations was obtained by iterating values of Cf rather than the exponent ($^1/n$).

The computer programme is detailed in Appendix 28. The calculations were carried out on an I.C.T. 1905 computer, the running times being; Power Law Programme $\simeq$ 40 secs., Coles Law Programme $\simeq$ 2 mins. Tests were carried out to prove the convergence of the methods, the step lengths and iteration limits chosen were such as to incur no significant error.

5-6-2 Initial Conditions

The calculations were initiated at two stations, one upstream of diffuser inlet, the other at the first convenient measuring station downstream of the inlet bend. The downstream station was chosen to avoid the disturbance due to the change in outer wall angle. In this way it was hoped to investigate the sensitivity of the predictions to inlet conditions. The inlet conditions are detailed in Appendix 29, calculations started downstream of the inlet bend required additional information regarding the experimental pressure rise, total pressure loss etc. up to the initial station. The theoretical cases considered are listed in Section 6-6, and the computer print-out for a selected number of cases is shown in Appendix 29.

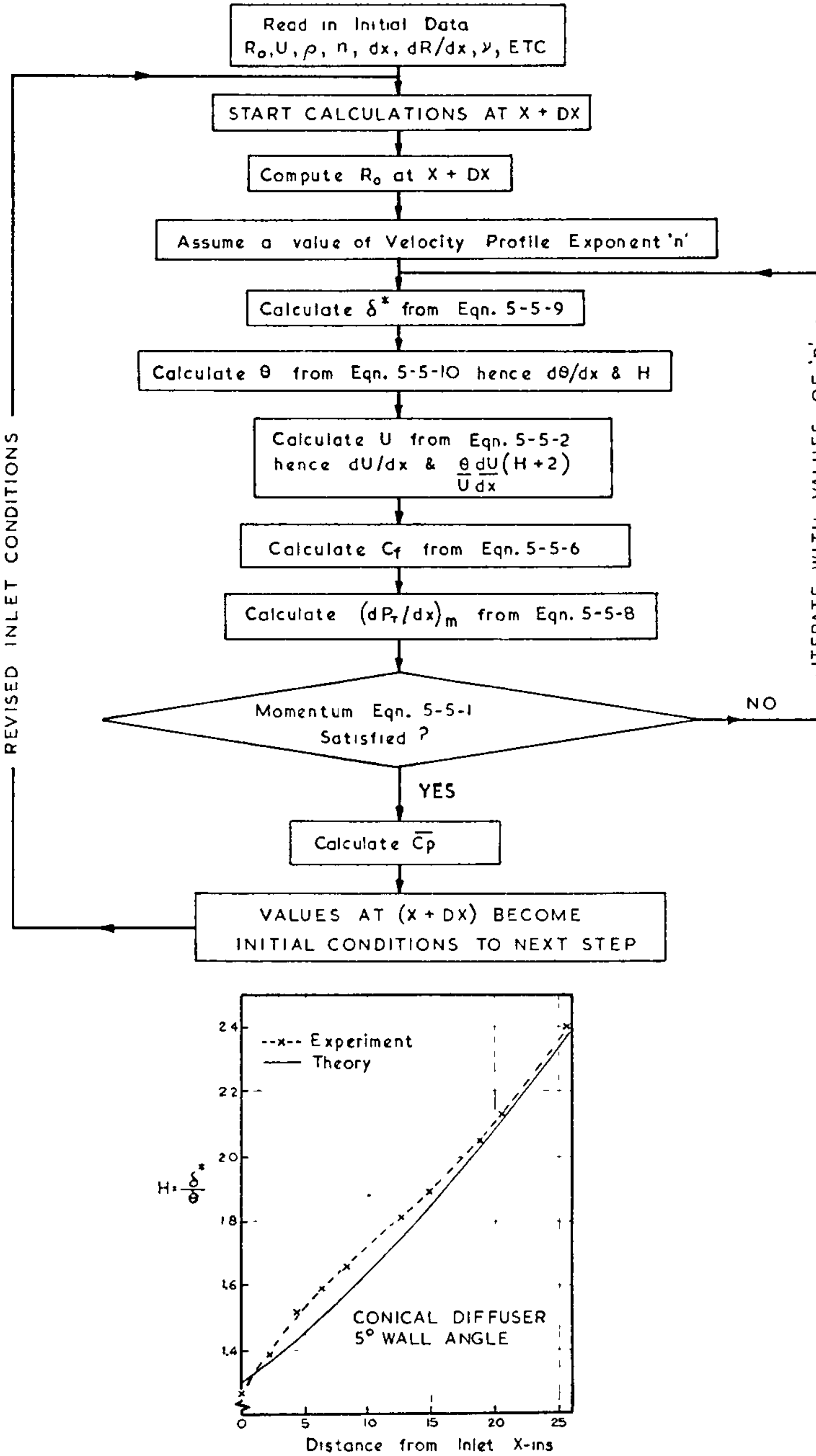

FIG. 5-5-1 FLOW DIAGRAM OF THE COMPUTER PROGRAMME (CONICAL DIFFUSER) AND COMPARISON BETWEEN THEORY AND EXPERIMENT AFTER STEVENS[33]

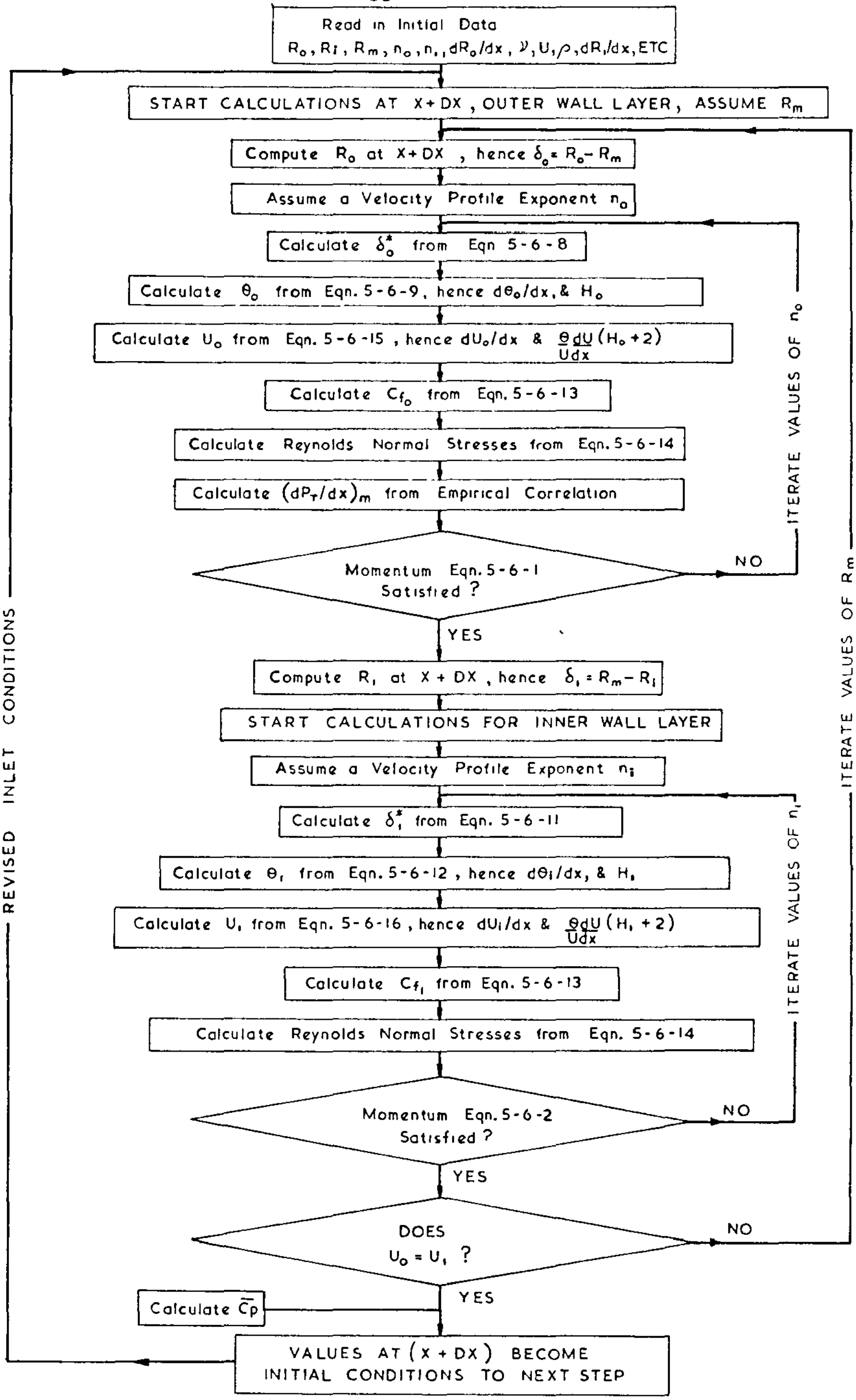

FIG. 5-5-2 FLOW DIAGRAM OF THE COMPUTER PROGRAMME FOR AN ANNULAR DIFFUSER

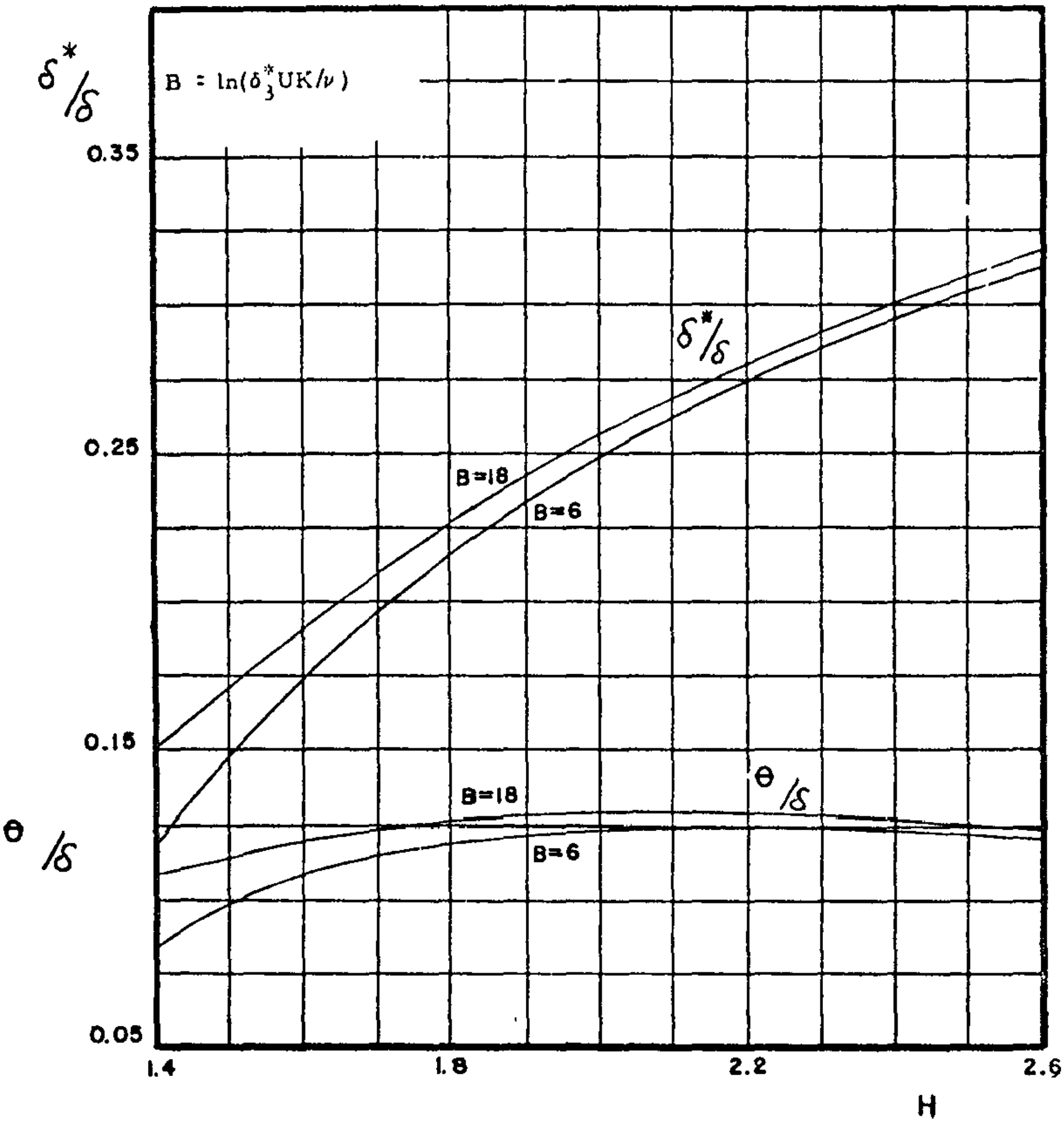

FIG. 5-6-1 BOUNDARY LAYER PARAMETERS AFTER TITCOMB AND FOX [67]

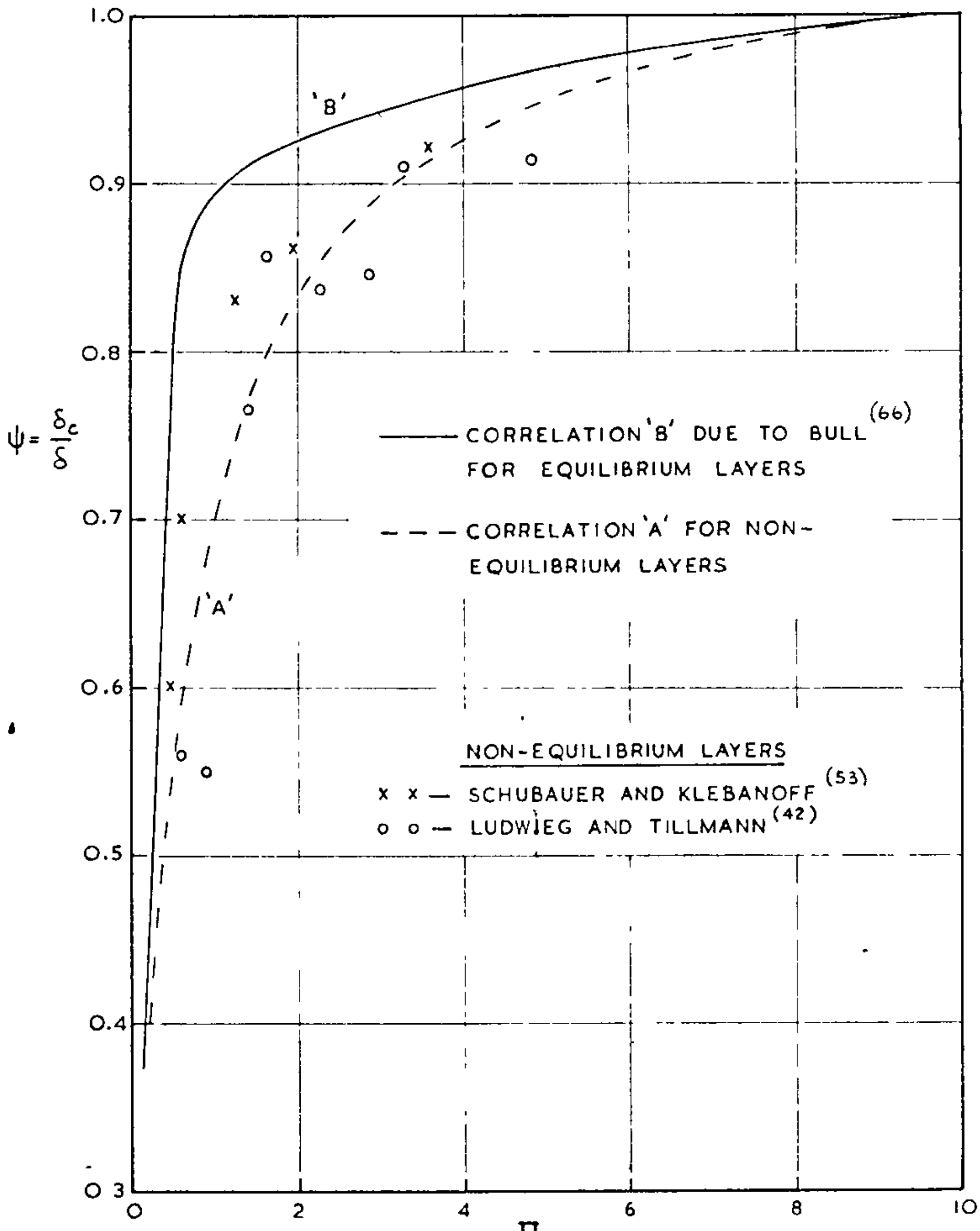

FIG. 5-6-2 VARIATION OF ψ WITH COLES PARAMETER Π

SECTION 6

DISCUSSION OF THEORETICAL RESULTS AND COMPARISON WITH EXPERIMENT

In seeking to compare the theoretical predictions with experiment, the following criteria are normally used:

(i) To calculate accurately the development of the velocity profile and hence the pressure recovery.

(ii) To indicate the imminence of stalling.

Criterion (i) implies that the momentum thickness θ, shape parameter H, and maximum velocity at any section are known, and that the velocity profile may be accurately represented by a single or two parameter equation. No suitable theory exists to satisfy the second criterion[34] although the shape parameter is often used as a guide, values ranging from 1.8 to 4.0 have been quoted as an indication of stalling.

One of the difficulties in assessing the large number of predictions used, is that in merely comparing θ, H, etc. the effect of the individual assumptions may well be lost. Thus in order to establish the accuracy of the prediction method adopted the validity of the assumptions will be examined by direct comparison with experiment. The theoretical approach adopted depends on:

(i) That no net mass transfer takes place between the inner and outer wall boundary layers.

(ii) The velocity profile equation.

(iii) An estimate of the total pressure loss along the streamline of maximum velocity.

(iv) An empirical correlation for the Reynolds normal stresses

(v) An estimate of the skin friction coefficient.

6-1 No Net Mass Transfer Assumption

The percentage mass flow in the outer wall boundary layer calculated by integrating the velocity profile at each station is shown in Fig. 6-1-1. Whilst such a calculation is sensitive to the estimated value of R_m, the results show that within the limits of experimental accuracy the mass flow in the outer wall boundary layer remains constant. Only at exit of the $L/\Delta R_1 = 5$ diffuser is any significant scatter noted, and this is attributed to the presence of a transitory stall.

The estimated position of the streamline of maximum velocity (Rm) and the location of the point of zero shear stress ($R_{\tau=0}$) are compared in Fig. 6-1-2. Changes in total pressure along a streamline are caused by momentum transfer between adjacent streamlines; thus if Reynolds shear stresses, which represent the mean momentum transfer in the 'R' direction of ' x ' component momentum per unit volume, are small in the vicinity of Rm, then the total pressure loss at this point should also be very small. Fig. 6-1-2 confirms that this is the case, and in view of the local symmetry of the velocity profile in this region, the indications are that both the momentum, and mass transfer, at the position of maximum velocity are indeed very small.

It is not possible to state conclusively that no net mass transfer takes place between the inner and outer wall boundary layers, but it can be stated that, within the limits of experimental accuracy, any net mass transfer which does take place is very small.

6-2 Mean Velocity Profiles

The simplest method of representing a turbulent velocity profile is the one parameter representation initiated by Prandtl for turbulent pipe flow. Pretsch[65] and Spence[68] have expressed this result in the form of the power law. However, it is now generally accepted on physical grounds, that the turbulent boundary layer can only be described in terms of a minimum of two regions (inner and outer), and this necessitates the use of at least two parameters to define the velocity profile. The Coles "Wake Law" which describes the departure of the profile in the outer region, from the universal "Law of the Wall" has been used in this investigation.

6-2-1 Relationship between Boundary Layer Parameters

Many authors (Goldberg[29] and Thompson[69]) have plotted the energy shape parameter $\overline{H}$ as a function of H to establish that the experimental data can be represented satisfactorily by a one or two parameter equation. The experimental results for inner and outer wall layers are plotted in a similar manner in Fig. 6-2-1; also shown are the power law and Coles law values. Whilst the inner wall data form a well defined line, some scatter is noted in the outer wall results. Since this method of analysis is rather insensitive at high values of H, an alternative method of comparison was adopted.

The theoretical prediction of flow in a diffuser with merged boundary layers requires that θ be calculated from assumed values of H, δ and U . In view of this the results are compared by plotting values of θ / δ as a function of H in Figs. 6-2-2/3 respectively. The inner wall values again form, within the limits of experimental error, a well defined line although some 20% lower than the predicted values. In the case of the outer wall the results do not collapse onto a unique line, although the results for individual diffuser tests appear to follow well defined variations with little scatter. As the diffuser non-dimensional length decreases so the disparity between experimental and predicted values becomes more evident, therefore in the case of outer wall profiles both the one and two parameter representations clearly fail.

The inadequacy of the accepted methods of profile representation could be due to one, or a combination of the following factors:

i) That in large adverse pressure gradients, the velocity profile equations are not well enough known; e.g. a failure of the universal law of the wall, and/or the law of the wake

ii) Upstream history effects

iii) The comparatively large turbulent fluctuations in the outer regions of the layers.

6-2-2 Proximity to Local Equilibrium in Boundary Layers with Adverse Pressure Gradients

In order to assess the severity of the pressure gradients the shape parameter H is plotted against the non-dimensional pressure gradient parameter ($\frac{\theta}{\tau_\omega}\frac{dP}{dx}$) in Figs. 6-2-4/5. Such an approach has been used by Rotta(61) to illustrate history effects in boundary layer development. Clauser(51) has shown that if $\left(\frac{\theta}{\tau_\omega}\frac{dP}{dx}\right)$, which expresses the ratio of the pressure gradient to skin friction forces, remains constant, the velocity profiles are of similar shape. These profiles which have a constant history are known as 'equilibrium' profiles, and Nash(70) has suggested the following relationship for equilibrium values of H

$$\sqrt{\frac{2}{C_f}}\left(1 - \frac{1}{H}\right) = 6.1\left(\frac{\delta^*}{\tau_w}\frac{dP}{dx} + 1.81\right)^{0.5} - 1.7$$

Nash analysed the data of Schubauer and Klebanoff[53], Newmann[71], and Ludwieg and Tillmann,[42] and found that the results were in good agreement with the line for equilibrium values. This is not to say that the boundary layers were in equilibrium, but that "the variation in shape parameter is the same as if the layers were passing through each possible equilibrium state". Nash therefore referred to the data, which has always been classified as "strong adverse pressure gradient", as being in "local equilibrium".

The results for the inner wall boundary layers, shown in Fig. 6-2-4 indicate that the profiles in the $L/\Delta R_1$ = 10 diffuser are in local equilibrium. However the layers in the $L/\Delta R_1$ = 7.5 & 10.0 diffusers initially depart from equilibrium, and then return as the pressure gradient is relaxed. The same tendency is observed in the relaxing pressure gradient data of Bradshaw[50]. Thus for the same pressure gradient parameter velocity profiles of different shape are produced, Rotta stated that "this demonstrates clearly that our system has a dynamic character and that the behaviour of the output is influenced by the previous history of the input."

The adverse pressure gradient data of Moses[28] and Ludweig and Tillmann[42] are included with the outer wall results in Fig. 6-2-5, also shown is the data due to Stratford (IDENT. 5200 & 5300[44]) for which Coles[44] is, "convinced of a real failure of the similarity laws". Again the results for the

$L/\Delta R_1 = 10$ diffuser are near to "local equilibrium" whereas there is a significant departure for the other test configurations, with no tendency for a return to equilibrium conditions. It is of interest that the "severe adverse pressure gradient" data of Moses(28) is in "local equilibrium", but the data of Stratford shows a marked departure followed by the characteristic return in a relaxing pressure gradient.

6-2-3 Comparison of Velocity Profiles

In view of the suspicion that history effects may be present it was decided to compare the measured velocity profiles with the accepted methods of representation i.e. using the power law and Coles law. Sufficient data was available to compare profiles of the same shape parameter having different upstream histories.

In comparing velocity profiles of the same H it is conventional to plot u/U against the non-dimensional distance from the wall (y/θ), θ being used because its value can be obtained more precisely than δ. For the power law

$$\frac{u}{U} = \left(\frac{y}{\theta}\right)\left[\frac{H-1}{H(H+1)}\right]^{\frac{H-1}{2}} \quad * \qquad 6\text{-}2\text{-}1$$

Such a calculation proceeds up to a value of $u/U = 0.99$, at which point it is generally assumed that the velocity is experimentally indistinguishable from the maximum value. However, many research workers go further and assume the value of y at $u/U = 0.99$, is equal to the boundary layer thickness δ. The error involved in such an assumption is usually neglected in view of the inaccuracy of the profile equation in this region, and the difficulty of obtaining an accurate value of δ. For a power law

$$\frac{\theta}{\delta} = \frac{H-1}{H(H+1)} \quad * \qquad 6\text{-}2\text{-}2$$

* two-dimensional version

In the theoretical approach adopted θ is calculated from assumed values of δ (i.e. $R_o - R_m$) and H, and the profile equations are assumed to hold up to the edge of the layer ($y = \delta$). Whilst in the normal manner of presentation, an error, typically 10%, is accepted between theoretical and experimental values of δ, in this investigation such a situation would result in a 10% error in the predicted value of θ. Therefore the theoretical approach adopted places a particularly severe test on the velocity profile equations. It was decided that for comparative purposes θ and H would be specified and values of $^u/U$ calculated at varying distances from the wall, in this way errors in δ could be observed directly.

<u>Power Law Velocity Profile</u>

In this case the profiles were treated as plane boundary layers, and the two-dimensional values of θ and H were specified. (the values differ by less than, 7.5% for θ, and 3% for H from the axisymmetric values, see appendix 4).

<u>Coles Law Velocity Profile</u>

As discussed in Section 5-6-1 particular care needs to be exercised in applying Coles law. Coles[44] in preparing data for the conference at Stanford University[34] recognised the deficiency in the equations near the edge of the boundary layer and took this into account by limiting the region of curve fitting. Coles stated "I have chosen to attack the data by finding values of the two parameters δ and u_τ for each of the profiles such that the R. m. s. deviation of the data from the formula (1) is minimised". The curve fitting region was limited to $y/\delta \leqslant 0.9$ when the wake component was large, to 0.75 for flow at constant pressure, and to 0.60 as the wake component vanished. Moreover in some cases significant disagreement was found between the experimental data and Eqn. 5-6-17 in the 10 to 15% of the profile near the wall. Coles[44] assumed that the discrepancy could be attributed to experimental error; only in the large pressure gradient data of Bradshaw[50] and Stratford[35] was he "convinced of a real failure of the similarity laws".

In comparing the data with the representation due to Coles, a number of methods of attack were considered, namely;

i) To follow the latest technique, curve fitting over a limited range of y/δ

ii) Solve the velocity profile Equation 5-16-7 to give the experimental values of θ and H in the manner illustrated below

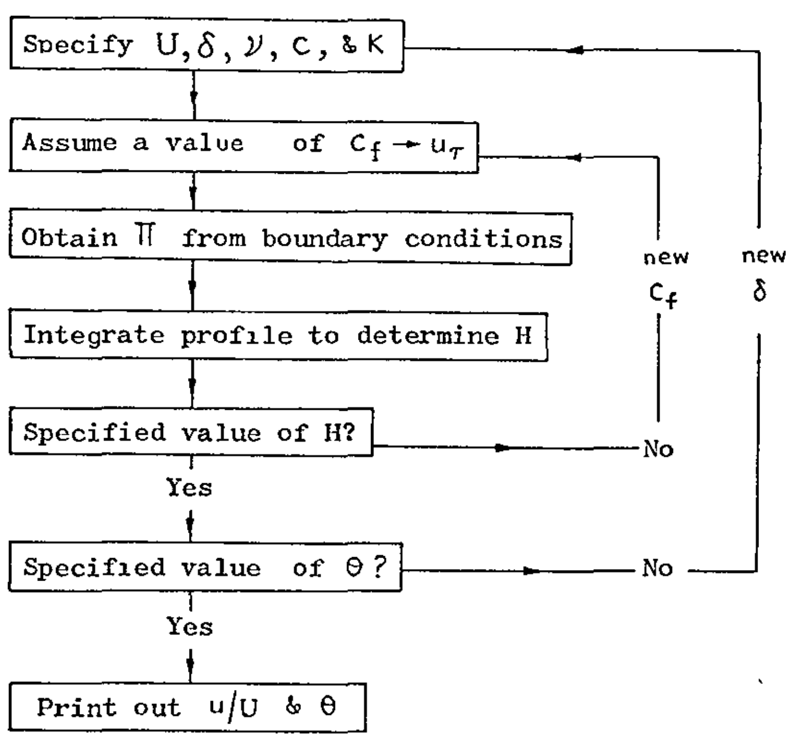

iii) Using experimental values of δ and Cf (from law of wall plot) compare the velocity defect with Coles wake function.

Approach (i) removes much of the simplicity which makes Coles law so attractive since additional relationships would be required to specify the shape of the profile in the outer regions of the layer. Titcomb and Fox(67) used approach (iii) and concluded that in order to fit experimental profiles over a wide range of values of H three different versions of Coles Law were required. Approach (ii) was therefore adopted with a view to obtaining a correlation between δ_{Coles} and δ_{expt}.

To assess the validity of approach (ii) the profiles due to Perry(72) were analysed, and the results compared with those of Coles who limited the range of curve fitting to values of y/δ between 0.125 and 0.90. The main results are given in Table 6-1 and the profiles compared in Fig. 6-2-6. It will be seen that there is excellent agreement.

In analysing the experimental data outer wall velocity profiles having shape parameters of 1.5, 1.69, 1.9 and 2.1 were investigated. For each shape parameter two profiles were chosen, one non-equilibrium, the other near to local equilibrium. On the inner wall three profiles were analysed. The location of the profiles relative to local equilibrium is indicated in Figs. 6-2-4/5. The experimental results are compared with the power law and Coles Law predictions in Figs. 6-2-7 to 6-2-12, the turbulent shear stress distribution is also included. The following initial observations may be made:

i) In nearly all the cases considered there is a significant difference between δ as given by Coles Law and the experimental value. The ratio ψ ($\psi = \delta_{coles}/\delta_{expt.}$) falling to as low as 0.76 for the outer wall profile at X = 1.35 ins., $L/\Delta R_1 = 5.0$.

ii) For the twelve profiles investigated, in only four can good agreement be claimed for the two parameter representation due to Coles. These profiles are at:

x = 6.0 ins., $L/\Delta R_1 = 7.5$, outer wall

x = 9.85ins., $L/\Delta R_1 = 10.0$, inner wall

x = 4.28ins., $L/\Delta R_1 = 5.0$, outer wall

x = 7.7 ins., $L/\Delta R_1 = 10.0$, outer wall

three of which are near to local equilibrium (the profile at x = 4.28 ins. is outside the range of the data upon which Nash's correlation is based). Also all of the profiles are in the latter stages of diffusion with relatively low pressure gradients ($\frac{dP}{dx}$)

iii) In those cases where significant disagreement occurs between experiment and Coles law the failure is always of the same character namely that the predicted values are; too high near the wall, too low in the middle of the layer, and too high at the edge of the layer. These findings are identical to those of Thompson(56) who compared a two parameter family with the results of Stratford(35) for a boundary layer in a large adverse pressure gradient. Titcomb and Fox(67) obtained similar results for boundary layers in a conical diffuser.

iv) In nearly all the cases where a failure of Coles law occurs, the power law is considerably better, particularly in the inner 60% of the layer. This is particularly surprising since the merit of Coles law is its good agreement near the wall. If it is accepted that some correction to δ will be required whichever profile representation is used, then for the majority of the profiles investigated the power law is to be preferred.

Since on physical grounds Coles law is normally preferred, it is important to establish, if possible, the physical reasons for its failure. It is therefore proposed to examine the two similarity laws.

6-2-4 The Law of the Wall

As already noted in Section 4-11 many of the velocity profiles fail to satisfy the law of the wall. In some cases no logarithmic variation can be detected even down to values of ($\frac{y u_\tau}{\nu}$) as low as 100. In view of this it is proposed to review the justification for the law of the wall. Prandtl assumed that, at large Reynolds numbers, the shear stress outside the laminar sublayer may be written as $\tau = \rho \ell^2 \left(\frac{du}{dy} \right)^2$

The mixing length 'ℓ' was assumed to proportional to the distance from the wall i.e. $\ell^2 = k^2 y^2$. The assumption was also made that for a thin layer near the wall the shear stress remains constant i.e. $\tau = \tau_\omega$

Thus $$\tau_\omega = \rho k^2 y^2 \left(\frac{du}{dy} \right)^2 \qquad 6\text{-}2\text{-}3$$

integration of Eqn. 6-2-3 yields

$$u = \frac{1}{\kappa} u_\tau \log_e y + \text{Const.} \qquad 6\text{-}2\text{-}4$$

where the friction velocity $u_\tau = \sqrt{\frac{\tau_\omega}{\rho}}$

Equation 6-2-4 known as the universal law of the wall has been found to be valid not only in the vicinity of the wall, but over a much larger proportion of the layer than would normally be expected. Following the experiments of Ludwieg and Tillman[42] the universal law was also assumed to hold in an adverse pressure gradient, although the extent of the logarithmic portion was reduced considerably. However as pointed out by Rotta[61] and Thompson[56] the pressure gradients in Ludwieg and Tillmanns' experiments were relatively small.

When a boundary layer is exposed to an extremely severe pressure gradient examination of the experimental shear stress distributions in the vicinity of the wall (see Figs. 4-9-1/2/3) reveals that;

(i) the wall shear stress decreases rapidly

(ii) there is a large gradient of shear stress normal to the wall.

Thus the constant shear stress hypothesis, upon which the universal law is based, is invalidated in a strong pressure gradient.

Using a mixing length approach, Stratford[35] considered the influence of a shear stress gradient on the flow near the wall when the skin friction is negligible. Since the inertia forces at a wall are zero, the mean flow equation reduces to;

$$\left(\frac{d\tau}{dy}\right)_{y=0} = \frac{dP}{dx} \qquad 6\text{-}2\text{-}5$$

Integration of Eqn. 6-2-5 across a small region close to the wall gives

$$\tau = y\frac{dP}{dx} \qquad 6\text{-}2\text{-}6$$

Eliminating τ between Eqns. 6-2-5 and 6-2-6

$$\frac{du}{dy} = \left(\frac{1}{\rho K^2}\frac{dP}{dx}\right)^{0.5} y^{-0.5}$$

Integrating, and using the no-slip condition gives

$$u = \left(\frac{4}{\rho K^2}\frac{dP}{dx}\right)^{0.5} y^{0.5} \qquad 6\text{-}2\text{-}7$$

Townsend(74) and McDonald(73) have considered the general case of a shear stress gradient combined with finite wall shear.

Writing $\tau = \tau_\omega + \left(\frac{dP}{dx}\right) y = \rho K^2 y^2 \left(\frac{du}{dy}\right)^2$

to give $\frac{du}{dy} = \frac{(ay + \tau_\omega)^{0.5}}{\rho^{0.5} K y}$ $\qquad a = \frac{dP}{dx}$

which integrates to

$$u = \frac{2}{\rho^{0.5}K}\left(ay + \tau_\omega\right)^{0.5} + \left(\frac{\tau_\omega}{\rho K^2}\right)^{0.5} \log_e\left[\frac{(ay + \tau_\omega)^{0.5} - \tau_\omega^{0.5}}{(ay + \tau_\omega)^{0.5} + \tau_\omega^{0.5}}\right] \qquad 6\text{-}2\text{-}8$$

Townsend has written the non-dimensional form of Eqn. 6-2-8 as

$$\frac{u}{u_\tau} = \frac{2}{K}\left[(\gamma y^+ + 1)^{0.5} - 1\right] + \frac{1}{K}\log_e\left[\frac{4(\gamma y^+ + 1)^{0.5} - 1}{\gamma(\gamma y^+ + 1)^{0.5} + 1}\right] \qquad 6\text{-}2\text{-}9$$

where

$$\gamma = \frac{dP}{dx}\frac{\nu}{\rho u_\tau^3}$$

$$y^+ = \frac{y u_\tau}{\nu}$$

and $B^+ = 5.0$ $\qquad K = 0.40$

The additive constant B^+ is obtained by matching the profiles at the edge of the sublayer. It was suggested by Townsend that the flow in the sublayer would not be affected by moderate pressure gradients and he therefore assumed the zero pressure gradient additive constant. Townsend's equation has recently been modified by McDonald(73) to take account of the influence of pressure gradient on the flow in the sublayer, and an allowance was also made for the departure from the wall value of the gradient of shear stress normal to the wall.

The correctness of the "conventional" universal equation is therefore seen to depend on the magnitude of the parameter $\gamma \left(\frac{\nu}{\rho u_\tau{}^3} \frac{dP}{dx} \right)$ as illustrated in Fig. 6-2-13. The "strong adverse pressure gradient" data of Ludwieg and Tillmann correspond only to values of $\gamma \leqslant 0.0035$, whilst in some of the profiles of Stratford, for which $\gamma \simeq 0.14$, no logarithmic portion can be found. Thompson has suggested that if $\gamma > 0.10$ estimates of Cf from the Coles two-parameter profile could be in error by as much as 60%.

Great difficulty arises in attempting to compare measured profiles with the predicted values from Eqn. 6-2-9 since the wall shear must be known before any meaningful comparison can be made. In the literature there is not one case where significant pressure gradient effects could be expected and where both the velocity profile and skin friction have been measured directly. An attempt was made to see if the approach due to Clauser(51) could be used to obtain more accurate values of Cf, since the experimental pressure gradient was known, and a plot of $^u/U$ against $\frac{(R_o - R)\,U}{\nu}$ could be obtained from Eqn. 6-2-9 for various values of Cf. Unfortunately this approach was not successful as the experimental points did not lie on a line of constant Cf. The reasons for this apparent failure can be traced to the underlying assumptions, since many authors, particularly Spangenberg et al.(46) have shown that away from the wall $\frac{d\tau}{dy} \neq \frac{dP}{dx}$. Bradshaw(34) found that $\frac{d\tau}{dy} \simeq \frac{1}{2}\frac{dP}{dy}$. Spangenberg suggested that the remainder of the force near the wall to overcome the pressure gradient is to be found in the Reynolds normal stress term. Also, the actual rate of development of the mean flow ($u\frac{\partial u}{\partial x} + v\frac{\partial u}{\partial R}$) and upstream history can be expected to have an effect. The influence of these effects, using the data presented in this thesis, is the subject of a continuing investigation.

Therefore the estimates of Cf from the conventional law of the wall equation in Section 4-11 can only be considered as approximate and the experimental values of γ given in Table 6-2 are only a guide to the relative significance of pressure gradient effects. It will be seen that in many cases the values of γ are an order of magnitude greater than those recorded in Ludwieg and Tillmann's experiments, whilst along the outer wall of the $L/\Delta R_1 = 5$ diffuser values are obtained that are higher than those achieved by Stratford. It can therefore be concluded that the failure of the experimental profiles to exhibit a logarithmic variation near the wall is due to the large adverse pressure gradients which have been encountered.

Since the experimental values of wall shear stress are relatively low it can be argued that the shear stress at a point in the vicinity of the wall is approximately equal to $\left(\frac{dP}{dx}\right) y$, in which case using the approach due to Stratford

$$\left(\frac{u}{U}\right)^2 = K_1 \left(R_0 - R\right) \qquad 6\text{-}2\text{-}10$$

where $K_1 = \frac{2}{\kappa^2}\left(\frac{2}{\rho U^2}\frac{dP}{dx}\right)$ 6-2-11

The experimental values of $(u/U)^2$ plotted against distance from the wall for the $L/\Delta R_1 = 5$ & 10 diffusers are shown in Figs. 6-2-14/15. Also indicated is the approximate position of the point of maximum shear stress.

In the case of the profiles measured in the $^{L}/\Delta R_1 = 5$ diffuser, nearly all follow the half-power law ($u/U = k\,y^{0.5}$). The failure at X = 4.28 ins. along the outer wall is considered to be due to the non-linearity in the turbulent shear stress profile. At a number of stations the experimental value of K_1' (Eqn. 6-2-11) was compared with the theoretical value assuming zero wall shear. Without exception the experimental values were found to be higher, by as much as 40% in some cases. The reason for this discrepancy is due in part to the fact that Prandtl's assumption i.e., $\ell = 0.40\,y$, is only true in the immediate vicinity of the wall. In the latter stages of diffusion the variation of mixing length follows a ramp function with the value of ℓ remaining constant over a large proportion of the layer.

Also indicated in Figs. 6-2-14/15 is the approximate position of maximum shear stress; it is surprising to see that the half-power law, based on the assumption of a constant shear stress gradient continues for some distance past this point. This is rather similar to the situation which prevails in equilibrium layers where a mixing length approach based on constant shear stress extends over a greater proportion of the profile than would normally be expected. It is difficult to state precisely why this should occur since many factors can influence the shape of the profile in the outer regions of the layer e.g. a variation in the shear stress gradient, Reynolds normal stress etc. The clarification of the relative influence of these effects is still under investigation.

Despite the lower overall pressure gradient a number of the velocity profiles in the $^{L}/\Delta R_1 = 10$ diffuser follow

Stratford's half-power law. Again the experimental values of K_1 were found to approximately 30% higher than the predicted values.

Recent experiments reported by Stevens and Eccleston[36] on an optimum $\overline{C}_p^*$ annular diffuser in which both wall angles were positive, have confirmed the half-power law in severe adverse pressure gradients. McDonald[73] has drawn similar conclusions after analysing the data of Spangenberg et al.[46] for which $\gamma \simeq 0.04$.

In summary, an initial analysis of the inner region of the velocity profiles indicates a clear failure of the conventional form of the "Law of the Wall". This is due to the large shear stress gradient which is required to balance the pressure forces near the wall. A large proportion of the velocity profiles follow Stratford's half-power law.

6-2-5 The Law of the Wake

The normalised velocity defect curves for the profiles analysed in the previous section were compared with Coles universal wake function $w\left(\frac{y}{\delta}\right)$. In the majority of cases the level of agreement was poor, the discrepancy increasing as the value of γ increased. In addition $w\left(\frac{y}{\delta}\right) = 2.0$ occurred at a value of $y/\delta < 1.0$. Similar conclusions were reached by Titcomb and Fox[67], who modified the wake function, and whilst some improvement was obtained the general level of agreement with experimental profiles was still unacceptable. Thus the failure of Coles Law to predict the shape of the outer region of the velocity profiles could be due to:

i) That the velocity defect curves do not follow a universal wake function

ii) That the velocity defect curves have been based on an incorrect 'law of the wall'.

iii) History effects

Non-Universal Velocity Defect Profile

Bull[66] in analysing the data of Mellor and Gibson[75] suggested that the normalised velocity defect curve is not a universal function. The inability of the function to extend to the edge of the layer, i.e. $w (y/\delta) = 2.0$ at $y/\delta < 1.0$, has been taken into account by Bull who plotted ψ (δ Coles/δ expt) against the Coles parameter Π which is a function of pressure gradient. The experimental values of ψ are shown in Fig.6-2-16 and compared with the two correlations used in the prediction method. Whilst the inner wall values of ψ correlate reasonably well, there is a large amount of scatter in the outer wall results. This is to be expected since the correlation is based on a two-parameter velocity profile equation which has been shown to be inadequate for a large number of the outer wall profiles.

A failure of the wake function for the profiles due to Stratford[35] has also been reported by Thompson[56]. In this case the conventional form of the 'law of the wall' was also used to obtain the velocity defect profile.

Incorrect 'Law of the Wall'

It has been shown in the previous section that in regions of severe adverse pressure gradient a modified law of the wall equation is required. The wake function due to Coles cannot therefore be expected to apply in such cases since it is based on a similarity law which is assumed to be independent of pressure gradient. The question arises, if a modified 'law of the wall' equation is used will the corresponding velocity defect curves follow a universal function? The answer hinges on the correctness of the modified law of the wall, which must be verified by direct measurement of wall shear stress. Until this has been done no conclusive remarks can be made, moreover the problem is further complicated by the influence of upstream history.

6-2-6 History Effects

Evidence of history effects can be observed in Figs.6-2-7 to 6-2-12 in the sense that at a given value of H different shear stress distributions are measured. Although the velocity profile cannot in many cases be characterised by a two-parameter family, neither can the shear stress be uniquely defined by the local velocity gradient. More information is needed concerning what has gone before, i.e. concerning the upstream history of the flow.

The classical case of history effects is observed in attempts to calculate the behaviour of a boundary layer in a relaxing pressure gradient. In such a case information regarding the initial shear stress distribution and its subsequent rate of development is required before meaningful calculations can be made. The relative importance of history effects can be studied by examining the equation of motion

$$u\frac{\partial u}{\partial x} + v\frac{\partial u}{\partial y} = -\frac{1}{\rho}\frac{dP}{dx} - \frac{\partial}{\partial x}\left(\overline{u'^2}\right) + \frac{\partial \tau}{\partial y}$$

History effects enter the equation via the last two terms on the right-hand-side, namely the Reynolds normal and shear stresses. If the pressure gradient term is large in comparison with the Reynolds stresses, history effects will have negligible influence on the development of the boundary layer. Stratford[76] assumed that in the outer part of the layer the shear stress is negligible if the pressure gradient is sufficiently strong. In which case the pressure force is in competition with inertia forces only, and the total head is approximately constant along a streamline. In order to assess the significance of history effects in the profiles shown in Figs. 6-2-7 to 6-2-12, the value of $\frac{d\tau}{dy}$ was calculated in the outer regions of the layers i.e. outside the range of the half-power law. The results of the calculations are tabulated below.

H	station x (ins)	wall	Diffuser $L/\Delta R_1$	Fig.No.	$\frac{d}{dy}\left(\frac{2\tau}{\rho U^2}\right)$ (approx)	$\frac{d}{dx}\left(\frac{2P}{\rho U^2}\right)$
1.50	0.75	outer	5.0	6-2-3	0.004	0.260
1.50	1.25	outer	7.5	6-2-3	0.0053	0.146
1.69	1.35	outer	5.0	6-2-1	0.006	0.185
1.69	4.70	outer	10.0	6-2-1	0.010	0.073
1.90	1.95	outer	5.0	6-2-4	0.0085	0.132
1.90	7.7	outer	10.0	6-2-4	0.0165	0.057
2.10	2.55	outer	5.0	6-2-2	0.0128	0.098
2.10	6.00	outer	7.5	6-2-2	0.032	0.068

In the above calculations the profiles were treated as plane boundary layers. Whilst history effects are present their influence is negligible during the initial stages of diffusion. This is mainly due to the large initial pressure gradient, and, to a lesser extent, to the lag in the shear stress distribution.

Only in the later stages of diffusion does the term $\frac{d\tau}{dy}$ become significant. In which case the pressure gradient should be compared with the difference between the gradient of Reynolds stress in the measured profile, and in an equilibrium profile having the same value of H (assuming $\frac{\partial \overline{u'^2}}{\partial x} \ll \frac{\partial \tau}{\partial y}$)
The profile at X = 7.7 ins. has, within experimental error, an equilibrium shear stress distribution (based on $\frac{\varepsilon}{U\delta^*}$) in the outer region of the layer. In the case of the profile at X = 6.0 ins. the measured shear stress distribution is lower than the equilibrium value but the discrepancy is not large enough to have a significant influence. Both profiles are in fact relatively close to equilibrium (see Fig. 6-2-5), and because of this history effects which can be observed in the lag of the shear stress distributions do not significantly influence the flow in the outer regions of the layers.

History effects are normally associated with the flow in the outer region, but there is evidence to suggest that the Reynolds normal stresses may influence the flow in the inner region. Spangenberget al.[46] in noting that $\left(\frac{d\tau}{dy}\right)_{y=0} < \frac{dP}{dx}$ suggested that the remainder of the force near the wall was to be found in the normal stresses. An investigation of this effect along the outer wall of the $L/\Delta R_1 = 5$ diffuser revealed that near the inlet $d\tau/dy = 0.8\ dP/dx$ decreasing to $0.25\ dP/dx$ at $X/L = 0.75$. Calculations at $X/L = 0.75$ indicate that the discrepancy could be ascribed to the influence of Reynolds normal stresses. On the outer wall of the $L/\Delta R_1 = 10$ diffuser at $X/L = .725$, $\frac{d\tau}{dy} = 0.9 \frac{dP}{dx}$ and in this case the longitudinal turbulence intensity distributions confirm that the contribution due to $\frac{\partial \overline{u'^2}}{\partial x}$ is small.

6-2-7 Velocity Distribution at the Edge of the Layer

It was anticipated that the higher turbulence intensities at the edge of the layers would influence the velocity distribution in that region. However no evidence to support this view was found, since the profile which is in good agreement with Coles law at the edge of the layer ($X = 7.7$ ins. $L/\Delta R_1 = 10$, Fig. 6-2-4) has a relatively high level of "edge" turbulence intensity. Whereas the profiles which are in poor agreement near the edge of the layer are often to be found in the initial stages of diffusion with a relatively low level of "edge" turbulence intensity. Therefore the frequent failure of Coles law to predict the velocity distribution near the edge of the layer is considered to be due to a breakdown of the similarity laws rather than the influence of "edge" turbulence intensity.

6-2-8 Concluding Remarks

The object of the analysis in this section has been to establish the reasons for the failure of Coles Law to adequately describe the outer wall velocity profiles in the $L/\Delta R_1 = 5$ & 7.5 diffusers. These profiles which have been developed in an extremely severe adverse pressure gradient are far removed from a state of local equilibrium and under such conditions it has been shown that:

i) The universal law of the wall which is the corner stone of most turbulent skin friction laws is invalid. The modified law proposed by Townsend[74] which takes account of the influence of pressure gradient is more applicable.

ii) In a severe adverse pressure gradient the velocity distribution in the inner region of the layer follows a half-power law.

iii) In a near-separating boundary layer the force required to overcome the pressure gradient is principally derived from the Reynolds normal stresses.

iv) The universal "Law of the Wake" in its present form is unsuitable

v) History effects do not have a significant influence in the outer region of the layer.

The outer wall velocity profiles in the $L/\Delta R_1 = 10$ diffuser and the majority of the inner wall profiles, can be adequately represented by Coles Law providing a suitable correction is made to the boundary layer thickness.

In conclusion, it appears that for velocity profiles near to a condition of local equilibrium the accepted methods of profile representation are adequate. However for profiles that are grossly non-equilibrium there is a real failure of the existing similarity laws.

6-3 Total Pressure Gradient along the Streamline of Maximum Velocity

Three methods of attack were used to obtain values of the total pressure loss along the streamline of maximum velocity. These were;

i) A theoretical calculation of the shear stress gradient in the vicinity of the position of maximum velocity.

ii) Energy Equation

iii) Empirical correlation of experimental data

The shear stress gradient was calculated using a mixing length approach. A value of $\ell/\delta^* = 0.2$ was assumed, and the slope of the velocity profile near the edge of the outer wall boundary layer was calculated using Coles law.

A number of methods were used to obtain the dissipation coefficient in the energy equation e.g. Goldberg[29], Rotta[61], and mixing length theory, but this approach was abandoned due to numerical difficulties. Examination of the relative magnitude of the terms in the energy equation (see Tables A24-1 to A24-3) indicates that the term incorporating the total pressure loss ($\frac{2}{\rho U^2}(\delta-\delta^*)\left(\frac{dP_T}{dx}\right)_m$) is small in comparison with the pressure gradient term ($3\frac{\delta^{**}}{U}\frac{dU}{dx}$) and therefore small errors in the prediction of the later produce disproportionate changes in the total pressure loss.

The correlation of $\frac{2}{\rho U^2}D_h(dP_T/dx)_m$ with the outer wall shape parameter Ho (see Fig. A10 - 6) was based on the experimental results quoted in Appendix 10, and a test carried out on a conical diffuser. Whilst in the conical diffuser the values of $(dP_T/dx)_m$ were obtained by direct measurement, the values in the annular diffusers have been calculated from the static pressure rise and the kinetic energy coefficient at each station.

A comparison of the experimental and predicted values is shown in Fig. 6-3-1. The gradient of shear stress at the position of maximum velocity was also estimated from the measured shear stress distributions, and the values obtained in this way are included in Fig. 6-3-1. Bearing in mind the difficulties involved in making accurate shear stress measurements, the values obtained are in reasonable agreement with the experimental data.

The momentum-balance plots indicate that the contribution from the term $\frac{R_o^2 - R_m^2}{R_o} \frac{1}{2\rho U^2} \left(dP_T/dx \right)_m$ increases with distance along the diffuser until at exit it represents approximately 35% of $\frac{d\theta_o}{dx}$. Fig. 6-3-1 shows that the empirical correlation predicts $\frac{2}{\rho U^2}\left(\frac{dP_T}{dx}\right)_m$ at diffuser exit to within 30% or better, representing at most a 10% error in the theoretical value of $\frac{d\theta}{dx}$ The lower empirical values of total pressure loss will lead to an overestimate of the shape parameter.

In attempting to calculate the shear stress gradient in the vicinity of the streamline of maximum velocity the value of ℓ/δ^* was chosen with a view to achieving a reasonably accurate estimate in the latter stages of diffusion. It can be seen that this approach has been partially successful although better agreement could be achieved by correlating ℓ/δ^* against a suitable mean flow parameter e.g. H_o. Nevertheless doubts must be expressed regarding the physical correctness (see Batchelor[81]) of using a mixing length approach near the edge of a boundary layer.

6-4 Reynolds Normal Stresses

A comparison of the measured outer wall values of $\left(\frac{1}{U^2}\frac{d}{dx}\int(\overline{u'^2}+\overline{v'^2_m}-\overline{v'^2})\,dR \right.$ with the correlation due to Goldberg[29] is shown in Fig. 6-4-1. The fact that Goldberg's correlation was based on results in a potential core situation, for which $\frac{d\overline{v'^2_m}}{dx} = 0$. has been shown in Appendix 23 to be of only minor importance. The results for the $^L/\Delta R_1 = 10$ diffuser are within the scatter band of the original data, but the results for the $^L/\Delta R_1 = 7.5$ & 5.0 diffusers are discrepant and follow the general trend of the data due to Schubauer and Klebanoff(53). The failure of Goldberg's correlation to predict the lower experimental values is considered to be due to the lag in the turbulence structure. Although a lag or history effect was present in Goldberg's experiments the values of pressure gradient in the $^L/\Delta R_1 = 5$ diffuser are very high and Nash(70) has shown that lag increases with pressure gradient.

The difference between the experimental and predicted values shown in Fig. 6-4-2 is not serious since the normal stress term is only of importance when the boundary layer is driven toward large values of shape parameter. No comparisons are included for the inner wall data as the normal stress term does not make a significant contribution to $\frac{d\theta_1}{dx}$.

The failure of Goldbergs correlation illustrates the fundamental weakness of relating turbulence to the local mean flow quantities.

6-5 Internal Performance

The results of the various prediction methods are summarised in Figs. 6-5-2 to 6-5-5; the following coding is used to identify the methods employed:

C - Coles Law only

CA - Coles Law incorporating a modification to the boundary layer thickness (Ref. Fig. 5-6-2)

CNA - Coles Law with modified thickness and including Goldberg's correlation for the Reynolds normal stress (N.S.C.)

CNEA - Coles Law with modified thickness, N.S.C., and $(dP_T/dx)_m$ obtained from an empirical correlation

CNSA - As above, but $(dP_T/dx)_m$ calculated from the shear stress gradient

P - Power Law

PN - Power Law with N.S.C.

PNE - Power Law with N.S.C. and $(dP_T/dx)_m$ obtained from empirical correlation.

The number in front of the coding indicates the axial distance (ins.) downstream of the diffuser throat at which the calculations commence. The computer print-out for a selected number of cases is given in Appendices 27 and 29. Apart from H and θ, values of the various terms in momentum and energy equations, and the energy thicknesses etc. are included. In the absence of any prediction criteria for turbulent separation the programmes were allowed to run to diffuser exit.

In the methods based on a power law velocity profile no attempt was made to calculate the shear stress gradient near the edge of the boundary layer, because of the known inaccuracy of the power law in this region. The majority of the calculations using Coles law, which commence downstream of the diffuser throat incorporate a modification to the boundary layer thickness based on correlation 'A' (see Fig. 5-6-2). This correlation is for essentially non-equilibrium flow, and for calculations commencing at the diffuser throat correlation 'B' was used to ensure the correct initial value of momentum thickness. In a number of cases both correlations were used for comparative purposes.

In attempting to judge the relative success of the theoretical predictions it must be emphasised that empirical corrections are included in all turbulent boundary layer calculations and a prediction of H and θ to within 10% can be considered to be good. If Coles law is used it is important that both parameters should be predicted accurately, otherwise the estimate of the velocity profile and static pressure rise coefficient will be impaired. Furthermore, the wide range of pressure gradients obtained in the test diffusers represents a severe test of the prediction methods. To assist in assessing the relative success of the methods used, the results of all the theoretical comparisons from the Stanford Conference[34] for the adverse pressure gradient data of Moses (Case 3) are shown in Fig. 6-5-1. It can be seen that all the differential methods fail, and of the integral methods only that due to Head[57] is successful. Head's method predicts final values of H and θ which are lower by approximately 10 and 20% respectively.

The calculations which commence at the diffuser throat eg. O,CNEA predict approximately the same shape parameter at exit, on both inner and outer walls. The failure to predict the asymmetric growth of the shape parameters is due to the inability of the methods to take account of the disturbance associated with the change in flow direction on the outer wall at inlet. Theoretically the calculation should take account of the streamline curvature. In view of this, the calculations were started downstream of the throat at a station where the flow was assumed to have adjusted to the initial disturbance; a similar approach has been adopted by Nicoll and Ramaprian[31]. Unfortunately, if calculations are started downstream of the throat more initial data is required e.g. $\overline{Cp}$, ΔP_T, etc., there is a dearth of information on flow in annular bends and such data is normally unlikely to be available.

Applying Coles law without incorporating a modification to the boundary layer thickness results in an overestimation of θ, and the pressure gradient term $\frac{\theta dU}{Udx}$ (H+2). Consequently the predicted values of shape parameter are too high in all the cases with the exception of the outer wall in the $^L/\Delta R_1 = 5$ diffuser. The inclusion of Reynolds normal stresses does not have any significant effect, and there is little overall difference between the two methods of estimating $(dP_T/dx)_m$. Due to the dominant influence of pressure gradient we may write:

$$\frac{d\theta}{dx} \simeq \frac{\theta}{U}\frac{dU}{dx}(H+2) \qquad 6\text{-}6\text{-}1$$

Comparing the 1.0 CNEA - correlation 'B' predictions with the experimental data it will be seen that there is good agreement for both θ and H in the $^L/\Delta R_1 = 10$ diffuser. In the case of $^L/\Delta R_1 = 7.5$ diffuser the 1.25 CNEA approach using correlation 'A' yields good agreement along the outer wall, but because of an incorrect calculation of the initial inner wall momentum thickness the predicted values of θ_i and H_i are lower by approximately 35% and 15% respectively. The failure to estimate θ correctly on the inner wall is due to the fact that correlation 'A' is for non-equilibrium flow whereas the flow along the inner wall tends towards a condition of local equilibrium. The calculations were repeated using correlation 'B' and as would be expected this gives good results along the inner wall but due to the higher estimated values of momentum thickness the predicted values of H_o are approximately 30% too high. Whilst reasonable agreement is obtained along the inner wall of the $^L/\Delta R_1 = 5$ diffuser there is a real failure in the prediction of H_o, the values being approximately 35% too low. Since the no net mass transfer assumption has been shown, within the limits of experimental error, to be correct, the failure of the predictions in the $^L/\Delta R_1 = 5$ diffuser and the partial failure in the $^L/\Delta R_1 = 7.5$ diffuser can be traced to a breakdown of the similarity laws in Coles equation as discussed in Section 6-2. Apart from the failure of the similarity laws, the need to include additional empiricism in the form of modifications to the boundary layer thickness removes a lot of the attraction in applying Coles formulation. Although calculations were carried out with differing correlations the results are not included since they did not produce any significant improvement. In fact, the main advantage of Coles law appears to lie in the analysis of experimental data.

In view of this calculations were also carried out using the power law velocity profile, which had previously been reasonably successful when applied to a symmetrical annular diffuser.[27] It can be seen that the power law overestimates θ resulting in higher predicted values of shape parameter. However, the values of shape parameter are only marginally inferior to the values obtained using the modified Coles law. In addition the calculations started at the diffuser throat are slightly better than the Coles law predictions. Thus the power law appears to be the better choice although on physical grounds it has less appeal.

Despite the fact that the integral method chosen has only been partially successful it can be stated with reasonable confidence that no other available integral method would have been any more successful. In fact many of those available rely on auxiliary equations which have been shown by Thompson[56] to be notoriously inaccurate, and the "best" integral method namely that due to Head[57] is not applicable for the case of fully developed flow at inlet.

The most disturbing feature of the results is the failure to calculate the behaviour of flow in the diffuser of engineering interest i.e. the optimum $\bar{C}p^*$ diffuser ($L/\Delta R_1 = 5$). The successful application of an integral method to this case requires the formulation of a new velocity profile equation which takes account of the influence of pressure gradient on the flow in the inner region of the layer. In view of the greater potential of differential methods, despite their failure to predict the Moses, Case 3, data[34], work is in hand[77] to modify the method due to Patankar and Spalding[78].

6-6 Overall Performance

The prediction of overall performance is centred on two parameters namely the loss coefficient and the static pressure rise coefficient.

6-6-1 Total Pressure Loss Coefficient

The experimental values of loss coefficient λ_{1-2} are compared with the predicted values in the table below

DIFFUSER $L/\Delta R_1$	5	7.5	10
Experimental value λ 1-2	0.080	0.065	0.077
Predicted values λ 1-2			
0.75/1.25/1.0 CNEA	0.065	0.074	0.055
0.75/1.25/1.0 CNSA	0.068	0.076	0.060
O/PNE	0.052	0.065	0.063

The experimental values are quoted relative to measurements taken at a plane 3 ins. upstream of the throat. The initial conditions supplied to the programme based on Coles law also include the loss between the measuring plane and the stations at which the calculations commence. In the case of the calculations using a power law velocity profile a value of 0.02 has been added to the predicted loss coefficient. This is the estimated loss based on a friction factor of 0.0033 between the measuring plane and the diffuser throat. It can be seen that within the limits of experimental error there is good agreement.

6-6-2 Static Pressure Rise Coefficient

The static pressure rise coefficient is obtained from the equation

$$\bar{C}_p = \left[\alpha_1 - \frac{\alpha_2}{AR^2} \right] - \lambda_{1-2} \qquad 1\text{-}3\text{-}3$$

Thus for specified inlet conditions the prediction of $\bar{C}p$ depends on the estimation of the loss coefficient λ 1-2 and the velocity profile energy coefficient α_2. The value of α_2 is determined by the shape of the exit velocity profile and is calculated in the case of the Coles law representation from the predicted values of θ_o, H_o, θ_i, H_i, U, and R_m. The experimental and predicted values of α_2 and $\bar{C}p$ are compared in Fig. 6-6-1. It can be seen that in the case of the $L/\Delta R_1$ = 7.5 and 10.0 diffusers although there are errors in the predicted values of α_2 they do not significantly affect the values of Cp, which are in good agreement with the measured data. Therefore whilst the theoretical approaches are less than totally adequate for boundary layer calculations, they do appear to be sufficient for predictions of overall performance. Similar conclusions have been reached by Cocanower et al[55]. However in the case of the outer wall boundary layer in the $^{L}/\Delta R_1 = 5$ diffuser there is a more serious failure of the prediction methods and as a consequence the estimated values of $\bar{C}p$ are approximately 20% too high.

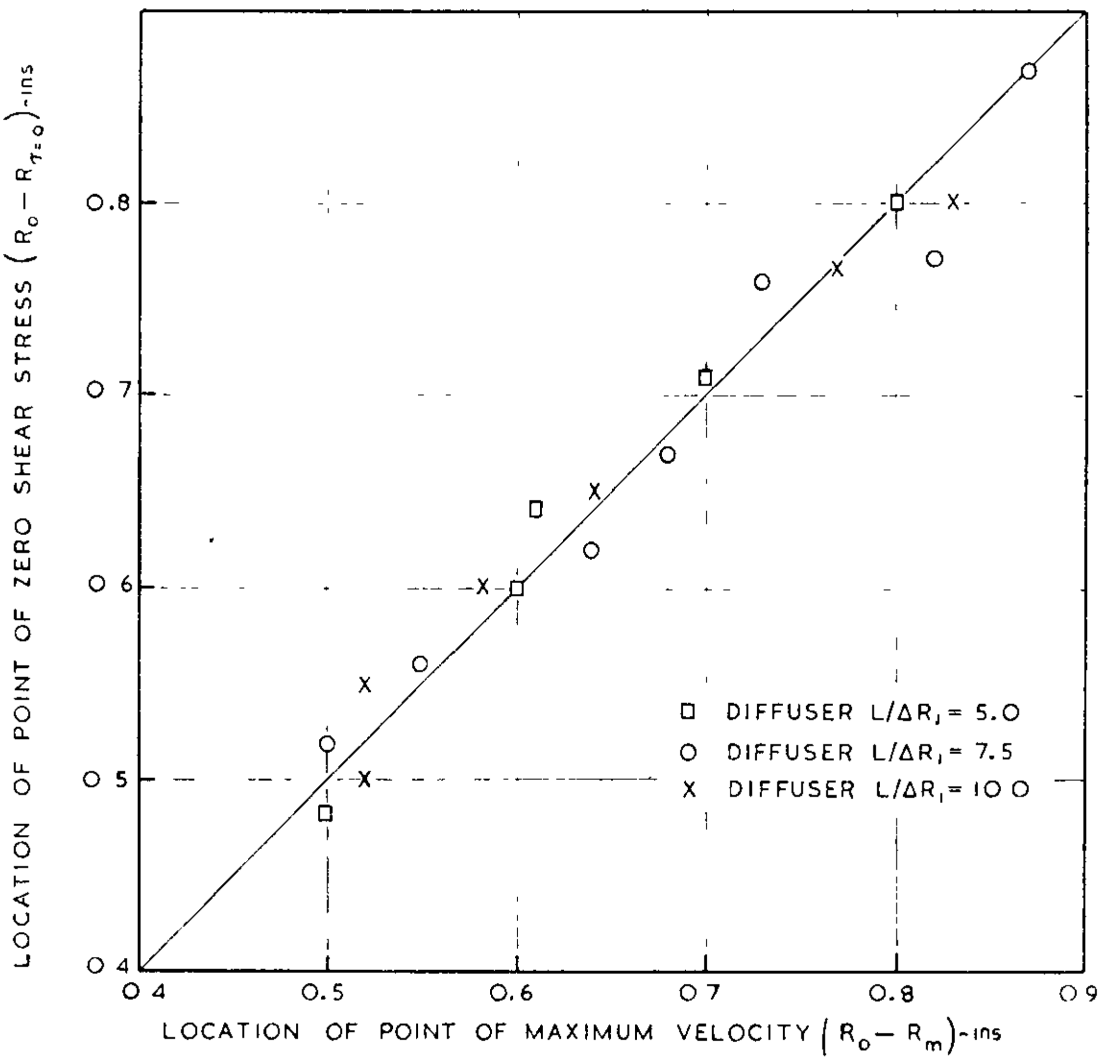

FIG. 6-1-2 COMPARISON OF LOCATION OF POINTS OF MAXIMUM VELOCITY AND ZERO SHEAR STRESS

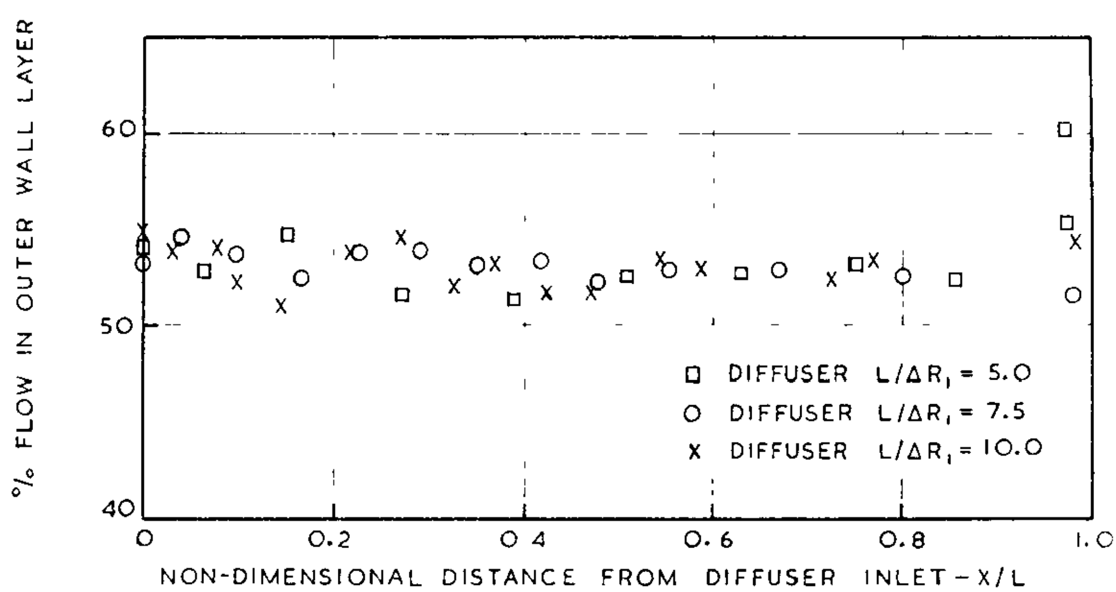

FIG. 6-1-1 PERCENTAGE FLOW IN OUTER WALL BOUNDARY LAYERS

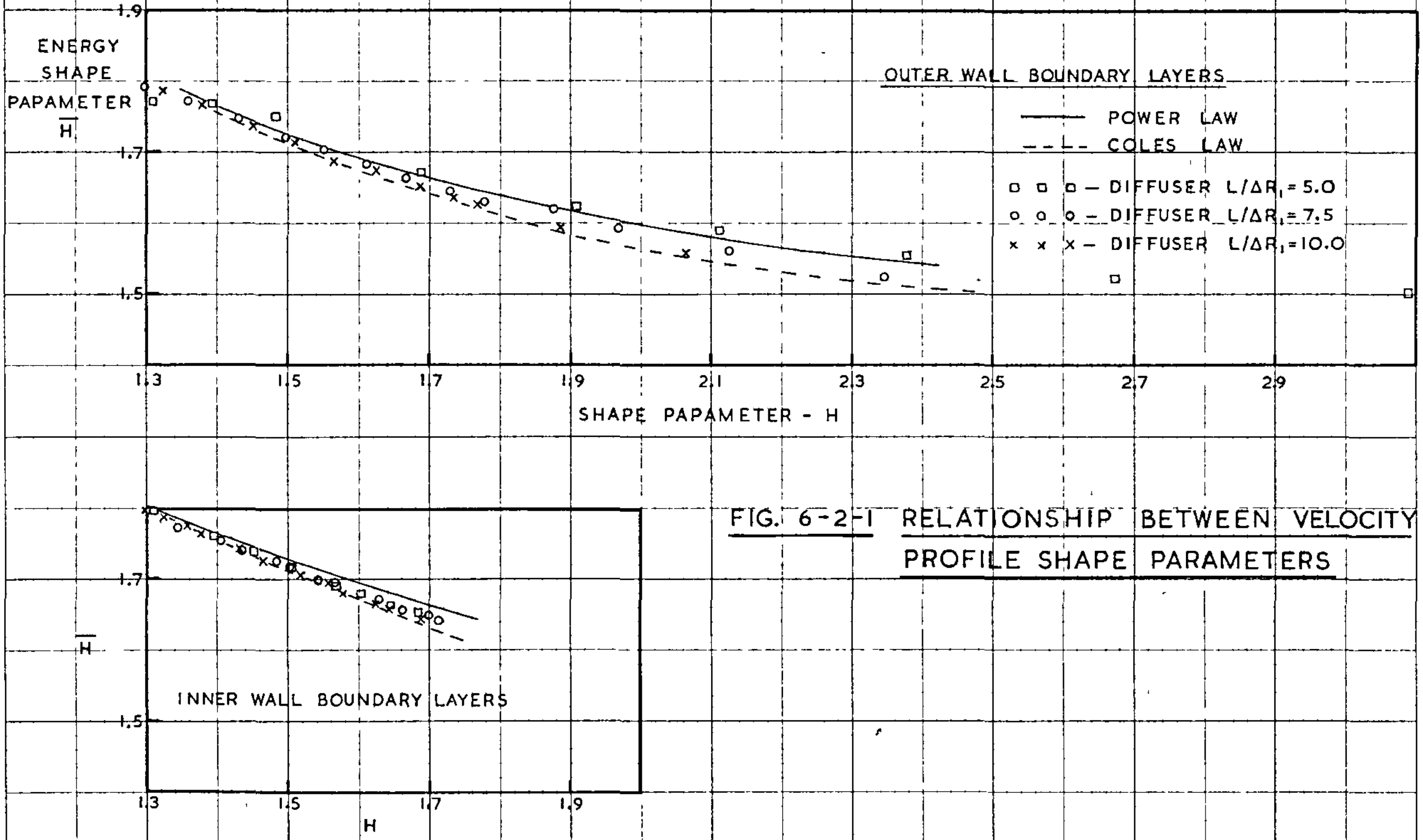

FIG. 6-2-1 RELATIONSHIP BETWEEN VELOCITY PROFILE SHAPE PARAMETERS

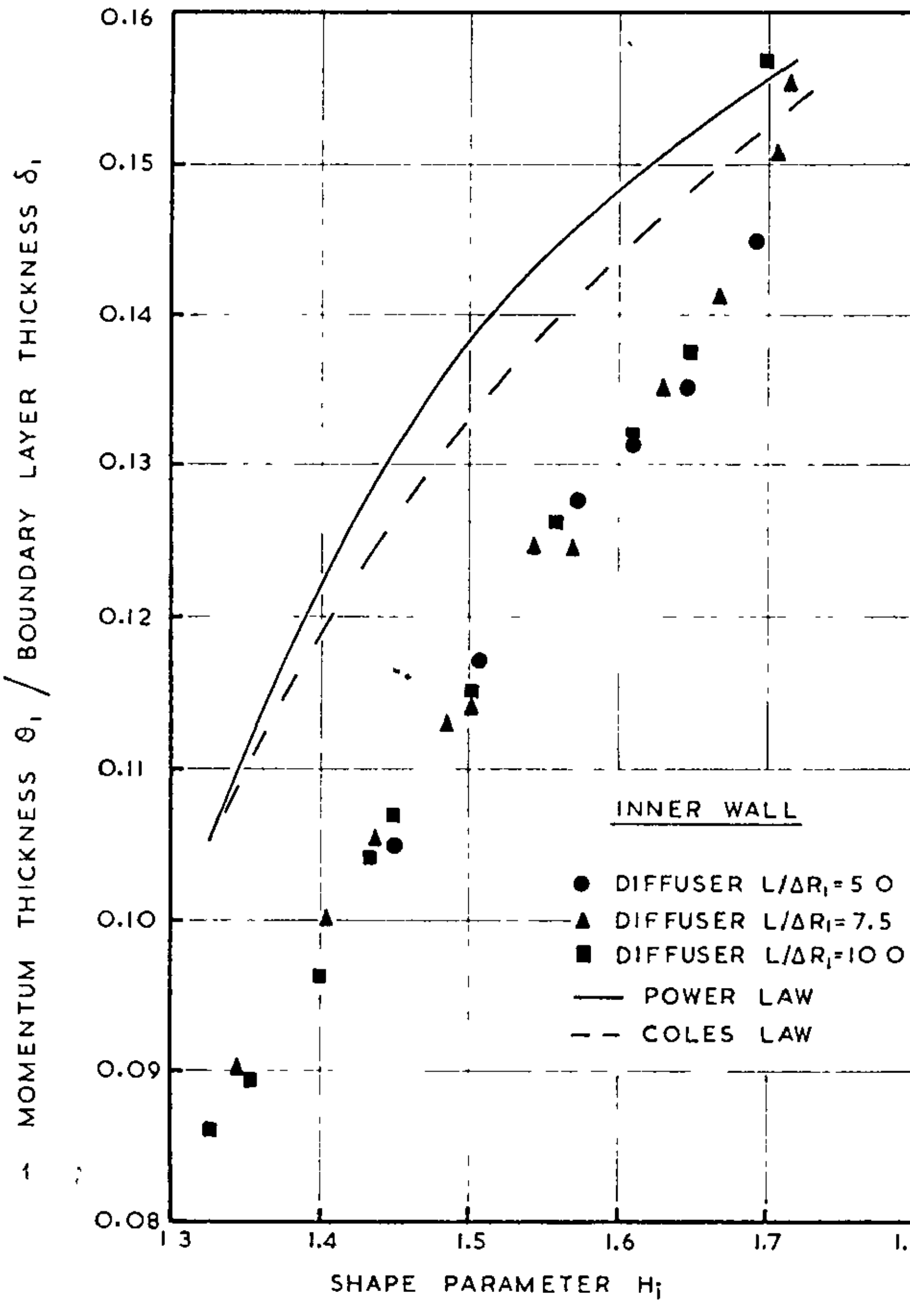

FIG. 6-2-2 RELATIONSHIP BETWEEN NON-DIMENSIONAL MOMENTUM THICKNESS AND SHAPE PARAMETER - INNER WALL

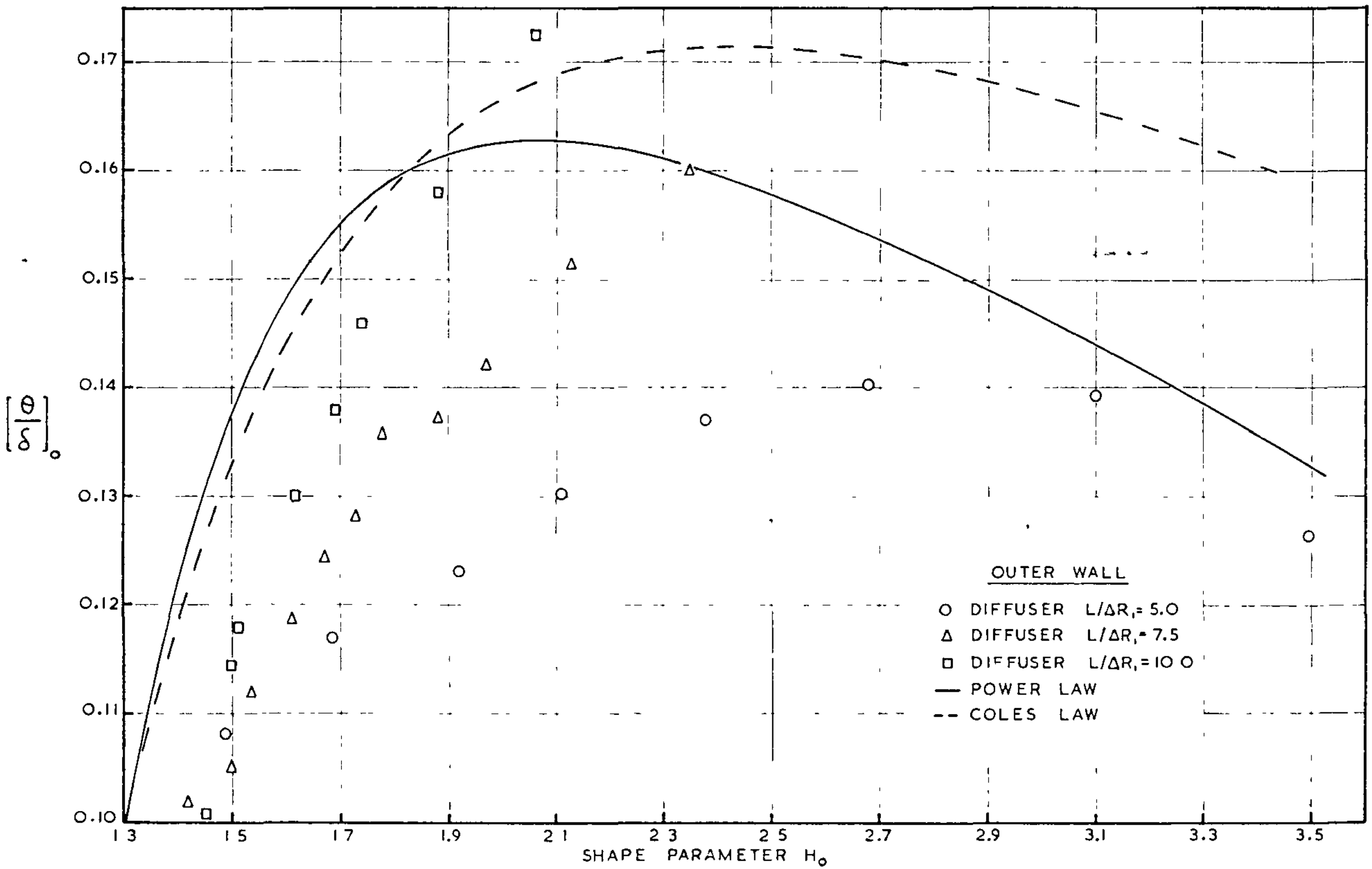

FIG. 6-2-3 RELATIONSHIP BETWEEN NON-DIMENSIONAL MOMENTUM THICKNESS AND SHAPE PARAMETER - OUTER WALL

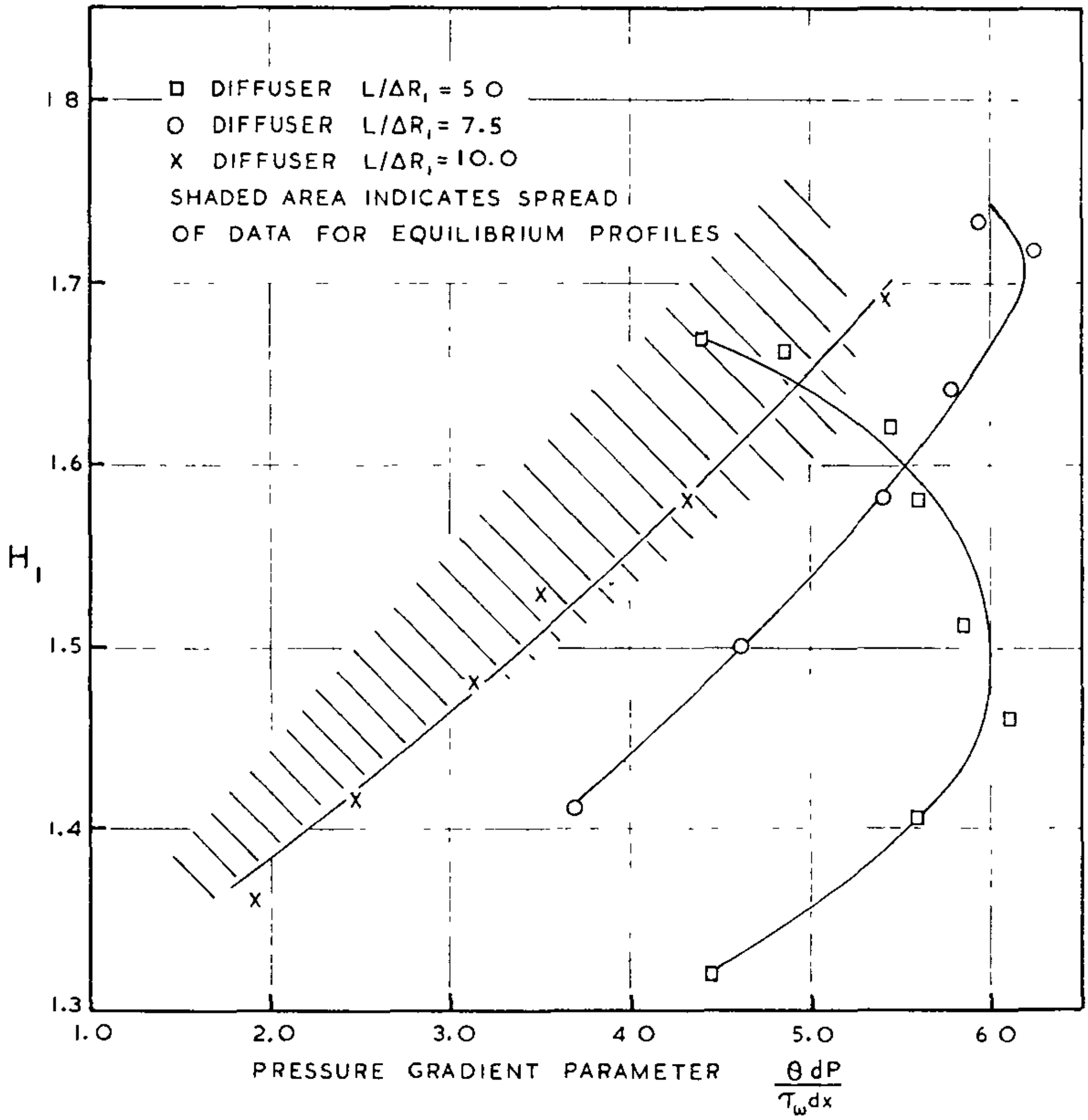

FIG. 6-2-4 PROXIMITY TO "LOCAL EQUILIBRIUM" OF INNER WALL BOUNDARY LAYERS

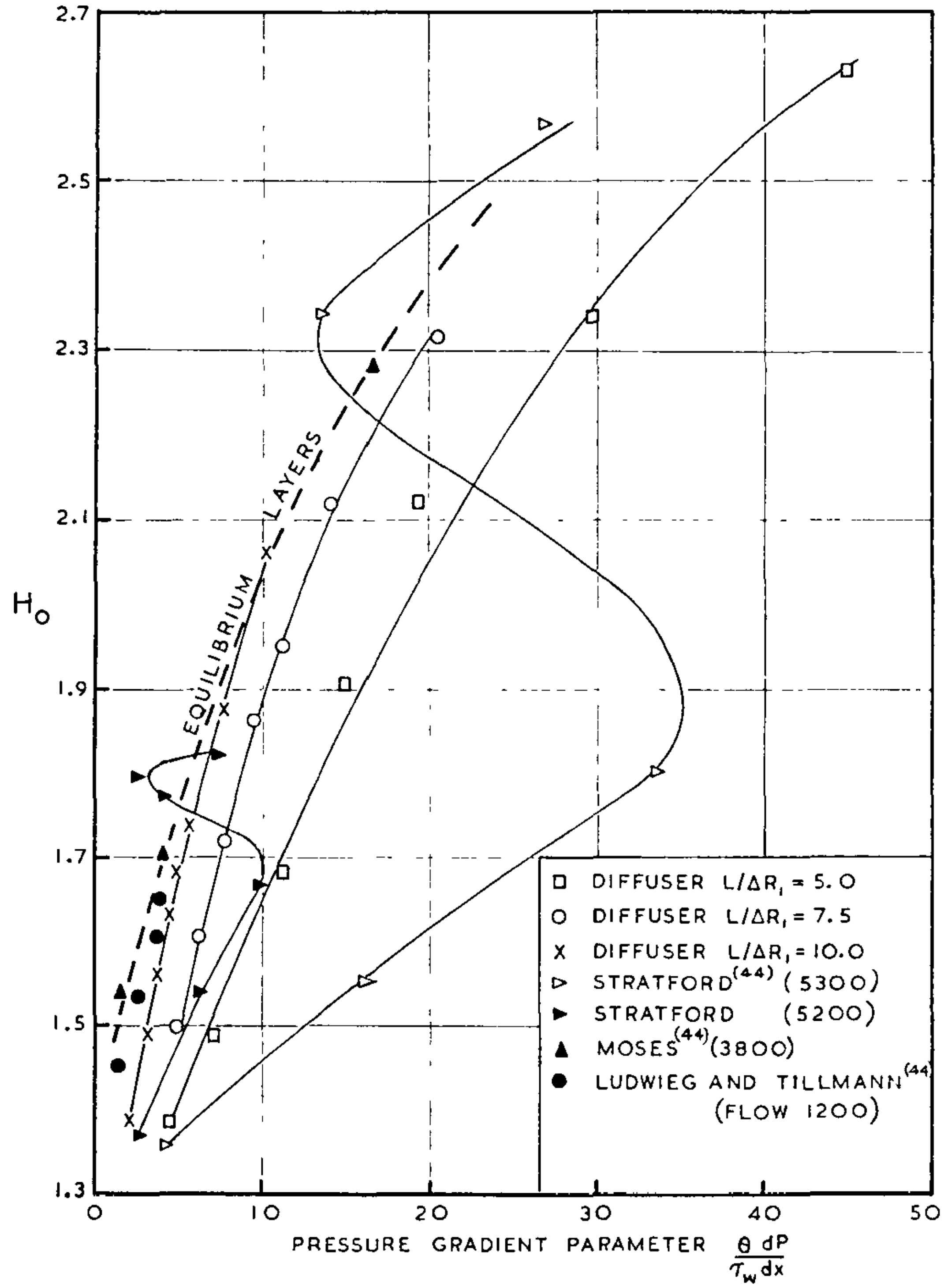

FIG. 6-2-5 PROXIMITY TO "LOCAL EQUILIBRIUM" OF OUTER WALL BOUNDARY LAYERS

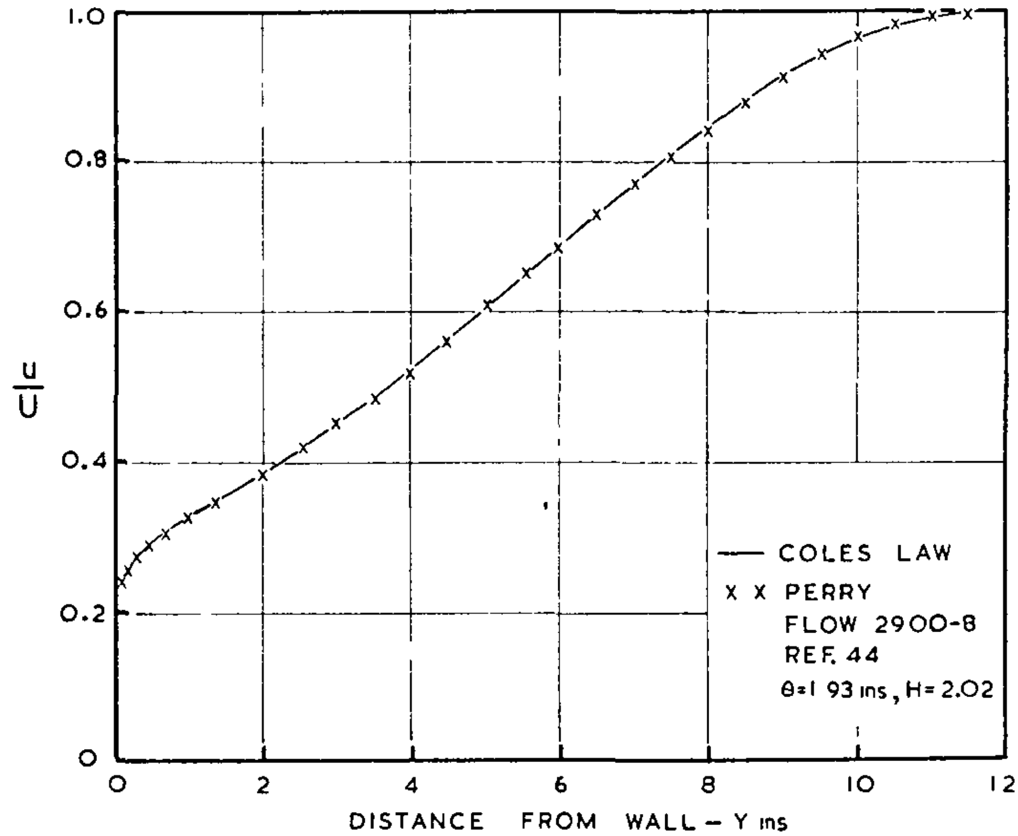

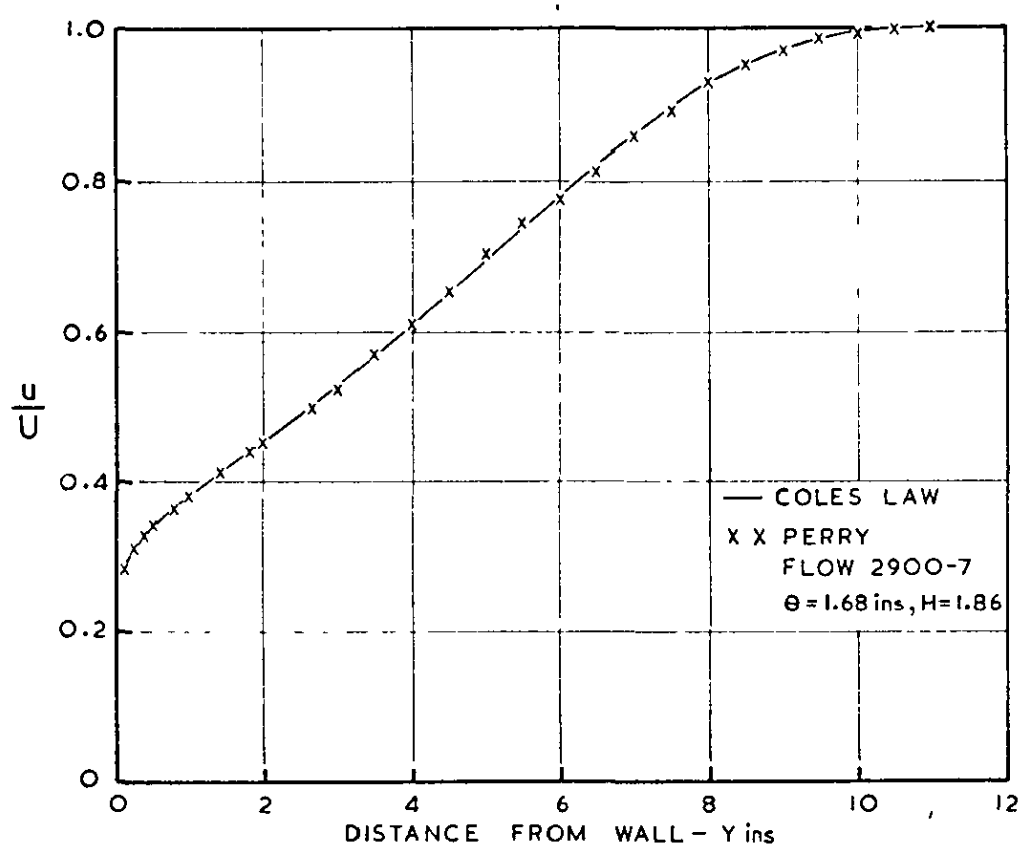

FIG. 6-2-6 COMPARISON OF VELOCITY PROFILES MEASURED BY PERRY[72] WITH THE PROFILES PREDICTED BY COLES LAW. BOTH PROFILES HAVE THE SAME VALUES OF θ AND H.

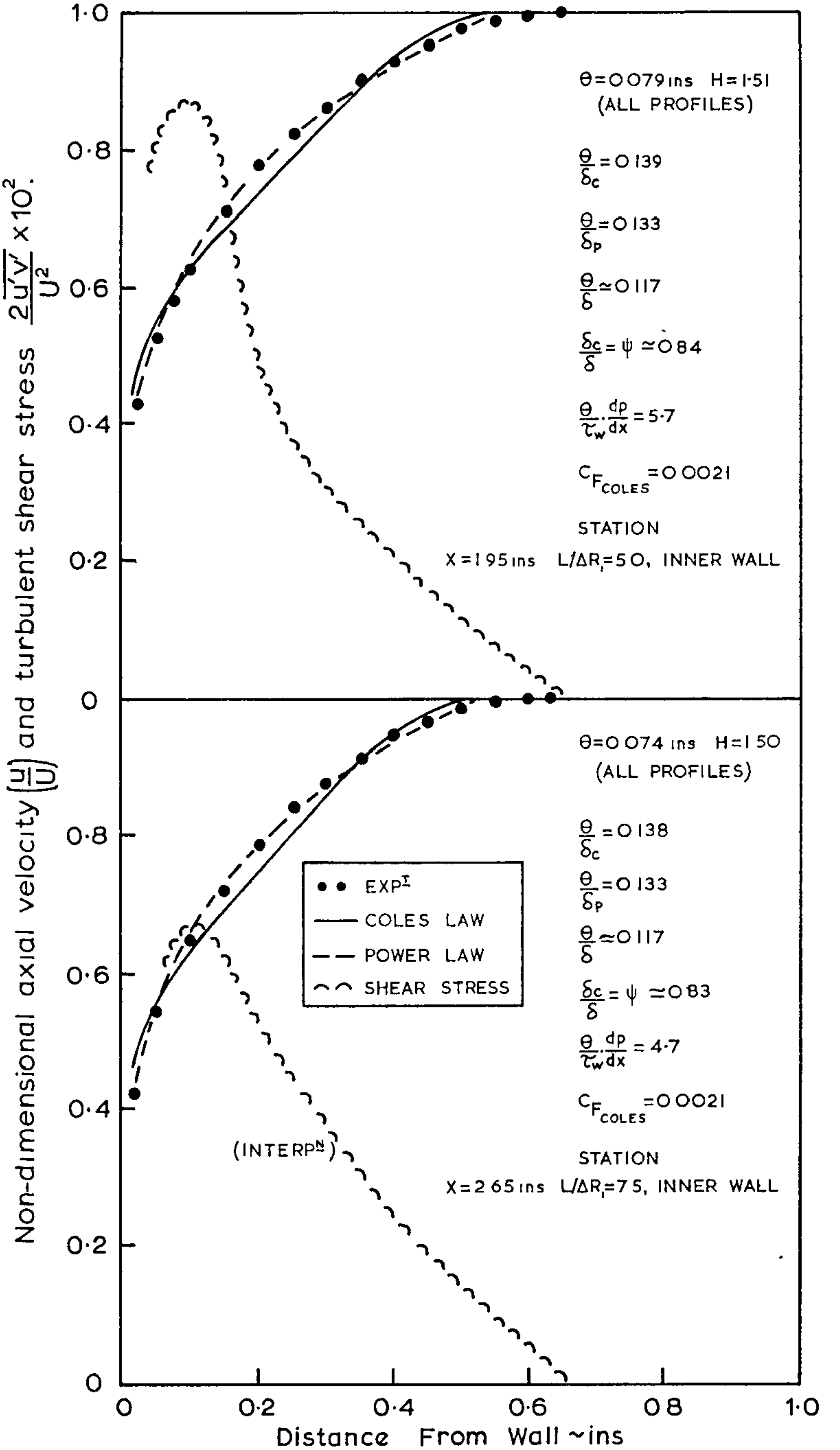

FIG 6-2-7 COMPARISON OF VELOCITY PROFILES. H=1·50

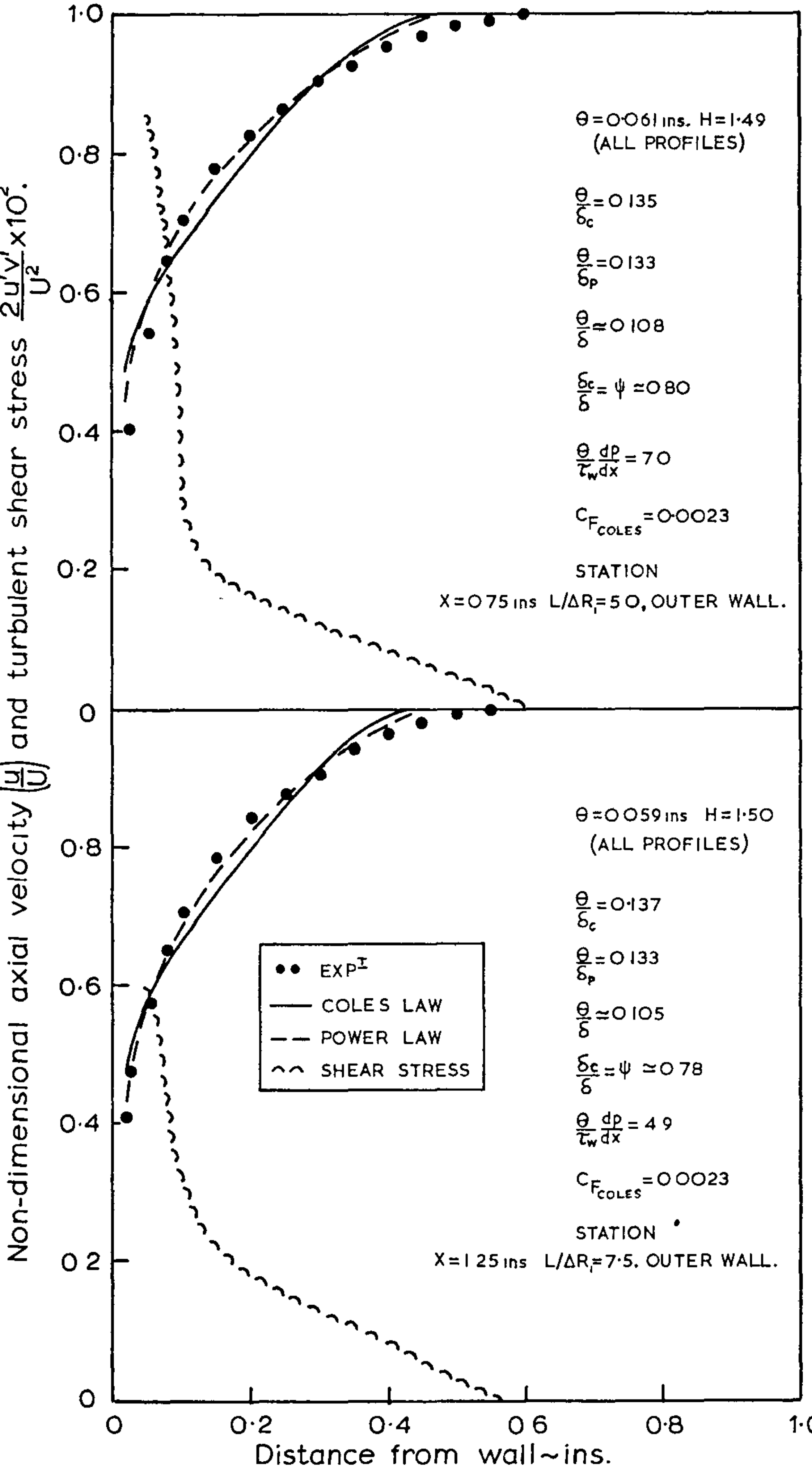

FIG. 6-2-8 COMPARISON OF VELOCITY PROFILES H=1·50

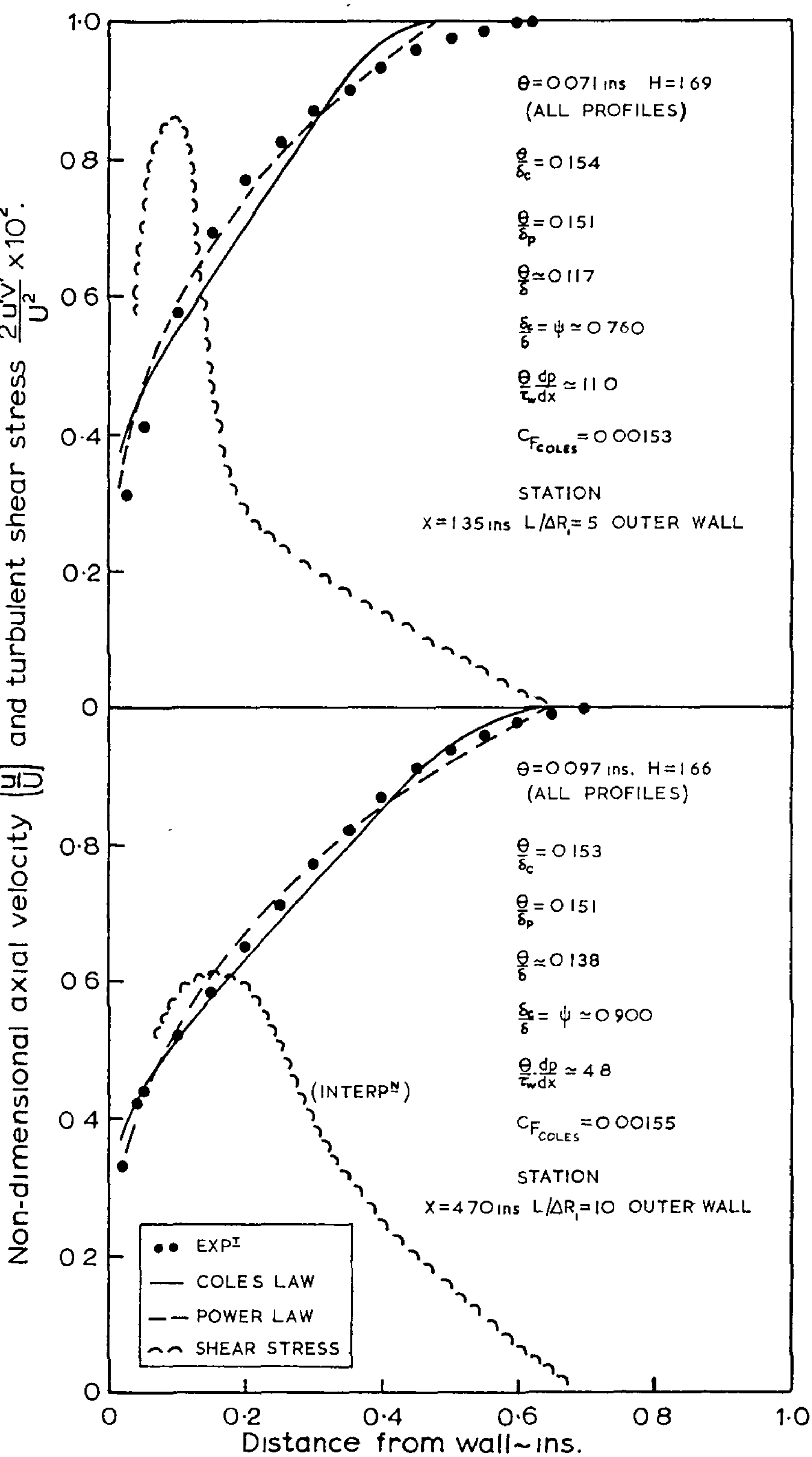

FIG 6-2-9 COMPARISON OF VELOCITY PROFILES H=1·69

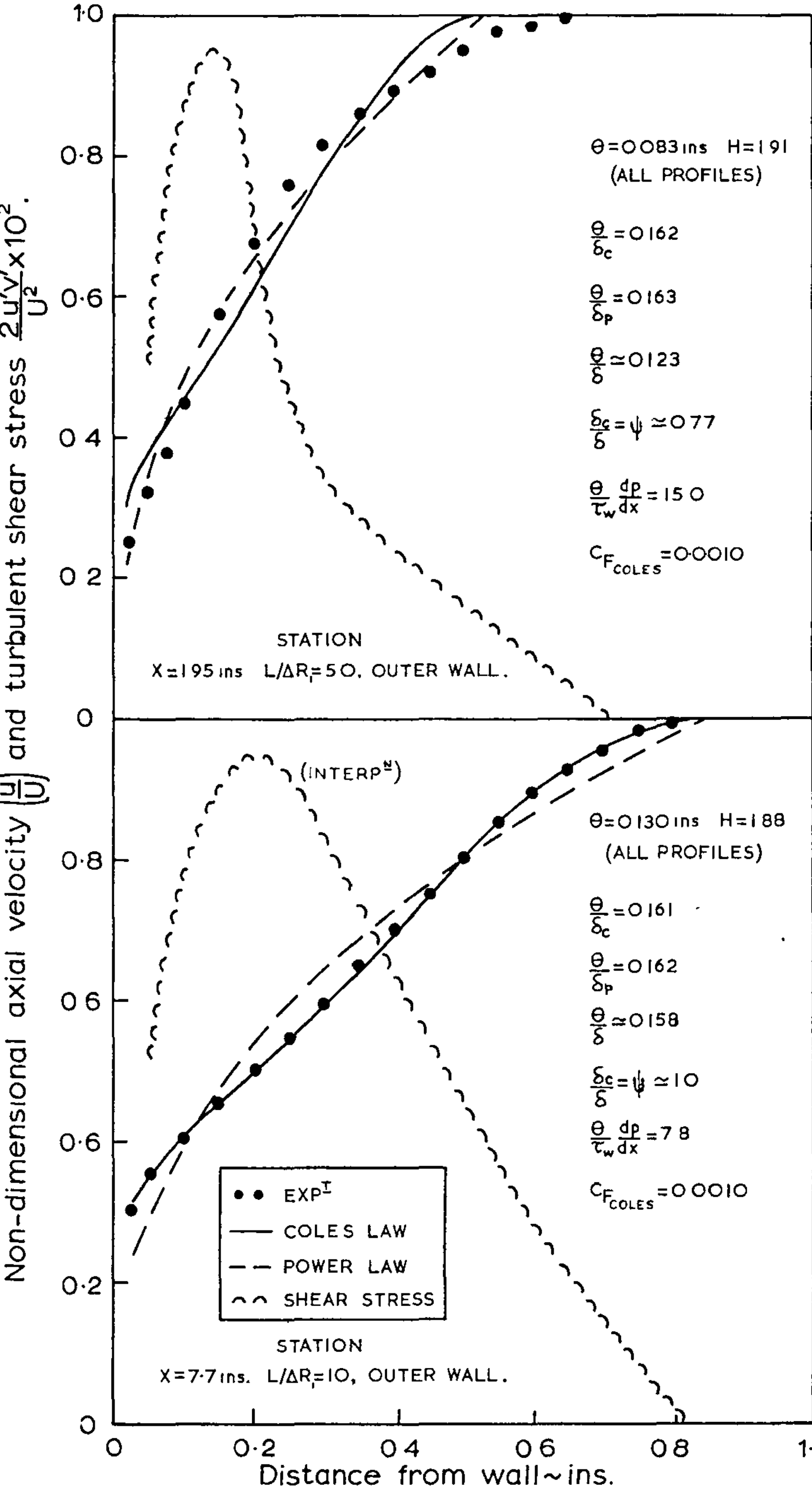

FIG 6-2-10 COMPARISON OF VELOCITY PROFILES H=1·90

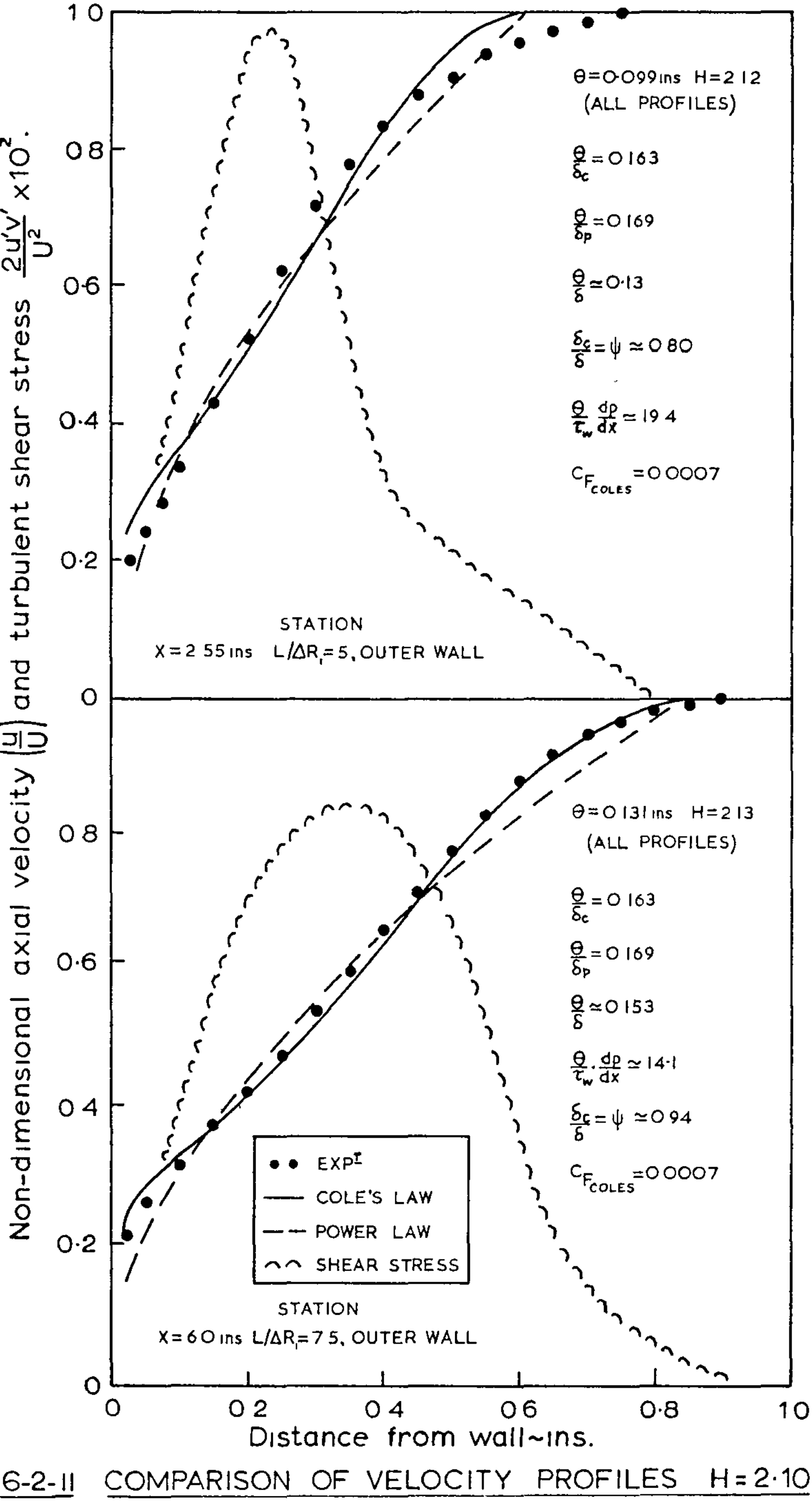

FIG 6-2-11 COMPARISON OF VELOCITY PROFILES H=2·10

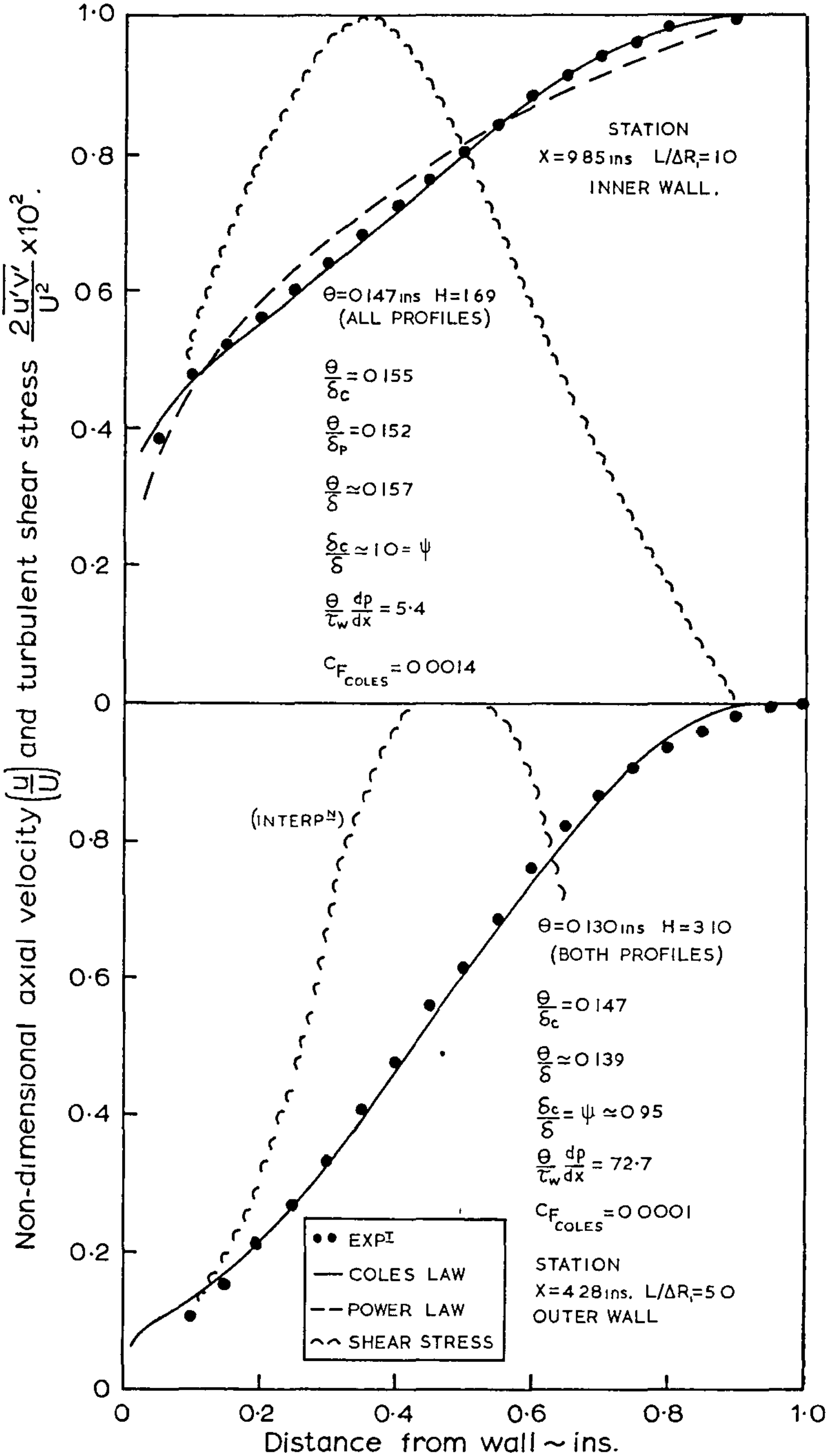

FIG 6-2-12 COMPARISON OF VELOCITY PROFILES H = 1·69 & H = 3·10

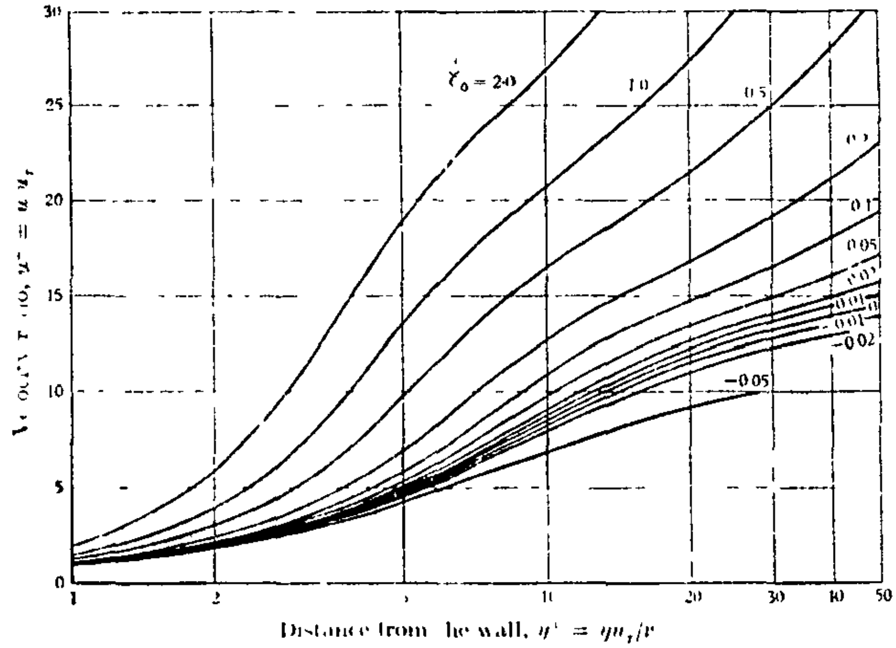

Effect of pressure gradient on the velocity profile near the wall A semi-logarithmic plot Stress gradient γ = pressure gradient $\gamma_0 = (\nu/\rho u_\tau^3)(dp/dx)$

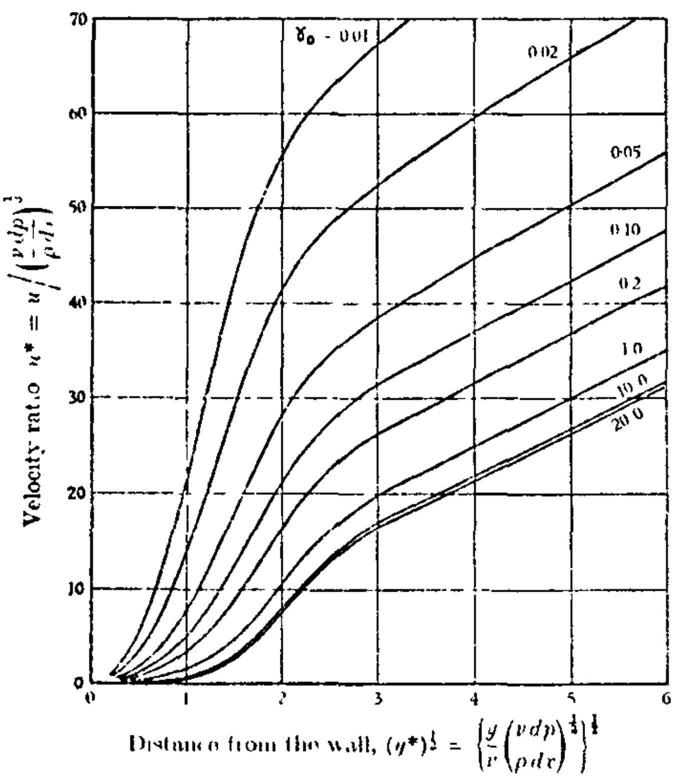

Figure 3 Effect of pressure gradient on the velocity profile near the wall A square root plot Stress gradient γ = pressure gradient $\gamma_0 = (\nu/\rho u_\tau^3)(dp/dx)$

FIG. 6-2-13 EFFECT OF PRESSURE GRADIENT ON THE VELOCITY PROFILE NEAR THE WALL AFTER McDONALD[73]

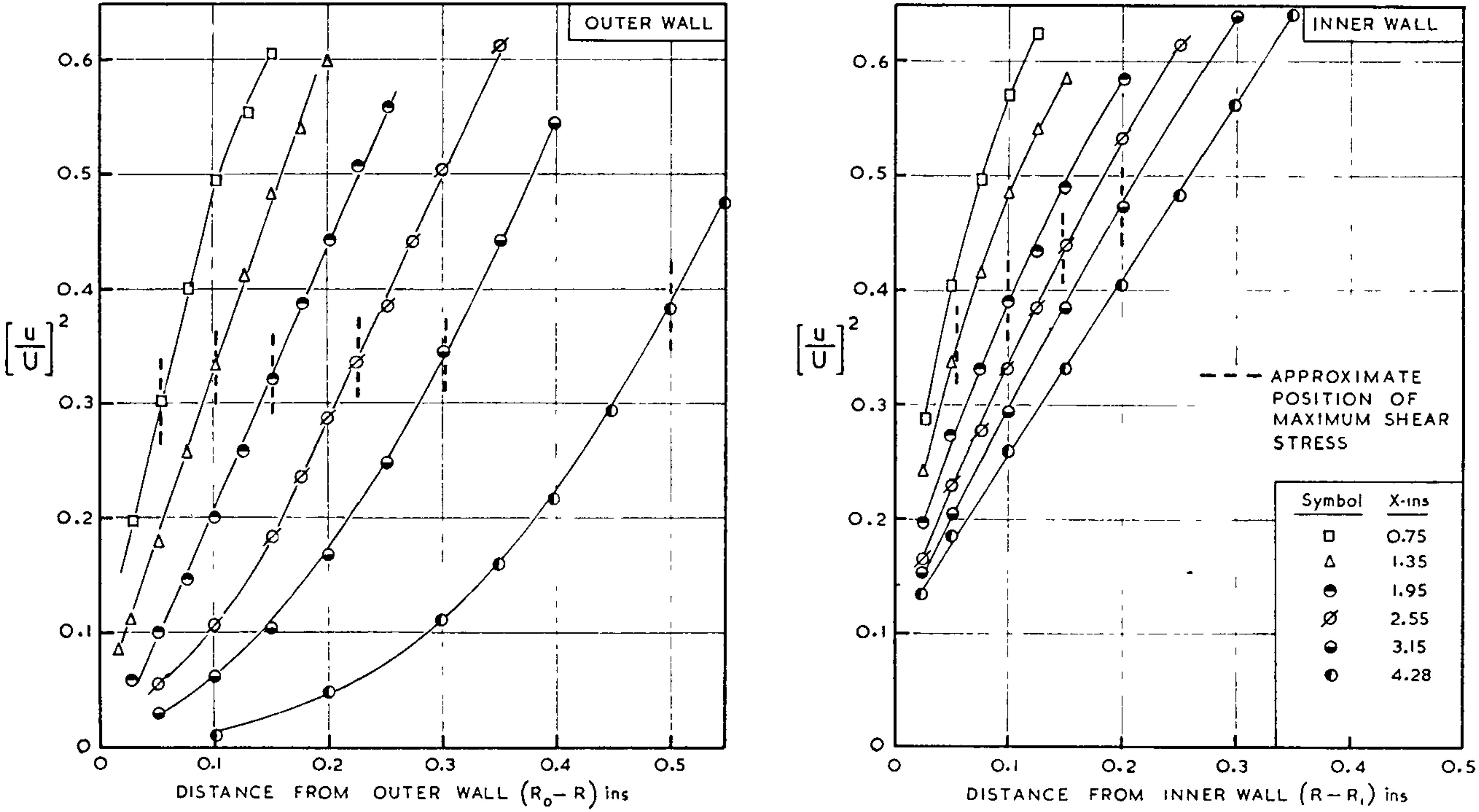

FIG. 6-2-14 DYNAMIC HEAD PROFILES IN THE $L/\Delta R_i = 5.0$ DIFFUSER

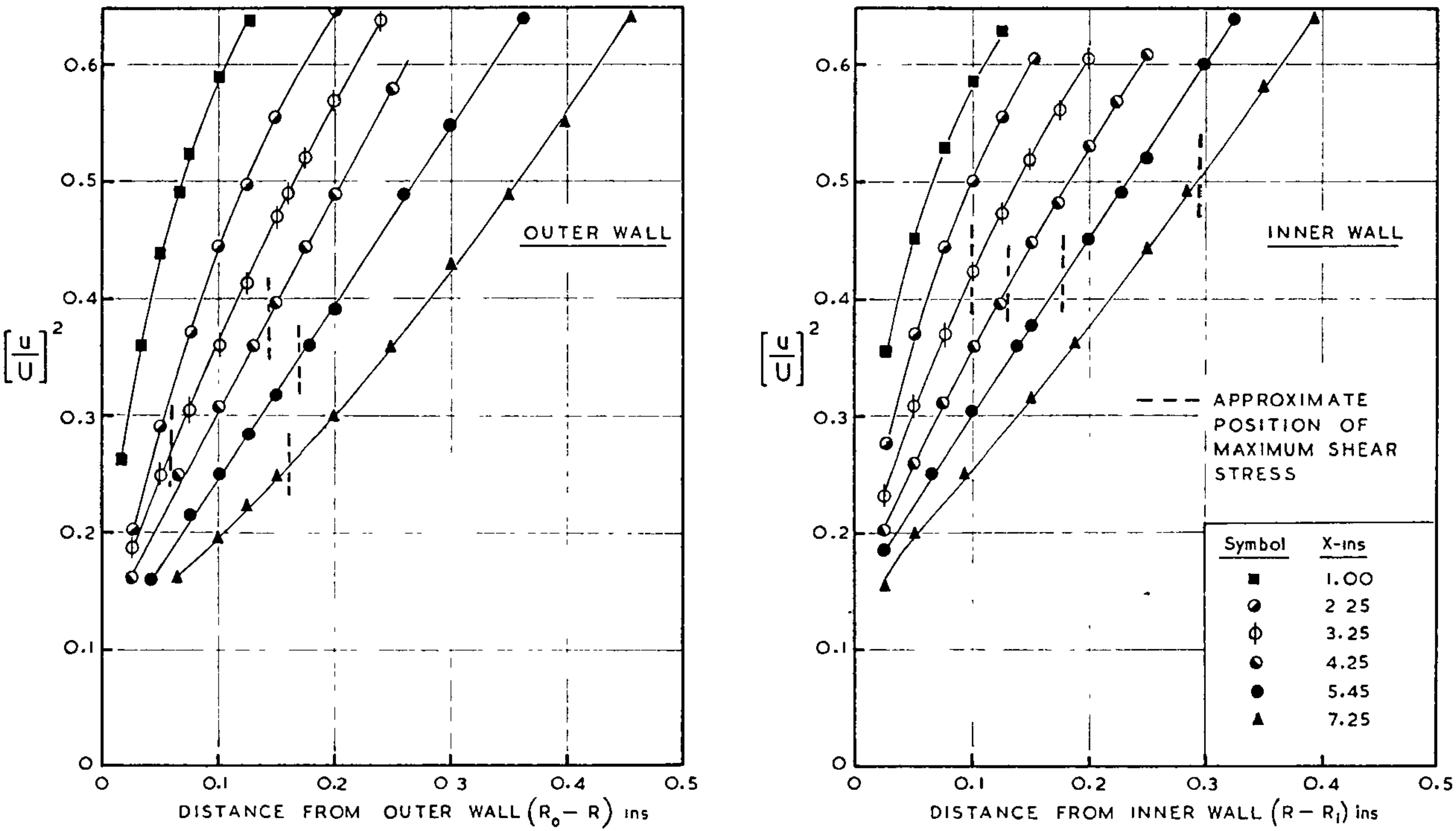

FIG. 6-2-15 DYNAMIC HEAD PROFILES IN THE $L/\Delta R_I = 10.0$ DIFFUSER

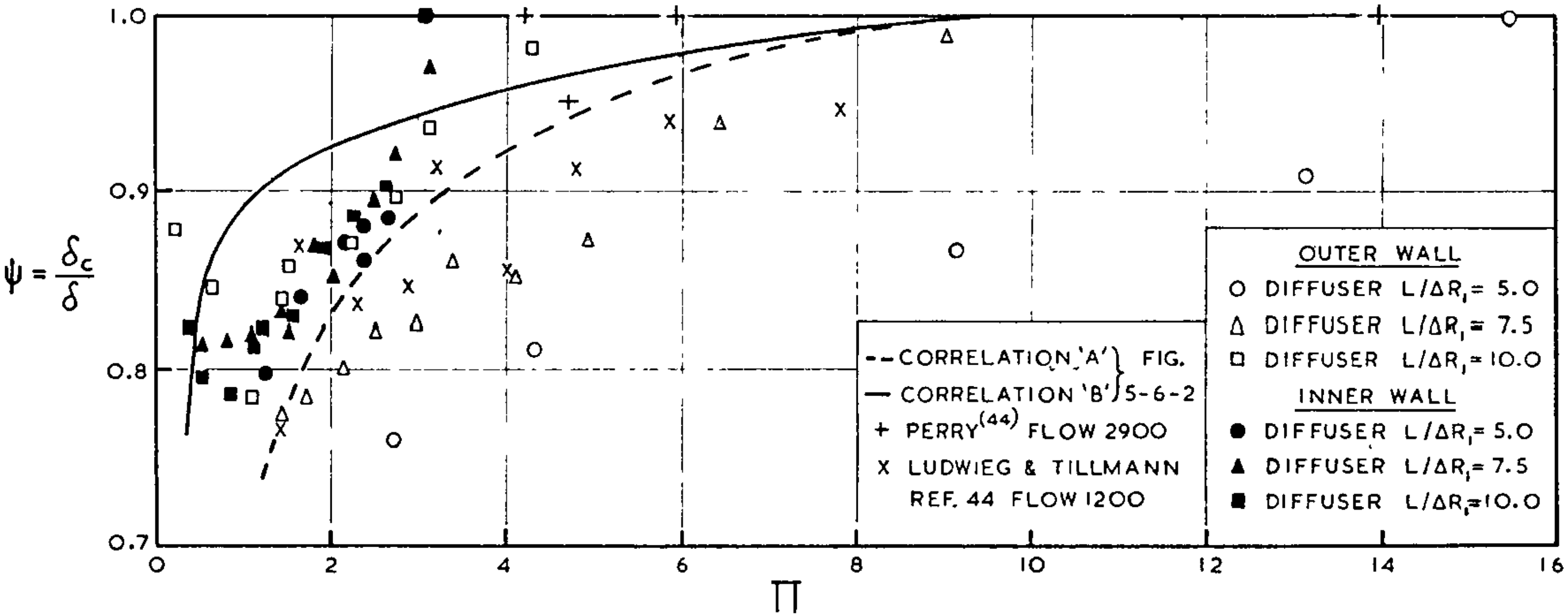

FIG. 6-2-16 COMPARISON OF THE EXPERIMENTAL VALUES OF ψ WITH THE VALUES OBTAINED FROM THE CORRELATION DUE TO BULL[66]

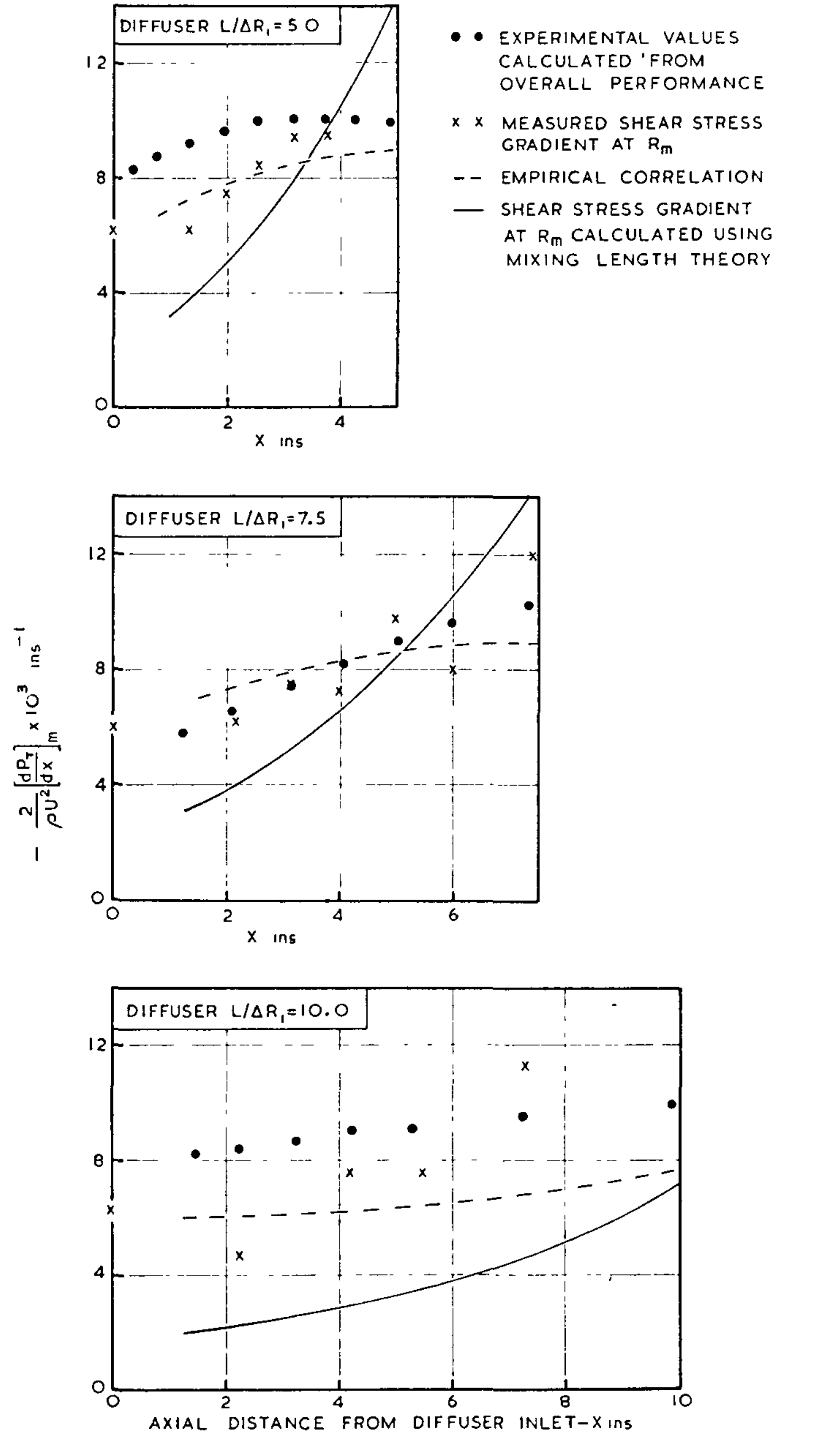

FIG. 6-3-1 COMPARISON OF EXPERIMENTAL AND PREDICTED VALUES OF THE TOTAL PRESSURE GRADIENT ALONG THE STREAMLINE OF MAXIMUM VELOCITY

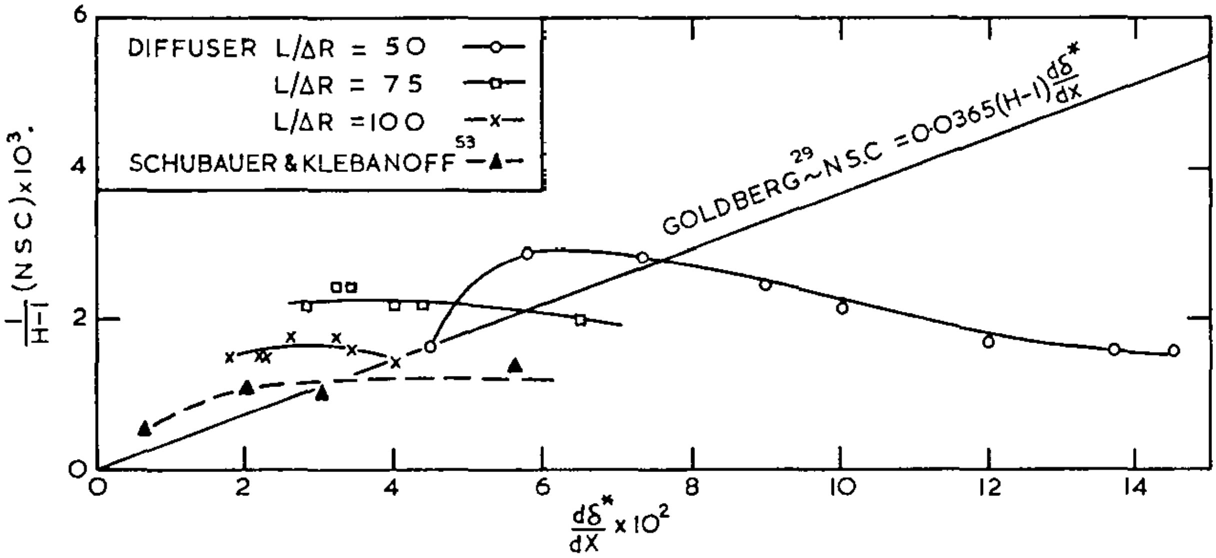

COMPARISON OF TEST DATA WITH CORRELATION DUE TO GOLDBERG[29]

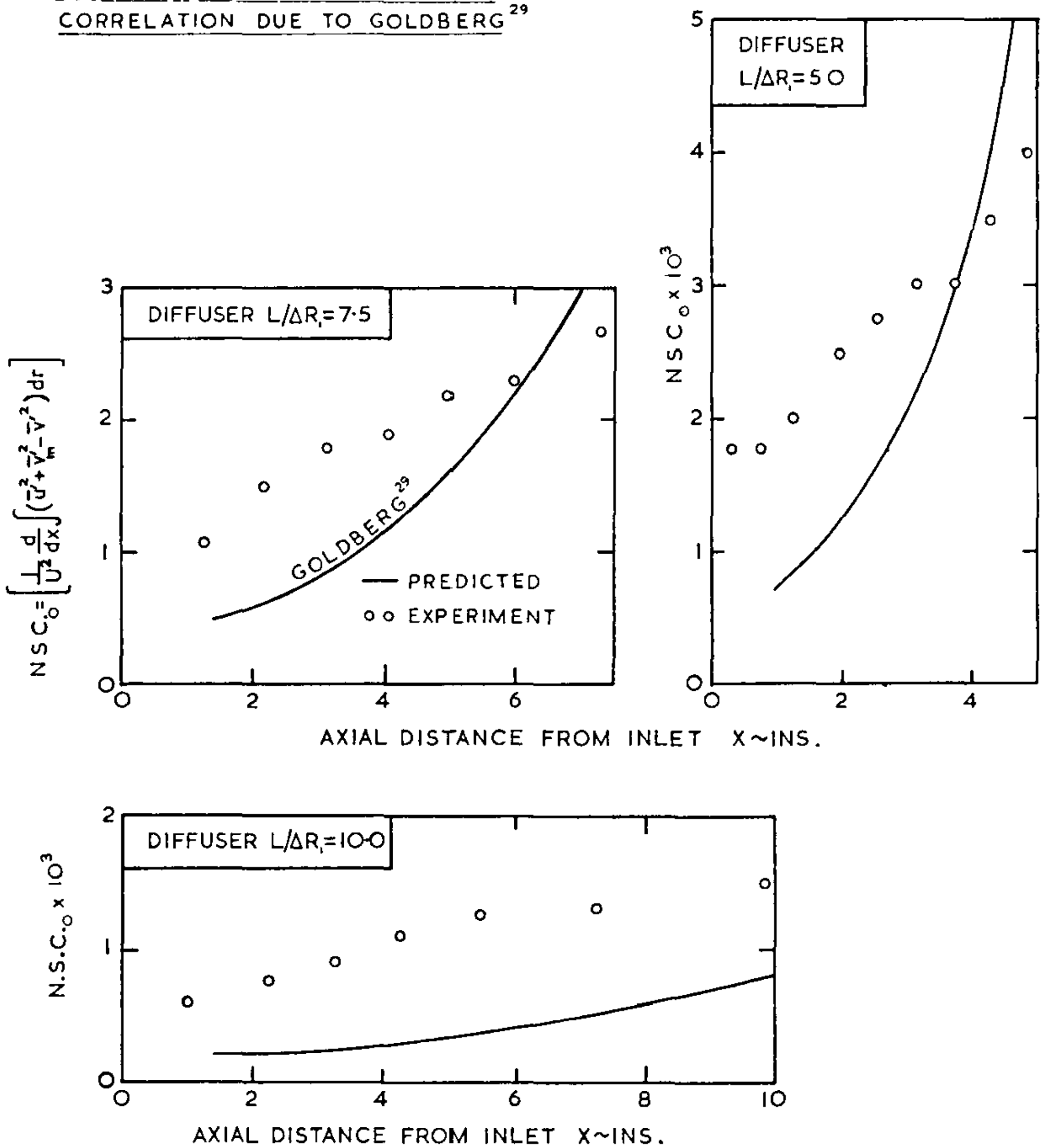

FIG. 6-4-1 COMPARISON OF EXPERIMENTAL AND PREDICTED VALUES OF REYNOLDS NORMAL STRESS IN OUTER WALL BOUNDARY LAYERS

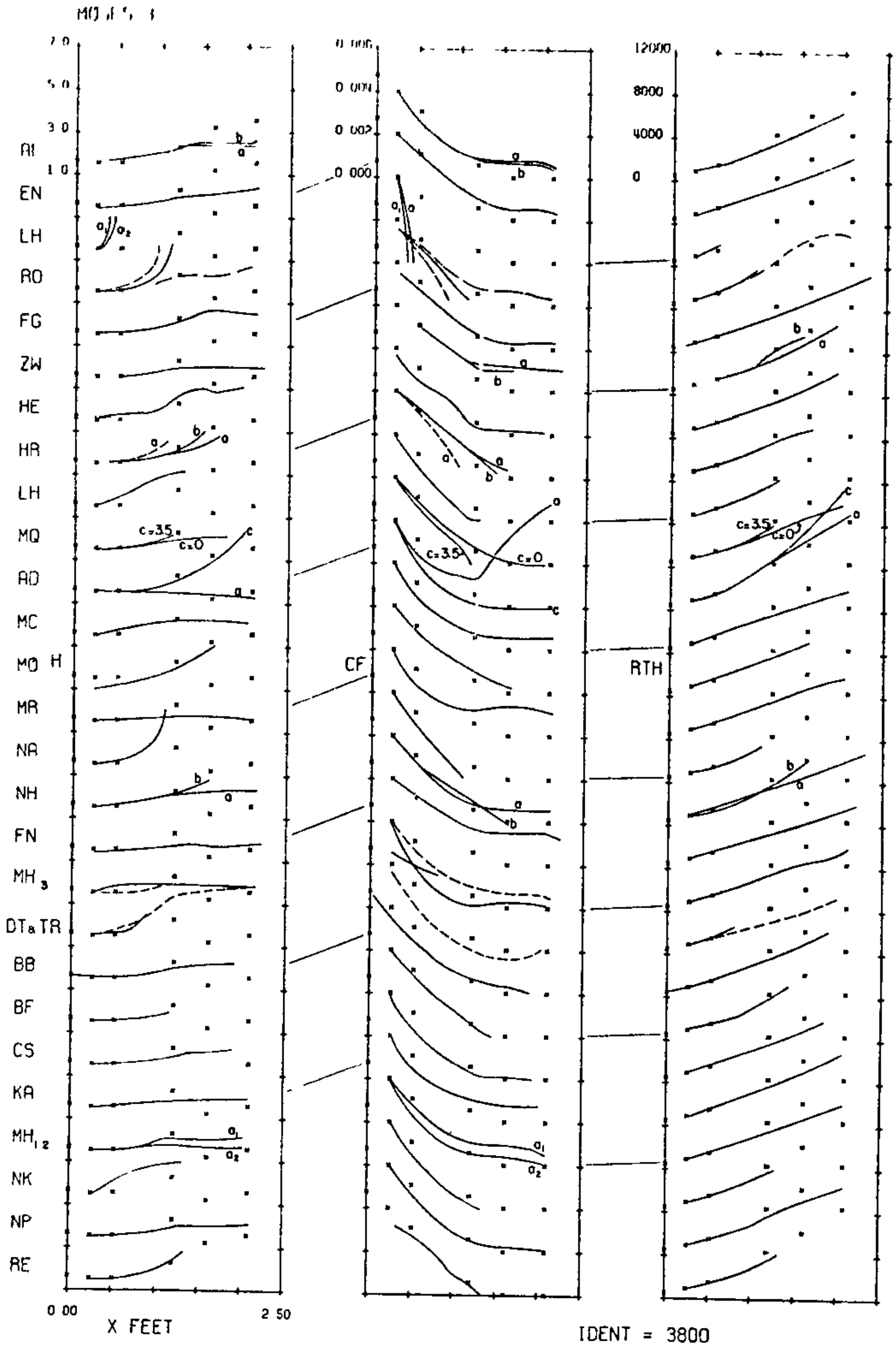

FIG. 6-5-1 STANFORD PREDICTION METHODS[34] APPLIED TO THE DATA OF MOSES[28]

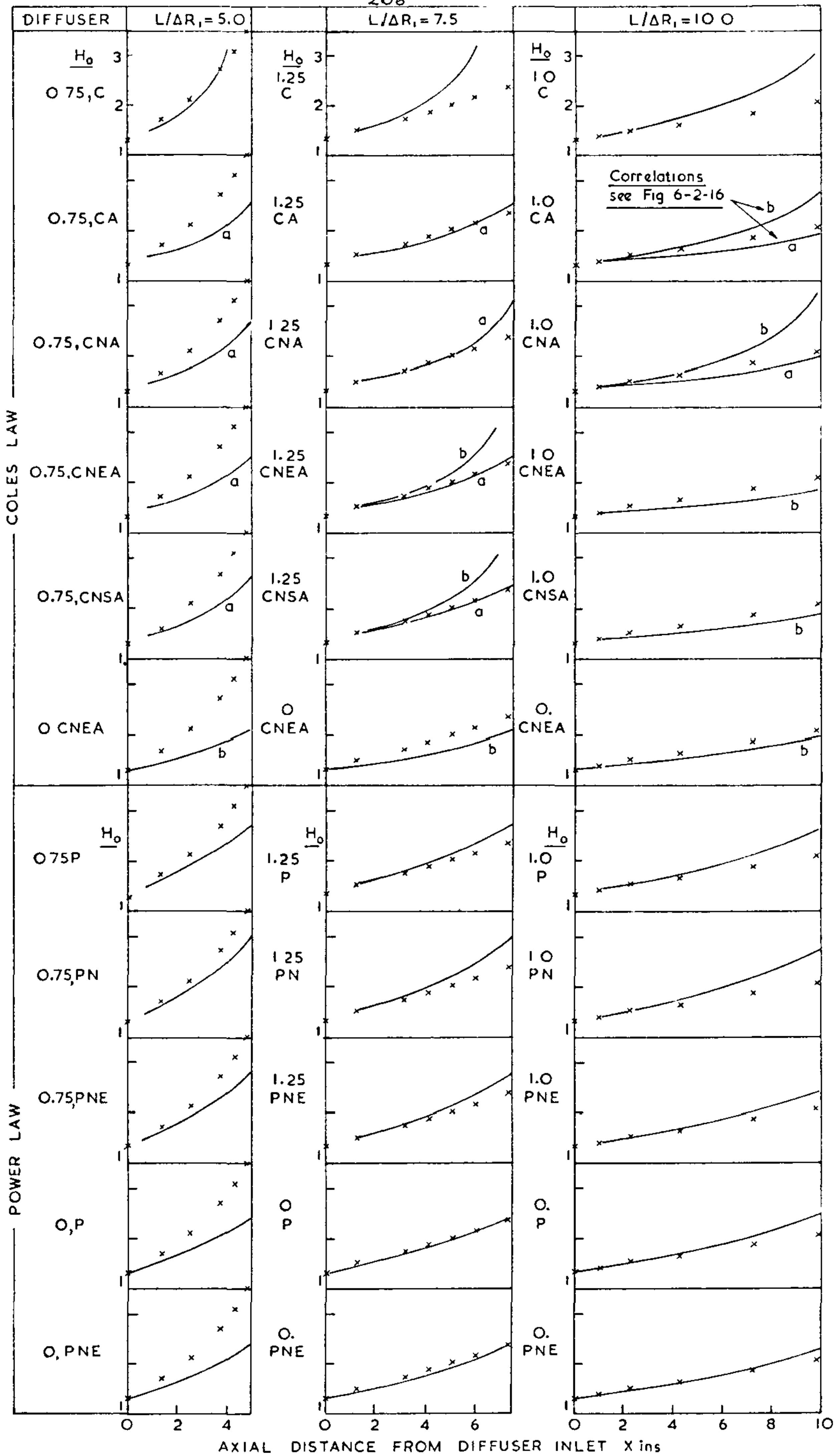

FIG. 6-5-2 SUMMARY OF PREDICTED RESULTS – H_0

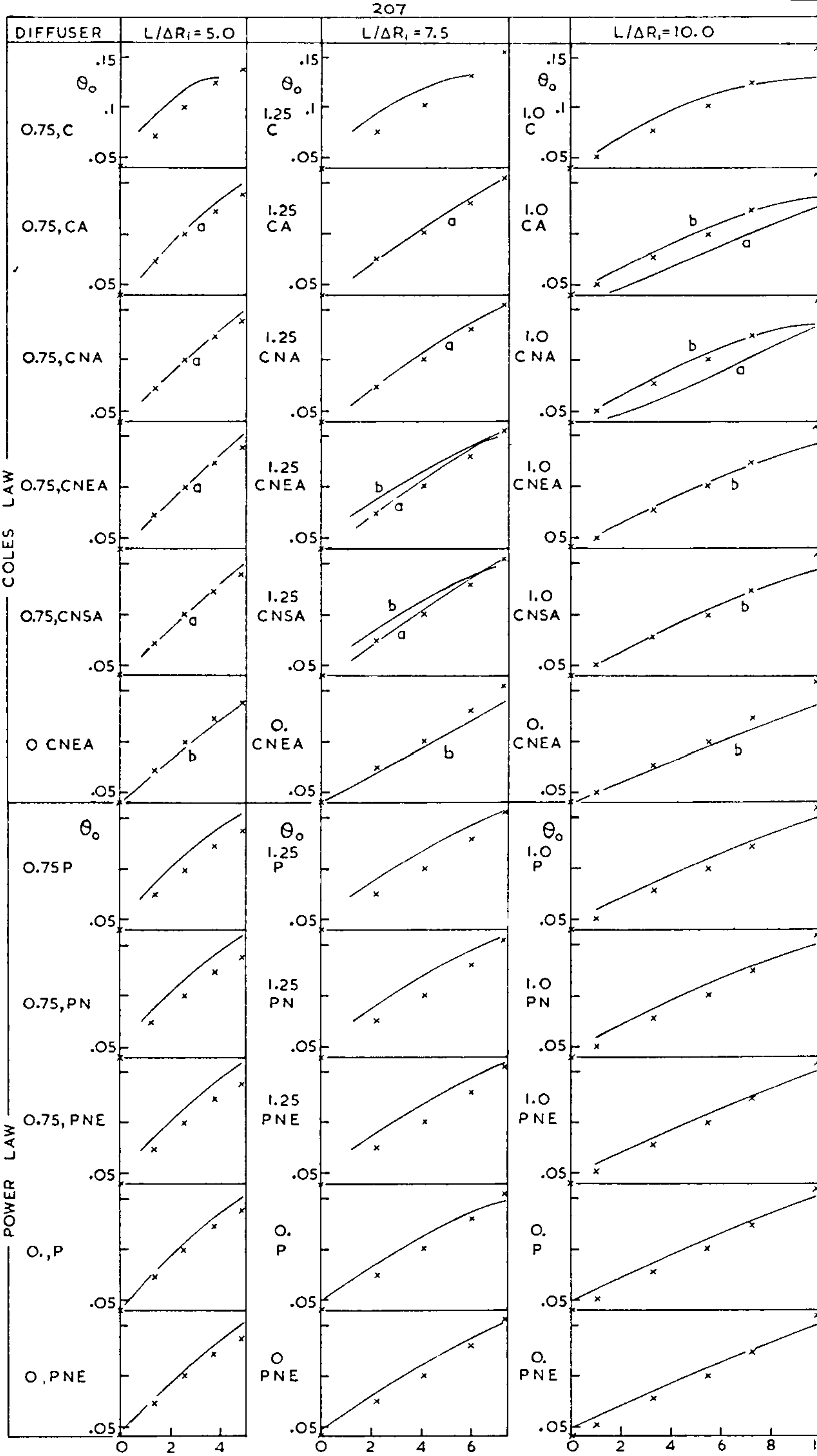

FIG. 6 - 5 - 3 SUMMARY OF PREDICTED RESULTS — θ_o Ins

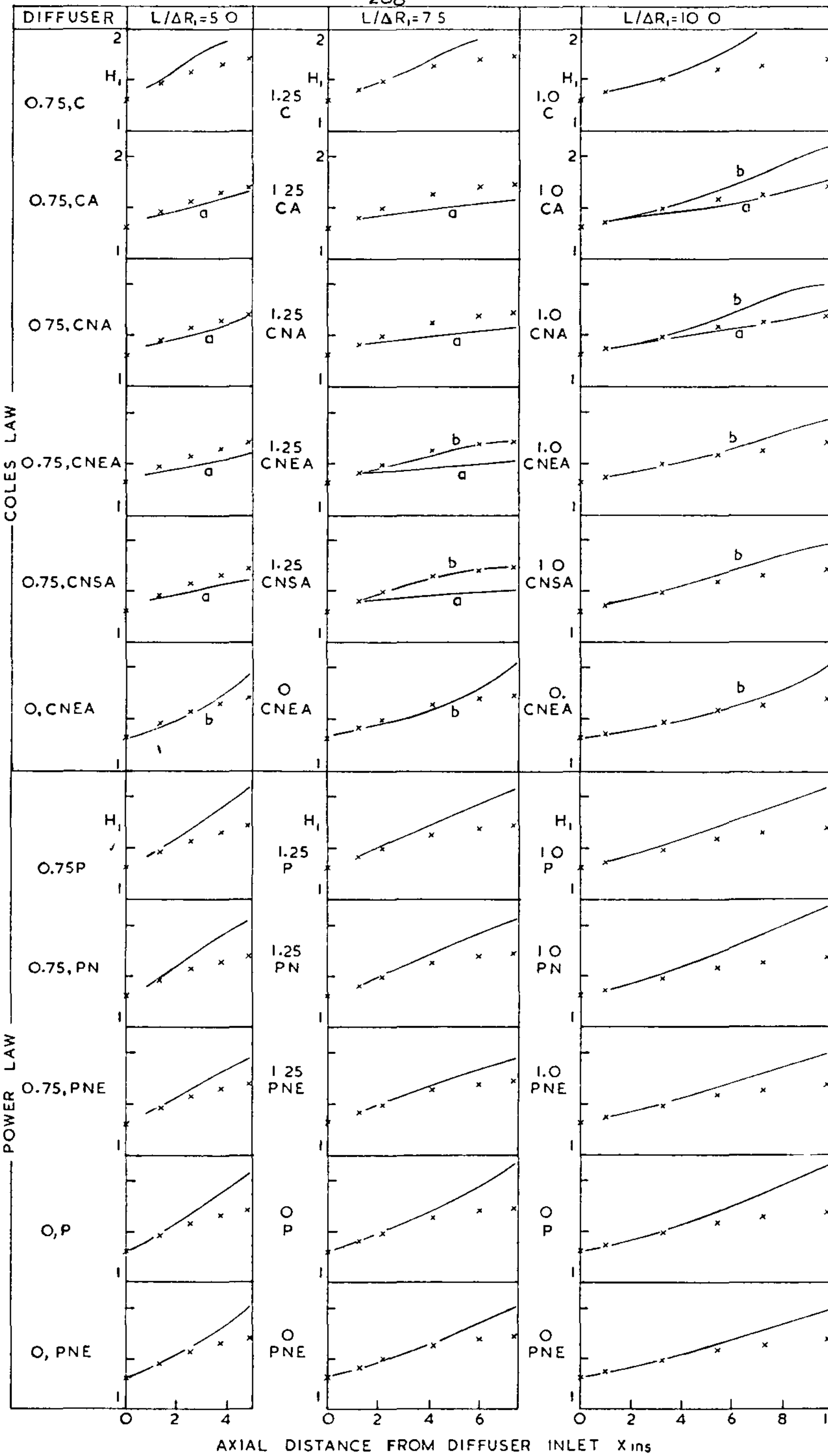

FIG. 6-5-4 SUMMARY OF PREDICTED RESULTS – H_1

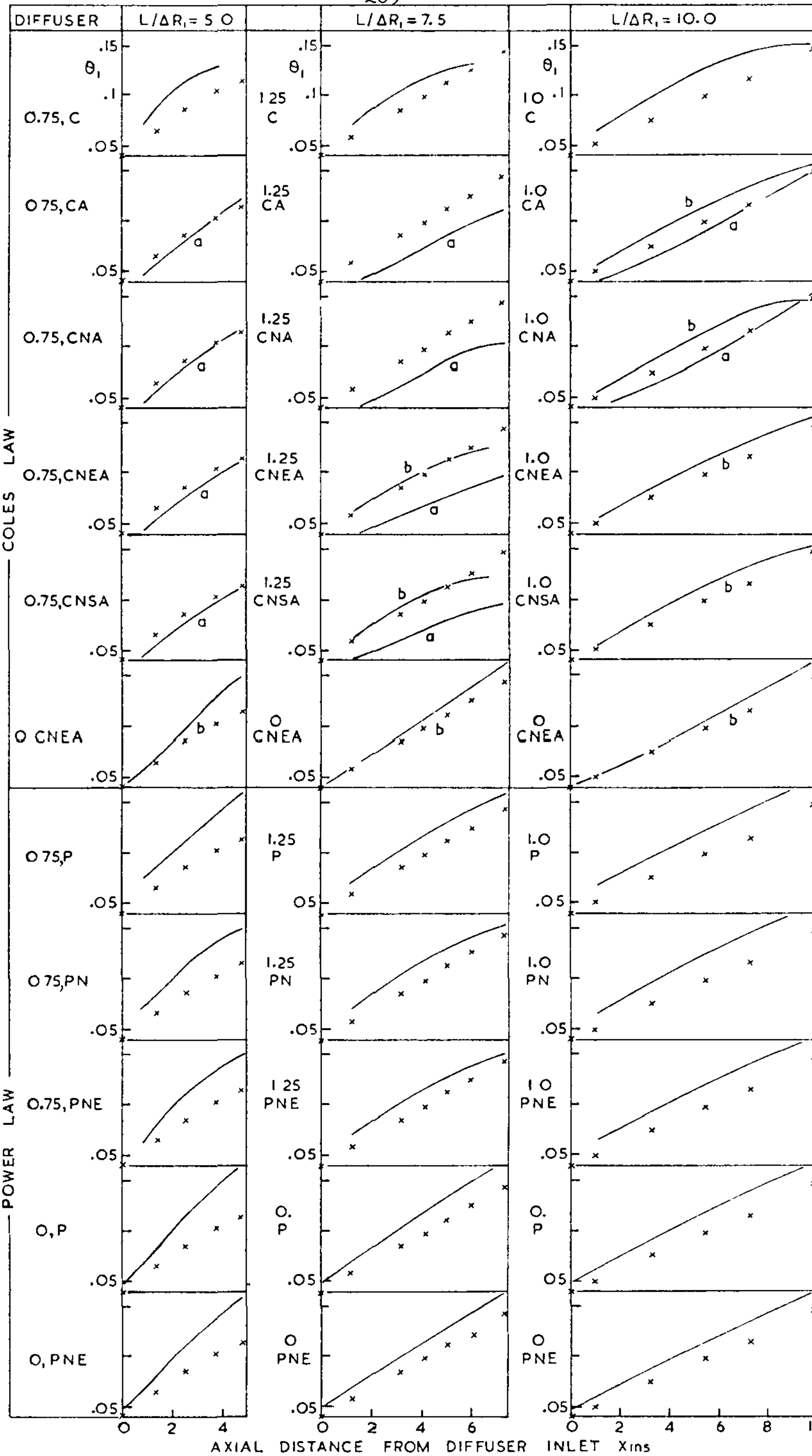

FIG. 6-5-5 SUMMARY OF PREDICTED RESULTS – θ_1 ins

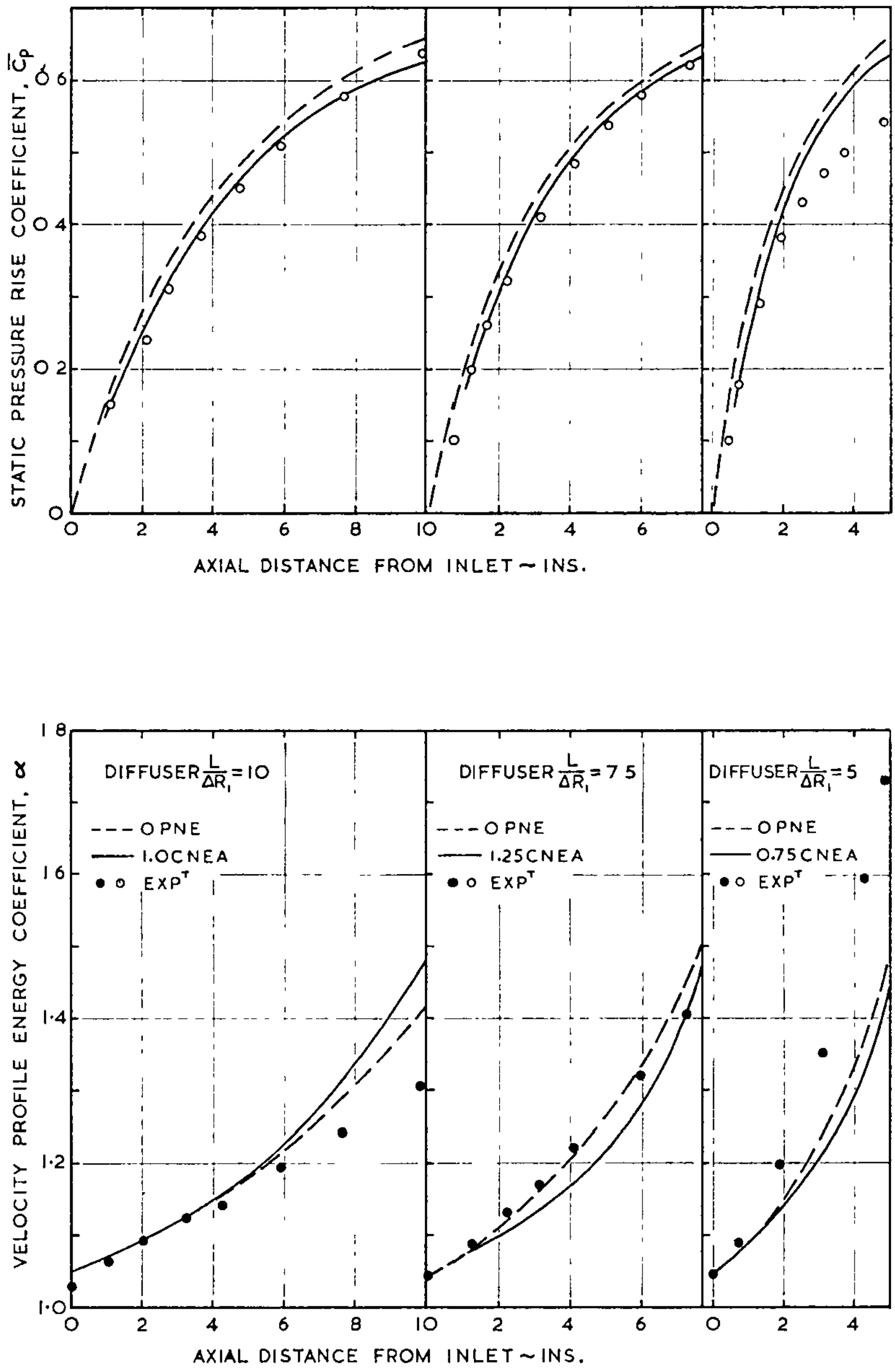

FIG. 6-6-1. COMPARISON OF DIFFUSER OVERALL PERFORMANCE.

TABLE 6-1

COMPARISON OF PROFILE PREDICTIONS

DATA DUE TO PERRY(72)

PROFILE INDENT. No.	2906	2907*	2908*	2909	2910
x ft.	10.0	11.0	12.5	14.0	15.0
U ft/sec	84.55	82.16	79.94	77.27	76.04
C_f COLES	0.00076	0.00064	0.00047	0.00033	0.000225
C_f AUTHOR	0.00079	0.00061	0.00045	0.00031	0.000210
Π COLES	4.778	5.955	7.771	10.48	13.921
Π AUTHOR	4.723	5.979	7.847	10.59	13.992
θ ins COLES	1.4415	1.682	1.930	2.327	2.486
θ ins. AUTHOR	1.442	1.680	1.930	2.324	2.479
δ ins. COLES	9.004	10.312	11.81	14.293	15.512
δ ins. AUTHOR	9.058	10.342	11.765	14.235	15.446
δ ins PERRY	9.50	11.00	11.50	13.5	15.50
ψ	0.955	0.941	1.02	1.055	1.00
H COLES	1.755	1.86	2.02	2.20	2.41
H AUTHOR	1.755	1.87	2.02	2.21	2.41

* compared graphically

TABLE 6-2

APPROXIMATE VALUES OF $\gamma = \frac{\nu}{\rho u_\tau^3} \frac{dP}{dx}$

$L/\Delta R_1 = 5$ DIFFUSER

X (ins)	0.75	1.35	1.95	2.55	3.15	3.75	4.28
γ Outer Wall	0.055	0.093	0.156	0.197	0.364	0.665	1.460
γ Inner Wall	0.043	0.043	0.038	0.038	0.036	0.0306	0.0276

$L/\Delta R_1 = 7.5$ DIFFUSER

X (ins)	1.25	2.2	3.15	4.10	5.05	6.0	7.35
γ Outer Wall	0.0388	0.048	0.060	0.076	0.093	0.120	0.189
γ Inner Wall	0.0273	0.033	0.038	0.038	0.041	0.038	0.031

$L/\Delta R_1 = 10.0$ DIFFUSER

X (ins)	1.0	2.25	3.25	4.25	5.45	7.25	9.85
γ Outer Wall	0.016	0.023	0.026	0.032	0.037	0.040	0.066
γ Inner Wall	0.015	0.017	0.020	0.023	0.028	0.028	0.029

SECTION 7

CONCLUSIONS

7-1 Extension of Theoretical Approach

7-1-1 Integral Methods

It has been shown that for diffusers of moderate overall pressure gradient ($^{L}/\Delta R_1$ = 7.5 and 10.0), reasonable agreement, sufficient for most engineering purposes, can be achieved between experimental and theoretical values of internal and overall performance. However, this agreement is restricted by the necessity to commence calculations at a station downstream of the inlet bend. Failure to take account of the disturbance due to the inlet bend results in a failure to predict the asymmetric growth of the boundary layers.

In attempting to apply integral methods to the calculation of the flow in a minimum length diffuser ($^{L}/\Delta R_1$ = 5.0), serious discrepancies arise. These discrepancies have been traced, in the main, to a failure of the existing methods of representing the mean velocity profile in a severe adverse pressure gradient. The failure of the two parameter representation due to Coles[(41)] has been shown to be due to a failure of the well known law of the wall, resulting in an overestimate of the skin friction coefficient and the local velocity.

In order to apply integral methods in severe adverse pressure gradients a new approach is required. This may take the form of a revised law of the wall as suggested by McDonald[(73)], which takes account of the influence of local pressure gradient, combined with a universal defect law. Another possible line of attack has been suggested by Coles[(44)], namely that the flow near the wall should be treated as "non-turbulent". Alternatively an approach based on the half-power law due to Stratford[76] appears promising.

Sufficient data has been obtained, in which history effects are present, to investigate the relaxation technique, proposed by Nelson[79] and Rotta[34], for the calculation of the dissipation integral. In addition, improved empirical relations are required for the Reynolds normal stress coefficient, taking account of turbulence lag, and again a relaxation technique may give the best leverage. In the absence of an accurate mean velocity profile equation, and the difficulties surrounding the correct choice of mixing length, the calculation of the total pressure gradient along the streamline of maximum velocity appears to be restricted to improved empirical correlations.

7-1-2 Differential Methods

Differential techniques are still in the initial stages of development and no "best" method has yet been determined. The recently published results from the AFOSR-IFP-Stanford 1968 Conference on Computation of Turbulent Boundary Layers, confirm the view expressed by Rotta[34] who stated that, "it appears doubtful that much improvement in prediction techniques will be gained by adopting mean-field methods." The data obtained in this investigation support this view, unless some means can be found to predict the values of mixing length in an adverse pressure gradient. An approach using a relaxation technique where the length scale is dependent on local pressure gradient may be possible. In view of this, a modified wall function and values of mixing length, based on the experimental data are to be incorporated in the Spalding GENMIX-4 programme[78] [77].

A more promising approach may be to use the data in a turbulent-field method notably that due to Beckwith and Bushnell[34]. Finally, an attempt must be made to incorporate the calculation of streamline curvature effects, so that the influence of the inlet bend may be included.

7-2 Extension of Experimental Work

The data obtained represents a detailed investigation of the flow through annular diffusers having centre bodies of uniform diameter, and operating with fully developed flow conditions at inlet. However there is a great need for further comprehensive data on other types of annular diffuser operating near to the lines of optimum performance. Such data should, where possible, be free from any significant three-dimensional effects, and in this respect the work reported in this thesis indicates that a fully annular rig is desirable.

In addition to detailed measurements of the mean velocity profile and turbulence structure attempts should be made to measure the wall shear directly. Such measurements are necessary for a complete analytical study of the flow near a wall in a severe adverse pressure gradient. Also apparatus should permit flow visualisation studies, in order to check for regions of intermittent transitory stalling which may not be detected by measurements along selected radii.

Apart from measurements within the diffuser there is a need for detailed data on the flow around the inlet bend which can serve as a basis for theoretical predictions. Very little information has been published on flow in annular bends. Another aspect which requires further work is the determination of acceptable prediction criteria for turbulent separation. This work is particularly difficult since separated flow is essentially three dimensional and unsteady, and consequently more complex instrumentation is required.

Finally most diffuser work is carried out on "clean" diffusers free from any internal obstructions, however in nearly all gas turbine applications struts are present. The struts, which can number as many as eighteen in certain combustion chamber applications, often extend over half the length of the diffuser. The interaction of these components in the presence of a turbulent shear flow frequently controls diffuser design. No published data are known to the author on this aspect of diffuser performance.

7-3 Conclusions

Overall performance data has been obtained for three annular diffusers having centre bodies of uniform diameter and conically diverging outer walls. The diffusers have a common area ratio of 2.0 : 1, and non-dimensional lengths ($^{L}/\Delta R_1$) of 5.0, 7.5, and 10.0 respectively. The tests were carried out with fully developed flow at inlet, the inlet conditions being obtained by natural development in a long annular entry length. For the optimum (Cp^*) diffuser the measured static pressure rise coefficient is in good agreement with published data after applying a correction to take account of the increased boundary layer thickness at inlet. Also for the diffuser area ratio investigated the non-dimensional length consistent with the onset of transitory stalling has been established.

In addition to the overall performance characteristics a detailed study has been made of the growth of the boundary layers along the inner and outer walls in each of the three diffusers. Measurements were made of the mean velocity profiles and turbulence structure at a number of stations along the length of the diffusers. The data shows excellent symmetry of flow, and momentum - balance plots, including the contribution due to Reynolds normal stresses, were in excellent agreement, indicating that no significant three-dimensional effects were present. It is considered that this data will be extremely useful as a basis of comparison for future theoretical studies.

The results indicate an asymmetric growth of the boundary layers along the inner and outer walls. The rate of increase in the shape parameters becoming significantly greater on the outer wall as the outer wall angle increases. This asymmetry is attributed, mainly, to the disturbance associated with the change in outer wall angle at inlet. The measured shear stress distributions exhibit considerable lag, and a large gradient of shear stress near the wall in regions of severe adverse pressure gradient. As a result of the large shear stress gradients a number of the velocity profiles do not obey the conventional form of the law of the wall, but follow more closely a half-power law. In these circumstances the use of the two-parameter method of profile representation gives rise to considerable error.

An integral approach has been used to predict the boundary layer growth, based on the assumption that no net mass transfer takes place between the inner and outer wall boundary layers. Within the limits of experimental error, this assumption has been verified, for the case of naturally developed inlet conditions.

For two of the diffusers ($^{L}/\Delta R_1 = 7.5$ and 10.0), good agreement, sufficient for most engineering purposes, has been achieved between the theoretical and experimental values of overall and internal performance. However this agreement is only obtained by commencing the calculations downstream of the disturbance associated with the inlet bend. In the case of the minimum length ($\overline{Cp}^*$) diffuser, the predicted values of shape parameter along the outer wall were too low. This is considered to be due to a failure of the accepted methods of velocity profile representation in severe adverse pressure gradients.

SECTION 8

REFERENCES

1. Renau, L.R., Johnston, J.P., and Kline, S.J., "Performance and Design of Straight, Two-Dimensional Diffusers," Report PD-8, Mech. Eng. Dept. Stanford University, 1964.

2. Kline, S.J., Abbott, D.E., and Fox, R.W., "Optimum Design of Straight-Walled Diffusers," Trans. A.S.M.E. J. Basic. Eng., Vol. 81, Series D, 1959.

3. Livesey, J.L., and Turner, J.T., "The Dependence of Diffuser Performance upon Inlet Flow Conditions," Jnl. of Royal Aero. Soc., Vol. 69, 1965.

4. Wolf, S., and Johnston, J.P., "Effects of Non-Uniform Inlet Velocity Profiles on Flow Regimes and Performance in Two-Dimensional Diffusers," Report PD-12, Mech. Eng. Dept. Stanford University, 1966.

5. Schlichting, H., and Gersten, K., "Calculation of the Flow in Rotationally Symmetric Diffusers with the Aid of Boundary Layer Theory," Zeitschrift fur Flugwissenschaften, Vol. 9, Nos. 4/5, 1961.

6. Sprenger, H., "Experimental Research on Straight and Curved Diffusers," Mitteilung aus dem Institute fur Aerodynamik an der E.T.H., Zurich, No. 27, 1959.

7. Sovran, G., and Klomp, E., "Experimentally Determined Optimum Geometries for Rectilinear Diffusers with Rectangular, Conical, or Annular Cross-Section," Fluid Mechanics of Internal Flow, Elsevier, 1967.

8. Waitman, B.A., Reneau, L.R., and Kline, S.J., "Effects of Inlet Conditions on Performance of Two-Dimensional Diffusers," Report PD-5, Mech. Eng. Dept. Stanford University, 1960.

9. Migay, V.K., "Effect of Initial Turbulence on the Efficiency of Diffuser Flows," Teploenergetika, No. 2, 1966.

10. Tyler, R.A., and Williamson, R.G., "Diffuser Performance with Distorted Inflow," Proceedings of Symposium on Subsonic Fluid Flow Losses in Complex Passages and Ducts, I. Mech. E. Proceedings Vol. 182, Part 3D, 1967-68.

11. Schwartz, I.R., "Investigation of an Annular Diffuser - Fan Combination Handling Rotating Flow," N.A.C.A. R.M. L9B28, 1949

12. Gibson, A.H., "On the Flow of Water through Pipes and Passages having Converging and Diverging Boundaries," Proc. Royal Soc. Series A, Vol. 83, No. 563, 1910.

13. McDonald, A.T., and Fox, R.W., "An Experimental Investigation of Incompressible Flow in Conical Diffusers," A.S.M.E. Preprint 65-FE-25, 1965.

14. Young, A.D., and Green, G.L., "Tests of High-Speed Flow in Diffusers of Rectangular Cross-Section," R. & M. No. 2201, A.R.C. 1944.

15. Little, B.H., and Wilbur, S.W., "Performance and Boundary Layer Data from 12-degree and 23-degree Conical Diffusers of Area Ratio 2.0 at Mach Numbers up to Choking and Reynolds Numbers up to 7.5×10^6, " N.A.C.A. Report 1201, 1954.

16. Migay, V.K., "Study of Ribbed Diffusers," Teploenergetika, No. 10, 1962.

17. Henderson, F.D., "The Effect of Profile and Length on the Efficiency of Pump Diffusers," R.P.E. Tech. Note No. 181, 1959.

18. Okiishi, T.H., and Servoy, G.K., "An Experimental Study of the Turbulent-Flow-Boundary-Layer Development in Smooth Annuli," A.S.M.E. Preprint 67-WA/FE-10, 1967.

19. Stevens, S.J., and Markland, E., "The Effect of Inlet Conditions on the Performance of Two Annular Diffusers," A.S.M.E. Preprint 68 - WA/FE - 38, 1968.

20. Ainley, D.G., "Investigation of Air Flow Through Some Annular Diffusers," Power Jets Report No. R1151, 1946.

21. Johnston, I.H., "The Effect of Inlet Conditions on the Flow in Annular Diffusers," A.R.C. Current Paper No.178, 1954.

22. Wood, C.C., and Higginbotham, J.T., "Effects of Diffuser and Centre Body Length on Performance of Annular Diffusers with Constant-Diameter Outer Walls and with Vortex Generator Controls," N.A.C.A. RML54G21, 1954.

23. Wilbur, S.W., and Higginbotham, J.T., "Investigations of Two Short Annular Diffuser Configurations Utilizing Suction and Injection as a Means of Boundary Layer Control," N.A.C.A. RM L54K18, 1955.

24. Horlock, J.H., "Boundary Layer Problems in Axial Turbomachines," Flow Research on Blading, Elsevier 1970.

25. Henry, J.R., Wood, C., and Wilbur, S.W., "Summary of Subsonic Diffuser Data," N.A.C.A. RM L56 F05, 1956.

26. Howard, J.H.G., Henseler, H.J., and Thornton-Trump, A.B., "Performance and Flow-Regimes for Annular Diffusers," A.S.M.E. Preprint 67 - WA/FE - 21, 1967.

27. Stevens, S.J., "The Performance of Annular Diffusers," M.Sc. Thesis, University of Nottingham, 1966.

28. Moses, H.L., "The Behaviour of Turbulent Boundary Layers in Adverse Pressure Gradients," M.I.T. Gas Turbine Lab Report No.73, 1964.

29. Goldberg, P., "Upstream History and Apparent Stress in Turbulent Boundary Layers," M.I.T. Gas Turbine Lab. Report No. 85, 1966.

30. Imbach, H.E., "Calculation of Rotationally Symmetrical Turbulent Flow through Diffusers," The Brown Boveri Review Vol.51, No.12, 1964.

31. Nicoll, W.B., and Ramaprian, B.R., "A Modified Entrainment Theory for the Prediction of Turbulent Boundary Layer Growth in Adverse Pressure Gradients," A.S.M.E. Preprint 69-FE-16, 1969.

32. Soo, S.L., "Auxiliary Functions of Three-Dimensional Turbulent Boundary Layers," Part 1, AGARDograph 97, 1965.

33. Stevens, S.J., "The Performance of Annular Diffusers," Proc. of Symposium on Subsonic Fluid Flow Losses in Complex Passages and Ducts, I. Mech. E. Proceedings Vol.182, Part 3D, 1967-68.

34. Kline, S.J., Morkovin, M.V., Sovran, G., and Cockrell, D.J. "Proceedings Computation of Turbulent Boundary Layers - 1968 AFOSR - IFP - Stanford Conference," Vol.1, Stanford University, 1969.

35. Stratford, B.S., "An Experimental Flow with Zero Skin Friction Throughout its Region of Pressure Rise," J. Fluid Mech., 5, 1959.

36. Stevens, S.J., and Eccleston, B., "The Performance of Combustion Chamber Annular Diffusers," Report No. TT 69 R02, Dept. of Transport Technology, Loughborough University of Technology, 1969.

37. Pankhurst, R.C., and Holder, D.W., "Wind-Tunnel Technique" pub. Pitman, 1952.

38. Young, A.D., and Maas, J.N., "The Behaviour of a Pitot-Tube in a Transverse Pressure Gradient," A.R.C. R.and M. 1770.

39. Brighton, J.A., and Jones, J.B., "Fully Developed Turbulent Flow in Annuli," Trans. A.S.M.E., Series D, vol.86, 1964.

40. Knudsen, J.G., and Katz, D.L., "Fluid Dynamics and Heat Transfer," pub. McGraw-Hill, 1958.

41. Coles, D., "The Law of the Wake in the Turbulent Boundary Layer," J. Fluid Mech., 1, 1956.

42. Ludwieg, H., and Tillman, W., "Investigations of the Wall Shearing Stress in Turbulent Boundary Layers," N.A.C.A. TM 1285.

43. Felsch, K.O., "Contribution to the Calculation of Turbulent Boundary Layers in Two-Dimensional Incompressible Flow," Ph.D. Thesis, T.H. Karlsruhe, 1965.

44. Coles, D.A., and Hirst, E.A., "Proceedings Computation of Turbulent Boundary Layers - 1968 AFOSR-IFP-Stanford Conference," Vol.II, Stanford University, 1969.

45. Sandborn, V.A., and Liu, C.Y., "On Turbulent Boundary Layer Separation," J. Fluid Mech., 32, 1968.

46. Spangenberg, W.G., Rowland, W.R., and Mease, N.E., "Measurements in a Turbulent Boundary Layer Maintained in a Nearly Separating Condition," Fluid Mechanics of Internal Flow, Elsevier, 1967.

47. Rotta, J.C., "Critical Review of Existing Methods for Calculating the Development of Turbulent Boundary Layers," Fluid Mechanics of Internal Flow, Elsevier, 1967.

48. Bradshaw, P., "Turbulent Boundary Layers," The Aero. Jnl. of The Royal Aero. Soc., Vol 72, No. 689, 1968.

49. Spalding, D.B., "Theories of the Turbulent Boundary Layer," Appl. Mech. Rev. 20, No. 8, 1967.

50. Bradshaw, P., and Ferriss, D.H., "The Response of a Retarded Equilibrium Turbulent Boundary Layer to the Sudden Removal of Pressure Gradient," N.P.L. Aero Rep. 1145, 1965.

51. Clauser, F.H., "Turbulent Boundary Layers in Adverse Pressure Gradients," Jnl. of Aero. Sci., Vol. 21, 1954.

52. McDonald, H., and Stoddart, J.A.P., "On the Development of the Incompressible Turbulent Boundary Layer," R and M No. 3484, 1965.

53. Schubauer, G.B. and Klebanoff, P.S., "Investigation of Separation of the Turbulent Boundary Layer," N.A.C.A. T.N. 2133, 1950.

54. Cockrell, D.J., "Boundary Layer Effects in Diffusers," Ph.D. Thesis, University of Nottingham, 1964

55. Cocanower, A.B., Kline, S.J., and Johnston, J.P.," A unified Method for Predicting the Performance of Subsonic Diffusers of Several Geometries," Report PD-10. Mech. Eng. Dept., Stanford University, 1965.

56. Thompson, B.G.J., "A Critical Review of Existing Methods of Calculating the Turbulent Boundary Layer," A.R.C. Report No. 26,109, 1964.

57. Head, M.R., "Entrainment in the Turbulent Boundary Layer," A.R.C. R. and M. No. 3152, 1960.

58. Spalding, D.B., "The Kinetic-Energy-Deficit Equation of the Turbulent Boundary Layer," AGARDograph. No. 97, 1965.

59. Escudier, M.P., and Spalding, D.B., "A Note on the Turbulent Uniform-Property Boundary Layer on a Smooth Impermeable Wall; Comparison of Theory and Experiment," A.R.C., C.P. No. 875, 1966.

60. Bradshaw, P., Ferriss, D.H., and Atwell, N.P., "Calculation of Boundary Layer Development Using the Turbulent Energy Equation," N.P.L. Aero. Report 1182, 1966.

61. Rotta, J.C., "Turbulent Boundary Layers in Incompressible Flow," Progress in Aeronautical Sciences, Vol. 2. Pergamon Press, 1962.

62. Kline, S.J., "Turbulent Boundary Layer Prediction," Flow Research on Blading, Elsevier 1970.

63. Lee, B.E., "Some Effects of History on Turbulent Fluid Flow," Ph.D. Thesis, University of Leicester, 1969.

64. Sandborn, V.A., and Slogar, R.J., "Study of the Momentum Distribution of Turbulent Boundary Layers in Adverse Pressure Gradients. N.A.C.A. T.N.3264, 1955.

65. Pretsch, J., "Zur Theoretischen Berechung des Profilwiderstandes" Jb. Dtsh. Luftfahrtforsch, I, 1938.

66. Bull, M.K., "Velocity Profiles of Turbulent Boundary Layers," The Aero Jnl. of the Royal Aero Soc., Vol. 73, 1969.

67. Fox, R.W., and Titcomb, C.S., "Prediction Methods for Turbulent Incompressible Flow in Conical Diffusers," Report FMTR-65-2, Mech. Eng. Dept. Purdue University, 1965.

68. Spence, D.A., "Development of Turbulent Boundary Layers," Jnl. of Aero. Sci., Vol. 23, 1956.

69. Thompson, B.G.J., "A New Two-Parameter Family of Mean Velocity Profiles for Incompressible Turbulent Boundary Layers on Smooth Walls," A.R.C. R. and M. 3463, 1965.

70. Nash, J.F., "Turbulent Boundary Layer Behaviour and the Auxiliary Equation," N.P.L. Aero. Rep. 1137, 1965.

71. Newman, B.G., "Some Contributions to the Study of the Turbulent Boundary Layer Near Separation," ACA-53, 1951.

72. Perry, A., "Turbulent Boundary Layers in Decreasing Adverse Pressure Gradients," Jnl. Fluid Mech., Vol. 26, 1966.

73. McDonald, H., "The Effect of Pressure Gradient on the Law of the Wall in Turbulent Flow," Jnl. Fluid Mech., Vol. 35, 1969.

74. Townsend, A.A., "The Behaviour of a Turbulent Boundary Layer near Separation," Jnl. Fluid Mech., Vol. 12, 1962.

75. Mellor, G.L., and Gibson, D.M., "Equilibrium Turbulent Boundary Layers," FLD Report No. 13, Dept. Aerospace Mech. Sci., 1963.

76. Stratford, B.S., "Prediction of Separation of the Turbulent Boundary Layer," Jnl. Fluid Mech., Vol. 5, 1959.

77. Nayak, U.L., and Stevens, S.J., "Calculation of the Boundary Layer Growth in an Annular Diffuser," (to be published as Dept. TT report, Dept. of Transport Technology, Loughborough University of Technology)

78. Patankar, S.V., and Spalding, D.B., "Heat and Mass Transfer in Boundary Layers," Morgan-Grampian, London, 1967.

79. Nelson, D.M., "Turbulent Boundary Layer Calculations Using A Law of the Wall of the Wake Method," U.S. Naval Ordinance Report, NOTS TP 4083, 1966.

80. Stevens, S.J., and Williams, G.J., "The Performance of Annular Diffusers," Gas Turbine Collaboration Committee, Report No. 299, Min. Tech., 1969.

81. Batchelor, G.K., "Note on Free Turbulent Flows, with Special Reference to the Two-Dimensional Wake," Jnl. of Aero.Sci., Vol. 17, 1950.

82. Nelson, W.J., and Popp, E.G., "Performance Characteristics of Two 6^{o} and Two 12^{o} Diffusers at High Flow Rates," N.A.C.A. R.M.L9H09, 1949.

83. Parthasarathy, S.P. and Tritton, D.J., "Impossibility of Linearising a Hot Wire Anemometer for Measurements in Turbulent Flows," A.I.A.A. Jnl., 1963

84. Schlichting, H., "Boundary Layer Theory", 6th Edition, published McGraw-Hill.

85. Goldstein, S., "Modern Developments in Fluid Dynamics," Vols. I and II, published Clarendon Press, Oxford.

86. Chaturvedi, M.S., "Flow Characteristics of Axisymmetric Expansions," Proc. of A.S.C.E., Hydraulics Div., May 1963